UNIVERSITY OF CALIFORNIA,

IRVINE

Information Content of Hydrologic Signatures and their Impacts on Watershed Model Calibration

THESIS

submitted in partial satisfaction of the requirements

for the degree of

MASTER OF SCIENCE

in Environmental Engineering

by

Mohammad Sassani

Thesis Committee:
Professor Amir AghaKouchak, Chair
Professor Mojtaba Sadegh
Professor Kuolin Hsu

2018

DEDICATION

To

my wonderful loving parents Ali Sassani and Roya Lolachi

TABLE OF CONTENTS

LIST OF Figures

Page

LIST OF TABLES

ACKNOWLEDGMENTS

The sons of Adam are limbs of each other,
Having been created of one essence.
When the calamity of time affects one limb
The other limbs cannot remain at rest.
If you have no sympathy for the troubles of others,
You are unworthy to be called by the name of a Human.

"Abū-Muhammad Muslih al-Dīn bin Abdallāh Shīrāzī(Saadi) "

First, I would like to thank my parents, Ali and Roya Sassani for the opportunity and encouragement to study as an undergraduate and graduate student. All of this could not have been possible without their constant unconditional love and support. I am forever indebted and grateful to them.

I would like to thank Professor Amir AghaKouchak, Mojtaba Sadegh and Kuo-lin Hsu, for serving on my committee and providing suggestions that improved the research presented in this thesis. I wish to give special thanks to Mojtaba Sadegh for his guidance, patience, and support as both the director of my research and a friend. I wish to thank Dr. Amir AghaKouchak for providing me with the opportunity, support, and freedom that made this work possible. And thanks to my friends Amir Kashfi and Hamed Nagsh Nilchi for giving me encouragement during this process.

ABSTRACT OF THE THESIS:

Information Content of Hydrologic Signatures and their Impacts on Watershed Model Calibration

By

Mohammad Sassani

Master of Science in Environmental Engineering

University of California, Irvine, 2018

Professor Amir AghaKouchak, Chair

Approximate Bayesian computation, also known as ABC, is a simulation-based method with its roots in Bayesian analysis, which is increasingly used in the past couple of years in the field of hydrology for parameter estimation and uncertainty analysis. ABC relaxes the need for an explicit likelihood function and uses multiple hydrologic metrics (signatures) to evaluate model simulations. If the hydrologic signatures are sufficient, and the distance between simulated metrics and their observed counterparts are less than a nominal threshold, model parameters are assumed to be derived from the posterior distribution. Since finding a sufficient set of summary statistics is difficult for complex environmental systems and high-order models, the inferred posterior parameter and

predictive distributions are constrained on the set of selected metrics and may not necessarily mirror the "true" posterior parameter distributions.

In this thesis, we have strived to shed some light on how different hydrologic signatures constrain watershed models. More specifically, we are interested to understand which portions of the hydrograph is constrained by each individual hydrologic signature, and ultimately move toward finding a set of sufficient metrics with least overlapping information. Throughout the years significant strides have been made in the field of calibration and uncertainty assessment of hydrologic models, but the constraining power of different hydrologic metrics have not yet been characterized. Using information theory, likelihood, entropy, and conventional metrics such as NSE, RMSE, and percent bias; we try to characterize constraining power and model parameter sensitivity to each metric. Sensitivity analysis of model parameters is performed using Kullback-Leiber divergence metric and Two Sample Kolmogorov Smirnov test. One interesting finding of this study is that hydrologic signatures are model specific and cannot be readily transferred between different models. The result of this study also depict that that each watershed possesses different and unique characteristics, which is also manifested in the hydrologic signatures that are selected for each watershed. In other word, hydrologic signatures are model- and watershed- specific. We also observe that more flexible watershed models, such as GR4J, react differently to hydrologic signatures as compared to less flexible model structures, such as HyMod. In more detail, more flexible model structures are associated with higher

information content, which might ultimately help the hydrologic signatures in constraining model behavior.

Chapter 1

INTRODUCTION:

Hydrologic models are important tools for improving our understanding of catchments behavior and generating prediction estimation of future environmental responses [Dmitri Kavetski, et al., 2006; Sadegh et al. 2018]. In the early 1960s, theoretical hydrology models such as The Stanford watershed Model that can deal with the continuous dynamics of hydrologic operations were proposed. These models were designed to profit from advancements in the computational power of computers in order to quantifiably illustrate the hydrologic processes that occur in a watershed. These advancements have taken place with respect to available knowledge of a watershed and computational power that both limitations have been decreasing over the years [John C. Schaake,2003].

The major limiting factor in hydrologic modeling is in making predictions and testing conclusions at space and time scales of interest. Another factor is imperfect and limited knowledge in regard to: vegetation and topographic characteristics, soil properties, water and energy forcing that alternate over time and space, and hydrologic processes at distinct scales. Due to these factors, real world modeling is both an art and a science of implementing finite and incomplete knowledge [John C. Schaake,2003].

Each theoretical model poses parameters that are coefficient and exponents within the model equations. These parameters usually cannot be measured in the field [Sadegh

and Vrught, 2013], and should be assessed for the catchment in question. Using a complex calibration process, parameters need to be estimated with respect to the physical characteristics or via parameter modification with the goal of the model responding to an approximate observed response [Naeini et al. 2018]. The process of calibration is more convoluted than it seems due to the inadequacy of available input and output data, insufficiency in regard to the available understanding of basin characteristics, limitations within models, and restrictions in one's skill to define quantitatively preferences for how best to fit the models to the data. Consequently, for any explicit watershed, there are no apparent parameter values and there exists an amount of uncertainty in regard to which parameter value would be optimal [John C. Schaake,2003].

When analyzing the model's output in association with the measured data, some differences between these two are observed. As a result, essential questions about the origin of this divergence emerge. This divergence can be the result of many different factors such as: limitations within the model structure, parameter short comings, and last but not least, errors with in the forcing data and/or in the output measurements [Sadegh and Vrugt, 2013]. The calibration scheme must clearly be account for input, state, model structural and parameter uncertainty, as well as model response uncertainty for various cases and forms of information and data. This process needs to take place simultaneously with the recurrent processing of data and new information as they become available and ready to use [Moradkhani et al. 2005].

Traditional model calibration methods minimized a distance metric between model simulations and observations such as mean square error (RMSE) or Nash-Sutcliffe Efficiency (NSE). Some of the major weaknesses of traditional methods includes their fundamental assumption that the model structure is appropriately exact, inefficiency to manage diverse sources of uncertainty, their insistence on finding a singular optimal parameter set when realistically there can be range of acceptable parameters, being dependable on a particular aggregate measure of performance model and foremost their inability to characterize between different model behavior [HoshinV. Gupt et all, 2003]. This has encouraged researchers to use Bayesian inference to account for modeling uncertainties in a robust and sound way [Sadegh et al., 2017 & 2018; and references therein]. However, the likelihood function in the Bayesian framework is also limited in terms of providing detailed information about model performance and lack the intrinsic capability to perform diagnostic model evaluation [Gupta et al. 2008]. Approximate Bayesian Computation (ABC) has become a favorable method of calibration due it powerful model evaluation scheme [Vrugt and Sadegh 2013; Sadegh and Vrugt 2013]. This method relaxes the demand for certain likelihood functions in support of multiple summary statistics that can extract independent pieces of information about model performance [Sadegh et al. 2015 & 2016]. ABC is also notably useful due to its superior capability (as opposed to traditional Bayesian approach) of using posterior distributions that correctly identify the role of model structure, parameter uncertainty, as well as calibration and forcing data [Vrugt and Sadegh, 2013].

Over the years significant strides have been made in the field of model calibration, analysis and developments, but analysis of the impacts of each individual hydrologic signature on the predictive performance of watershed models has not received much attention. Therefore, there remains a need for assessing the constraining power of individual hydrologic metrics. This analysis is performed herein by calibrating the GR4J and HyMod models for several watershed data and calculating mean ensemble RMSE, NSE, and percent bias for the posterior samples of the analysis with each metric. Coverage of observations within the predictive uncertainty ranges, as well as spread of the uncertainty range have also been analyzed. Moreover, Entropy of model simulations and likelihood of the observations given the model simulations' distribution, at each time step, have been computed to demonstrate the constraining power of each hydrologic signature on different portions of the hydrograph. Ultimately, the Kullback Leibler divergence metric and Two-sample Kolmogorov-Smirnov test was used to evaluate the sensitivity of each model parameter for each metric used.

Results of this study present importance of understanding distinctive characteristics of a watershed and its relation to the hydrologic model implemented, as well as its connection to calibration metrics used. Analyzing of a watershed, it is critical evaluate the model's performance using sets of performance evaluation metrics alongside predictive uncertainty plots. Furthermore, this research study indicates that metrics such as FDC Low Segment Volume less than 30 Percentile, Auto Correlation of Hydrograph with 1Day Lag, Rising LIMB Destiny, Declining LIMB Destiny and 1st Flow Percentile render more

constraining power over the GR4J hydrologic model, whereas FDC High Segment Volume more than 90 Percentile and 99th Flow Percentile are performing more adequately with HyMod hydrologic model that is a less flexible model. In general, hydrologic signatures are both model- and watershed- specific.

Chapter 2

METHODOLOGY

1.1. Bayesian Analysis

Bayesian inference is a statistical approach that uses Bayes' theorem to extract meaningful information from observation data to constrain model realizations. As more data, information, or material become available, Bayes' theorem is implemented with the purpose of updating the probability of a hypothesis. The Bayesian method is named after Reverend Thomas Bayes (1701–1761), minister and mathematician; who worked extensively on scheming distribution for the probability parameters of a binomial distribution [Sadegh and Vrugt 2013].

Over the years, the Bayesian analysis has found application in many different fields [Geweke, 1989], such as hydrology [Wood and Rodr ıguez-Iturbe, 1975], medicine [L.Bernardinelli,D et al. 1995], ecology [G.B. Arhonditsis a,et al. 2005], geology[Chih-HsiangHo, 1990], oceanography[L. Mark Berliner, 1997], meteorology[David J. Spiegelhalter, et al. 1993], and much more. This analysis is used for uncertainty quantification purposes and model inference [Huelsenbeck, et al. 2001].

Quantitative measurement of the probability of a hypothesis by using available data, describing probabilities as individual degrees of a notion in a likelihood of an event, and

delineating the posterior space of model parameters as random variables are just some of important aspects that make Bayesian inference a very important statistical tool [Aaron M. Ellison, 2004].

In hydrology, the Bayesian method has become increasingly popular for uncertainty analysis, fitting models to data, and many more (e.g., estimating modeling uncertainties of streamflow, pollution dispersion in water bodies, groundwater table depth, soil moisture pressure head, snow water equivalent) [Mojtaba Sadegh, Jasper A. Vrugt, 2014].

Bayes' law conveniently attributes all modeling uncertainties to model parameters and estimates the posterior distribution of model parameters [Sadegh et al. 2018]. A Major advantage of the Bayesian approach is that by employing informative prior probability distribution function the parameter uncertainty would be lowered [Guillermo et al., 1975]. Posterior distribution of model parameters using Bayes' law is defined as

$$p\left(\theta\middle|\tilde{Y}\right) = \frac{p(\theta)p\left(\tilde{Y}\middle|\theta\right)}{p\left(\tilde{Y}\right)} \quad (1)$$

In this equation $p\left(\theta\middle|\tilde{Y}\right)$ and $p(\theta)$ represent posterior and prior parameter distributions, respectively. The likelihood function is shown by $p\left(\tilde{Y}\middle|\theta\right) \cong \mathcal{L}\left(\theta\middle|\tilde{Y}\right)$, and $p\left(\tilde{Y}\right) = \int_{\theta} p(\theta)p\left(\tilde{Y}\middle|\theta\right) d\theta$. The latter indicates information and evidence, which is a constant value in a modeling practice. When the main objective is to estimate the posterior distribution of parameters, evidence can be removed from the analysis, and posterior parameter distribution can be estimated with

$$p(\theta|\tilde{Y}) \propto p(\theta)p(\tilde{Y}|\theta). \quad (2)$$

When there is a lack of useful information about the prior distribution of parameters, flat uniform prior can be employed [M. Thiemann et al., 2001]. Now the only remaining piece is defining a likelihood function, which assuming error residuals are uncorrelated, homoscedastic (same variance) and Gaussian-distributed with mean zero can be formulated by [Sorooshian and Dracup, ,1980].

$$\mathcal{L}(\theta|\tilde{Y}) = \prod_{i=1}^{n} \frac{1}{\sqrt{2\pi\tilde{\sigma}^2}} exp\left\{-\frac{1}{2}\tilde{\sigma}^{-2}[\tilde{y}_i - y_i(\theta)]^2\right\} \quad (3)$$

The standard deviation of measurements errors is signified by $\tilde{\sigma}$ in the above equation, and this equation can be logarithmically transformed for simplicity and numerical stability to

$$\ell(\theta|\tilde{Y}) = -\frac{n}{2}ln(2\pi) - \frac{n}{2}ln\,\tilde{\sigma}^2 - \frac{1}{2}\tilde{\sigma}^{-2}\sum_{i=1}^{n}[\tilde{y}_i - y_i(\theta)]^2. \quad (4)$$

Furthermore, $\tilde{\sigma}$ can be estimated as

$$\tilde{\sigma} = \sqrt{\frac{\sum_{i=1}^{n}[\tilde{y}_i - y_i(\theta)]^2}{n}}. \quad (5)$$

Equation 4 can be further simplified by removing the constant terms, as they does not impact the inference [Sadegh, M., E. Ragno, and A. AghaKouchak, 2017],

$$\ell\left(\theta\middle|\tilde{Y}\right) \cong -\frac{n}{2} ln\left\{\frac{\sum_{i=1}^{n}[\tilde{y}_i - y_i(\theta)]^2}{n}\right\}. \quad (6)$$

1.2. Approximate Bayesian Computation (ABC)

Over the years models are becoming more and more complex. Increasing computational power and advancements in measurement technologies have increased the availability and accuracy of hydrologic data and raised the need for higher diagnostic computational power [Sadegh et al. 2016]. Since traditional likelihood-based calibration and system analysis algorithms are insufficient to distinguish and find flaws in model structures, novel statistical techniques are required to extract independent pieces of information from model behavior and pinpoint potential shortcomings of modeling approach [Vrugt and Sadegh, 2013]. Note, however, that although significant strides are made in this direction, accommodating higher order system models with a considerable amount of field information is still a challenge [Turner, B. M., & Van Zandt, T. ,2012].

Approximate Bayesian computation (ABC) has become popular to address the search for a more powerful model evaluation, an absolute necessity raised by several researchers such as Gupta et al. 2008. This statistical methodology softens the need for accurate likelihood function and replaces it with one or more summary statistics rooted in environmental theory and doing so has provided a great diagnostic power for hydrological theory assessments [Turner, B. M., & Van Zandt, T. ,2012].

ABC was originally developed by Diggle and Gratton in 1984 and has been broadly used where evaluation of likelihood is exorbitant and/or for situations that specific objective function/likelihood cannot be supported [Brandon M. et al., 2012]. ABC has gained popularity in different fields of study such as genetics and has become an essential tool for human behavior models that endure extremely complex likelihoods [Turner, B. M., & Van Zandt, T. ,2012] and [Beaumont, M. et al. ,2002]. ABC was introduced to the field of hydrology by the early works of Nott et al., 2012 and Vrugt and Sadegh, 2013.

The proper implementation of ABC lies in the careful selection of summary metrics that appropriately extract nearly all available information from calibration data, assigning an appropriate tolerance value and proper sampling procedure for complex multidimensional spaces involving tens to hundreds of parameters [Mojtaba Sadegh and Jasper A. Vrugt, 2014]. ABC replaces the likelihood function calculation in Bayesian equation,

$$p\left(\theta\middle|\tilde{Y}\right) = \frac{p\left(\tilde{Y}\middle|\theta\right)p(\theta)}{\int p\left(\tilde{Y}\middle|\theta\right)p(\theta)\,d\theta}, \tag{7}$$

with some representative summary metrics that ideally extract as much information as the underlying "true" likelihood function. Note that the "true" likelihood function is not simple to derive in a complex environmental problem and is instead formulated given some assumptions about the system behavior which are often violated by the model response [Sadegh et al. 2016]. In short, intention of ABC is to gain estimation of posterior distribution for model parameters, without computation of an explicit likelihood function.

Without implementing likelihood, a θ^* can be assumed to be a sample from the posterior distribution, if distance value, $p\ (Y, \tilde{Y})$, that evaluates the divergence between model simulations, Y, and measurements, $\tilde{Y}$, is less than a tolerance threshold value ε . For a small value of tolerance threshold, the posterior distribution can be defined as: [Pritchard, J. K., Seielstad, M. T., Perez-Lezaun, A., & Feldman, M. W. ,1999].

$$p\left(\theta \middle| \rho\left(\ Y,\tilde{Y}\right) \leq \varepsilon\ \right) \cong\ p(\theta \mid \tilde{Y}) \tag{8}$$

Approximate Bayesian computation algorithm progresses by first sampling a parameter set, θ^*, form a prior distribution $p(\theta)$. Then, information gained from the 1st step is used to generate a vector of model simulations, Y, similar in dimension to observation data, $\tilde{Y}$. Next step is computing $\rho\ (Y, \tilde{Y})$ which is estimated by comparing the distance between Y (simulated data) and $\tilde{Y}$ (observed data) and if the value of $\rho\ (Y, \tilde{Y})$ is less than a nominal threshold, ε , the distance is regarded as small and parameter θ^* has a nonzero probability of being within the range of the approximate posterior distribution. When such case is true, θ^* is kept as a posterior sample; otherwise would be disregarded and a new θ^* would be chosen and the discussed process would take place again.

Instead of measuring the distance between a vector of observations, $\tilde{Y}$, and simulations, Y, one may characterize the distance between a set of their representative summary metrics. Summery metrics, $S(\ .\ )$, could represent different statistics such as sample mean, standard deviation, etc. More importantly, these metrics could have roots in the environmental theory to extract some clear and compelling information from the data

[Sadegh and Vrugt, 2014]. Information content of these metrics should be sufficient to delineate the posterior distribution of model parameters. Ideally, appropriate statistics, $S(\,.\,)$, offer the same amount of information about the parameters as the original data set ($\tilde{Y}$,), and hence the posterior distribution can be written as:

$$p\left(\theta\middle|\rho(S(Y),S(\tilde{Y})\leq\varepsilon\right)\ \cong p\left(\theta\middle|\tilde{Y}\right) \tag{9}$$

In summary, the assumption behind ABC is when $\rho\left(\,Y,\tilde{Y}\right)$ is characterized by satisfactory statistics, the resulting approximation to the posterior would be sufficient, as long as $\rho\left(S(Y),S(\tilde{Y})\right)<\varepsilon$. Some factors that need to be kept in mind are when the value of ε is very small, the rejection would increase dramatically, and choosing sufficient summary metrics is not simple partly due to its dependency on unknown likelihood $p\left(\tilde{Y}\middle|\theta\right)$ [Turner, B. M., & Van Zandt, T., 2012].

Sampling algorithms within approximate Bayesian computation framework can be organized into three wide categories: Rejection algorithm, Markov Chain Monte Carlo (MCMC) algorithms, and Sequential Monte Carlo methods also known as SMC [Sadegh and Vrugt, 2014]. We use the MCMC algorithm of Sadegh et al. 2017 to delineate the posterior distribution of hydrologic model parameters within an ABC framework in this study. The adaptive sampling of this algorithm mitigates the high rejection rates of the posterior samples within an ABC framework.

1.3. Hydrologic Models

1.3.1. GR4J

GR4J is a modified version of a GR3J model which was proposed by Edijianto and Michel in 1989 and substantially improved by Nascimento in 1995 and Edijantoet et al in 1999 [Charles Perrin, Claude Michel, Vazken Andréassian, 2003]. GR4J is a lumped conceptual model with four parameters and two reservoirs (a production reservoir and a routing reservoir). With precipitation and potential evapotranspiration as inputs, this model provides streamflow and evapotranspiration prediction at the catchment outlet.

Two-unit hydrograph-based methods are used in GR4J to represent the time lag between precipitation and stream flow. This model also takes into account a transfer function between unit hydrograph and the routing store. By subtracting potential evapotranspiration from precipitation, GR4J divides the inputs into net precipitation and net potential evapotranspiration. In cases where the potential evapotranspiration demand is not met from rainfall (precipitation), a portion of the production store would be dedicated to potential evapotranspiration. When net precipitation exists, parts of it would go to production store and the routing unit hydrograph function. Another factor that contribute to unit hydrograph is the output of production store. Unit hydrograph is divided into section one and section two; 90% of inputs to unit hydrograph would go to section one (UH1) and the remaining 10% would go to section two (UH2). Outputs of UH1 will then contribute to the routing reservoir, whereas UH2 outputs interact with the routing reservoir (based on surplus on either side) and contribute to runoff generation. Routing stores outlet, and net aggregate flow from section one of unit hydrograph and ground water exchange (f and, $Exch_T$) combine to estimate

streamflow at the catchment outlet [Sadegh et al., 2017]. Table 3.1 presents GR4J Hydrologic model's parameters, their descriptions and their units. In addition, figure 3.1 represents a schematic overview of the GR4J hydrologic model's structure.

Table 2.1 Description of parameters of conceptual rainfall-runoff for GR4J hydrologic model.

	Parameter Symbol	Parameter Description	Range	Unit
1	S1max	Max Capacity of Production Store	50 - 500	mm
2	Exch	Catchment Water Exchange Coefficient	-15 - 4	mm
3	S2max	One Day Maximal Capacity of the Routing Reservoir	10 - 1300	mm
4	UHB	Hydrograph Time Base	0.5 - 5	days
5	DD	Snow Module	0.7 - 9	mm/C/day

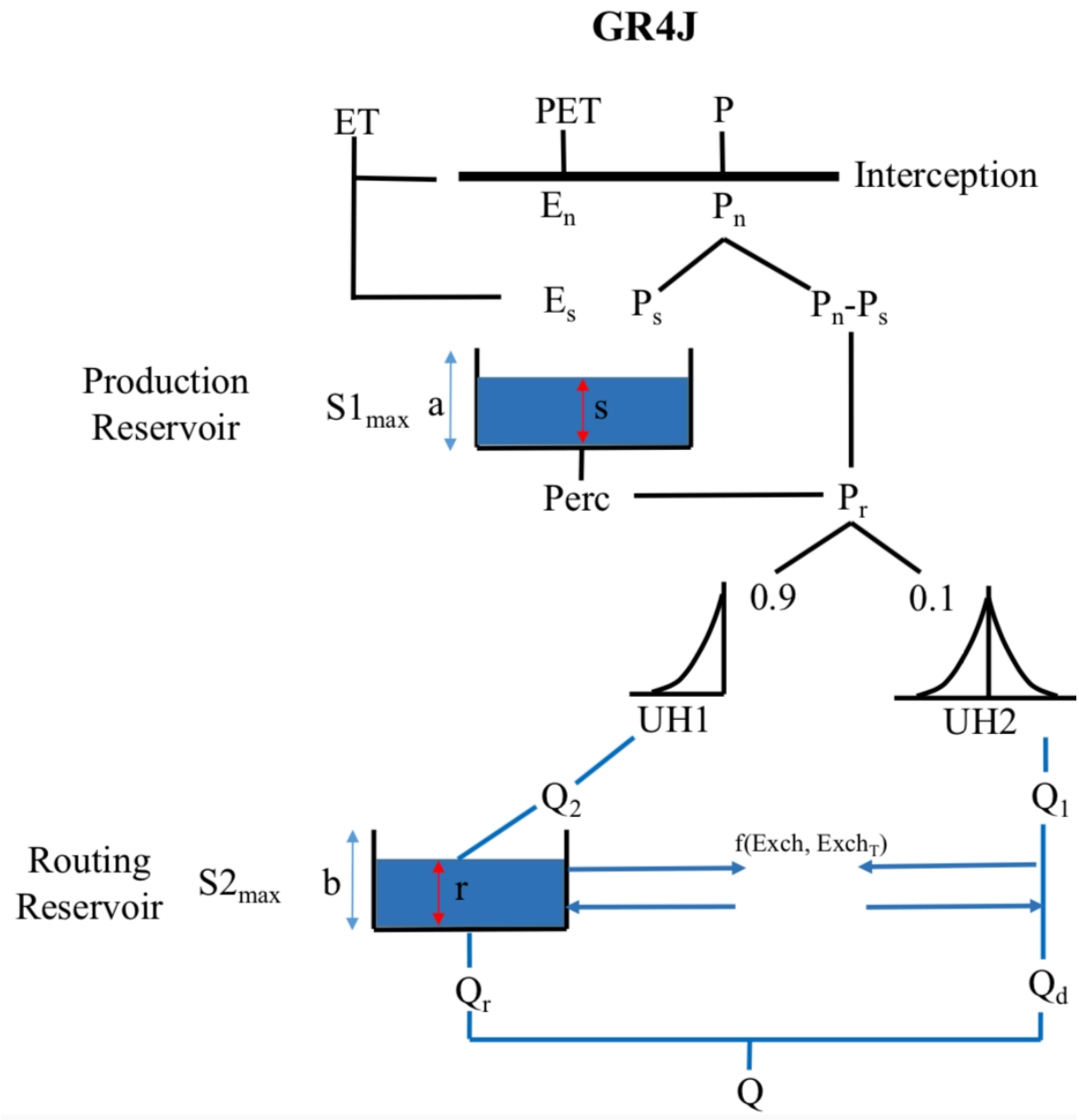

Figure 2.1. Diagrammatic structure of GR4J hydrologic model.

1.3.2. HyMod

HyMod was introduced by Boyle in 2000 and further developed by Wagner in 2001 as a flexible hydrologic model that by using a minimal number of modeling units and function parameters can represent hydrologic processes within a watershed [Boyle, Douglas Patrick, 2001].

HyMod is a parsimonious lumped conceptual model with five parameters and five storage compartments, including one soil moisture reservoir, three serial fast flow reservoirs and one slow flow reservoir, which is parallel to the fast flow reservoirs. In this model, precipitation is processed, and potential evapotranspiration is controlled by two parameters of storage capacity and spatial variability of soil moisture. Precipitation and potential evapotranspiration enters the first compartment (reservoir) the output would enter into fast and slow flow reservoirs working in parallel. The fast segment which includes three reservoirs and the slow segment which include one reservoir, act as routing functions, and their outlets will represent streamflow at the catchment outlet (2). Table 3.2 presents HyMod Hydrologic model's parameters, their descriptions and their units. In addition, figure 3.2 represents a schematic overview of the HyMod hydrologic model's structure.

Table 2.2 Description of parameters of conceptual rainfall-runoff for HyMod hydrologic model.

	Parameter Symbol	Parameter Description	Range	Unit
1	Cmax	Maximum Soil Moisture Reservoir	1 - 500	mm
2	BEXP	Spatial Variability of Soil Moisture Storage	0.1 – 2.00	____
3	Alpha (α)	Distribution Factor Between Fast and Slow Routing Reservoirs	0.1 – 0.99	____
4	Rs	Residence Time of Slow Flow Reservoir	0.001 – 0.1	days
5	Rq	Residence Time of Quick Flow Reservoirs	0.1 – 0.99	days
6	DD	Snow Module	0.7 - 9	mm/C/day

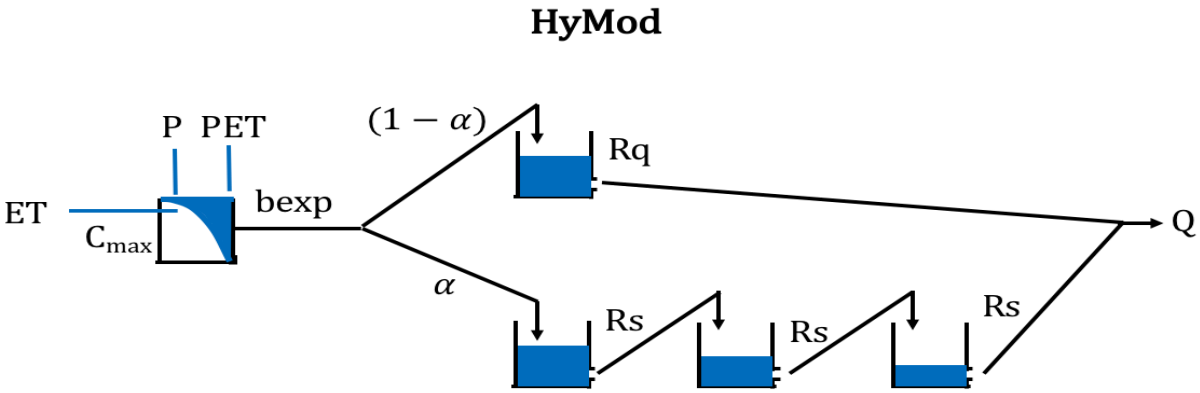

Figure 2.2 Diagrammatic structure of HyMod hydrologic model.

1.3.3. Snow Module

We adopt snow module from the HBV model of Aghakouchak and Habib (2010) with the purpose of determining snow accumulation and melt with respect to temperature. Snow module processes precipitation and temperature data for each given date to determine whether precipitation occurs in the form of rainfall or snow. If temperature is below freezing point (zero degrees Celsius, in this study), this module will accumulate snow, otherwise model would operate by the aggregate of snow melt and rainfall [Sadegh et al., 2017] . This module is separated from the HBV model of Aghakouchak and Habib (2010) and added as a separate module to GR4J and HyMod.

Snow melt is estimated based on $S_m = DD(T - T_0)$, in which T is observed temperature, and T_0 represents the predefined freezing threshold, whereby if temperature exceeds its value, snow melt takes place and when it stays below this threshold snow accumulation occurs. DD is degree day factor that governs the snowmelt volume taking place due to 1℃ temperatures above the freezing threshold, $T_0 = 0$ in this study, for one day. Degree day factor, DD, can range between 0.7 to 9 mm/ C/day [Aghakouchak, AmirHabib, Emad, 2010]. In addition, figure 3.3 represents a schematic overview of the snow module.

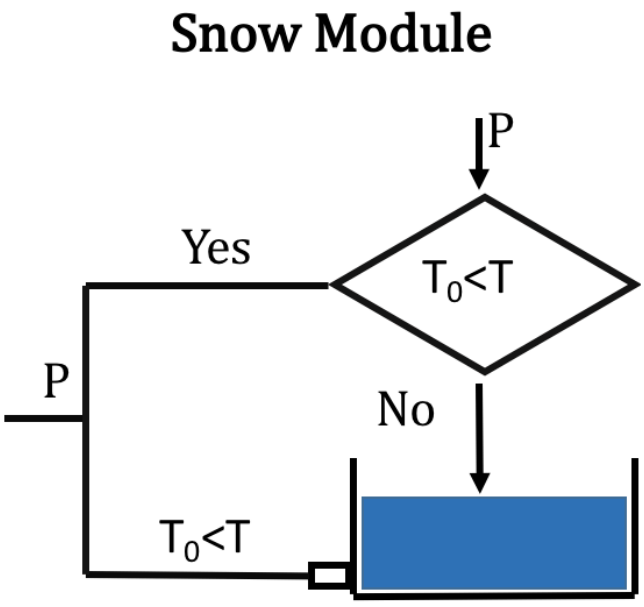

Figure 2.3. Diagrammatic structure of the Snow module. Observed precipitation(P) is first filtered through the snow module to conclude likely snow build up or melt. Tolerance threshold is presumed to be zero degrees Celsius (T0 = 0 C).

2. Performance Evaluation Metrics:

Estimating the precision of model simulations is necessary not only to characterize the accuracy of model's prediction but also for model selection and averaging. In this thesis, different performance evaluation metrics are used to estimate how accurately a predictive model would execute in practice. In the following, performance metrics used to evaluate model simulations in this thesis are briefly described.

2.1. Entropy

Entropy (H) is a measure of uncertainty, variability or disorder of random variables. Entropy is a logarithmic measurement of different states with the substantial lower possibility of occurrence [Liu, M-Y; Tuzel, O.; Ramalingam, S.; Chellappa, R., 2011]. Entropy for a distinct nonspecific arbitrary variable (X) with probability mass function (p_X) is characterized as [Liu, M-Y; Tuzel, O.; Ramalingam, S.; Chellappa, R., 2011].:

$$H(X) = -\sum_{x \in X}(x) p_X log p_X(x) \quad (10)$$

2.2. Likelihood

The likelihood function is implemented in order to outline the gap between observations and model simulations; in another word, it is employed to summarize the divergence among the observations and simulations in a scalar value. Therefore, it can be implemented to find the best fit to the observation data. The equation below calculates

likelihood values according to observations, $\tilde{Y}$, simulation, Y , parameter θ, estimation of standard deviation of measurement error $\tilde{\sigma}$, if residuals (divergence between model simulations and observational data) are assumed independent, homosckedastic, and Gaussian distributed with mean zero [Mojtaba Sadegh, Elisa Ragno, Amir AghaKouchak, 2017].

$$\mathcal{L}(\theta|\tilde{Y}) = \prod_{i=1}^{n} \frac{1}{\sqrt{2\pi\tilde{\sigma}^2}} exp\left\{-\frac{1}{2}\tilde{\sigma}^{-2}[\tilde{y}_i - y_i(\theta)]^2\right\} \quad (14)$$

2.3. Nash-Sutcliffe efficiency (NSE):

The Nash-Sutcliffe efficiency, NSE, is an established statistic of goodness-of-fit[Nash, J. E., and J. V. Sutcliffe,1970]. By using the equation below, NSE shows how accurately the plot of observed vs. simulated data fits the 1:1 line.

$$NSE = 1 - \left[\frac{\sum_{i=1}^{n}(\tilde{y}_i - y_i)^2}{\sum_{i=1}^{n}(\tilde{y}_i - \bar{\tilde{Y}})^2}\right] \quad (15)$$

In the above equation, the i^{th} observation is represented by Y_i^{obs}, the i^{th} simulated value is represented by Y_i^{sim}, the average(mean) of data is represented by $\bar{\tilde{Y}}$ and the total number of observations is shown by n.

The value of NSE ranges between one and negative infinity ($-\infty \leq NSE \leq 1.0$), the ideal NSE value is one. When NSE value drop below 0.0, this is a suggestion that the mean observation value provide a superior prediction than the simulated value; commonly, in

this case, the simulation performance, is not acceptable [D. N. Moriasi, J. G. Arnold, M. W. Van Liew, R. L. Bingner, R. D. Harmel, T. L. Veith, 2007].

NSE is a commonly used metric that can be applied to a range of model types. NSE has been recommended by ASCE Watershed Management Committee (ASCE 1993) and Legates and McCabe (1999). The strength of NSE on reflecting the overall fit of a hydrograph have been proven by Sevat and Dezetter (1991) [Sevat, E., and A. Dezetter, 1991].

2.4. Root Mean Square Error (RMSE):

Root mean square error, RMSE, historically has been one of the most popular methods to measure the difference between simulated values and observed data (model error) over the years [Rob J. Hyndmana, Anne B. Koehler, 2006] and is represented as:

$$RMSE = \sqrt{\frac{1}{n}\sum_{i}^{n}(\ \tilde{y}_i \quad - y_i\ (\theta))^2} \tag{16}$$

In the above equation discharge represented as y, the set of model parameters as θ, the total number of observations as n is (Thomas Meixner1, Hoshin V. Gupta, Luis A. Bastidas and Roger C. Bales, 2013). A Smaller the value of RMSE ($0 \leq$ RMSE) means a smaller error (the difference between data and simulated values. When the value of RMSE is equal to zero, it signifies perfect fit which is very rare [D. N. Moriasi, J. G. Arnold, M. W. Van Liew, R. L. Bingner, R. D. Harmel, T. L. Veith, 2007].

2.5. Percent Bias (PBIAS):

The Percent Bias, PBIAS, calculates the average (mean) tendency of the simulated values to be greater or less than the observation [Gupta et al., 1999]. PBIAS is the evaluation process for the deviation of data (simulated and observed) that represents this deviation and it is stated in the form of percentage. The equation below is used for this calculation process:

$$PBIAS = 100 * \frac{\sum_{i=1}^{n}\left(Y_i - \tilde{Y}_i\right)}{\sum_{i=1}^{n}\tilde{Y}_i} \quad (17)$$

In the above equation, the total number of observations is shown by n.

The value of PBIAS ranges between negative infinity $(-\infty)$ and positive infinity $(+\infty)$ with an optimal value of 0.0, and the small magnitude value of PBIAS represents an accurate water balance in the modeling process. When the value of PBIAS is positive, it represents an overall overestimation of discharge values, whereas its negative values represent overall underestimation of discharges.

2.6. Threshold

Threshold is used in the approximate Bayesian framework to accept or reject a model simulation, and can be used as a proxy metric to show whether model inference is sensitive to a hydrologic signature or not. We use percent divergence of simulated hydrologic signatures from their observed counterpart as the distance metric, and hence

threshold adopts a percentage nature. We iteratively search for a threshold value that renders a coverage of 90% of observation data in the uncertainty range of the inferred model simulation (posterior/behavioral samples).

The premise behind this analysis is that the parameter vector should be a sample of the posterior distribution if the distance between the observed and the simulated data is less than some nominal positive threshold. Whenever the simulated data does not satisfy the threshold value then it expresses that this model might prompt to weak performance.

A threshold value of 0% shows a perfect fit with regard to the hydrologic signature of interest, and as it increases model fit degrades [Mojtaba Sadegh, Jasper A Vrugt, Chonggang Xu, Elena Volpi, 2015]. We select the threshold separately for each metric, by finding the variation among summary metrics that is normalized with the observed metric, the results are found in percentage format and presented as a fraction value in this study.

2.7. Distance between Simulations and Acceptance Range

This metric is the average distance between the observations that have fallen out of the acceptance range and the range limit. The Distance without zero metric is very similar to the Distance metric, with one difference that for this metric the simulation points that are overlapping perfectly with the acceptance range are not taken into account when calculating the average distance.

2.8. Mean Uncertainty Spread

Mean Uncertainty Spread takes into account the spread of the acceptance range to measure the performance of each metric for each model.

2.9. Coverage

Coverage as a performance evaluation metric that measures the average of coverage of observations within the uncertainty range and presents the results in form of percentage. When values of evaluation are closer to 100%, the model simulations are perfect, with respect to the metric of interest given the uncertainty ranges (acceptance area).

3. Sensitivity Surrogate Metrics

3.1. Kullback-Leibler Divergence (KL Divergence)

An ideal method for measuring the variance among two distributions is the Kwullback-Leibler Divergence, KLD. Describing the statistical variance among two data sets is a complex task, and KLD summarizes this complex divergence by describing it as a single positive scalar.

Due to Kullback-Leibler Divergence's unique nature and quality, it has found many different applications such as in image recognition [C.Lin and H-Y Shum, 2003], analyzing

neural firing patterns [H.Nakahara and S.-I. Amari, 2002], financial forecasting [J. Robertson, E. W. Tallman, and C. H. Whiteman, 2002], and many more.

Kullback-Leibler Divergence is a measure of how one probability distribution, p, varies from another probability distribution q. Its equation is defined below:

$$D(p \parallel q) = \sum_{x \in X} p(x) \, log \frac{p(x)}{q(x)} \tag{18}$$

In the above equation X represents the outcome of all possible events. Due to not fulfilling triangle inequality and usually non-symmetric difference between two probability mass functions (PMFs) ($D(p \parallel q) \neq D(q \parallel p)$), KLD is not considered a true distance metric. This statement would not hold if and only if both probability distributions are identical; otherwise KLD is a non-zero positive number. In any case, KLD provides a measure of distance between two distributions, with zero corresponding to two distributions with similar (if not identical) statistical properties. KLD values of one depicts the maximum divergence of the two distributions from one another.

Kullback-Leibler Divergence is a member of the probability theory known as *f*-divergence [M. Basseville, 1989]. To compute the variation of two data sets by implementing KLD, the following steps are commonly used [Mostafa Afgani ; Sinan Sinanovic ; Harald Haas, 2008] :

1) Determining the sets of data that would be compared against one another, if needed data sets can be broken down to segments so ones with similar features are

compared with one another.

2) With data sets that are collected in a continuous fashion, it is important to assign restriction for the number of samples used to create each set.
3) After all data sets are gathered, extraction of chosen aspects for both data sets would take place.
4) With implementing equation number one, PMF of each data set over the aspects would be selected and calculated.
5) Presence of an anomaly is shown when the KLD value is greater than the set threshold, which also indicates that the there is a major variance between the data sets.

3.2. Two Sample Kolmogorov Smirnov Test

In the field of statistics, the distribution-free test of the equality of continuous, one dimensional probability distribution, known as Kolmogorov Smirnov (KS) test, can be implemented for finding distance between a sample with a reference probability distribution, and finding distance between two samples also known as two sample KS test. In 1933 the goodness-of-fit test for a sample was developed by Andrey Nikolaevich Kolmogorov, and in 1939 Vladimir Ivanovich Smirnov established Kolmogorov-Smirnov test for two samples [Yadolah Dodge, 2008].

A Kolmogorov-Smirnov test can be implemented with the purpose of finding a correlation between two unknown distributions. Particularly, $F_1(x)$ and $F_2(x)$ are not

identified for any x, but estimation for $F(x)$ and $G(x)$ is possible by implementing random samples from each group with the aim of analyzing H_0: $F_1(x) \cong F_2(x)$ for all x with the assumption equality of both distributions.

The highest potential outcome of $|F_1(x) - F_2(x)|$ is known as the Kolmogorov distance. A Kolmogorov distance of zero represents identicality of distributions ($F_1(x) \cong F_2(x)$ for all x). In graphs, Kolmogorov distance is the largest vertical space among the distribution functions [R. Wilcox, 2005].

As previously mentioned, the nonparametric hypothesis test that can be implemented to assess the variation among the cumulative distribution function (CDF) of the distributions of two sample data vectors is known as the two-sample Kolmogorov-Smirnov test. In other words, the two-sided test implements the highest (maximum) departure among the cumulative distribution functions (CDFs) of the distributions of two data vectors

$$D^* = max\ _x\left(\left|\widehat{F_1}(x) - \widehat{F_2}(x)\right|\right) \tag{19}$$

in which $\widehat{F_1}(x)$ and $\widehat{F_2}(x)$ are sections of sample data from the first set of samples, stated in vector format x_1 and x_2 respectively with values equal or less than x.

3.3. Hydrologic Signatures

As mentioned before in this study hydrologic models of GR4J and HyMod are

constrained against watersheds of SF Boise, Skykomish and Henry Fork using Monte Carlo, Runoff Ratio, Base Flow Index, Base Flow Runoff Ratio, Slope of Log FDC 5& 95 Percentile, Slope of Log 33 & 66 Percentile, Slope of Log FDC 20 & 70 Percentile, FDC High Segment Volume more than 90 Percentile , FDC Low Segment Volume less than 30 Percentile, FDC Medium Segment Volume , Auto Correlation of Hydrograph with 1 Day Lag , Peak Distribution, Rising LIMB Destiny, Declining LIMB Destiny, 1^{st} Flow Percentile, 5^{th} Flow Percentile, 15^{th} Flow Percentile, 50^{th} Flow Percentile, 95^{th} Flow Percentile, 99^{th} Flow Percentile metrics. Table 2.3 presents list of these metrics name and the symbols designated to them for this study.

Table 2.3. Hydrologic Metric's Names and their Symbols designated to each for this study, in this Study FDC stands for Flow Duration Curve

Metric Number	Metric Name	Metric Symbol
1	Runoff Ratio	RR
3	Base Flow Index	BFI
4	Base Flow Runoff Ratio	BFR
5	Slope of Log FDC 5& 95 Percentile	SL FDC $Q5^{th}$&$Q95^{th}$
6	Slope of Log 33 & 66 Percentile	SL $Q33^{th}$&$Q66^{th}$
7	Slope of Log FDC 20 & 70 Percentile	SL FDC $Q20^{th}$&$Q70^{th}$
8	FDC High Segment Volume more than 90 Percentile	FDC HSV $Q90^{th}$
9	FDC Low Segment Volume less than 30 Percentile	FDC LSV $Q30^{th}$
10	FDC Medium Segment Volume	FDC MSV
11	Auto Correlation of Hydrograph with 1 Day Lag	AC
12	Peak Distribution (Slope of Peak Flows)	PD
13	Rising LIMB Destiny	RLD
14	Declining LIMB Destiny	DLD
16	1^{st} Flow Percentile	$Q1^{st}$
17	5^{th} Flow Percentile	$Q5^{th}$
18	15^{th} Flow Percentile	$Q15^{th}$
19	50^{th} Flow Percentile	$Q50^{th}$
20	95^{th} Flow Percentile	$Q95^{th}$
21	99^{th} Flow Percentile	$Q99^{th}$

Chapter 3

STUDY AREA AND DATA RECOURSES

In this analysis, three different watersheds from National Weather Service's MOPEX data set is analyzed. Table 1 contains name, location, and size of each catchment, as well as mean annual precipitation, potential evapotranspiration, and runoff coefficient. These watersheds are located across the United States with different hydroclimatic characteristics, and their sizes vary from 83.2 mi^2 (215.487 km^2) to 641 mi^2 (1660.18 km^2).

The computation and calculations done on this thesis is based on 10 years of recorded daily data of watershed. Such length of calibration data (10 years) is sufficient for a robust calculation of summary metrics and hypothesis testing. Indeed, Yapo et al., 1996 suggested that 8 years of calibration data is sufficient to derive stable parameter distributions that are relatively insensitive to the period of calibration. Table 3.1. presents the description, name, region, USGS ID, drainage area, for the watersheds that has been used in this research study.

Table 3.1. Watersheds information and their area,

Name	City(Region) Sate, Country	USGS ID	Area (Km^2)
SF Boise	Elmore County, Idaho, USA	13186000	1660.18
Skykomish	Snohomish County, Washington, USA	12134500	1385.64
Henry Fork	Catawba County, North Carolina, USA	02143000	215.487

Chapter 4

RESULTS

This study strives to find the constraining power of different hydrological signatures in the approximate Bayesian framework using two parsimonious hydrologic models namely GR4J and HyMod evaluated against historical observations from three river basins in the United States. In doing so, each model is iteratively calibrated using one hydrological signature against each watershed, and a plethora of performance evaluation metrics are employed to assess the success/failure of each signature in sufficiently constraining the model response. We are specifically concerned with the constraining power of each metric for different sections of the hydrograph, in an attempt to moving toward finding as set of sufficient summary metrics to constrain hydrological models. Performance evaluation metrics include Entropy, Likelihood, NSE, RMSE and percent bias. We also have used Kullback Leibler divergence metric and two-sample Kolmogorov Smirnov test as sensitivity surrogate metrics to determine whether or not the posterior distribution of different model parameters have significantly changed from the uniform prior as a result of model calibration.

We analyze hydrological behavior of SF Boise river (USGS ID #13186000), Skykomish river (USGS ID #12134500) and Henry Fork river (USGS ID #02143000) in a temporal span of 10 years, starting from January 1, 1948 to January 1, 1958 using GR4J and

HyMod conceptual models. The conclusions and discoveries found from these watersheds in regard to constraining capabilities of various hydrologic metrics, their characteristics and sensitivities are discussed within this section. The outcomes and results of this study features various critical findings that have been gained by analyzing the model's outcome through multiple graphs, figures and tables discussed and analyzed in this section. In the following, we show some example predictive uncertainty ranges with calibrated GR4J and HyMod models using different individual hydrologic signatures, followed by a broader and comparative picture that is presented in performance evaluation tables. More predictive uncertainty range plots are provided in the supplementary information.

Figure 4.1 displays the predictive uncertainty ranges of GR4J model calibrated against the South Fork (SF) Boise river watershed historical record represented by the FDC High Segment Volume more than 90th Percentile Metric (FDC HSV Q^{90th}) and figure 4.2 displays predictive uncertainty ranges of HyMod model calibrated against the stated watershed using same metric. In these figures unconstrained model predictive range (derived by 10,000 Monte Carlo samples from the uniform prior parameter distributions) is represented with blue, posterior distribution of simulated flow (derived from posterior parameter distribution constrained with the FDC HSV Q^{90th} metric) is represented with green and observed data are represented with red. The x-axis of these plots represents the time in form of day-month-year and the y-axis represents the stream flow data ($\frac{m^3}{s}$).

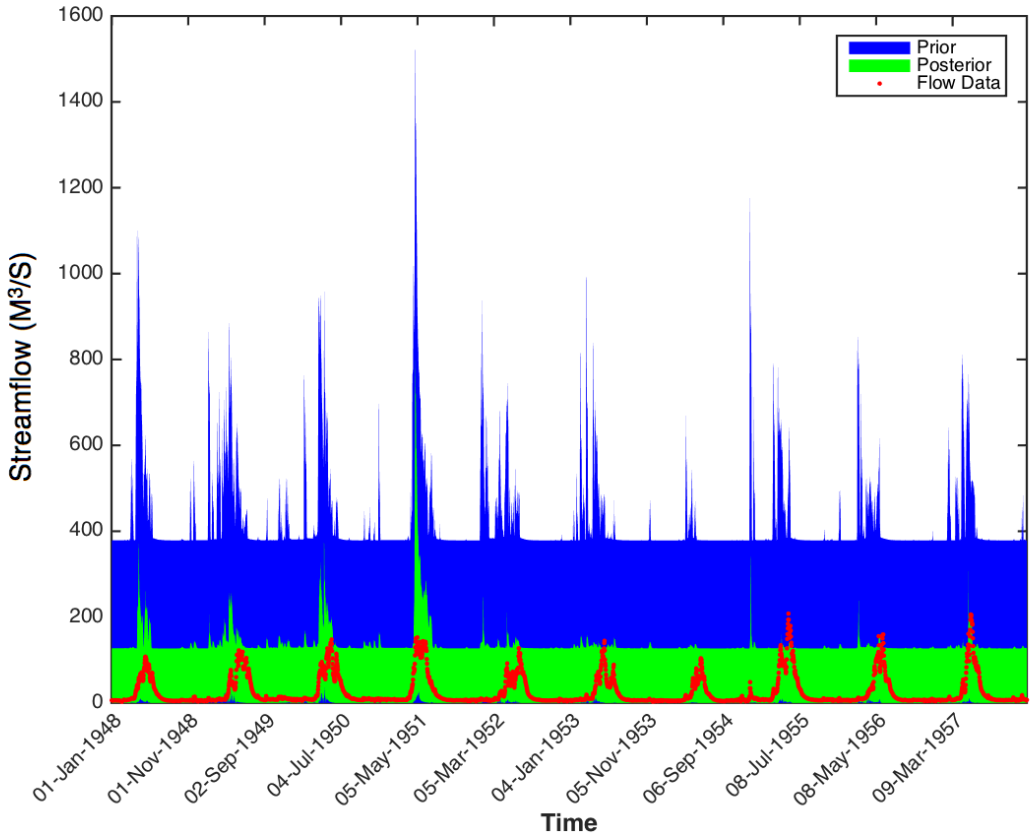

Figure 4.1. Predictive uncertainty ranges of GR4J model constrained against SF Boise watershed (USGS ID 13186000) using FDC High Segment Volume more than 90th Percentile Metric (FDC HSV Q^{90th}). Prior channel inflow in blue, posterior channel flow in green and observed data in red

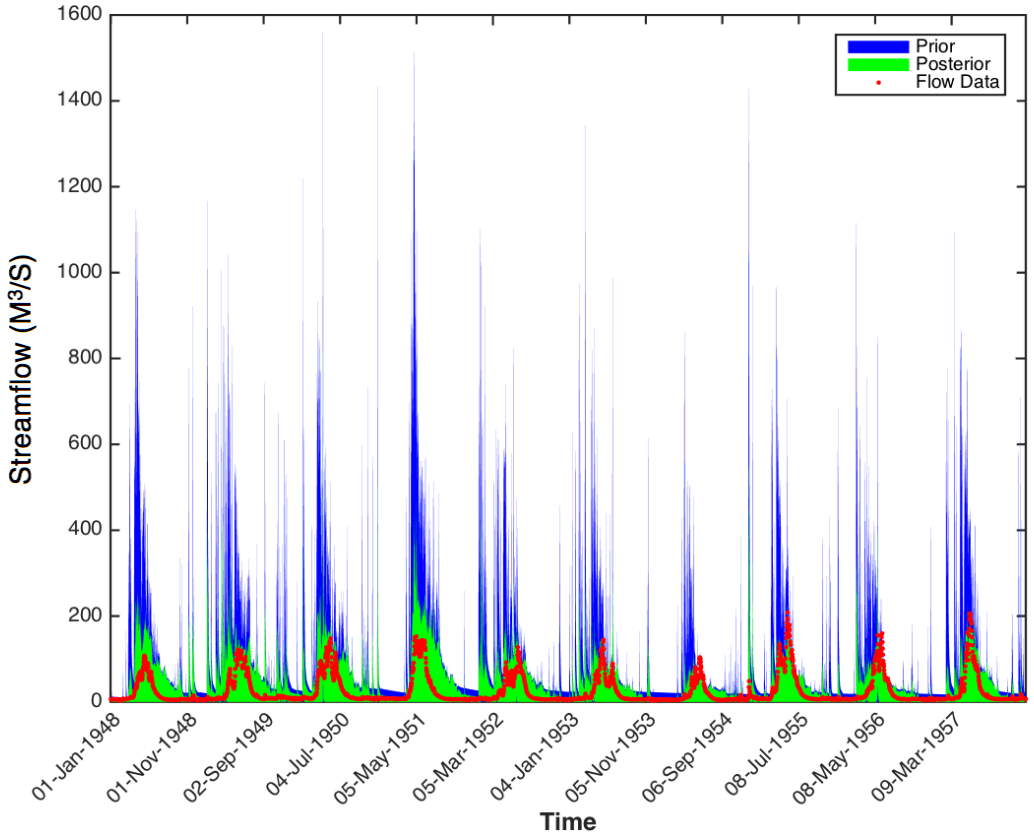

Figure 4.2 Predictive uncertainty ranges of HyMod model constrained against SF Boise watershed (USGS ID 13186000) using FDC High Segment Volume more than 90th Percentile Metric (FDC HSV Q^{90th}). Prior channel inflow in blue, posterior channel flow in green and observed data in red

Figure 4.1 displays that the GR4J hydrologic model calibrated with the FDC High Segment Volume more than 90th Percentile Metric (FDC HSV Q^{90th}) metric as compared to HyMod hydrologic model calibrated with the same metric (figure 4.2) is over estimating base flow. Indeed, HyMod simulates the base flow for SF Boise river watershed closer to the observed data. This rather disagreeable behavior of the GR4J can be attributed to the flexibility of model structure and impacts of tunable parameters on the model outcome. The HyMod model structure, however, is stricter in how it responds to the forcing, and is less dependent on the parameter values. When model is calibrated using a less informative metric such as FDC HSV Q^{90th}, model parameters are rather dispersed over the entire prior range, and hence a less flexible model structure such as HyMod outperforms its flexible counterpart, GR4J; as it depends more on the forcing. Surprisingly, this metric even fails to constrain peak flows for a flexible model structure such as GR4J (see, for example, 08/July/1995 in figure 4.1), but it has a more favorable behavior for HyMod model. In figure 4.2 it can be seen that posterior channel flow is much closer representation of the flow observed data. In general, one hypothesis could be that the FDC HSV Q^{90th} individually is insufficient to constrain a flexible model, but if the information content of FDC HSV Q^{90th} is matched with information from a stricter model structure (HyMod) it can constrain the model response to some extent. Note that if constraining is defined by the divergence of the posterior simulations from the unconstrained model simulations (blue to green in these figures) the FDC HSV Q^{90th} shows some merit for GR4J model, but if one is concerned about model performance this metric is certainly not sufficient. Figure 4.3 displays posterior parameter distributions of the GR4J and HyMod models constrained against SF Boise

watershed (USGS ID 13186000) using the FDC high segment volume more than 90th percentile hydrologic signature. The x axis represents parameters minimum and maximum values.

Posterior Parameter Distributions for Watershed SF Boise					
	$S1_{max}$	Exch	$S2_{max}$	UHB	
GR4J	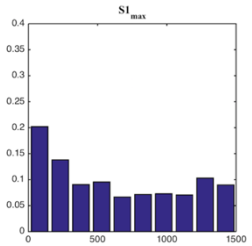	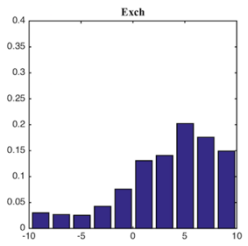	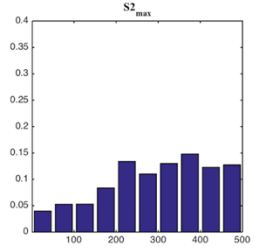	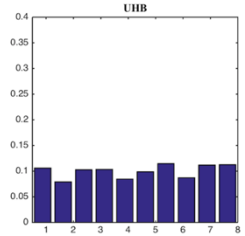	
	C_{max}	BEXP	Alpha (α)	Rs	Rq
HyMod	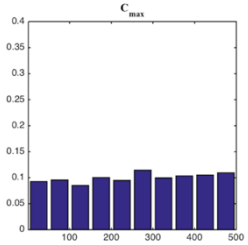	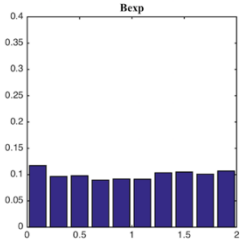	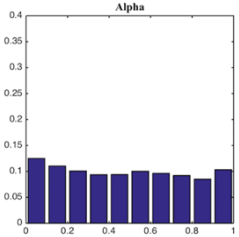	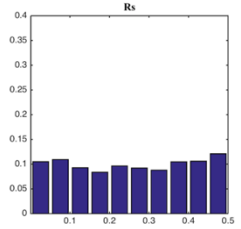	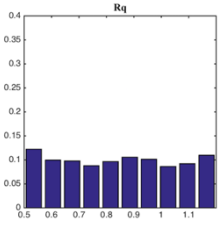

Figure 4.3. Posterior Parameter Distributions of GR4J and HyMod model constrained against SF Boise watershed (USGS ID 13186000), the x axis represents parameters minimum and maximum values

Figure 4.4 displays the predictive uncertainty ranges of GR4J model calibrated against the SF Boise river watershed using FDC less than 30th Percentile Metric (FDC LSV Q^{30th}) and figure 4.5 displays predictive uncertainty ranges of HyMod model calibrated against the stated watershed using same metric. Similar to previous figures, unconstrained model simulations are shown with blue, posterior predictive flow range is represented with green and observed data are represented with red.

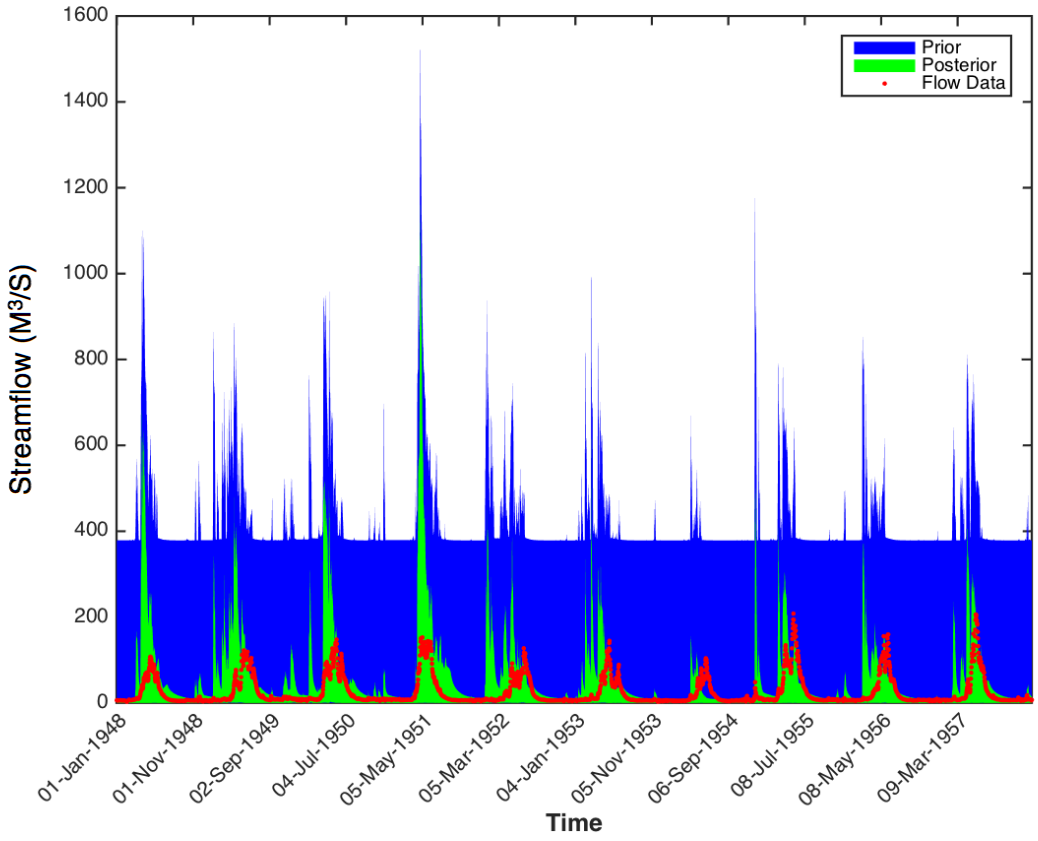

Figure 4.4. Predictive uncertainty ranges of GR4J model constrained against SF Boise watershed (USGS ID 13186000) using FDC Low Segment Volume less than 30th Percentile Metric (FDC LSV Q^{30th}). Prior channel inflow in blue, posterior channel flow in green and observed data in red

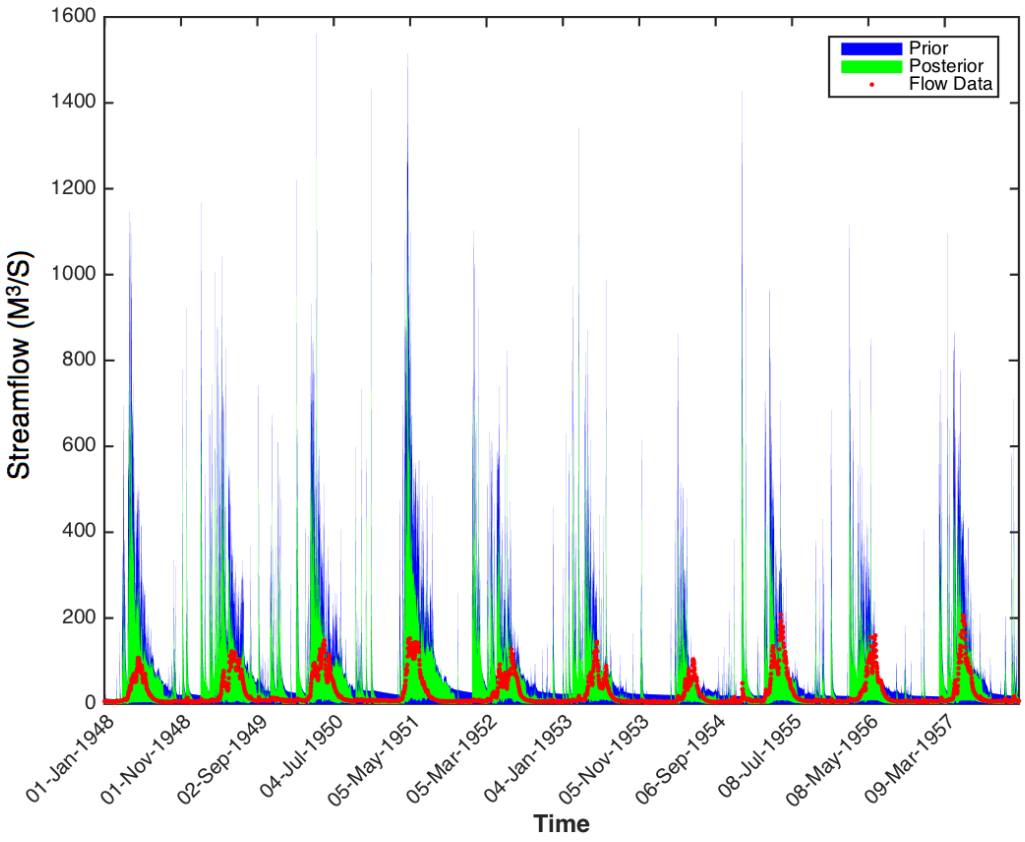

Figure 4.5 Predictive uncertainty ranges of HyMod model constrained against SF Boise watershed (USGS ID 13186000) using FDC Low Segment Volume less than 30th Percentile Metric (FDC LSV Q^{30th}). Prior channel inflow in blue, posterior channel flow in green and observed data in red

Figure 4.4 displays posterior predictive flow range for GR4J hydrologic model constrained with FDC less than 30th percentile metric (FDC LSV Q30th), and is capturing the base flow and to some extent the peak flows for the SF Boise river watershed. Interestingly, model predictions with GR4J model in this case are even superior to predictive uncertainty ranges of the HyMod model (see figure 4.5), as HyMod overestimates the recession portion of the hydrograph and baseflows. Both models overestimate peak flows showing the FDC LSV Q30th metric is not sufficient to capture both low and high flows. Further research is required to show if this metric in combination with another can capture both high and low flows or not.

Figure 4.6 displays the predictive uncertainty ranges of GR4J model calibrated against the SF Boise river watershed using Peak Distribution (PD) metric also known as Slope of Peak Flow, and figure 4.7 displays predictive uncertainty ranges of HyMod model for this watershed and hydrologic signature. Figure 4.6 displays that the GR4J hydrologic model using Peak Distribution metric over estimates base flow, whereas HyMod is representing base flow for SF Boise watershed closer to the observed data. This behavior is rather similar to that of FDC HSV Q^{90th}, except PD is less successful in reducing the uncertainty range compared to the unconstrained uncertainty ranges (green versus blue). Moreover, uncertainty ranges for peak flows are rather similar between constrained and unconstrained ranges. One might argue that the PD metric would not add much information to the calibration process and should not be used.

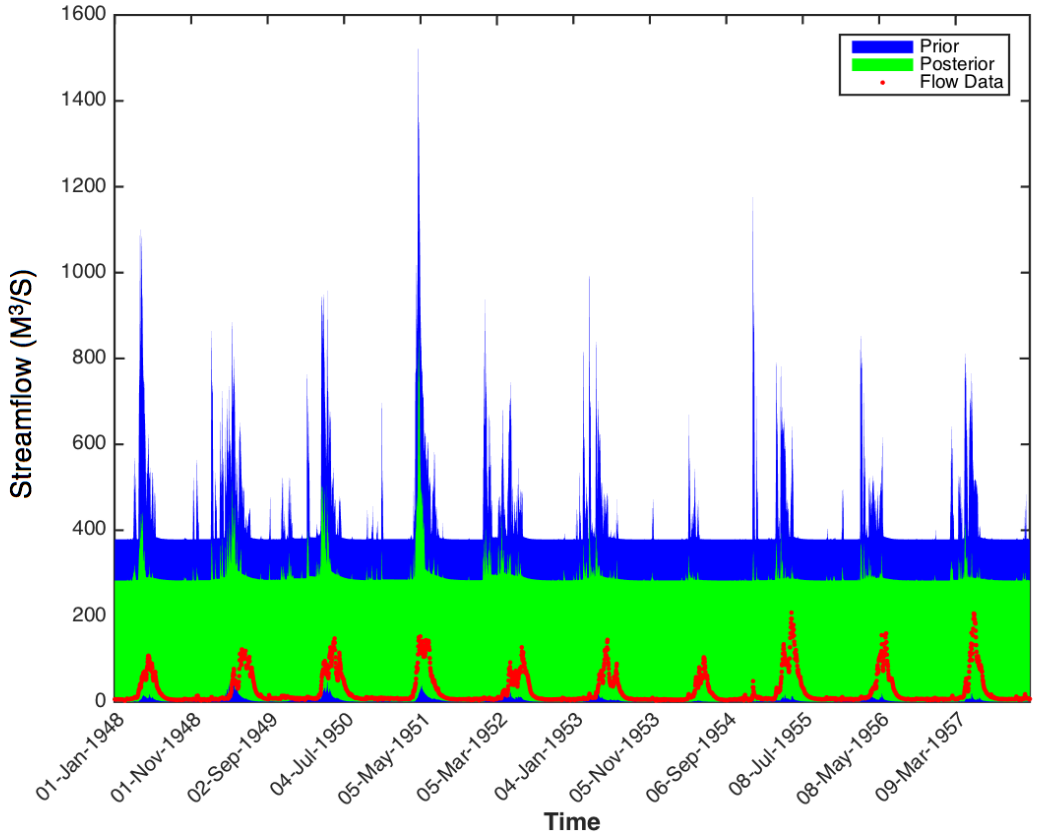

Figure 4.6 Predictive uncertainty ranges of GR4J model constrained against SF Boise watershed (USGS ID 13186000) using Peak Distribution metric also known as Slope of Peak Flow Metric (PD). Prior channel inflow in blue, posterior channel flow in green and observed data in red

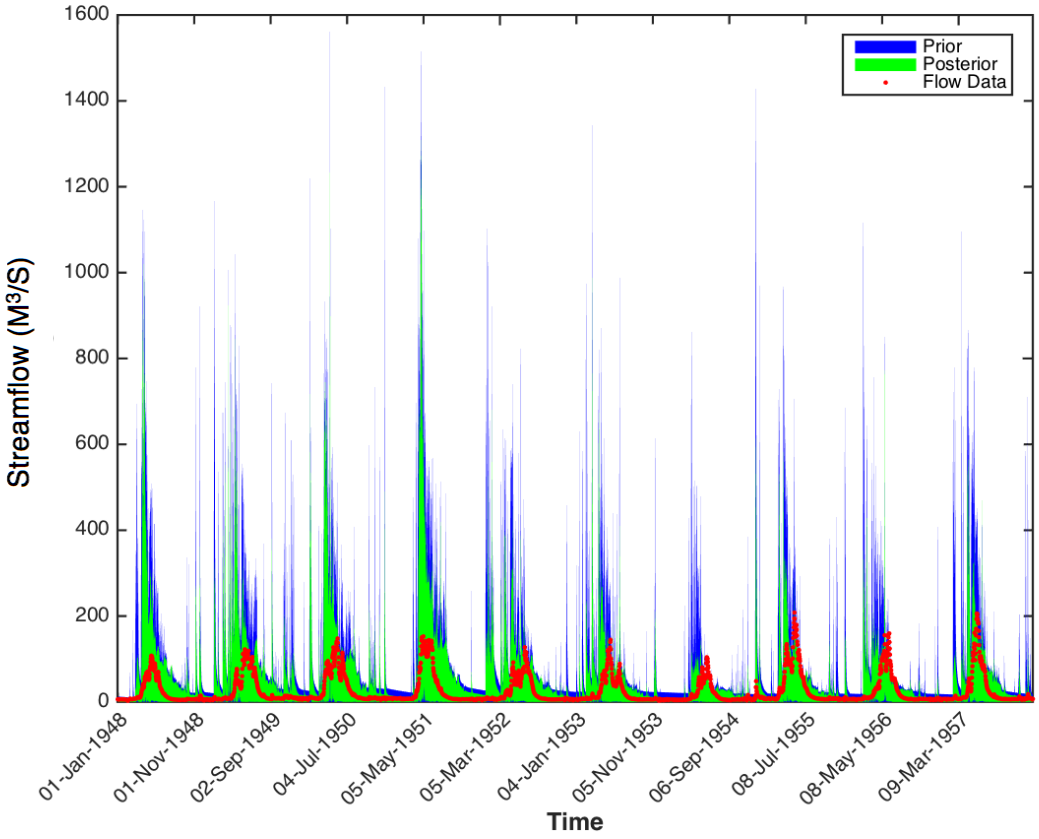

Figure 4.7 Predictive uncertainty ranges of HyMod model constrained against SF Boise watershed (USGS ID 13186000) using Peak Distribution metric also known as Slope of Peak Flow Metric (PD). Prior channel inflow in blue, posterior channel flow in green and observed data in red

Figure 4.8 displays the predictive uncertainty ranges of the GR4J model calibrated against the SF Boise river watershed using 1st Flow Percentile Metric (Q1st) and figure 4.9 displays predictive uncertainty ranges of the HyMod model constrained against the stated watershed using the same metric. Model simulations calibrated with this metric fail to correctly capture the peak flows. For base flows, GR4J shows some level of constraining, but HyMod is not constrained for low and base flows. Conjunctive use of this metric with others might add some information to the calibration process.

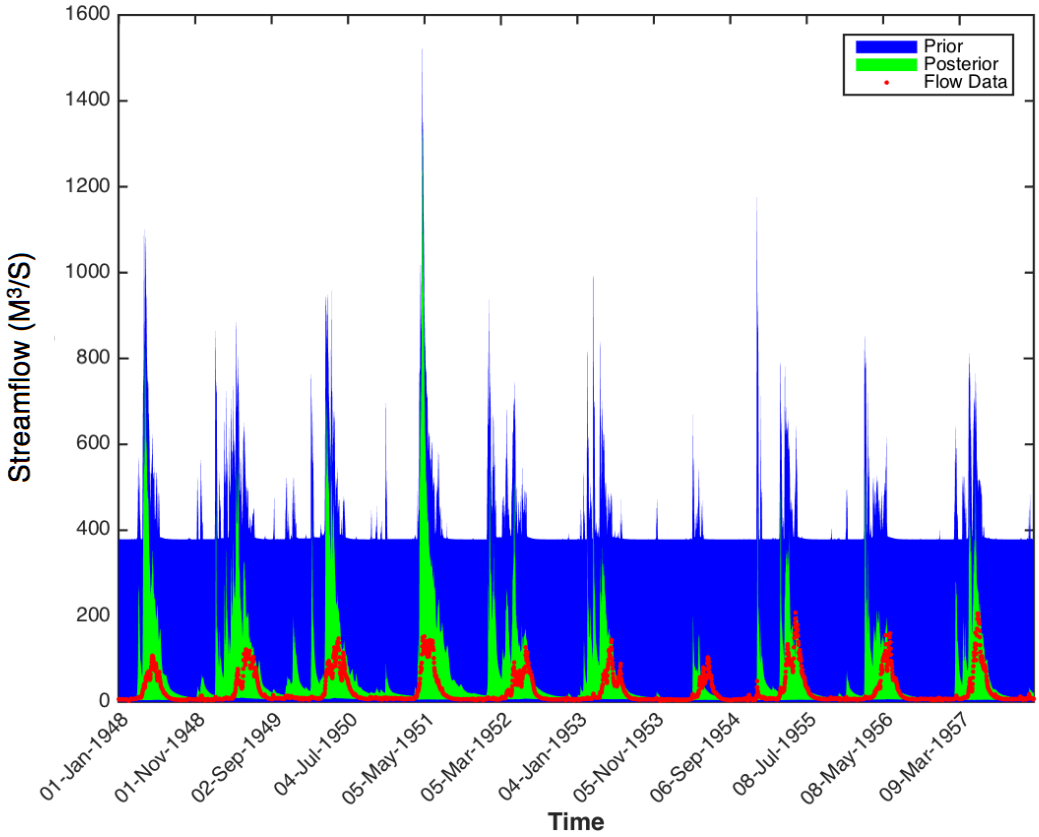

Figure 4.8 Predictive uncertainty ranges of GR4J model constrained against SF Boise watershed (USGS ID 13186000) using 1st Flow Percentile Metric (Q1st). Prior channel inflow in blue, posterior channel flow in green and observed data in red

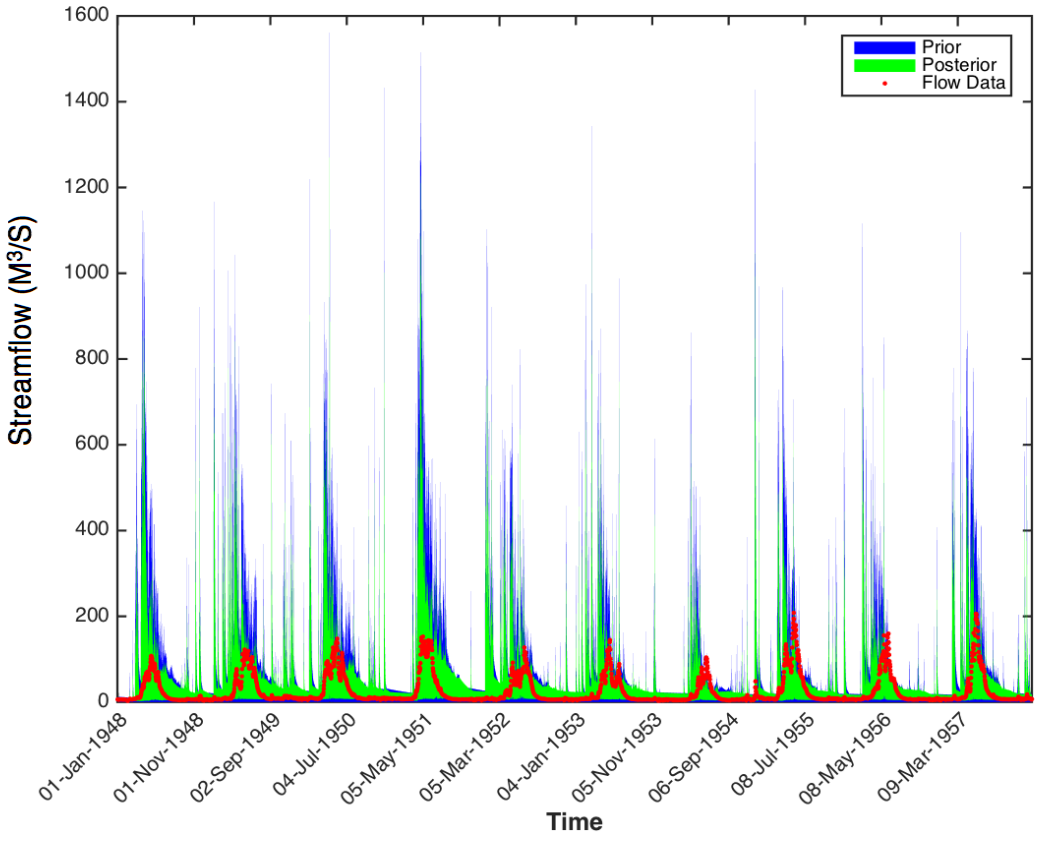

Figure 4.9 Predictive uncertainty ranges of HyMod model constrained against SF Boise watershed (USGS ID 13186000) using 1st Flow Percentile Metric (Q1st). Prior channel inflow in blue, posterior channel flow in green and observed data in red

Figure 4.10 displays the predictive uncertainty ranges of GR4J model constrained against the SF Boise river watershed using 99th Flow Percentile Metric (Q99th) and figure 4.11 displays predictive uncertainty ranges of HyMod model constrained against the stated watershed using same metric. It is interesting how this hydrologic metric fails to capture the peaks for GR4J, whereas is basically focused on the high flows. The model response for HyMod, however, is much more desirable, which can be attributed to the information content of the Q99th signature going hand in hand with the information content of the HyMod model.

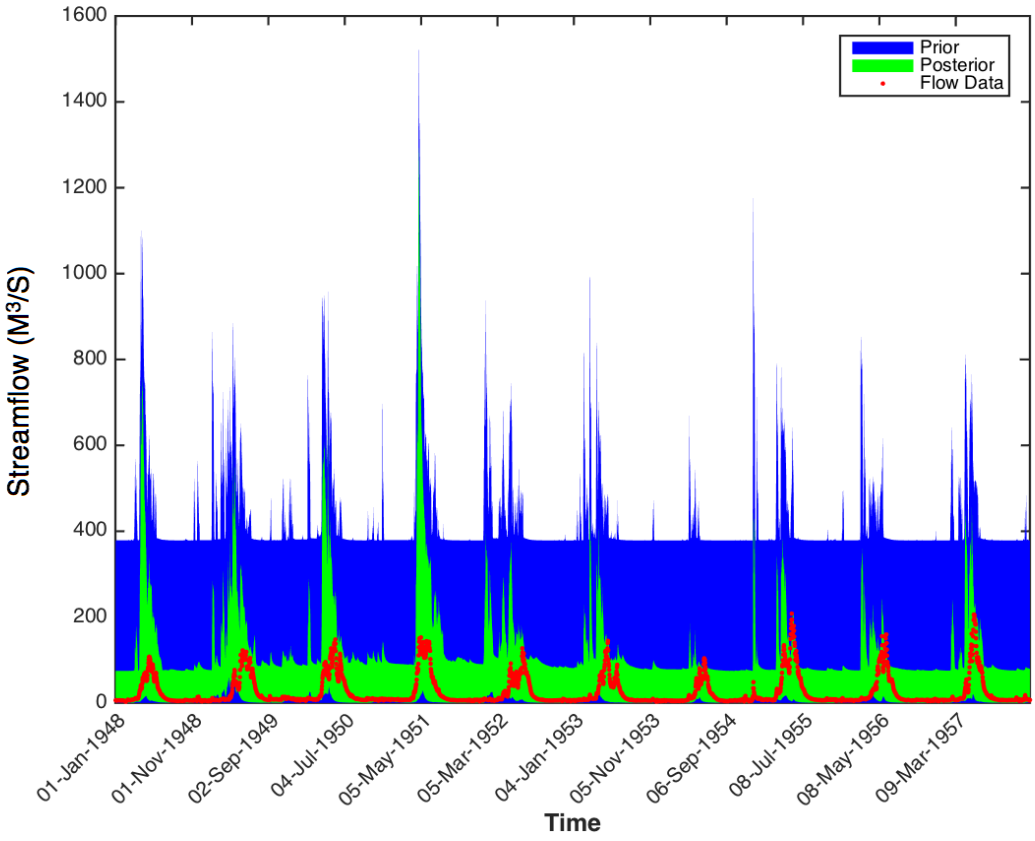

Figure 4.10. Predictive uncertainty ranges of GR4J model constrained against SF Boise watershed (USGS ID 13186000) using 99th Flow Percentile Metric (Q99th). Prior channel inflow in blue, posterior channel flow in green and observed data in red

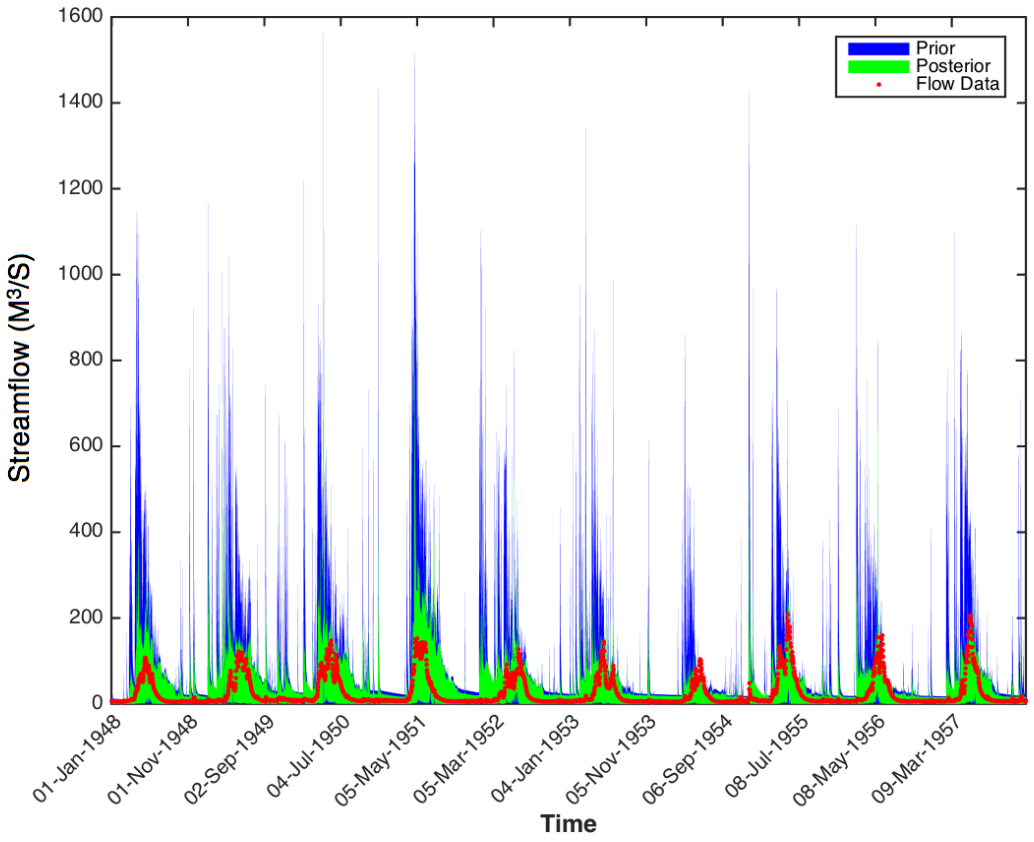

Figure 4.11. Predictive uncertainty ranges of HyMod model constrained against SF Boise watershed (USGS ID 13186000) using 99th Flow Percentile Metric (Q99th). Prior channel inflow in blue, posterior channel flow in green and observed data in red

Using performance evaluation metrics of Likelihood, Entropy, NSE, RMSE, PBIAS, Distance, Distance, Mean Uncertainty Spread, Coverage, and Threshold, Tables 4.1 and 4.2 list the posterior predictively result of GR4J and HyMod hydrologic models, respectively, which are being constrained against SF Boise river watershed using different metrics, namely Runoff Ratio (RR), Base Flow Index (BFI), Base Flow Runoff Ratio (BFR), Slope of Log FDC 5th & 95th Percentile (SL FDC Q5th&Q95th), Slope of Log 33rd & 66th Percentile (SL Q33th&Q66th), Slope of Log FDC 20th & 70th Percentile (SL FDC Q20th&Q70th), FDC High Segment Volume more than 90th Percentile (FDC HSV Q90th), FDC Low Segment Volume less than 30th Percentile (FDC LSV Q30th), FDC Medium Segment Volume (FDC MSV), Auto Correlation of Hydrograph with 1 Day Lag (AC), Peak Distribution(PD), Rising LIMB Destiny(RLD), Declining LIMB Destiny(DLD), 1st Flow Percentile (Q1st), 5th Flow Percentile(Q5th), 15th Flow Percentile(Q15th), 50th Flow Percentile(Q50th), 95th Flow Percentile(Q95th), 99th Flow Percentile(Q99th).

Superior predictions are associated with higher likelihood and NSE values, and lower RMSE and Distance values. Distance is defined as average distance of observed data that are not covered in the uncertainty range to the upper (lower) bound of the uncertainty range. It is also desired that a higher coverage of observed points is obtained in a lower entropy. Entropy is a proxy measure of the spread of the predictive range. As explained earlier, acceptance threshold for each hydrologic signature is iteratively selected in this study to ensure at least 90% of observation points are covered. So a larger threshold is indicative of sensitivity of the analysis to that specific hydrologic signature. Mean predictive uncertainty spread also informs the width of the predictive uncertainty ranges.

Moreover, we have included in this table whether the posterior distribution of different model parameters are significantly different from their prior uniform distribution or not, using a KS test.

It is noteworthy in this table that mean ensemble NSE values are negative for all hydrologic signatures, indicating that no single metric is good enough to constrain the hydrologic models. Some metrics such as autocorrelation (AC) show a very tight tolerance threshold (0.01) which might suggest insensitivity of such metric to variation of model simulations. This is also reflected in the large posterior predictive uncertainty range associated with this metric. Even worse is the Peak Distribution (PD) metric that not only bears the disadvantageous properties of AC, but also suffers from a lower coverage rate of observational points in higher posterior predictive uncertainty range. Such information can help us rule out metrics such as PD and AC from the approximate Bayesian analysis. Also, some metrics fail to constrain some specific parameters. For example, the 50^{th} percentile of flow distribution does not constrain 1^{st} (Max Capacity of Production Store, S1max) and 4^{th} (Hydrograph Time Base, UHB) parameters of the GR4J model. The 15^{th} percentile of the flow distribution also does not constrain the 4^{th} parameter of the GR4J model. These two hydrologic signatures, however, do relatively good in terms of the mean predictive uncertainty ranges, entropy and NSE compared to other metrics. The modeler should be aware of selecting a metric that is sensitive to the 1^{st} and 4^{th} parameters of the GR4J model along with these two hydrologic signatures.

	SF Boise WatershedGR4J Hydrologic Model										
	Likelihood	Entropy	NSE	RMSE	PBIAS	Distance	Distance /NoZero	Mean Uncertainty Spread	Coverage	Threshold	Sensitive Parameters
Monte Carlo	0.03289	3.32778	-1.2184	41.2570	-20.6036	0.00000	NaN	428.18560	100.000		
RR	0.05974	3.19503	-0.2496	36.1017	-8.75657	0.74915	11.03191	91.42350	93.2092	0.30000	1,2,3,4,5
BFI	0.04086	2.85226	-0.1526	35.5006	-38.7232	0.72876	20.63113	88.17880	96.4677	0.01000	1,2,3,4,5
BFR	0.07006	3.09660	-0.2812	36.5253	-2.08463	0.94588	9.78573	97.18420	90.3341	0.15000	1,2,3,4,5
SL FDC Q5th&Q95th	0.03928	2.27386	-0.3469	37.1779	-43.9251	1.63970	22.42768	81.11300	92.6889	0.01000	1,2,3,4,5
SL Q33th&Q66th	0.03047	3.10872	-0.9272	40.9804	7.32142	1.05741	20.21817	111.19950	94.7700	0.02000	1,2,3,4,5
SL FDC Q20th&Q70th	0.07144	2.9233	-0.0169	32.9227	-26.7784	0.39993	18.03143	103.50120	97.7820	0.05000	1,2,3,4,5
FDC HSV Q90th	0.04579	3.0335	-0.1933	33.6260	-21.7864	0.26414	17.86338	137.28360	98.5214	0.03500	1,2,3,4,5
FDC LSV Q30th	0.01814	2.3876	-0.1949	36.3729	-62.8689	2.02578	21.75929	68.61540	90.6900	0.35000	1,2,3,0,5
FDC MSV	0.08460	2.6790	-0.1755	35.2456	-28.0266	1.14889	13.23579	82.69250	91.3198	0.35000	1,2,3,4,5
AC	0.04498	3.1648	-0.2120	35.1961	-38.5594	0.00000	NaN	226.43710	100.000	0.01000	1,2,3,4,5
PD	0.03179	4.1244	-4.2223	58.8651	126.433	0.14744	6.99298	292.64960	97.8916	0.01000	1,2,3,4,5
RLD	0.03971	2.6913	-2.7538	46.2239	-10.7259	0.00000	NaN	314.85860	100.000	0.02000	1,2,3,4,5
DLD	0.00626	-2.3855	-1.1370	43.4418	-80.0751	0.00000	NaN	379.49970	100.000	0.60000	1,2,3,4,5
Q1st	0.10025	2.56421	-0.1277	34.56335	-19.8753	0.88084	11.74029	81.96000	92.4973	0.10000	1,2,3,4,5
Q5th	0.09383	2.67980	-0.0955	33.96476	-18.1359	0.69920	7.05378	85.77590	90.0876	0.25000	1,2,3,4,0
Q15th	0.10191	2.69197	-0.1873	35.05425	-15.8295	0.93288	12.52531	92.30010	92.55200	0.20000	1,2,3,0,5
Q50th	0.08199	2.61328	-0.1009	34.38038	-32.8173	0.99290	10.33067	78.89070	90.38880	0.30000	0,2,3,0,5
Q95th	0.02693	3.95883	-0.8411	44.33849	42.75870	0.76805	9.84181	126.41170	92.19610	0.10000	1,2,3,4,5
Q99th	0.03199	3.03875	-0.0321	33.58489	-29.199	2.15686	26.70117	52.37700	91.92220	0.02000	1,2,3,4,5

Table 4.1. Table of posterior predictively result of GR4J model constrained against SF Boise watershed (USGS ID 13186000) in terms of Monte Carlo simulation (not constrained), and constrained against Runoff Ratio (RR), Base Flow Index (BFI), Base Flow Runoff Ratio (BFR), Slope of Log FDC 5th & 95th Percentile (SL FDC Q5th&Q95th), Slope of Log 33rd & 66th Percentile (SL Q33rd &Q66th), Slope of Log FDC 20th & 70th Percentile (SL FDC Q20th&Q70th), FDC High Segment Volume more than 90 Percentile (FDC HSV Q90th), FDC Low Segment Volume less than 30th Percentile (FDC LSV Q30th), FDC Medium Segment Volume (FDC MSV), Auto Correlation of Hydrograph with 1 Day Lag (AC), Peak Distribution(PD), Rising LIMB Destiny(RLD), Declining LIMB Destiny(DLD), 1st Flow Percentile (Q1st), 5th Flow Percentile(Q5th), 15th Flow Percentile(Q15th), 50th Flow Percentile(Q50th), 95th Flow Percentile(Q95th), and 99th Flow Percentile(Q99th) metrics.

	SF Boise Watershed HyMod Hydrologic Model										
	Likelihood	Entropy	NSE	RMSE	PBIAS	Distance	Distance/ NoZero	Mean Uncertainty Spread	Coverage	Threshold	Sensitive Parameters
Monte Carlo	0.01247	1.4011	-2.3308	58.15793	-9.4345	0.16342	13.56353	142.19290	98.79520		
RR	0.01277	1.2391	-1.8586	55.13448	0.0228	1.06951	13.75300	90.70120	92.22340	0.01000	1,2,3,4,5,6
BFI	0.03237	3.1212	0.1460	30.65279	-11.5655	1.11008	13.88357	59.28280	92.00440	0.01000	1,2,3,4,5,6
BFR	0.03092	3.1703	-0.6268	40.60564	8.4698	0.78093	8.07920	92.42480	90.33410	0.05000	1,2,3,4,5,6
SL FDC Q5th&Q95th	0.06128	3.0885	-0.3221	36.45272	-5.9358	1.26955	20.79100	76.42090	93.89380	0.03500	1,2,3,4,5,6
SL Q33th&Q66th	0.05135	3.2371	-0.8323	42.08314	-13.7540	2.25493	23.59598	78.81850	90.44360	0.02000	1,2,3,4,5,6
SL FDC Q20th&Q70th	0.04608	3.3493	-0.9642	44.10189	-15.5147	1.59213	24.12632	86.73800	93.40090	0.05000	1,2,3,4,5,6
FDC HSV Q90th	0.02675	2.6630	-0.0054	33.12273	-26.6357	0.55635	8.75775	62.30760	93.64730	0.05000	1,2,3,4,5,6
FDC LSV Q30th	0.03955	3.2850	-1.1278	45.64067	-15.1828	1.38025	20.57415	88.93070	93.29130	0.02000	1,2,3,4,5,6
FDC MSV	0.04024	2.9287	-0.9780	45.07757	-10.5453	0.69164	9.18500	86.67620	92.46990	0.07500	1,2,3,4,5,6
AC	0.02090	2.5722	0.0339	32.10763	-13.3548	0.59458	11.80121	70.90870	94.96170	0.01000	1,2,3,4,5,6
PD	0.01538	1.8337	-0.6350	41.37991	-25.8369	0.63599	13.74344	82.68720	95.37240	0.10000	1,2,3,4,5,6
RLD	0.01777	2.2162	-1.3448	48.50053	-13.6104	0.46502	13.92013	91.33780	96.65940	0.05000	1,0,3,4,5,6
DLD	0.01269	1.3831	-2.5313	59.81705	-8.3371	0.24481	14.90054	131.92860	98.35710	1.00000	0,0,0,0,5,0
Q1st	0.05091	3.2302	-0.4886	38.47688	-2.0288	0.99807	12.87965	91.27790	92.25080	0.50000	1,2,3,4,5,6
Q5th	0.06044	3.2065	-0.6144	39.87712	-5.1489	0.86835	18.54519	92.52100	95.31760	0.50000	1,2,3,4,5,6
Q15th	0.06557	3.1004	-0.7048	41.09136	-5.1135	1.00860	11.51070	90.79330	91.23770	0.20000	1,2,3,4,5,6
Q50th	0.03178	2.9490	-0.9063	44.45036	-7.4692	0.95250	10.05357	89.63520	90.52570	0.12500	1,2,3,4,5,6
Q95th	0.01411	1.6859	-1.5494	50.78372	-13.4298	1.00007	15.74246	98.15460	93.64730	0.10000	1,2,3,4,5,6
Q99th	0.01861	2.3565	0.0267	32.66147	-22.7205	0.48118	15.55113	68.13870	96.90580	0.07500	1,2,3,4,5,6

Table 4.2. Table of posterior predictively result of HyMod model constrained against SF Boise watershed (USGS ID 13186000) in terms of Monte Carlo simulation (not constrained), and constrained against Runoff Ratio (RR), Base Flow Index (BFI), Base Flow Runoff Ratio (BFR), Slope of Log FDC 5th & 95th Percentile (SL FDC Q5th&Q95th), Slope of Log 33rd & 66th Percentile (SL Q33rd &Q66th), Slope of Log FDC 20th & 70th Percentile (SL FDC Q20th&Q70th), FDC High Segment Volume more than 90th Percentile (FDC HSV Q90th), FDC Low Segment Volume less than 30th Percentile (FDC LSV Q30th), FDC Medium Segment Volume (FDC MSV), Auto Correlation of Hydrograph with 1 Day Lag (AC), Peak Distribution(PD), Rising LIMB Destiny(RLD), Declining LIMB Destiny(DLD), 1st Flow Percentile (Q1st), 5th Flow Percentile(Q5th), 15th Flow Percentile(Q15th), 50th Flow Percentile(Q50th), 95th Flow Percentile(Q95th), and 99th Flow Percentile(Q99th)

metrics.

Using performance evaluation metrics of Likelihood, Entropy, NSE, RMSE, PBIAS, Distance, Distance/NoZero, Mean Uncertainty Spread, Coverage, and Threshold ,tables 4.3 and 4.4 respectively lists the posterior predictively result of GR4J and HyMod hydrologic models that been constrained against Skykomish watershed with regards to metrics of RR, BFI, BFR, SL FDC $Q5^{th}$&$Q95^{th}$, SL $Q33^{rd}$ &$Q66^{th}$, SL FDC $Q20^{th}$&$Q70^{th}$, FDC HSV $Q90^{th}$, FDC LSV $Q30^{th}$, FDC MSV, AC, PD, RLD, DLD, $Q1^{st}$, $Q5^{th}$, $Q15^{th}$, $Q50^{th}$, $Q95^{th}$ and $Q99^{th}$. These tables also demonstrate the Monte Carlo simulation results, which are basically random draws from the prior distribution of parameters and correspond to the information content of specific models without any constraining.

Similar conclusions as those of Tables 4.1 and 4.2 can be drawn with this watershed as well. What is specifically noticeable in Tables 4.3 and 4.4 is the difference between constraining power of the hydrologic signatures of this study for the GR4J and HyMond models. For GR4J, all hydrologic signatures except for Q^{1st}, Q^{15th} and Q^{50th} can constrain all GR4J model parameters, whereas only FDC LSV $Q30^{th}$ can constrain all HyMod model parameters. This confirms our previous discussion that GR4J model structure is much more flexible with little intrinsic model information, which responds to any level of information that hydrologic signatures impose in the calibration process. HyMod model structure, on the contrary, holds significant level of information, and doesn't respond to little constraining information that the hydrologic signatures provide single-handedly.

	Skykomish Watershed GR4J Hydrologic Model										
	Likelihood	Entropy	NSE	RMSE	PBIAS	Distance	Distance /NoZero	Mean Uncertainty Spread	Coverage	Threshold	Sensitive Parameters
Monte Carlo	0.00613	4.9485	-0.3686	128.8	-18.89	0.0210	15.3659	526.69030	99.8631		
RR	0.00732	4.7669	-0.3345	127.6	-9.286	3.5834	43.4779	300.47900	91.7579	0.3000	1,2,3,4,5
BFI	0.00625	4.4539	-0.2770	125.3	-23.86	4.0212	52.0760	299.17980	92.2782	0.0200	1,2,3,4,5
BFR	0.00675	4.7534	-0.3056	126.6	-20.00	2.93908	50.6298	314.78560	94.1950	0.5000	1,2,3,4,5
SL FDC Q5th&Q95th	0.01150	4.6143	-0.2163	122.0	-8.36	4.1777	50.6886	270.75620	91.7579	0.0750	1,2,3,4,5
SL Q33th&Q66th	0.01067	4.7123	-0.2812	124.5	-4.02	4.1645	55.7109	304.86010	92.5246	0.0500	1,2,3,4,5
SL FDC Q20th&Q70th	0.01027	4.7157	-0.2860	124.3	-6.038	3.9691	60.1468	351.58140	93.4009	0.1000	1,2,3,4,5
FDC HSV Q90th	0.00615	4.7920	-0.3609	129.3	-7.071	2.4617	45.4060	303.82510	94.5783	0.0200	1,2,3,4,5
FDC LSV Q30th	0.00626	4.3344	-0.1926	121.2	-34.24	5.3590	61.5442	246.39860	91.2924	0.1000	1,2,3,4,5
FDC MSV	0.00802	4.8017	-0.2785	124.5	-5.998	2.9942	36.4498	325.36630	91.7853	0.2500	1,2,3,4,5
AC	0.00368	4.7488	-0.4321	130.1	-15.89	0.1519	23.1257	425.74510	99.3428	0.0100	1,2,3,4,5
PD	0.00563	4.6762	-0.2852	126.3	-25.45	3.4596	69.4207	286.06080	95.0164	0.0200	1,2,3,4,5
RLD	0.00454	4.9624	-0.6780	137.7	-5.714	0.4020	35.8089	438.38060	98.8773	0.0100	1,2,3,4,5
DLD	0.00349	5.6284	-0.8686	145.3	18.51	0.2485	47.7773	456.62340	99.4797	0.0100	1,2,3,4,5
Q1st	0.00627	4.7876	-0.3258	127.6	-25.52	3.1454	57.4358	328.48780	94.5235	1.0000	0,2,3,4,0
Q5th	0.01318	4.5239	-0.2339	122.7	-7.577	4.3705	50.5105	285.75820	91.3472	0.2500	1,2,3,4,5
Q15th	0.00789	4.7225	-0.2981	125.6	-11.74	3.5147	56.5455	321.20960	93.7842	0.6000	1,2,3,0,5
Q50th	0.00806	4.7281	-0.2856	125.2	-8.525	3.6178	39.5584	301.38490	90.8543	0.4000	1,2,3,0,5
Q95th	0.00761	4.7721	-0.2295	123.2	-15.24	4.8371	51.2038	242.01210	90.5531	0.0350	1,2,3,4,5
Q99th	0.00769	4.6925	-0.3714	130.5	-8.126	4.3310	49.2737	256.57120	91.2103	0.0200	1,2,3,4,5

Table 4.3. Table of posterior predictively result of GR4J model constrained against Skykomish watershed (USGS ID 12134500) in terms of Monte Carlo simulation (not constrained), and Runoff Ratio (RR), Base Flow Index (BFI), Base Flow Runoff Ratio (BFR), Slope of Log FDC 5th & 95th Percentile (SL FDC Q5th&Q95th), Slope of Log 33rd & 66th Percentile (SL Q33rd &Q66th), Slope of Log FDC 20th & 70th Percentile (SL FDC Q20th&Q70th), FDC High Segment Volume more than 90th Percentile (FDC HSV Q90th), FDC Low Segment Volume less than 30th Percentile (FDC LSV Q30th), FDC Medium Segment Volume (FDC MSV), Auto Correlation of Hydrograph with 1 Day Lag (AC), Peak Distribution(PD), Rising LIMB Destiny(RLD), Declining LIMB Destiny(DLD), 1st Flow Percentile (Q1st), 5th Flow Percentile(Q5th), 15th Flow Percentile(Q15th), 50th Flow Percentile(Q50th), 95th Flow Percentile(Q95th), 99th Flow Percentile(Q99th) metrics.

	Skykomish Watershed HyMod Hydrologic Model										
	Likelihood	Entropy	NSE	RMSE	PBIAS	Distance	Distance /NoZero	Mean Uncertainty Spread	Coverage	Threshold	Sensitive Parameters
Monte Carlo	0.00366	4.16518	-0.81430	145.5624	-17.8967	3.71691	52.20835	309.32930	92.88060		
RR	0.00367	4.07712	-0.79250	144.7629	-17.4885	5.32452	53.71583	288.29800	90.08760	0.30000	1,0,0,4,5,0
BFI	0.00372	4.16459	-0.85050	146.7863	-18.1970	5.15014	51.81352	292.24810	90.06020	1.00000	0,0,3,4,0,6
BFR	0.00370	4.17384	-0.74436	143.2728	-17.5396	5.43605	54.53967	284.61360	90.03290	0.50000	0,0,3,4,5,6
SL FDC Q5th&Q95th	0.00388	4.17404	-0.80545	144.9365	-17.9017	5.16608	54.68563	293.24410	90.55310	5.00000	0,2,0,0,5,0
SL Q33th&Q66th	0.00402	4.22279	-0.65742	139.3486	-18.2613	5.19290	57.64282	288.13480	90.99120	3.00000	0,2,3,0,5,0
SL FDC Q20th&Q70th	0.00591	4.76967	-0.49286	131.4471	-19.7995	5.69433	57.28845	276.12190	90.06020	1.00000	1,2,3,4,5,6
FDC HSV Q90th	0.00419	4.23316	-0.55059	136.0249	-18.7675	5.04750	55.52254	268.88730	90.90910	1.00000	1,2,3,0,5,6
FDC LSV Q30th	0.00596	4.86351	-0.86499	143.8571	-18.9501	5.75596	58.88171	287.11840	90.22450	1.00000	1,2,3,4,5,6
FDC MSV	0.00389	4.20040	-0.72639	142.3941	-18.2757	4.77147	55.85071	293.04910	91.45670	2.00000	0,0,3,0,0,0
AC	0.00357	4.09507	-0.83450	146.6738	-18.4333	5.07922	56.55279	294.49750	91.01860	1.00000	0,0,0,4,0,6
PD	0.00365	4.17592	-0.90330	149.2085	-17.8467	5.37421	53.91932	287.58220	90.03290	3.00000	0,0,0,0,5,0
RLD	0.00381	4.15291	-0.79366	144.5296	-18.2352	5.23937	53.89907	290.49120	90.27930	0.50000	0,2,3,0,5,0
DLD	0.00388	4.13022	-0.73833	142.9001	-18.0247	5.31073	54.02443	285.87780	90.16980	0.40000	0,2,0,0,0,6
Q1st	0.00365	4.16459	-0.85700	147.1575	-18.4490	5.18808	57.58929	291.95570	90.99120	1.00000	0,2,3,0,5,0
Q5th	0.00380	4.24209	-0.77902	144.2077	-18.3300	5.25483	57.28546	288.92080	90.82690	1.00000	0,0,3,4,0,0
Q15th	0.00366	4.16364	-0.92517	149.2760	-17.8255	5.15936	56.92439	292.45740	90.93650	1.00000	1,0,3,4,0,0
Q50th	0.00373	4.16115	-0.85088	146.3977	-18.0336	4.57981	55.56634	297.04560	91.75790	1.00000	1,2,0,0,5,0
Q95th	0.00377	4.21364	-0.83975	146.9802	-18.1268	4.78327	50.92856	290.72200	90.60790	1.00000	0,0,0,4,5,0
Q99th	0.00396	4.16767	-0.64495	140.2647	-18.8332	5.46443	56.37318	269.01710	90.30670	1.00000	1,2,3,0,5,6

Table 4.4. Table of posterior predictively result of HyMod model constrained against Skykomish watershed (USGS ID 12134500) in terms of Monte Carlo simulation, and Runoff Ratio (RR), Base Flow Index (BFI), Base Flow Runoff Ratio (BFR), Slope of Log FDC 5th & 95th Percentile (SL FDC Q5th&Q95th), Slope of Log 33rd & 66th Percentile (SL Q33rd &Q66th), Slope of Log FDC 20th & 70th Percentile (SL FDC Q20th&Q70th), FDC High Segment Volume more than 90th Percentile (FDC HSV Q90th), FDC Low Segment Volume less than 30th Percentile (FDC LSV Q30th), FDC Medium Segment Volume (FDC MSV), Auto Correlation of Hydrograph with 1 Day Lag (AC), Peak Distribution(PD), Rising LIMB Destiny(RLD), Declining LIMB Destiny(DLD), 1st Flow Percentile (Q1st), 5th Flow Percentile(Q5th), 15th Flow Percentile(Q15th), 50th Flow Percentile(Q50th), 95th Flow Percentile(Q95th), 99th Flow Percentile(Q99th) metrics.

Using performance evaluation metrics of Likelihood, Entropy, NSE, RMSE, PBIAS, Distance, Distance/NoZero, Mean Uncertainty Spread, Coverage, and Threshold ,tables 4.5 and 4.6 respectively list the posterior predictively result of GR4J and HyMod hydrologic models that has been constrained against the Henry Fork watershed in regards to metrics of RR, BFI, BFR, SL FDC $Q5^{th}$&$Q95^{th}$, SL $Q33^{rd}$ &$Q66^{th}$, SL FDC $Q20^{th}$&$Q70^{th}$, FDC HSV $Q90^{th}$, FDC LSV $Q30^{th}$, FDC MSV, AC, PD, RLD, DLD, $Q1^{st}$, $Q5^{th}$, $Q15^{th}$, $Q50^{th}$, $Q95^{th}$ and $Q99^{th}$, as well as unconstrained model simulations derived through Monte Carlo sampling.

These tables also confirm our previous findings, with a distinct difference in how GR4J model parameters are sensitive to different hydrologic signatures. In this watershed, GR4J model parameters actually show a higher level of sensitivity to calibration against different hydrologic metrics, compared to the Skykomish watershed. HyMod model's performance seems to be more stable across different watersheds. This points out to an interesting finding that the quest for sufficient hydrologic signatures not only is model dependent but also watershed dependent to some extent.

	Henry Fork Watershed GR4J Hydrologic Model										
	Likelihood	Entropy	NSE	RMSE	PBIAS	Distance	Distance /NoZero	Mean Uncertainty Spread	Coverage	Threshold	Sensitive Parameters
Monte Carlo	0.24191	2.14773	-0.95434	5.65359	37.86578	0.00000	NaN	57.14850	100.00000		
RR	0.34134	0.91536	0.10523	4.58868	-0.635927	0.07527	1.02563	7.90380	92.66160	0.07500	1,2,3,0,5
BFI	0.24927	1.03648	-0.04823	4.93045	-18.19707	0.11940	2.30714	8.55070	94.82480	0.01000	1,2,3,4,5
BFR	0.46248	0.66418	0.13128	4.53957	-15.3241	0.18360	1.89941	6.55170	90.33410	0.15000	1,2,3,0,0
SL FDC $Q5^{th}$&$Q95^{th}$	0.31939	0.91999	0.01920	4.78789	-8.930315	0.14992	1.71635	7.76900	91.26510	0.02000	1,2,3,4,5
SL $Q33^{th}$&$Q66^{th}$	0.29651	1.35369	-0.02569	4.90313	7.076422	0.13056	2.25970	9.57350	94.22230	0.01000	1,2,3,4,5
SL FDC $Q20^{th}$&$Q70^{th}$	0.36055	1.17782	-0.12092	5.03507	5.372624	0.05817	1.02134	11.50980	94.30450	0.01000	1,2,3,4,5
FDC HSV $Q90^{th}$	0.05216	2.06876	-1.51166	7.60886	150.4614	0.09045	3.88596	13.80700	97.67250	0.02000	1,2,3,4,5
FDC LSV $Q30^{th}$	0.23755	1.07090	0.05447	4.71728	-32.99666	0.07578	0.78850	9.89500	90.38880	0.45000	1,2,3,0,5
FDC MSV	0.45738	0.72021	0.12530	4.54243	-13.16349	0.10190	1.06323	8.02220	90.41620	3.00000	0,2,3,0,5
AC	0.10939	1.20878	-3.59604	7.41008	55.14792	0.00000	NaN	51.28240	100.00000	0.02000	1,2,3,4,5
PD	0.16031	1.82251	-0.16353	5.11481	53.33856	0.17034	9.01573	11.10750	98.11060	0.02000	1,2,3,4,5
RLD	0.15199	2.50386	-1.45160	6.46637	103.5701	0.00664	0.93318	26.46750	99.28810	0.01000	1,2,3,4,5
DLD	0.09956	-0.70015	-0.84096	5.69105	-66.80629	0.00402	14.66938	51.61550	99.97260	0.30000	1,2,3,4,5
$Q1^{st}$	0.29458	0.98825	0.05315	4.72491	-31.18262	0.08457	0.87744	10.61380	90.36140	1.00000	1,2,3,0,5
$Q5^{th}$	0.42131	0.83215	0.10389	4.60027	-20.57927	0.06938	0.89534	9.01950	92.25080	0.50000	0,2,3,4,5
$Q15^{th}$	0.43969	0.84452	0.12265	4.55804	-16.10641	0.15626	1.78328	7.63400	91.23770	0.40000	1,2,3,4,0
$Q50^{th}$	0.44348	0.74681	0.12780	4.55046	-19.38730	0.18659	2.19110	6.20100	91.48410	0.30000	1,2,3,0,5
$Q95^{th}$	0.28558	1.05998	0.09816	4.62495	-6.284200	0.15883	3.35288	6.22380	95.26290	0.02000	1,2,3,4,5
$Q99^{th}$	0.08618	1.71115	-0.58659	6.09107	70.29356	0.14608	6.06241	11.57110	97.59040	0.02000	1,2,3,4,5

Table 4.5. Table of posterior predictively result of GR4J model constrained against Henry Fork watershed (USGS ID 02143000) in terms of Monte Carlo simulation (not constrained), as well as Runoff Ratio (RR), Base Flow Index (BFI), Base Flow Runoff Ratio (BFR), Slope of Log FDC 5^{th} & 95^{th} Percentile (SL FDC $Q5^{th}$&$Q95^{th}$), Slope of Log 33^{rd} & 66^{th} Percentile (SL $Q33^{rd}$ &$Q66^{th}$), Slope of Log FDC 20^{th} & 70^{th} Percentile (SL FDC $Q20^{th}$&$Q70^{th}$), FDC High Segment Volume more than 90^{th} Percentile (FDC HSV $Q90^{th}$), FDC Low Segment Volume less than 30^{th} Percentile (FDC LSV $Q30^{th}$), FDC Medium Segment Volume (FDC MSV), Auto Correlation of Hydrograph with 1 DayLag (AC), Peak Distribution(PD), Rising LIMB Destiny(RLD), Declining LIMB Destiny(DLD), 1^{st} Flow Percentile ($Q1^{st}$), 5^{th} Flow Percentile ($Q5^{th}$), 15^{th} Flow Percentile($Q15^{th}$), 50^{th} Flow Percentile($Q50^{th}$), 95^{th} Flow Percentile($Q95^{th}$), 99^{th} Flow Percentile($Q99^{th}$) metrics.

	Henry Fork Watershed HyMod Hydrologic Model										
	Likelihood	Entropy	NSE	RMSE	PBIAS	Distance	Distance /NoZero	Mean Uncertainty Spread	Coverage	Threshold	Sensitive Parameters
Monte Carlo	0.15838	1.66111	-2.477	8.149	60.48	0.0109	1.66519	19.56800	99.3428		
RR	0.14952	0.87103	-0.970	6.442	0.047	0.0442	1.00456	9.82090	95.5915	0.0200	1,2,3,4,5,6
BFI	0.17991	1.50631	-0.735	6.204	59.26	0.0230	1.13706	13.30250	97.9737	0.3000	1,2,3,4,5,0
BFR	0.15210	1.29017	-4.810	10.28	60.19	0.0851	0.94770	15.65610	91.0186	0.1250	1,2,3,4,5,6
SL FDC Q5th&Q95th	0.22577	1.52094	-0.770	5.825	59.16	0.0727	0.77951	11.68180	90.6627	0.0750	1,2,3,4,5,6
SL Q33th&Q66th	0.21746	1.50662	-1.206	6.175	63.74	0.0893	0.93752	13.91130	90.4710	0.1000	1,2,3,4,5,6
SL FDC Q20th&Q70th	0.19834	1.70889	-1.119	6.240	65.54	0.0388	0.85487	14.12480	95.4545	0.3000	1,2,3,4,0,0
FDC HSV Q90th	0.19775	1.38054	0.113	4.571	50.04	0.1487	2.23590	8.24360	93.3461	0.1000	1,2,3,4,5,0
FDC LSV Q30th	0.20461	1.77862	-1.034	6.441	57.36	0.0571	1.01378	13.16320	94.3593	0.0200	1,2,3,4,5,6
FDC MSV	0.17561	1.23880	-1.695	7.522	62.66	0.0957	0.96626	13.86970	90.0876	5.0000	1,2,3,4,5,0
AC	0.15212	1.10581	-1.927	8.180	58.44	0.1784	4.90023	10.21900	96.3582	0.0750	1,2,3,4,5,6
PD	0.18612	1.59991	0.142	4.477	48.96	0.1024	1.13037	9.02610	90.9365	0.5000	1,2,3,4,5,6
RLD	0.16441	1.51355	-2.702	8.399	52.97	0.0605	2.23403	16.64070	97.2892	0.0100	1,2,3,4,5,6
DLD	0.12450	1.16496	-8.285	14.34	72.58	0.4482	4.90111	14.25570	90.8543	0.2000	1,2,3,4,5,6
Q1st	0.15503	1.53612	-2.921	8.522	59.94	0.0756	1.03818	16.78320	92.7163	1.0000	0,0,0,4,5,0
Q5th	0.22551	1.57258	-1.078	6.428	61.45	0.0556	0.82654	13.85020	93.2640	0.5000	0,2,3,4,5,6
Q15th	0.20963	1.54835	-1.341	6.745	62.80	0.0535	0.86891	15.59870	93.8390	0.6000	1,2,3,4,5,0
Q50th	0.17192	1.26744	-1.955	7.784	60.53	0.0803	1.22224	14.21360	93.4283	0.40000	1,2,3,4,5,0
Q95th	0.12034	1.47988	-3.731	9.336	30.53	0.1489	2.14214	10.08910	93.0449	0.01000	1,2,3,4,5,6
Q99th	0.19001	1.56169	0.064	4.685	51.74	0.0725	3.44246	9.69850	97.8916	0.30000	1,2,3,4,5,6

Table 4.6. Table of posterior predictively result of HyMod model constrained against Henry Fork watershed (USGS ID 02143000) in terms of Monte Carlo simulation (not constrained), as well as Runoff Ratio (RR), Base Flow Index (BFI), Base Flow Runoff Ratio (BFR), Slope of Log FDC 5th & 95th Percentile (SL FDC Q5th&Q95th), Slope of Log 33rd & 66th Percentile (SL Q33rd &Q66th), Slope of Log FDC 20th & 70th Percentile (SL FDC Q20th&Q70th), FDC High Segment Volume more than 90th Percentile (FDC HSV Q90th), FDC Low Segment Volume less than 30th Percentile (FDC LSV Q30th), FDC Medium Segment Volume (FDC MSV), Auto Correlation of Hydrograph with 1 Day Lag (AC), Peak Distribution(PD), Rising LIMB Destiny(RLD), Declining LIMB Destiny(DLD), 1st Flow Percentile (Q1st), 5th Flow Percentile(Q5th), 15th Flow Percentile(Q15th), 50th Flow Percentile(Q50th), 95th Flow Percentile(Q95th), 99th Flow Percentile(Q99th) metrics.

Chapter 5

SUMMARY AND CONCLUSION

In this thesis, we address an important topic of characterizing the constraining power different hydrological signatures in an approximate Bayesian computation framework. We are specifically concerned with analyzing how different hydrologic signatures constrain distinct sections of the model response, hoping to shed some light on selection of a set of sufficient hydrologic signatures for rainfall runoff model calibration. Although significant strides have been made in the field of hydrologic model calibration using Bayesian inference and beyond, the constraining power of particular hydrologic metrics have not been analyzed. We calibrate two parsimonious rainfall-runoff models, namely GR4J and HyMod, using different hydrologic signatures in an approximate Bayesian computation framework against three watersheds in the United State; and compare the performance of each metric using goodness-of-fit metrics such as information theory, likelihood, entropy, NSE, RMSE, and percent bias. In more detail, posterior model parameters delineated by each of the hydrologic signatures are used to run the hydrologic models, goodness-of-fit of simulations of which shed light the advantages and disadvantages of using certain hydrologic signature in the calibration process. We also further the analysis by comparing the prior and posterior model distributions constrained with each metric using Kullback-Leiber divergence metric and Two-Sample Kolmogorov Smirnov test to identify which

metrics pose statistically significant change on each of the model parameters.

In summary, the analysis shows that there is no single metric that can perform satisfactorily with a hydrologic model, and hence a combination of metrics with different capabilities are required to constrain a hydrologic model. We have identified metrics such as Peak Distribution of 1st quantile of flow distribution that fail to constrain any specific portion of the model response, and hence are not recommended to be used in model calibration. We also noticed that the impact of hydrologic signatures on model calibration is both model- and watershed- specific. For a given watershed, a certain hydrologic metric might constrain one parameter of the GR4J model, while same metric might be insensitive to the response of another watershed. This is less of an issue for a more confined model structure such as HyMod. Moreover, some hydrologic signatures perform superior in a less flexible model structure such as HyMod, as opposed to a more flexible model structure such as GR4J. This points to the intrinsic information content of the HyMod model, which in conjunction with certain metrics can constrain the model response. This information is however lacking in a flexible model structure, such as GR4J, which doesn't provide the extra help to hydrologic signature to constrain model behavior.

BIBLIOGRAPHY

Afgani, Mostafa, Sinan Sinanovic, and Harald Haas. "Anomaly detection using the Kullback-Leibler divergence metric." Applied Sciences on Biomedical and Communication Technologies, 2008. ISABEL'08. First International Symposium on. IEEE, 2008.

Aghakouchak, Amir, and Emad Habib. "Application of a conceptual hydrologic model in teaching hydrologic processes." (2010): 963-973.

Arhonditsis, G. B., et al. “Exploring Ecological Patterns with Structural Equation Modeling and Bayesian Analysis.” Ecological Modelling, vol. 192, no. 3-4, 2006, pp. 385–409.

ASCE Task Committee on Definition of Criteria for Evaluation of Watershed Models of the Watershed Management Committee, Irrigation and Drainage Division. "Criteria for evaluation of watershed models." Journal of Irrigation and Drainage Engineering 119.3 (1993): 429-442.

Basseville, Michele. "Distance measures for signal processing and pattern recognition." Signal processing 18.4 (1989): 349-369.

Beaumont, Mark A., Wenyang Zhang, and David J. Balding. "Approximate Bayesian computation in population genetics." Genetics 162.4 (2002): 2025-2035.

Berliner, L. Mark. "Bayesian Analysis for Oceanographers." National Center for Atmospheric Research and Ohio State University (1997).

Bernardinelli, L., et al. “Bayesian Analysis of Space—time Variation in Disease Risk.” Statistics in Medicine, vol. 14, no. 21-22, 1995, pp. 2433–43.

Boyle, Douglas Patrick. "Multicriteria calibration of hydrologic models." (2001).

Dodge, Yadolah. The concise encyclopedia of statistics. Springer Science & Business Media, 2008.

Ellison, Aaron M. “Bayesian Inference in Ecology.” Ecology Letters, vol. 7, no. 6, 2004, pp. 509–20.

Geweke, John. “Bayesian Inference in Econometric Models Using Monte Carlo Integration.” Econometrica: Journal of the Econometric Society, vol. 57, no. 6, 1989, p. 1317.

Gottschalk, Lars, and Rolf Weingartner. "Distribution of peak flow derived from a distribution of rainfall volume and runoff coefficient, and a unit hydrograph." Journal of hydrology 208.3-4 (1998): 148-162.

Gupta, Hoshin V., Thorsten Wagener, and Yuqiong Liu. "Reconciling theory with observations: elements of a diagnostic approach to model evaluation." Hydrological Processes 22.18 (2008): 3802-3813.

Gupta, Hoshin Vijai, Soroosh Sorooshian, and Patrice Ogou Yapo. "Status of automatic calibration for hydrologic models: Comparison with multilevel expert calibration." Journal of Hydrologic Engineering 4.2 (1999): 135-143.

Ho, Chih-Hsiang. “Bayesian Analysis of Volcanic Eruptions.” Journal of Volcanology and Geothermal Research, vol. 43, no. 1-4, 1990, pp. 91–98.

Huelsenbeck, John P., et al. "Bayesian inference of phylogeny and its impact on evolutionary biology." science 294.5550 (2001): 2310-2314.

Hyndman, Rob J., and Anne B. Koehler. "Another look at measures of forecast accuracy." International journal of forecasting 22.4 (2006): 679-688.

John C. Schaake, et. al "Calibration of Watershed Models Water Science and Application Volume6. " American Geophysical Union.

Kavetski, Dmitri, George Kuczera, and Stewart W. Franks. "Bayesian analysis of input uncertainty in hydrological modeling: 1. Theory: Input Uncertainty in Hydrology." Water Resources Research 42.3 (2006).

Legates, David R., and Gregory J. McCabe. "Evaluating the use of “goodness-of-fit” measures in hydrologic and hydroclimatic model validation." Water resources research 35.1 (1999): 233-241.

Liu, Ce, and Hueng-Yeung Shum. "Kullback-leibler boosting." Computer Vision and Pattern Recognition, 2003. Proceedings. 2003 IEEE Computer Society Conference on. Vol. 1. IEEE, 2003.

Liu, Ming-Yu, et al. "Entropy rate superpixel segmentation." Computer Vision and Pattern Recognition (CVPR), 2011 IEEE Conference on. IEEE, 2011.

Massey Jr, Frank J. "The Kolmogorov-Smirnov test for goodness of fit." Journal of the American statistical Association 46.253 (1951): 68-78.

McCuen, Richard H., Zachary Knight, and A. Gillian Cutter. "Evaluation of the Nash–Sutcliffe efficiency index." Journal of Hydrologic Engineering 11.6 (2006): 597-602.

Meixner, Thomas, et al. "Estimating Parameters and Structure of a Hydrochemical Model Using Multiple Criteria." Calibration of Watershed Models (2003): 213-228.

Meixner, Thomas, et al. "Estimating Parameters and Structure of a Hydrochemical Model Using Multiple Criteria." Calibration of Watershed Models (2003): 213-228.

Merz, Ralf, and Günter Blöschl. "Regionalisation of catchment model parameters." Journal of hydrology 287.1-4 (2004): 95-123.

Moradkhani, Hamid, et al. "Uncertainty assessment of hydrologic model states and parameters: Sequential data assimilation using the particle filter." Water resources research 41.5 (2005).

Moriasi, Daniel N., et al. "Model evaluation guidelines for systematic quantification of accuracy in watershed simulations." Transactions of the ASABE 50.3 (2007): 885-900.

Naeini, Matin Rahnamay, et al. "Shuffled Complex-Self Adaptive Hybrid EvoLution (SC-SAHEL) optimization framework." Environmental Modelling & Software 104 (2018): 215-235.

Nakahara, Hiroyuki, and Shun-ichi Amari. "Information-geometric measure for neural spikes." Neural Computation 14.10 (2002): 2269-2316.

Nash, J. Eamonn, and Jonh V. Sutcliffe. "River flow forecasting through conceptual models part I—A discussion of principles." Journal of hydrology 10.3 (1970): 282-290.

Perrin, Charles, Claude Michel, and Vazken Andréassian. "Improvement of a parsimonious model for streamflow simulation." Journal of hydrology 279.1-4 (2003): 275-289.

Pokhrel, Prafulla, Koray K. Yilmaz, and Hoshin V. Gupta. "Multiple-criteria calibration of a distributed watershed model using spatial regularization and response signatures." Journal of Hydrology 418 (2012): 49-60.

Pritchard, Jonathan K., et al. "Population growth of human Y chromosomes: a study of Y chromosome microsatellites." Molecular biology and evolution 16.12 (1999): 1791-1798.

Robertson, John, Ellis Tallman, and Charles Whiteman. "Forecasting using relative entropy." (2002).

Sadegh, M., and J. A. Vrugt. "Bridging the gap between GLUE and formal statistical approaches: approximate Bayesian computation." Hydrology and Earth System Sciences 17.12 (2013): 4831-4850.

Sadegh, M., and J. A. Vrugt. “Bridging the Gap between GLUE and Formal Statistical Approaches: Approximate Bayesian Computation.” Hydrology and Earth System Sciences, vol. 17, no. 12, 2013, pp. 4831–50.

Sadegh, M., et al. "The soil water characteristic as new class of closed-form parametric expressions for the flow duration curve." Journal of Hydrology 535 (2016): 438-456.

Sadegh, Mojtaba, and Jasper A. Vrugt. "Approximate bayesian computation using markov chain monte carlo simulation: Dream (abc)." Water Resources Research 50.8 (2014): 6767-6787.

Sadegh, Mojtaba, Elisa Ragno, and Amir AghaKouchak. "Multivariate Copula Analysis Toolbox (MvCAT): Describing dependence and underlying uncertainty using a Bayesian framework." Water Resources Research (2017).

Sadegh, Mojtaba, et al. "The Quest for Hydrological Signatures: Effects of Data Transformation on Bayesian Inference of Watershed Models." Water Resources Management 32.5 (2018): 1867-1881.

Sadegh, Mojtaba, et al. "The stationarity paradigm revisited: Hypothesis testing using diagnostics, summary metrics, and DREAM (ABC)." Water Resources Research 51.11 (2015): 9207-9231.

Servat, Eric, and Alain Dezetter. "Selection of calibration objective fonctions in the context of rainfall-ronoff modelling in a Sudanese savannah area." Hydrological Sciences Journal 36.4 (1991): 307-330.

Sorooshian, Soroosh, and John A. Dracup. "Stochastic parameter estimation procedures for hydrologie rainfall-runoff models: Correlated and heteroscedastic error cases." Water Resources Research 16.2 (1980): 430-442.

Spiegelhalter, David J., et al. "Bayesian analysis in expert systems." Statistical science (1993): 219-247.

Thiemann, M., et al. "Bayesian recursive parameter estimation for hydrologic models." Water Resources Research 37.10 (2001): 2521-2535.

Turner, Brandon M., and Per B. Sederberg. "Approximate Bayesian computation with differential evolution." Journal of Mathematical Psychology 56.5 (2012): 375-385.

Turner, Brandon M., and Trisha Van Zandt. "A tutorial on approximate Bayesian computation." Journal of Mathematical Psychology 56.2 (2012): 69-85.

Vicens, Guillermo J., Ignacio Rodriguez-Iturbe, and John C. Schaake. "A Bayesian framework for the use of regional information in hydrology." Water Resources Research 11.3 (1975): 405-414.

Wilcox, R. "Kolmogorov–smirnov test." Encyclopedia of biostatistics (2005).

Wood, Eric F., and Ignacio Rodríguez-Iturbe. “Bayesian Inference and Decision Making for Extreme Hydrologic Events.” Water Resources Research, vol. 11, no. 4, 1975, pp. 533–42.

SUPPLEMENTARY INFORMATION

In the following, we show predictive uncertainty range plots of GR4J and HyMod models constrained against SF Boise river (USGS ID #13186000), Skykomish river (USGS ID #12134500) and Henry Fork river (USGS ID #02143000) in a temporal span of 10 years, starting from January 1, 1948 to January 1, 1958; Using Monte Carlo ,Runoff Ratio (RR), Base Flow Index (BFI), Base Flow Runoff Ratio (BFR), Slope of Log FDC 5th & 95th Percentile (SL FDC Q5th&Q95th), Slope of Log 33rd & 66th Percentile (SL Q33th&Q66th), Slope of Log FDC 20th & 70th Percentile (SL FDC Q20th&Q70th), FDC High Segment Volume more than 90th Percentile (FDC HSV Q90th), FDC Low Segment Volume less than 30th Percentile (FDC LSV Q30th), FDC Medium Segment Volume (FDC MSV), Auto Correlation of Hydrograph with 1 Day Lag (AC), Peak Distribution(PD), Rising LIMB Destiny(RLD), Declining LIMB Destiny(DLD), 1st Flow Percentile (Q1st), 5th Flow Percentile(Q5th), 15th Flow Percentile(Q15th), 50th Flow Percentile(Q50th), 95th Flow Percentile(Q95th), 99th Flow Percentile(Q99th). The plots in this section includes the plots that was not analyzed in result and discussion section.

13186000 GR4J

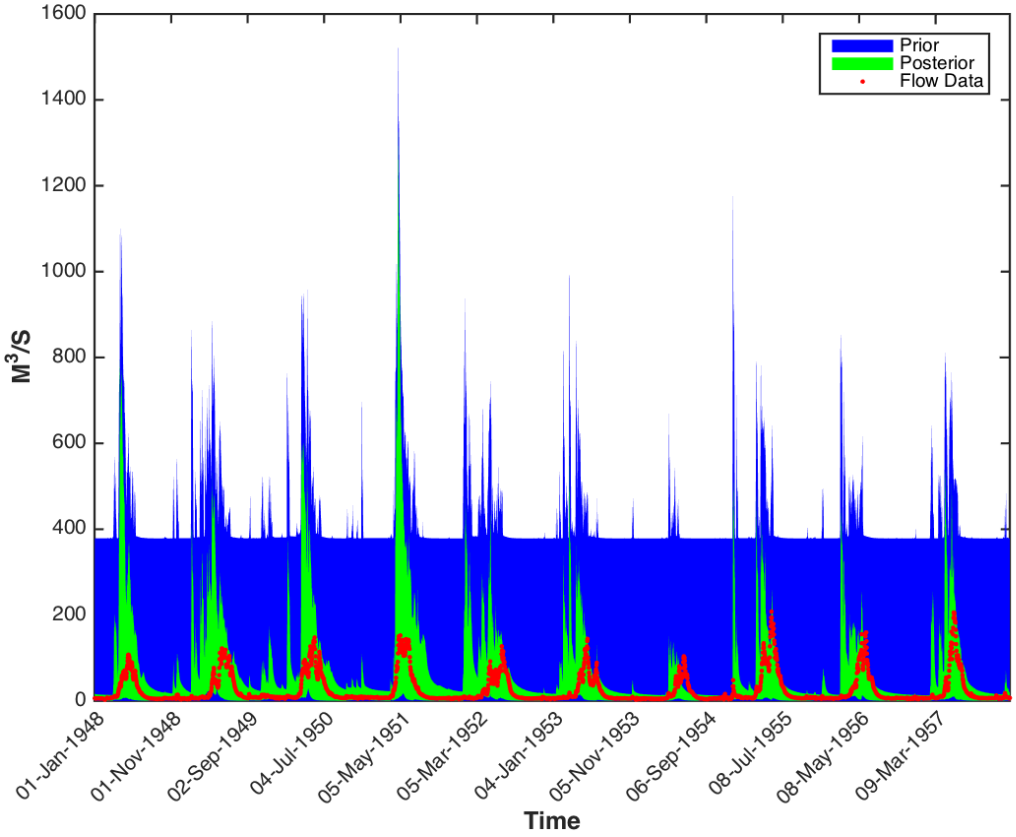

Figure 6.1. Predictive uncertainty ranges of GR4J model constrained against SF Boise watershed (USGS ID 13186000) using Runoff Ratio Metric (RR). Prior channel inflow in blue, posterior channel flow in green and observed data in red

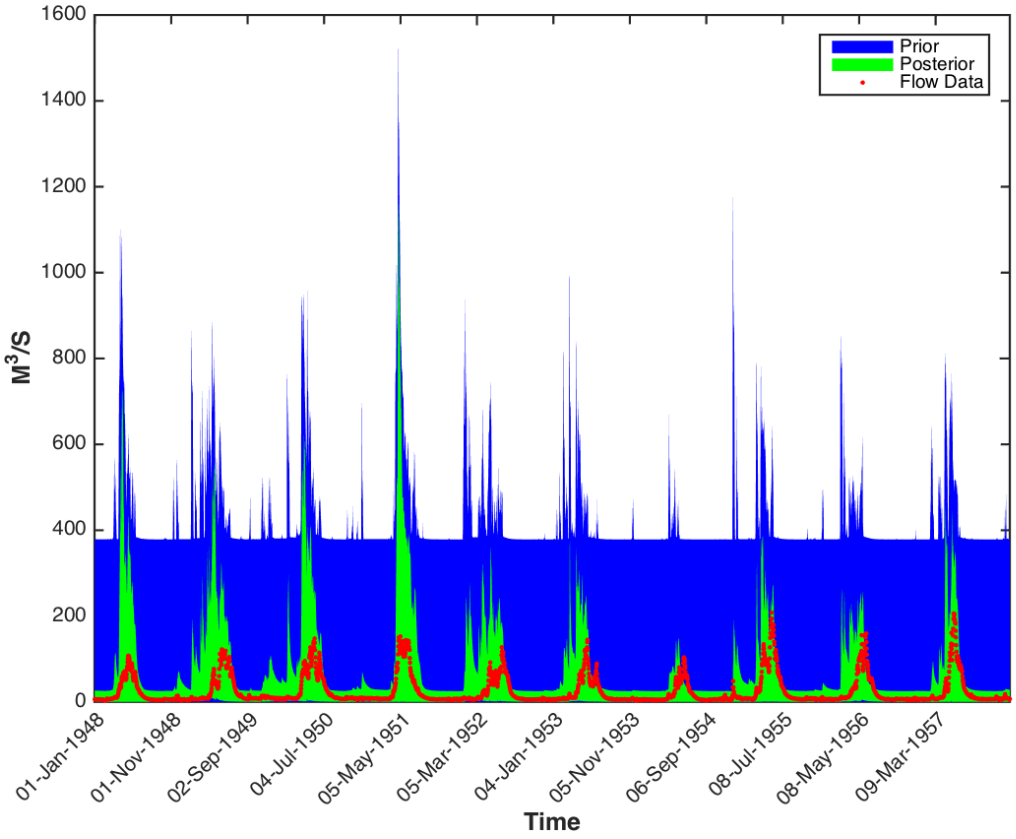

Figure 6.2 Predictive uncertainty ranges of GR4J model constrained against SF Boise watershed (USGS ID 13186000) using Base Flow Index (BFI). Prior channel inflow in blue, posterior channel flow in green and observed data in red

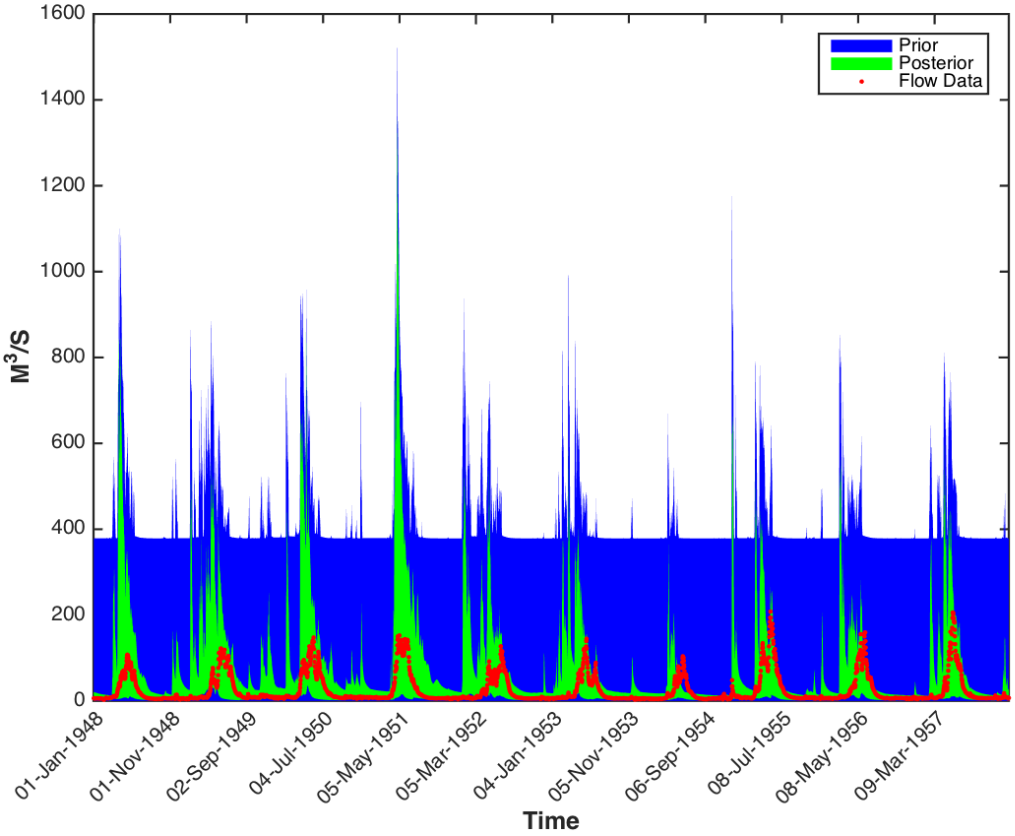

Figure 6.3. Predictive uncertainty ranges of GR4J model constrained against SF Boise watershed (USGS ID 13186000) using Base Flow Runoff Ratio (BFR). Prior channel inflow in blue, posterior channel flow in green and observed data in red

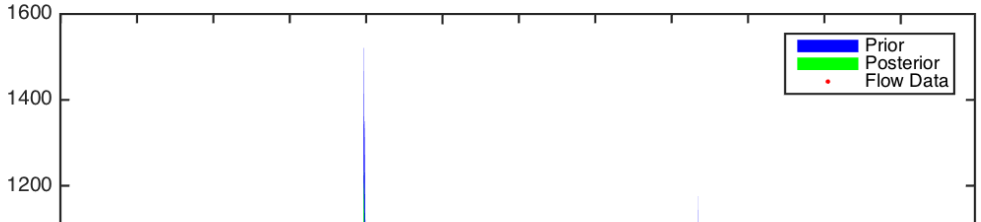

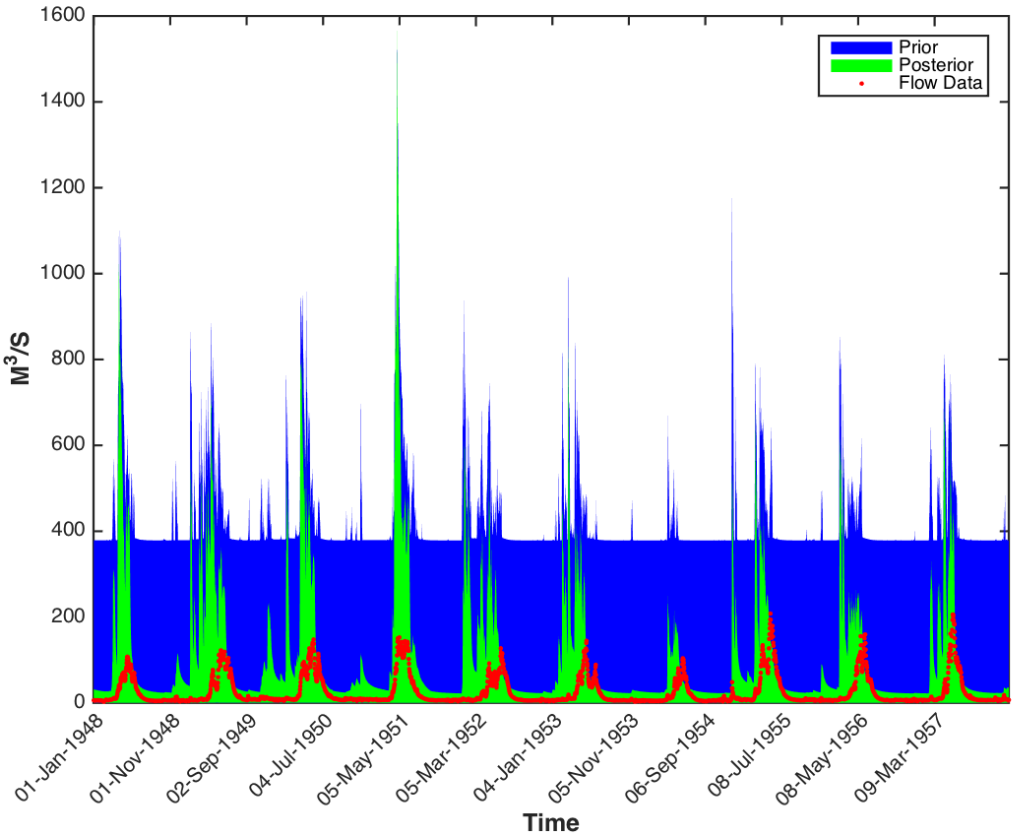

Figure 6.5 Predictive uncertainty ranges of GR4J model constrained against SF Boise watershed (USGS ID 13186000) using Slope of Log FDC 5& 95 Percentile (SL Q33th&Q66th). Prior channel inflow in blue, posterior channel flow in green and observed data in red

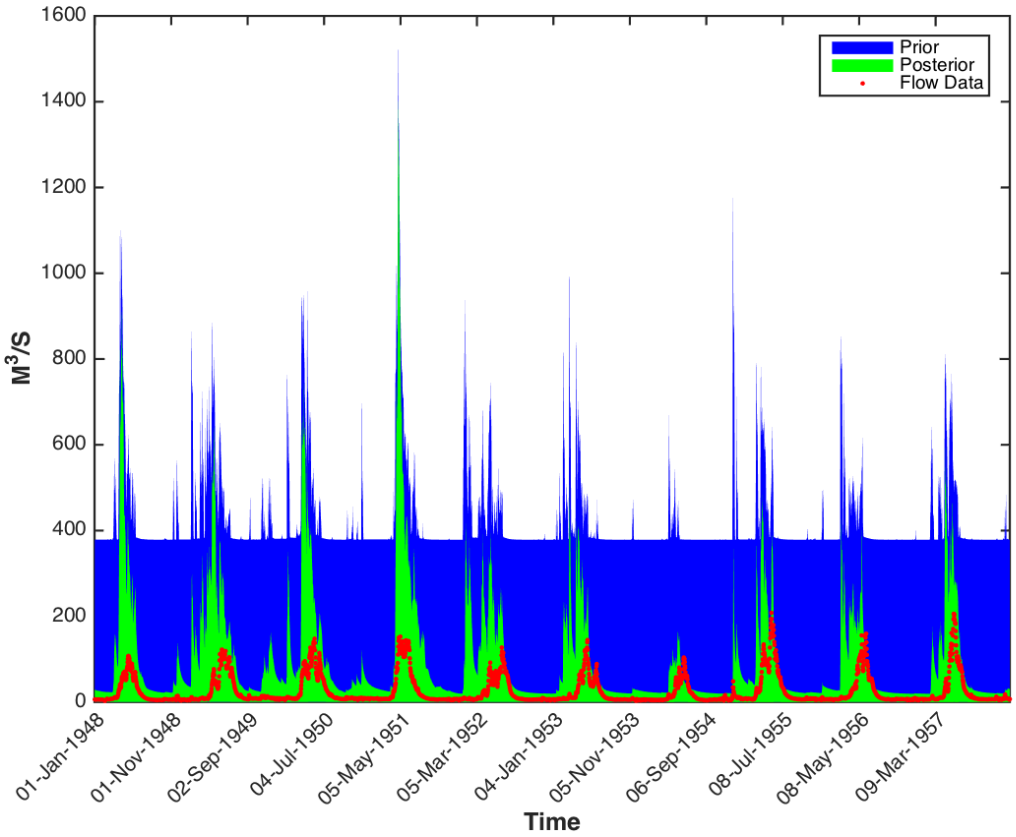

Figure 6.6. Predictive uncertainty ranges of GR4J model constrained against SF Boise watershed (USGS ID 13186000) using Slope of Log FDC 20 & 70 Percentile (SL FDC Q20th&Q70th). Prior channel inflow in blue, posterior channel flow in green and observed data in red

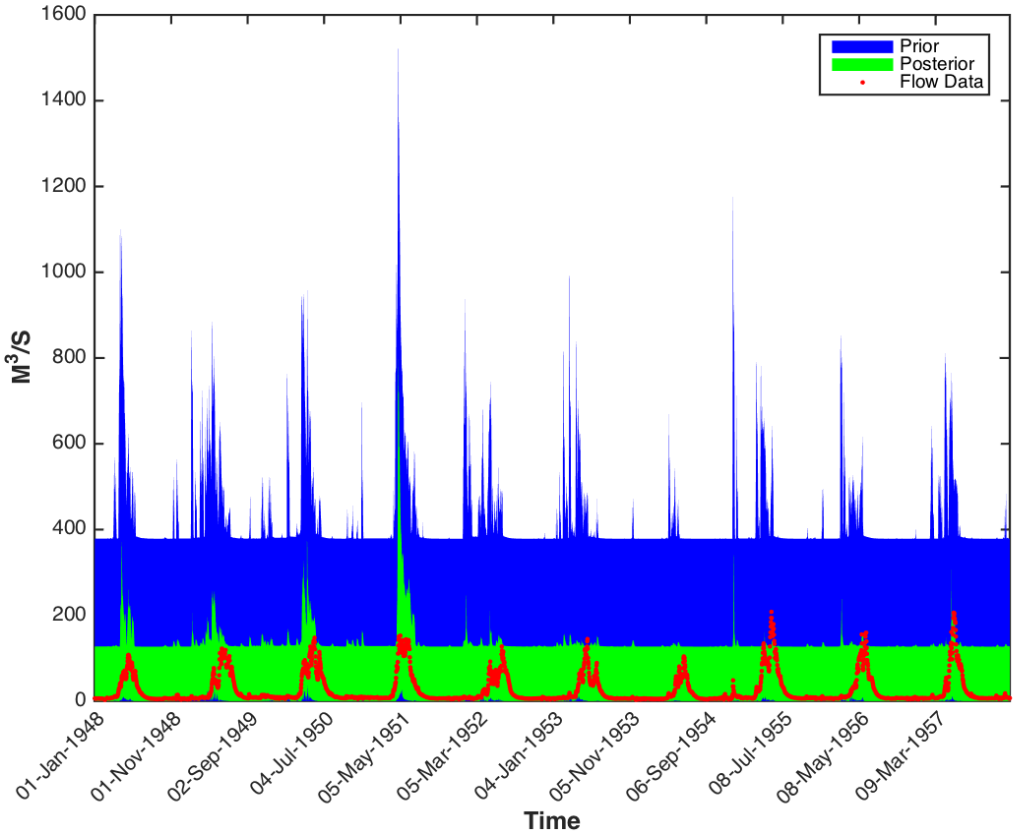

Figure 6.7. Predictive uncertainty ranges of GR4J model constrained against SF Boise watershed (USGS ID 13186000) using FDC High Segment Volume more than 90 Percentile (FDC HSV Q90th). Prior channel inflow in blue, posterior channel flow in green and observed data in red

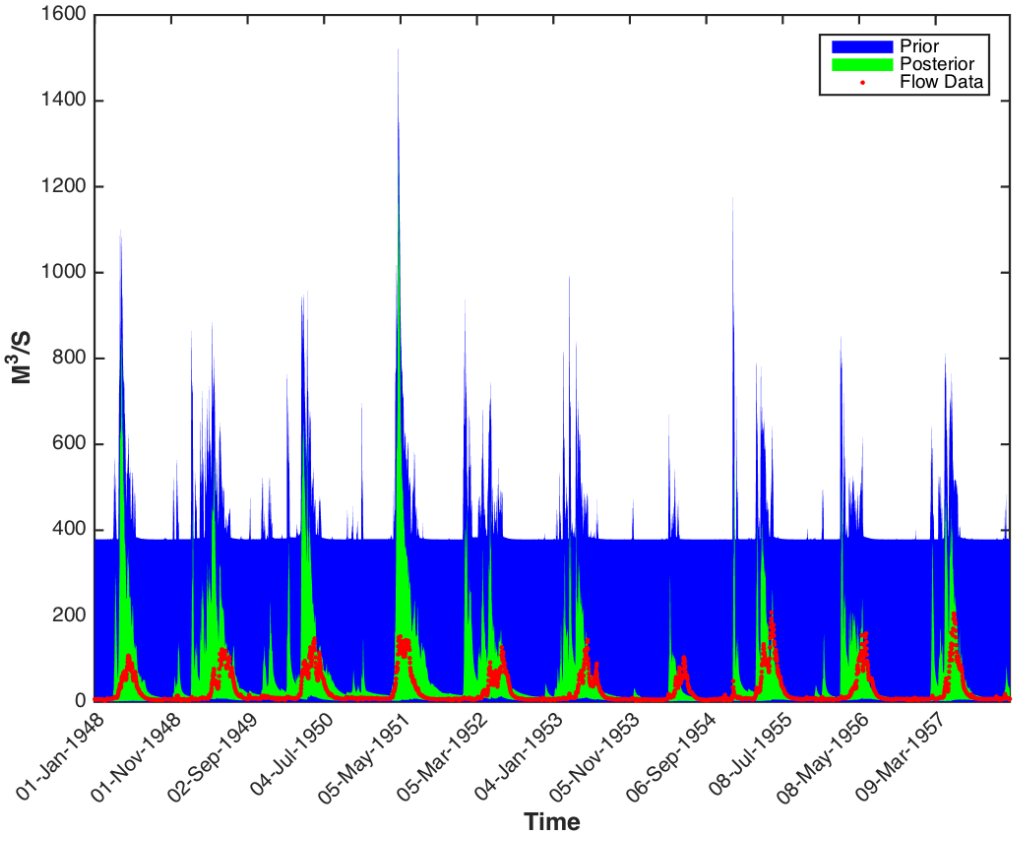

Figure 6.9. Predictive uncertainty ranges of GR4J model constrained against SF Boise watershed (USGS ID 13186000) using FDC Medium Segment Volume (FDC MSV) Prior channel inflow in blue, posterior channel flow in green and observed data in red

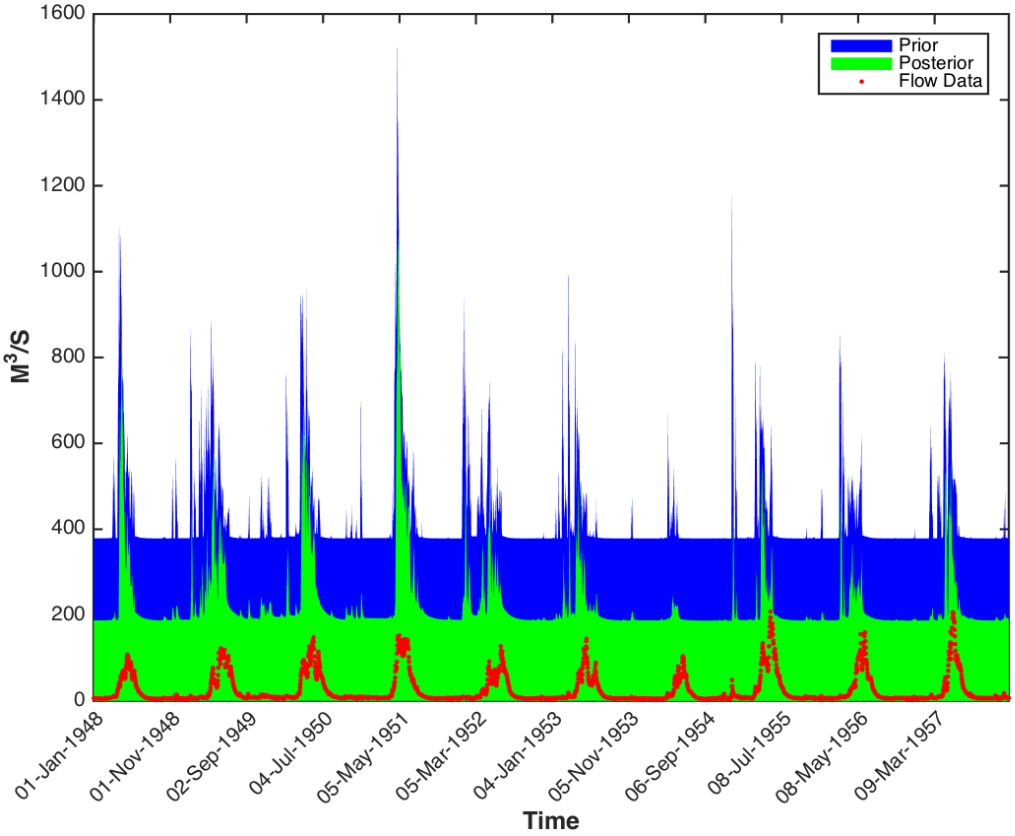

Figure 6.10. Predictive uncertainty ranges of GR4J model constrained against SF Boise watershed (USGS ID 13186000) using Auto Correlation of Hydrograph with 1 Day Lag (AC) Prior channel inflow in blue, posterior channel flow in green and observed data in red

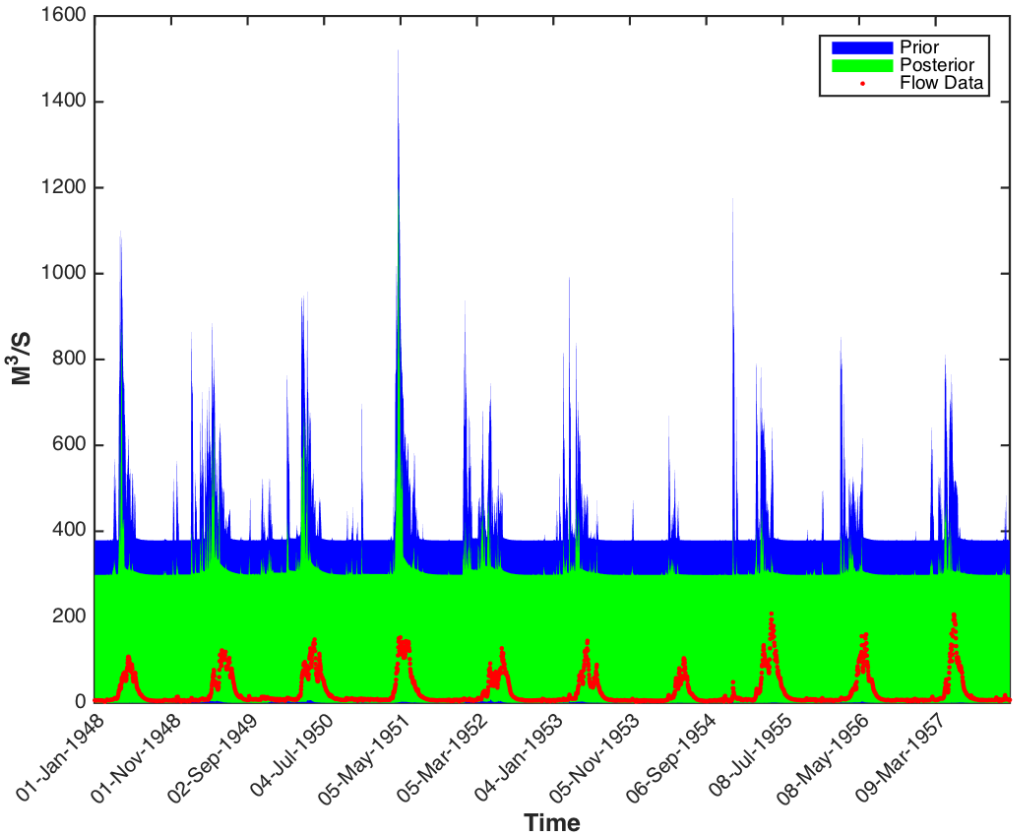

Figure 6.11. Predictive uncertainty ranges of GR4J model constrained against SF Boise watershed (USGS ID 13186000) Peak Distribution (Slope of Peak Flows) (PD) Prior channel inflow in blue, posterior channel flow in green and observed data in red

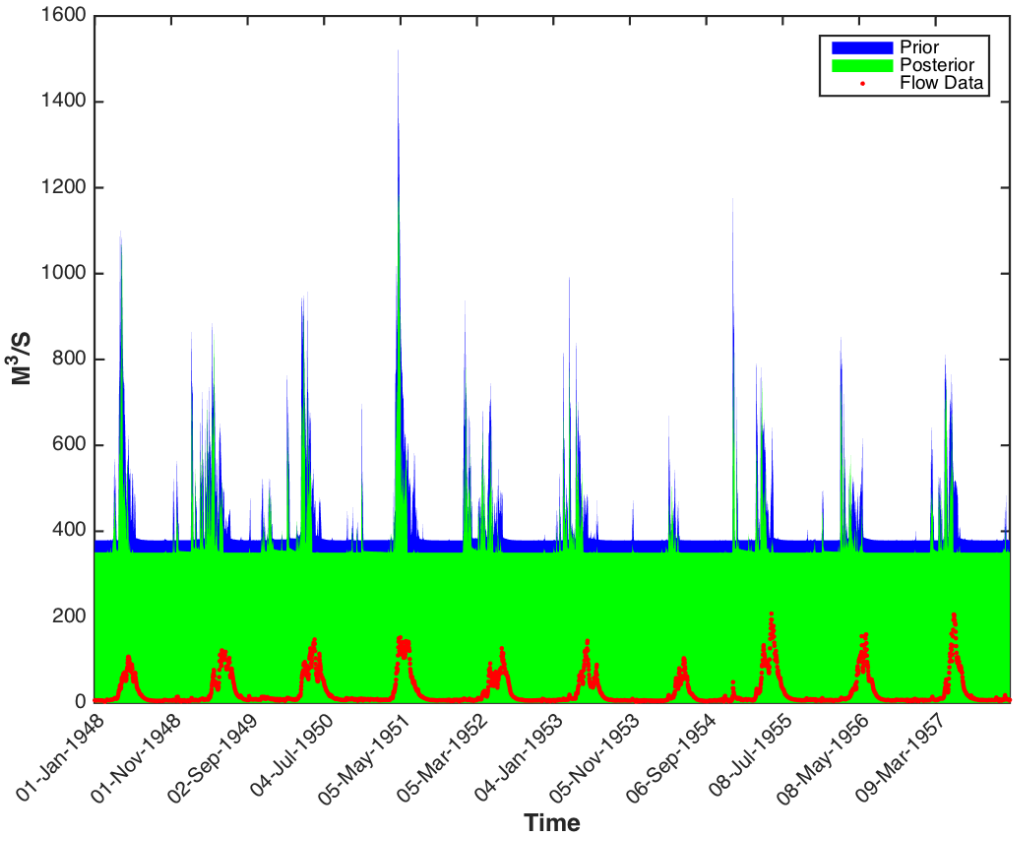

Figure 6.12. Predictive uncertainty ranges of GR4J model constrained against SF Boise watershed (USGS ID 13186000) using Declining LIMB Destiny (DLD) Prior channel inflow in blue, posterior channel flow in green and observed data in red

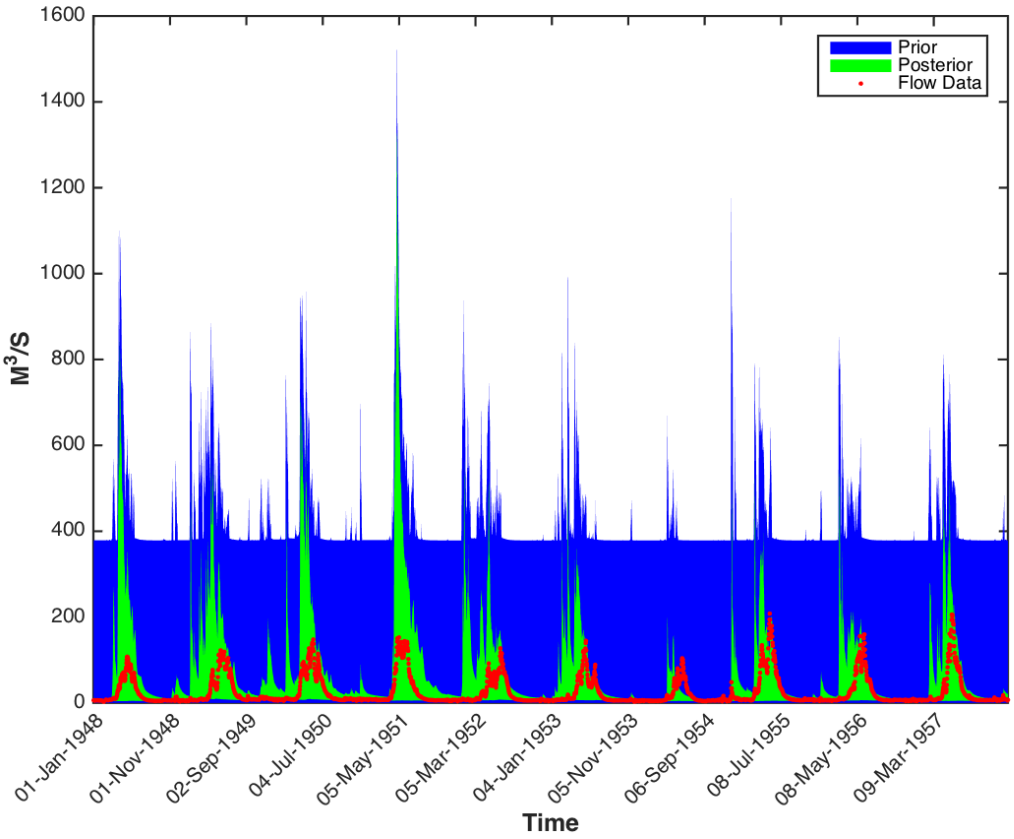

Figure 6.13. Predictive uncertainty ranges of GR4J model constrained against SF Boise watershed (USGS ID 13186000) using 1st Flow Percentile (Q1st) Prior channel inflow in blue, posterior channel flow in green and observed data in red

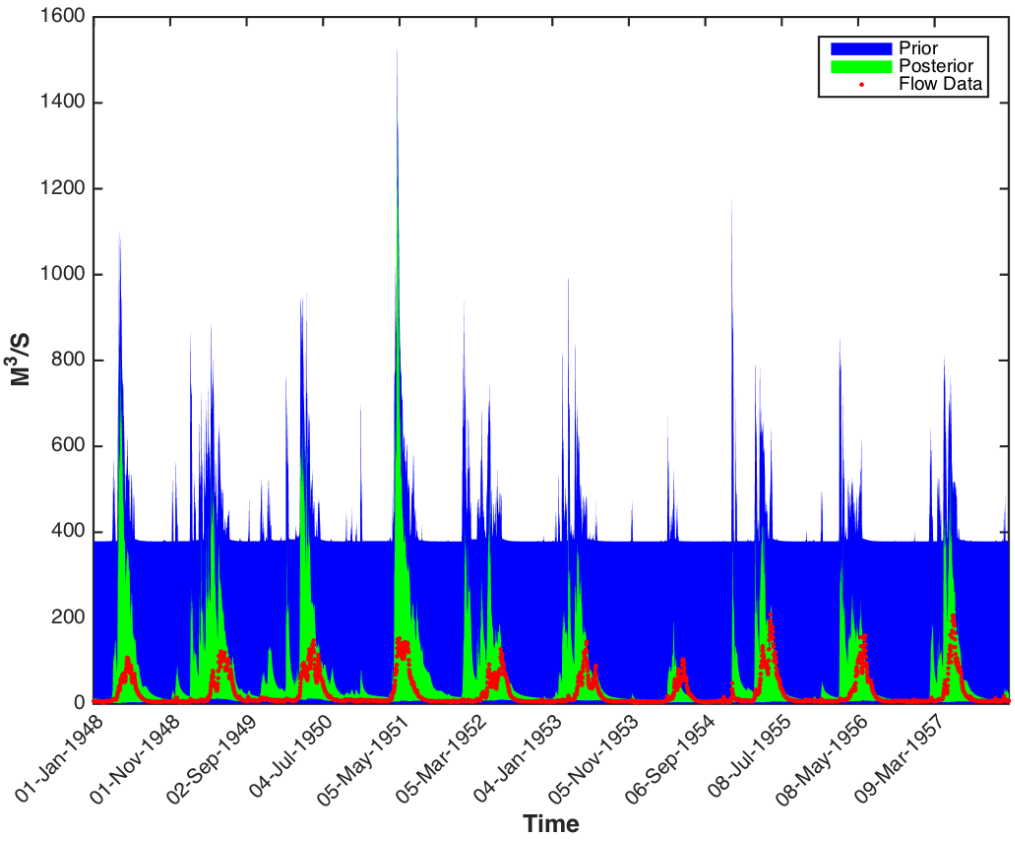

Figure 6.14. Predictive uncertainty ranges of GR4J model constrained against SF Boise watershed (USGS ID 13186000) using 5th Flow Percentile (Q5th) Prior channel inflow in blue, posterior channel flow in green and observed data in red

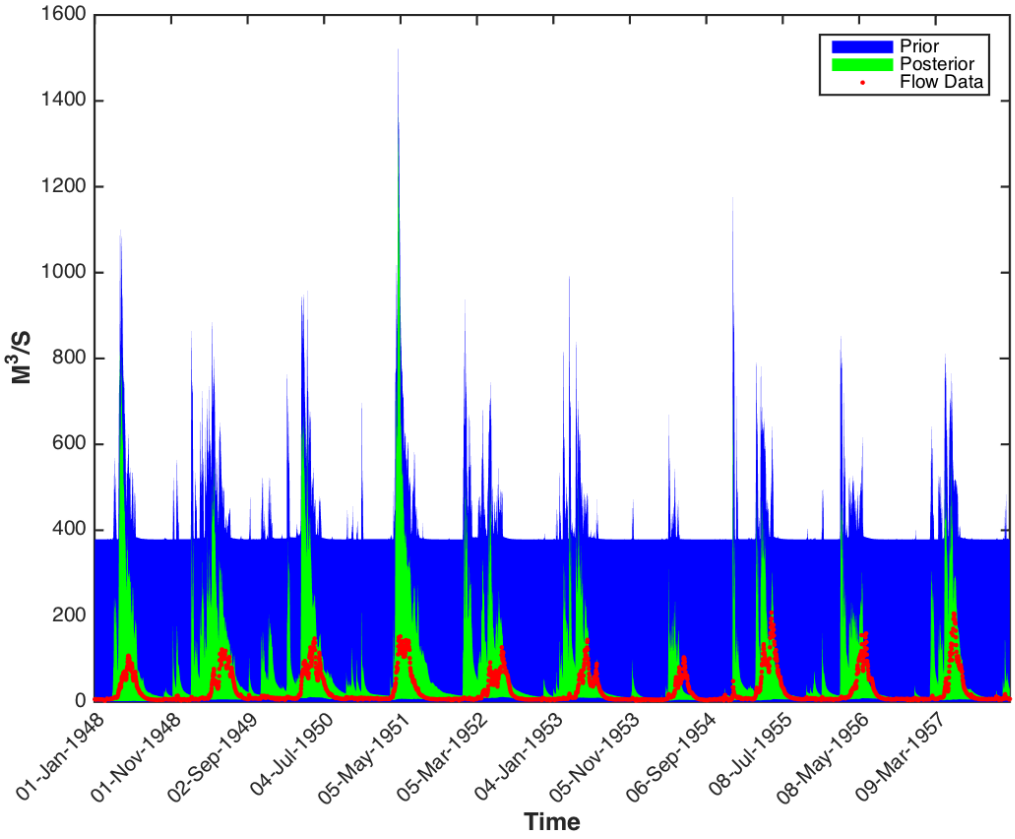

Figure 6.15. Predictive uncertainty ranges of GR4J model constrained against SF Boise watershed (USGS ID 13186000) using 15th Flow Percentile (Q15th) Prior channel inflow in blue, posterior channel flow in green and observed data in red

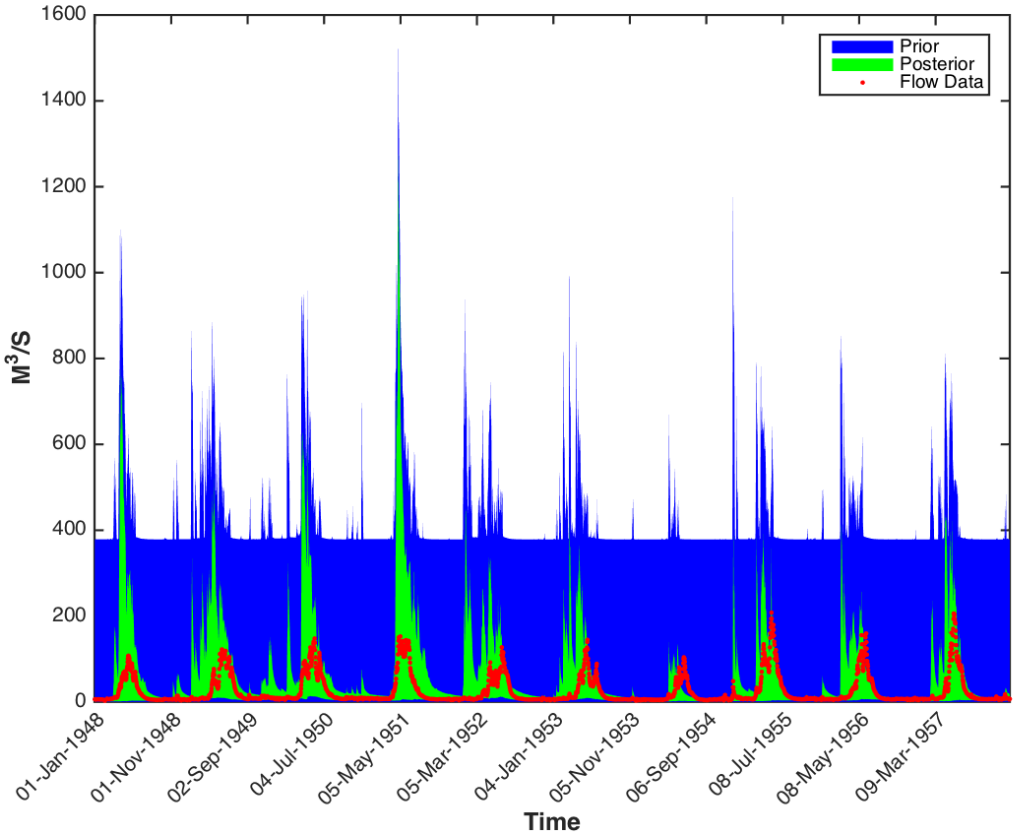

Figure 6.16. Predictive uncertainty ranges of GR4J model constrained against SF Boise watershed (USGS ID 13186000) using 50th Flow Percentile (Q50th) Prior channel inflow in blue, posterior channel flow in green and observed data in red

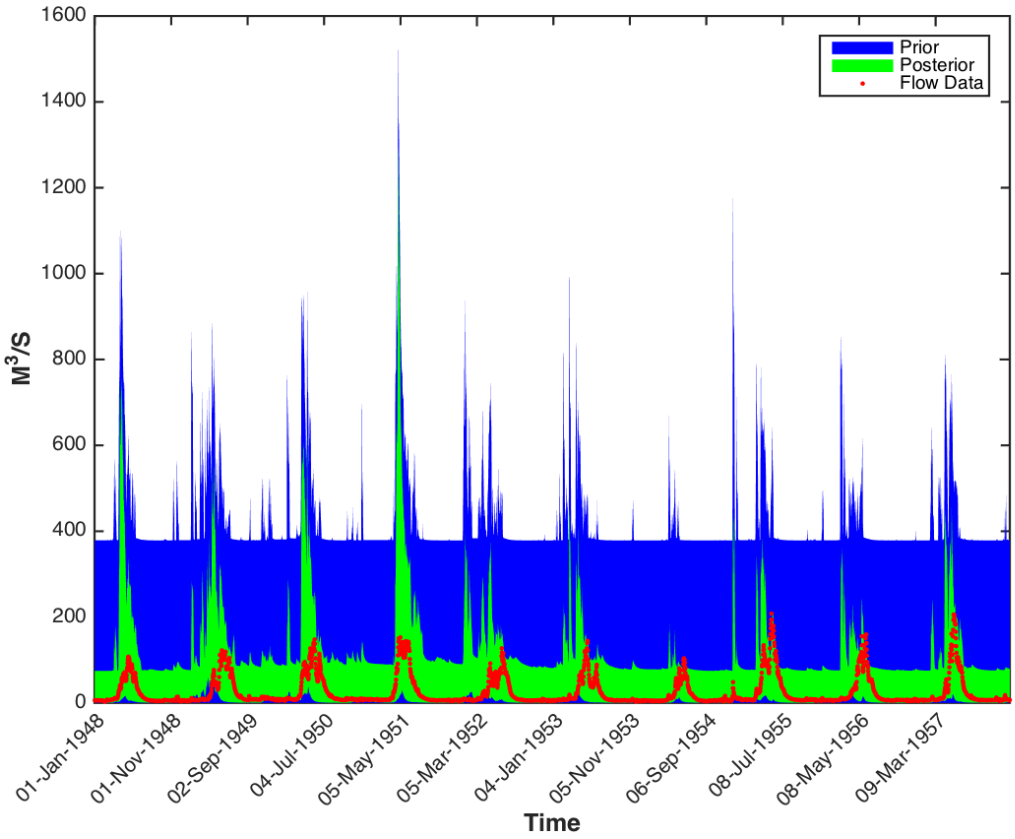

Figure 6.17. Predictive uncertainty ranges of GR4J model constrained against SF Boise watershed (USGS ID 13186000) using 95th Flow Percentile (Q95th) Prior channel inflow in blue, posterior channel flow in green and observed data in red

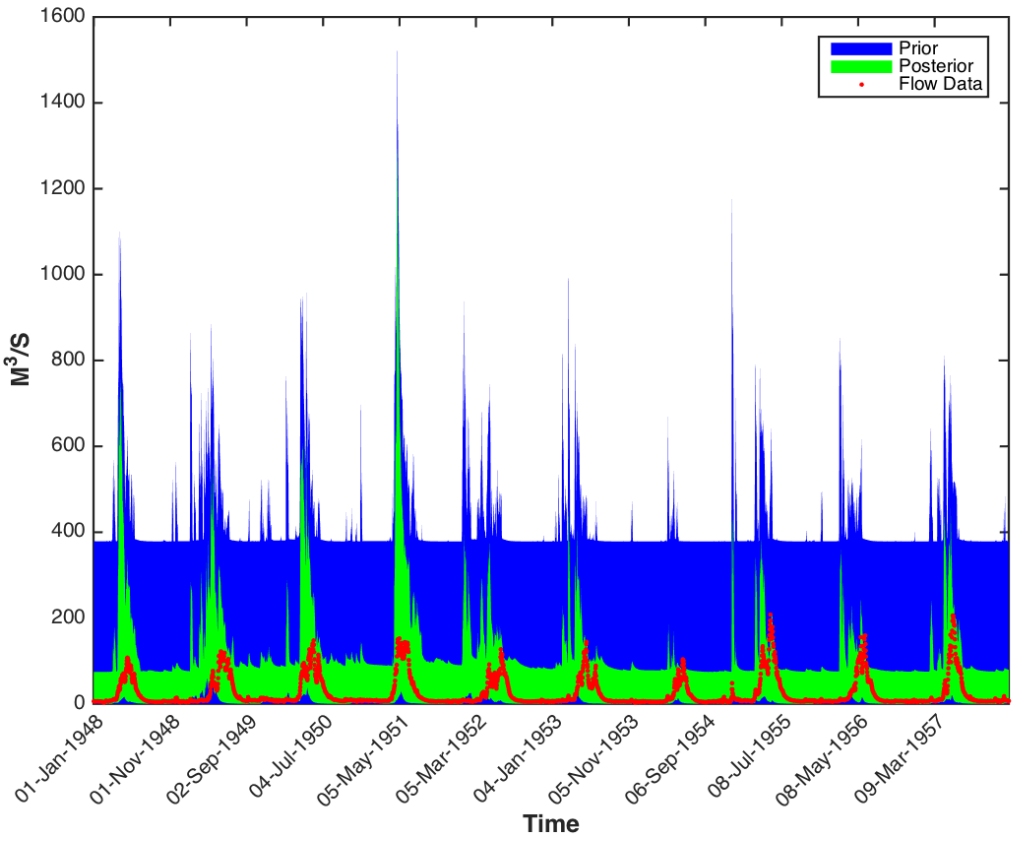

Figure 6.18. Predictive uncertainty ranges of GR4J model constrained against SF Boise watershed (USGS ID 13186000) using 99th Flow Percentile (Q99th) Prior channel inflow in blue, posterior channel flow in green and observed data in red

13186000 HYMOD

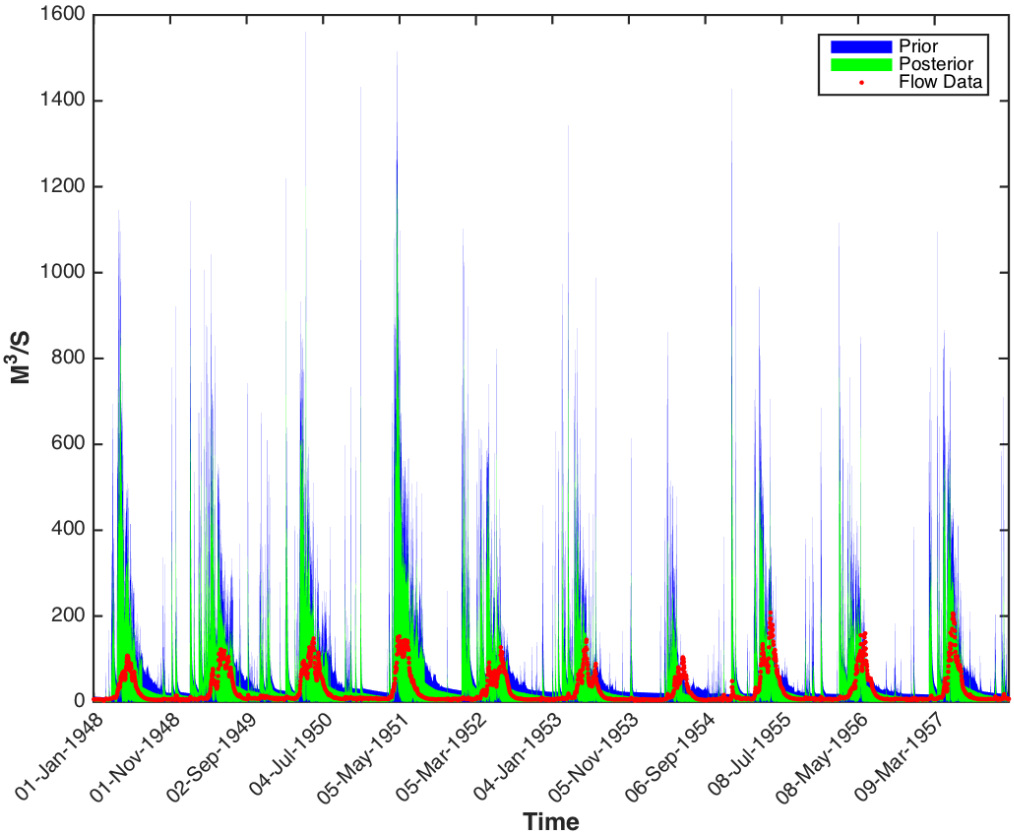

Figure 6.18. Predictive uncertainty ranges of HyMod model constrained against SF Boise watershed (USGS ID 13186000) using Runoff Ratio Metric (RR). Prior channel inflow in blue, posterior channel flow in green and observed data in red

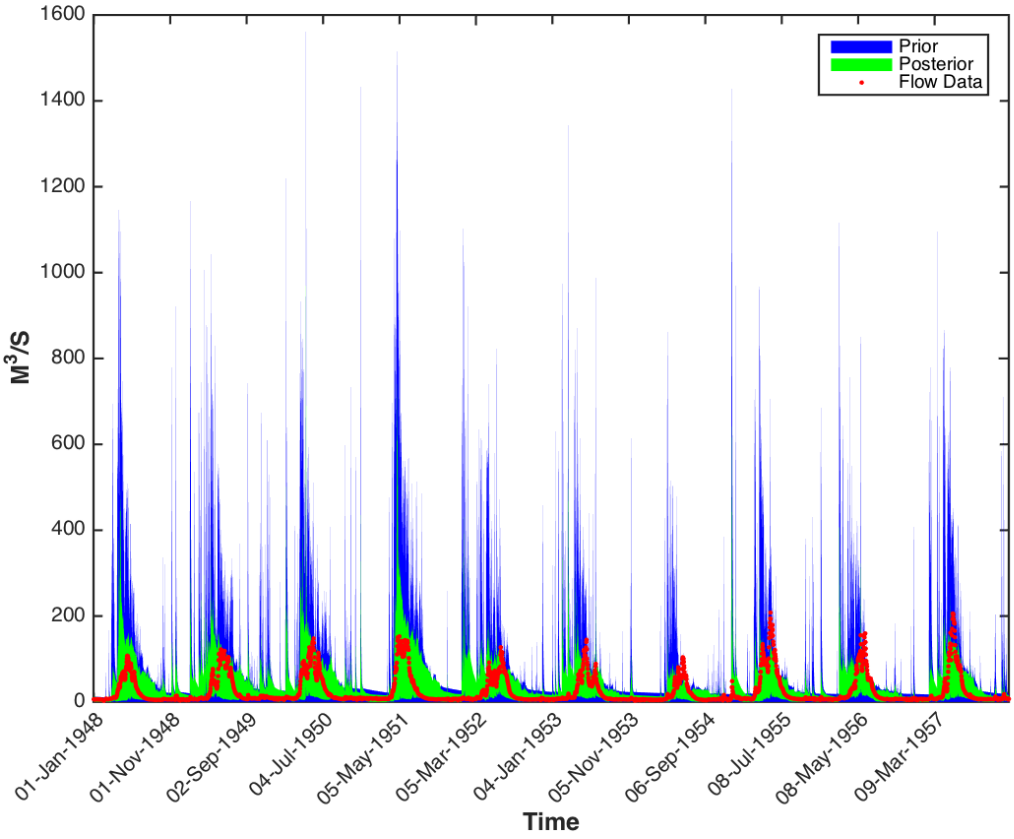

Figure 6.19 Predictive uncertainty ranges of HyMod model constrained against SF Boise watershed (USGS ID 13186000) using Base Flow Index (BFI). Prior channel inflow in blue, posterior channel flow in green and observed data in red

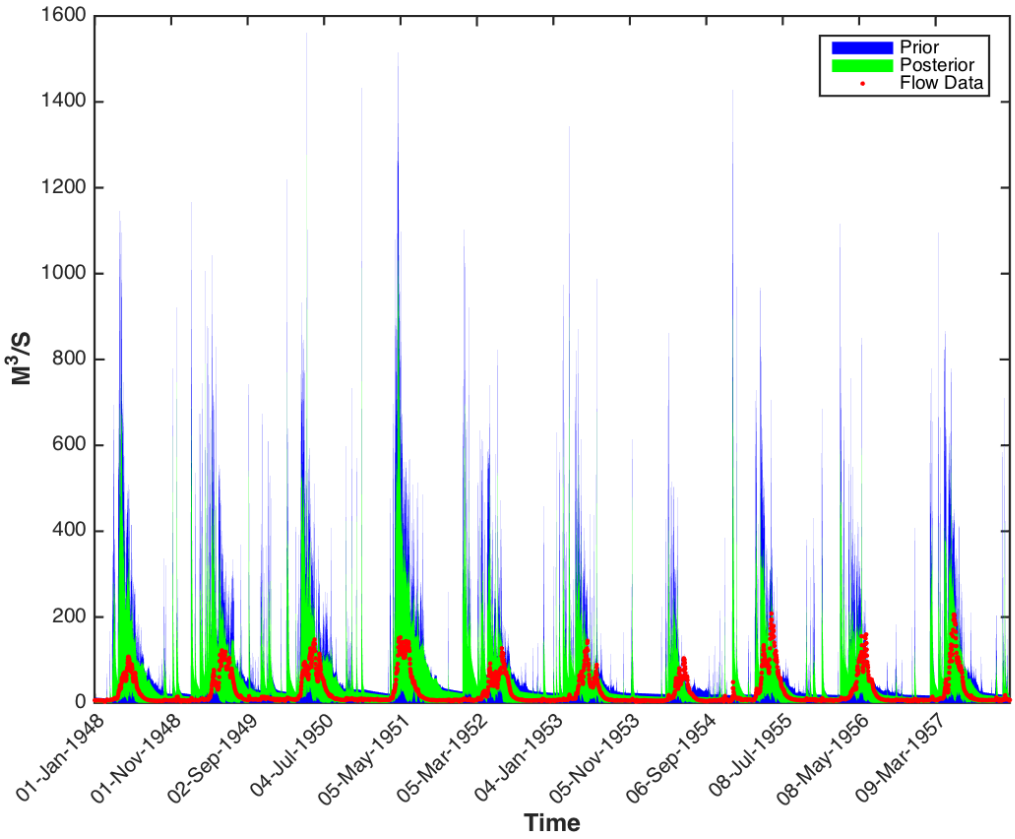

Figure 6.20. Predictive uncertainty ranges of HyMod model constrained against SF Boise watershed (USGS ID 13186000) using Base Flow Runoff Ratio (BFR). Prior channel inflow in blue, posterior channel flow in green and observed data in red

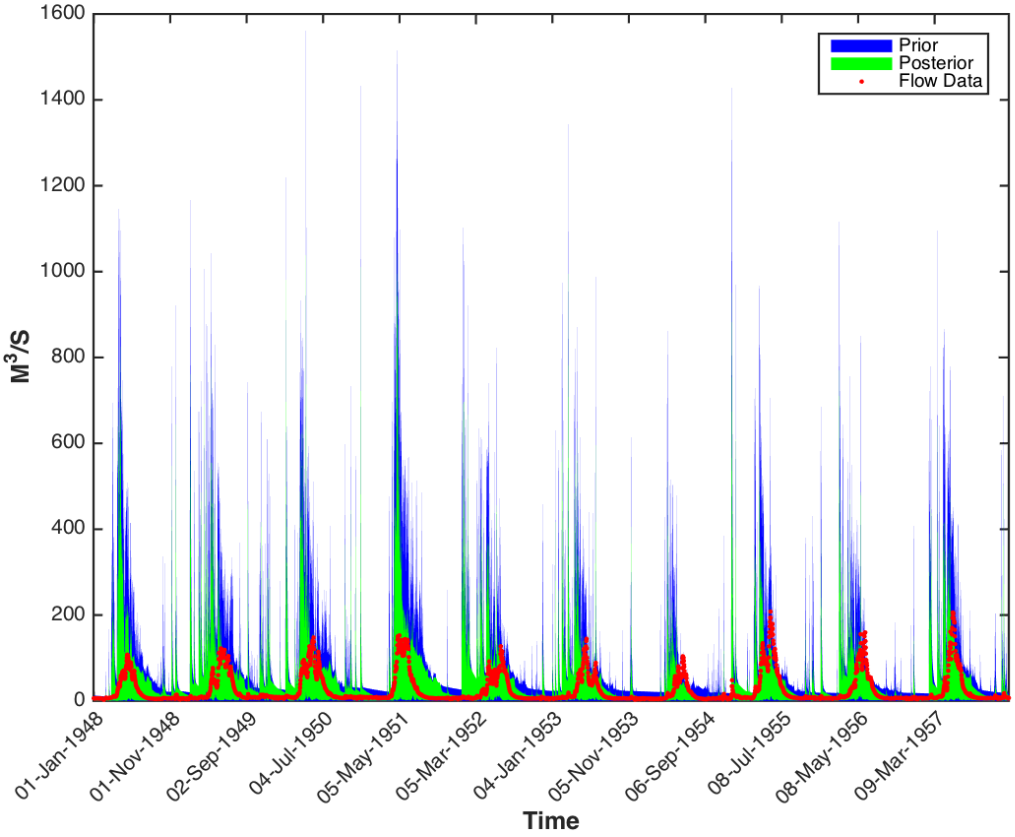

Figure 6.21. Predictive uncertainty ranges of HyMod model constrained against SF Boise watershed (USGS ID 13186000) using Slope of Log FDC 5th & 95th Percentile (SL FDC Q5th&Q95th). Prior channel inflow in blue, posterior channel flow in green and observed data in red

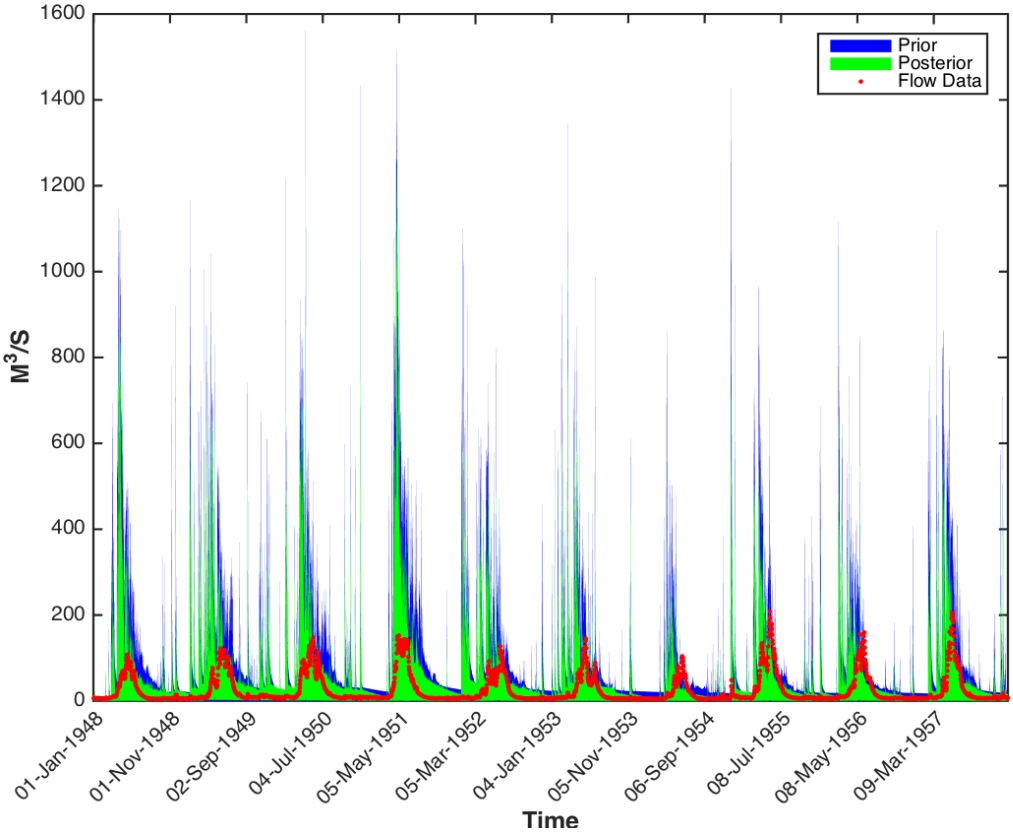

Figure 6.22. Predictive uncertainty ranges of HyModJ model constrained against SF Boise watershed (USGS ID 13186000) using Slope of Log FDC 5& 95 Percentile (SL Q33th&Q66th). Prior channel inflow in blue, posterior channel flow in green and observed data in red

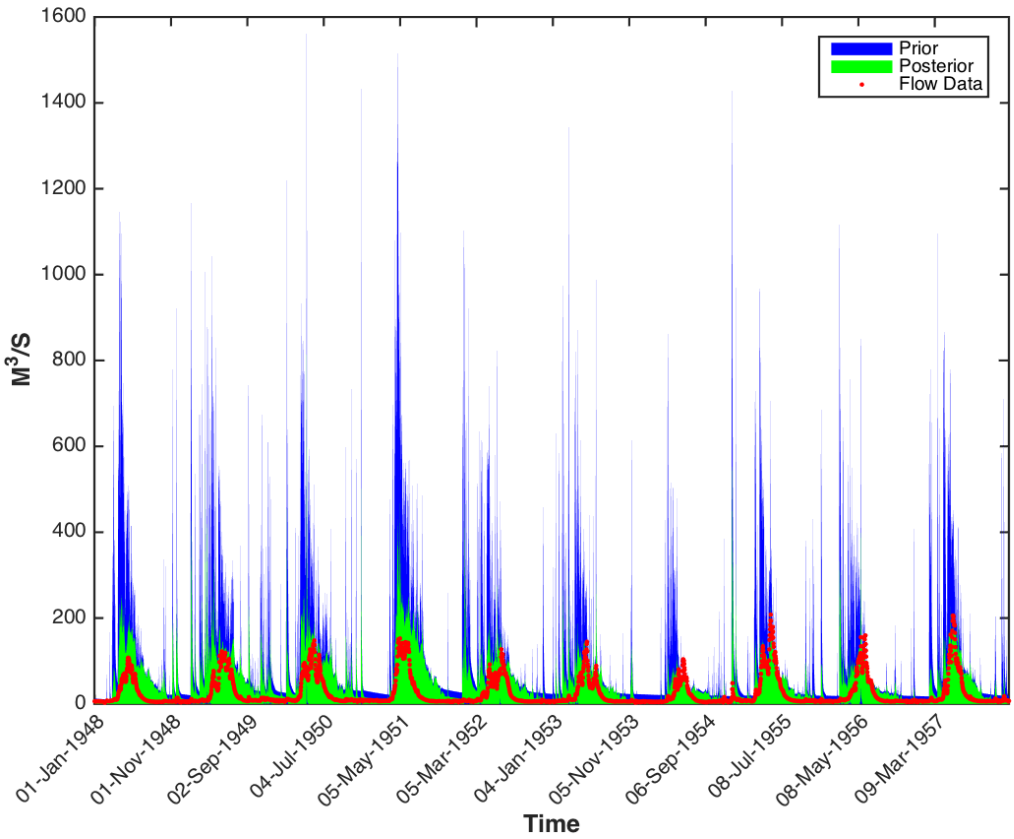

Figure 6.23. Predictive uncertainty ranges of HyMod model constrained against SF Boise watershed (USGS ID 13186000) using Slope of Log FDC 20 & 70 Percentile (SL FDC Q20th&Q70th). Prior channel inflow in blue, posterior channel flow in green and observed data in red

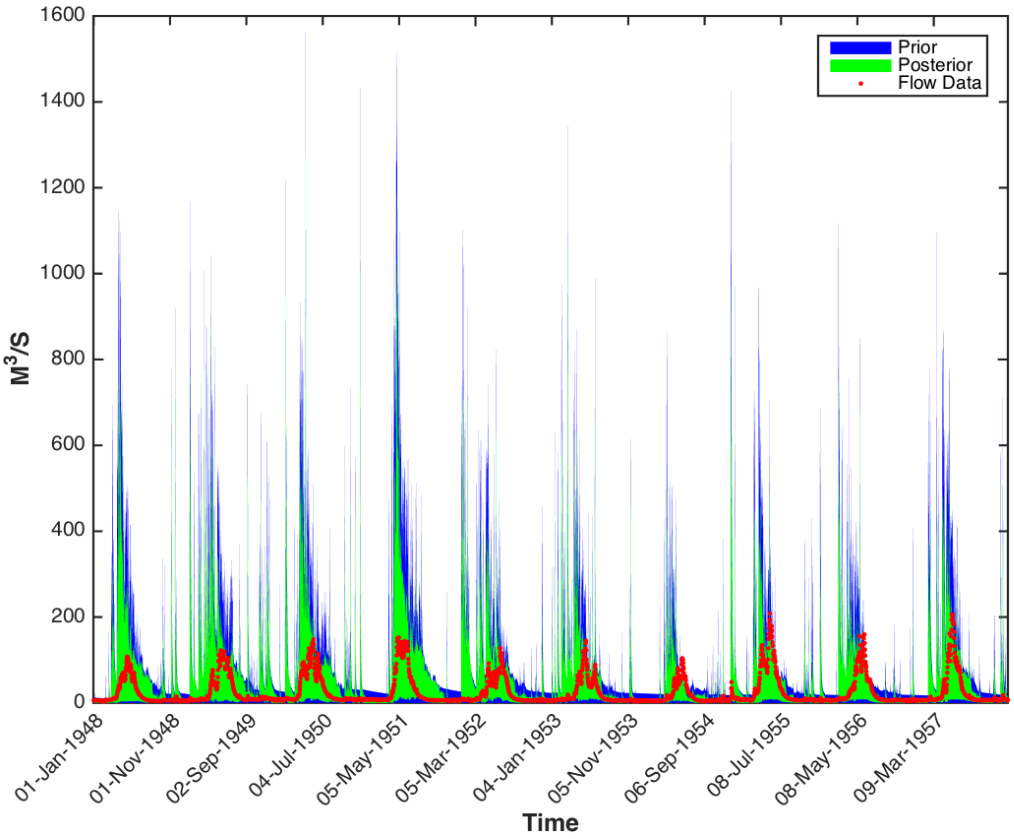

Figure6.24. Predictive uncertainty ranges of HyMod model constrained against SF Boise watershed (USGS ID 13186000) using FDC High Segment Volume more than 90 Percentile (FDC HSV Q90th). Prior channel inflow in blue, posterior channel flow in green and observed data in red

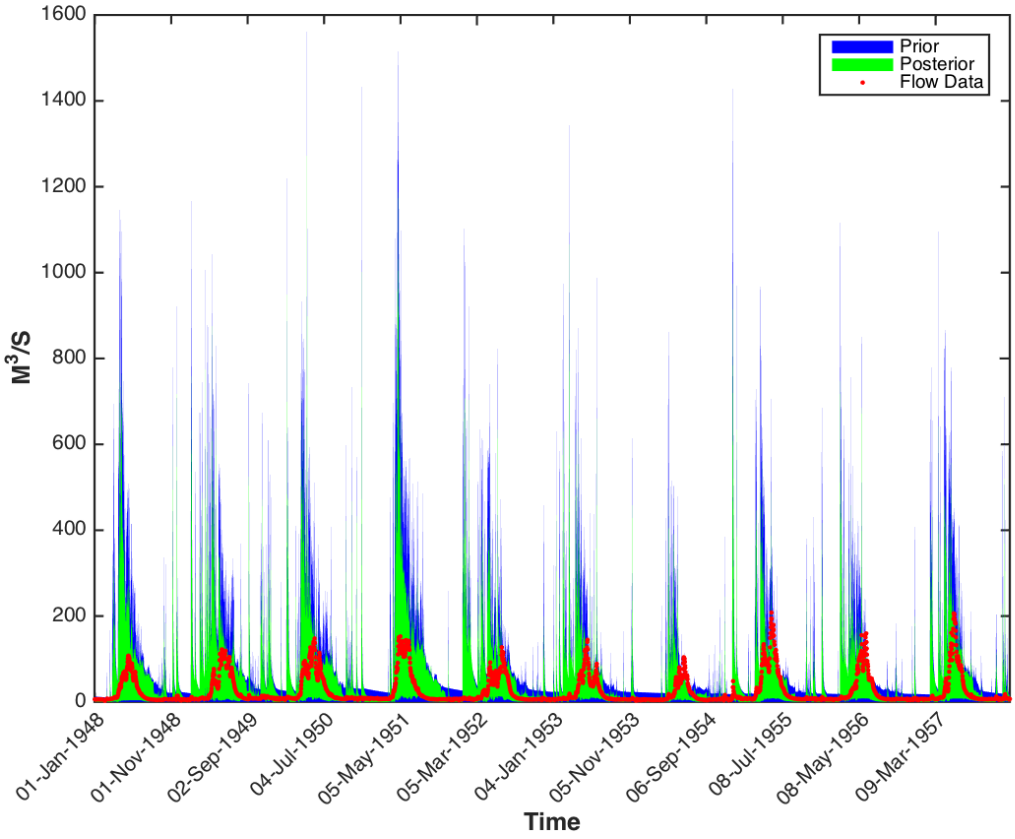

Figure 6.26.. Predictive uncertainty ranges of HyMod model constrained against SF Boise watershed (USGS ID 13186000) using FDC Medium Segment Volume (FDC MSV) Prior channel inflow in blue, posterior channel flow in green and observed data in red

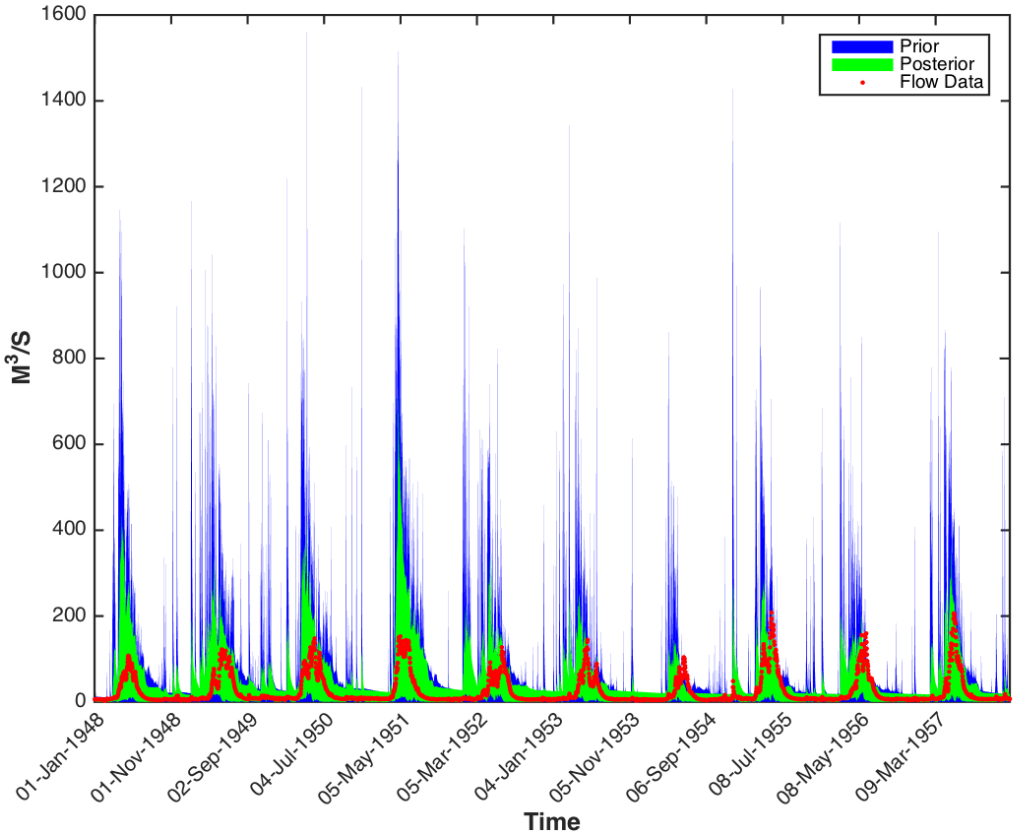

Figure6.27.. Predictive uncertainty ranges of HyMod model constrained against SF Boise watershed (USGS ID 13186000) Auto Correlation of Hydrograph with 1 Day Lag (AC) Prior channel inflow in blue, posterior channel flow in green and observed data in red

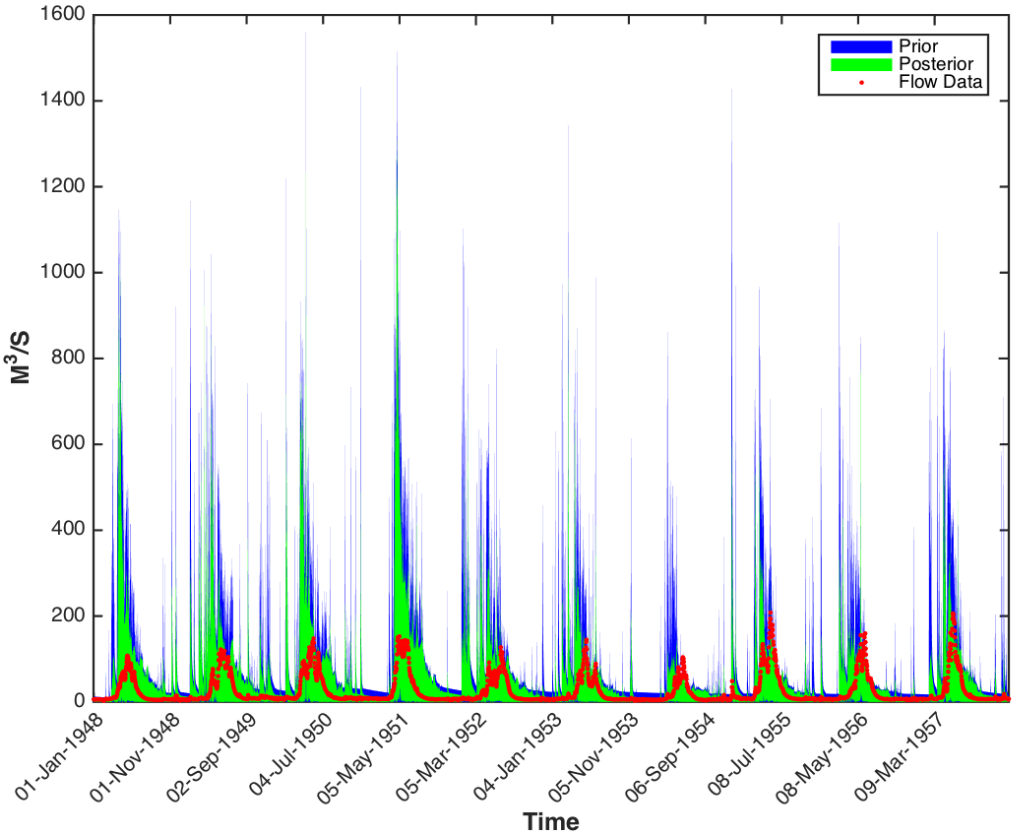

Figure 6.28. Predictive uncertainty ranges of HyMod model constrained against SF Boise watershed (USGS ID 13186000) Peak Distribution (Slope of Peak Flows) (PD) Prior channel inflow in blue, posterior channel flow in green and observed data in red

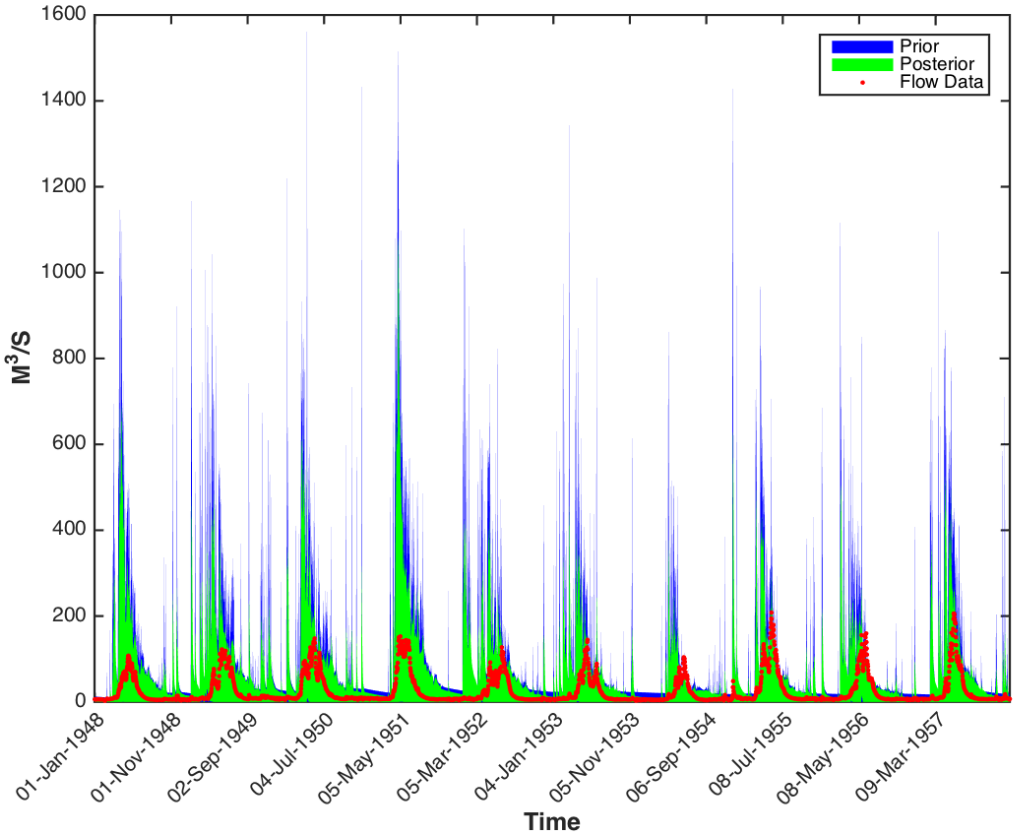

Figure 6.29. Predictive uncertainty ranges of HyMod model constrained against SF Boise watershed (USGS ID 13186000) using Declining LIMB Destiny (RLD) Prior channel inflow in blue, posterior channel flow in green and observed data in red

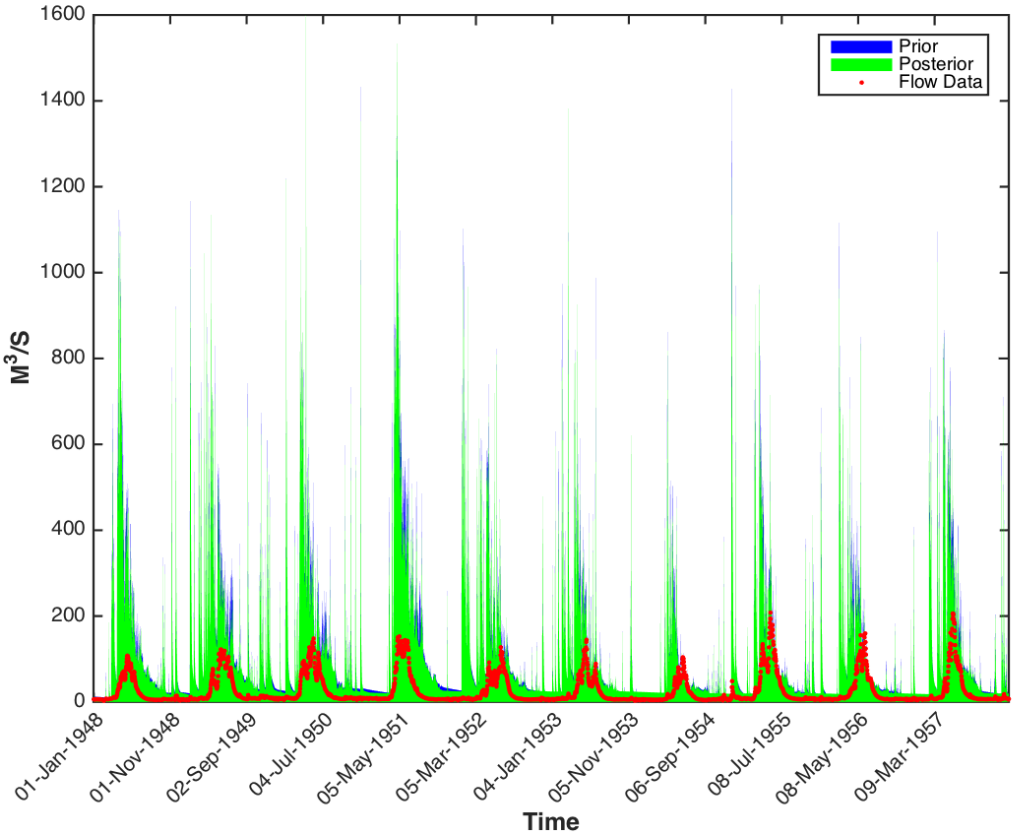

Figure 6.30. Predictive uncertainty ranges of HyMod model constrained against SF Boise watershed (USGS ID 13186000) using Declining LIMB Destiny (DLD) Prior channel inflow in blue, posterior channel flow in green and observed data in red

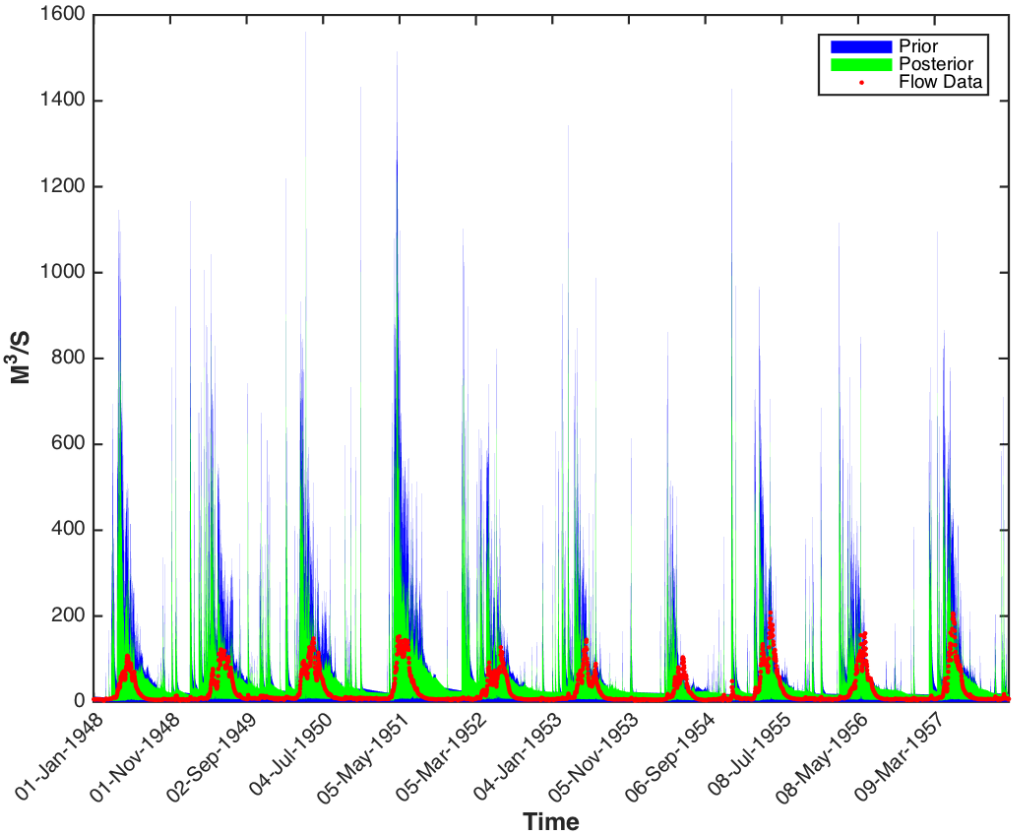

Figure 6.31. Predictive uncertainty ranges of HyMod model constrained against SF Boise watershed (USGS ID 13186000) using 1st Flow Percentile (Q1st) Prior channel inflow in blue, posterior channel flow in green and observed data in red

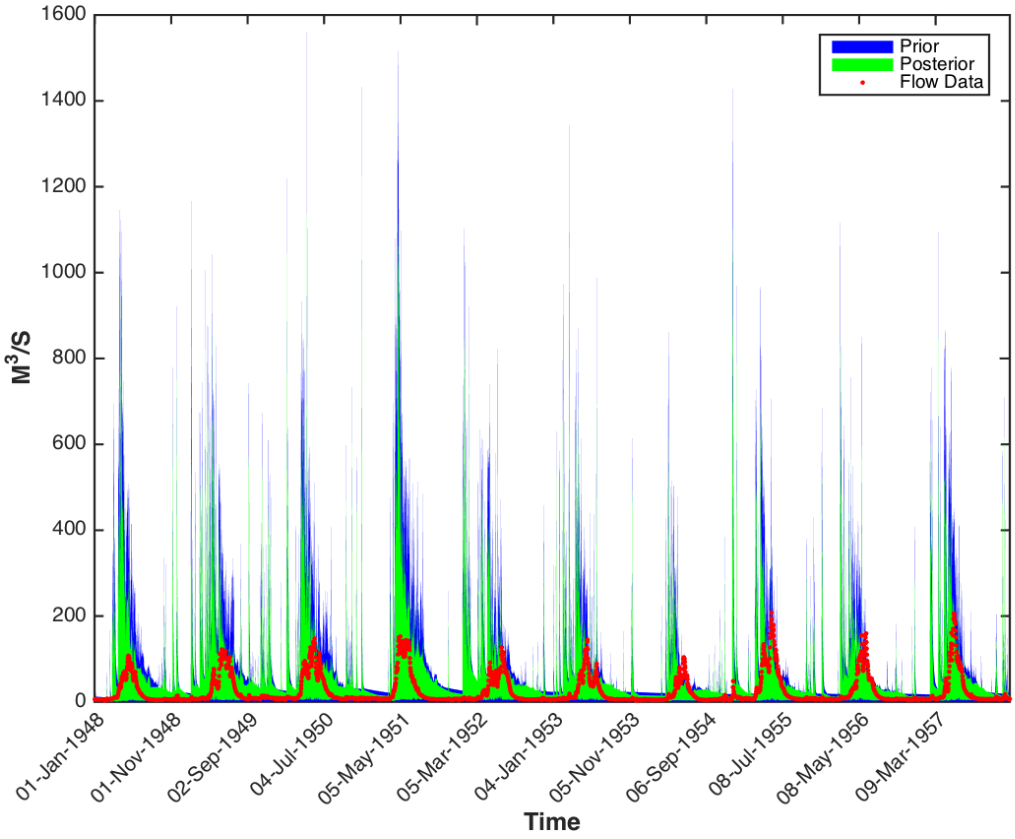

Figure 6.32. Predictive uncertainty ranges of HyMod model constrained against SF Boise watershed (USGS ID 13186000) using 5th Flow Percentile (Q5th) Prior channel inflow in blue, posterior channel flow in green and observed data in red

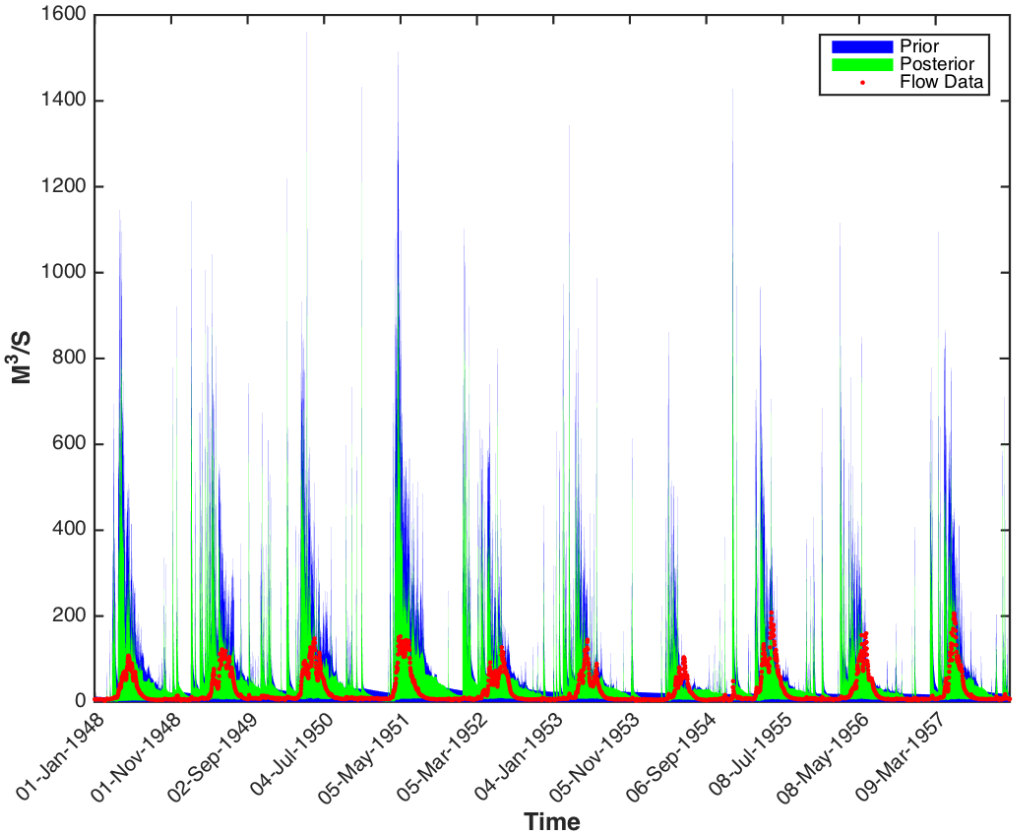

Figure 6.33. Predictive uncertainty ranges of HyMod model constrained against SF Boise watershed (USGS ID 13186000) using 15th Flow Percentile (Q15th) Prior channel inflow in blue, posterior channel flow in green and observed data in red

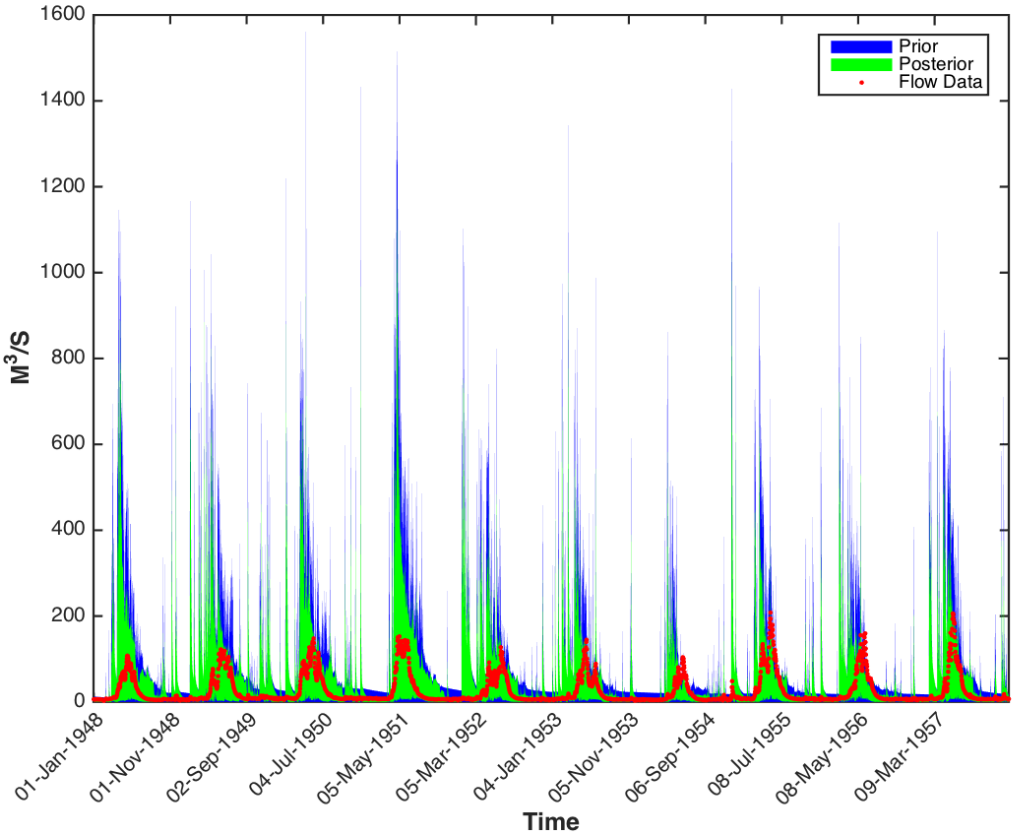

Figure 6.34. Predictive uncertainty ranges of HyMod model constrained against SF Boise watershed (USGS ID 13186000) using 50th Flow Percentile (Q50th) Prior channel inflow in blue, posterior channel flow in green and observed data in red

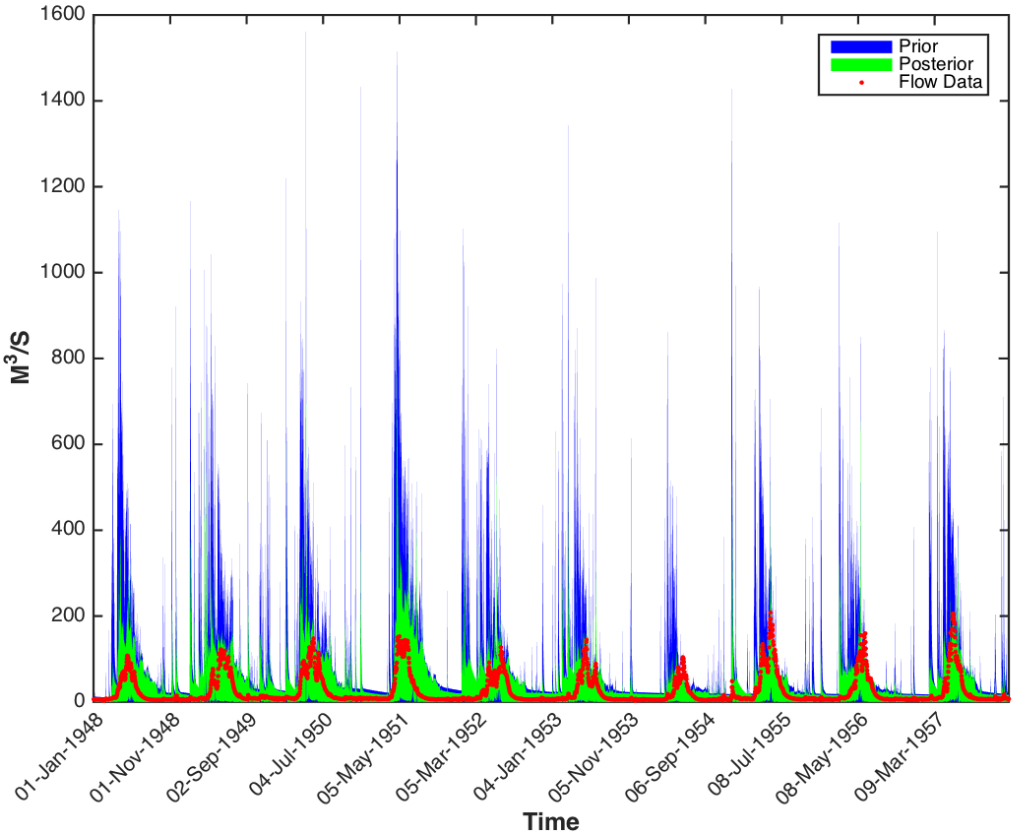

Figure 6.35. Predictive uncertainty ranges of HyMod model constrained against SF Boise watershed (USGS ID 13186000) using 99th Flow Percentile (Q99th) Prior channel inflow in blue, posterior channel flow in green and observed data in red

12134500 GR4J

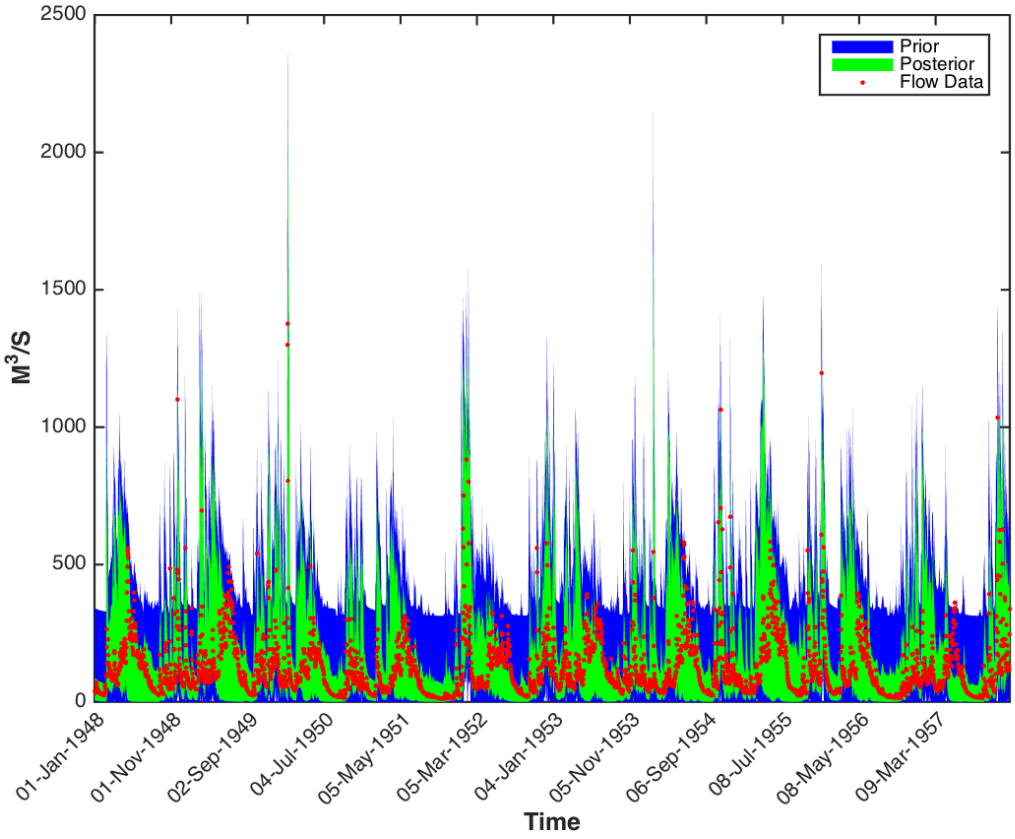

Figure 6.36 Predictive uncertainty ranges of GR4J model constrained against Skykomish watershed (USGS ID 12134500) using Runoff Ratio Metric (RR). Prior channel inflow in blue, posterior channel flow in green and observed data in red

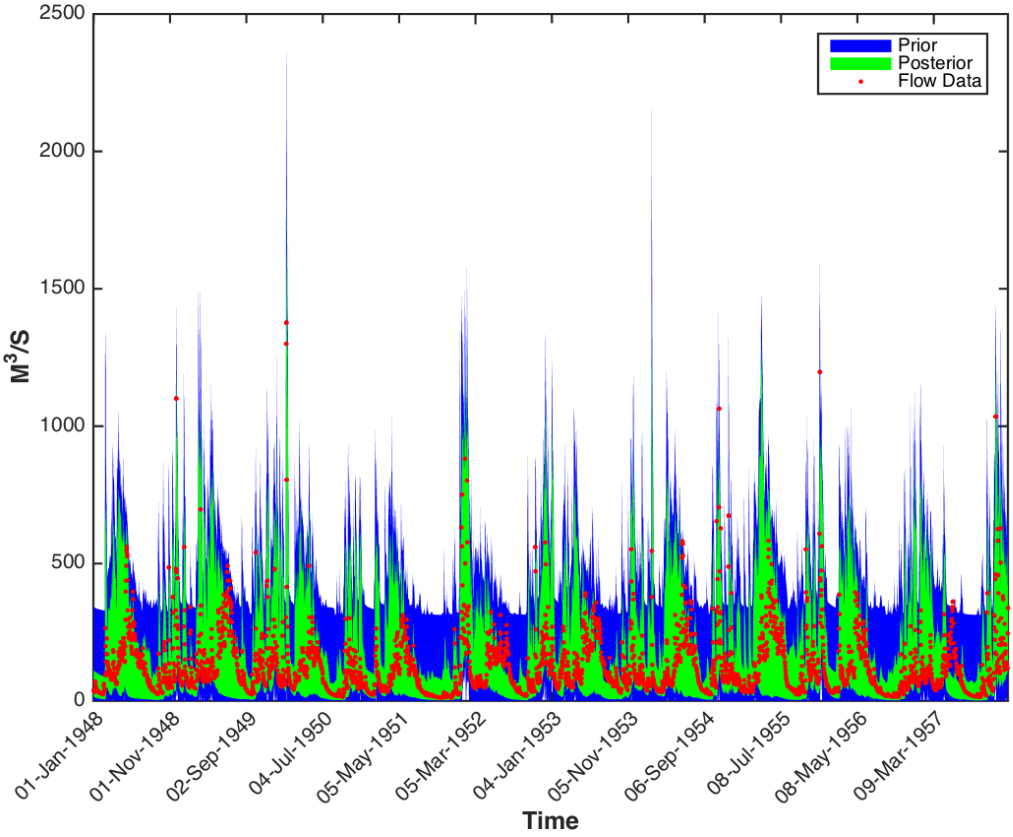
Prior
Posterior
Flow Data
2500
2000
1500
1000
500
0
M3/S
01-Jan-1948
01-Nov-1948
02-Sep-1949
04-Jul-1950
05-May-1951
05-Mar-1952
04-Jan-1953
05-Nov-1953
06-Sep-1954
08-Jul-1955
08-May-1956
09-Mar-1957
Time

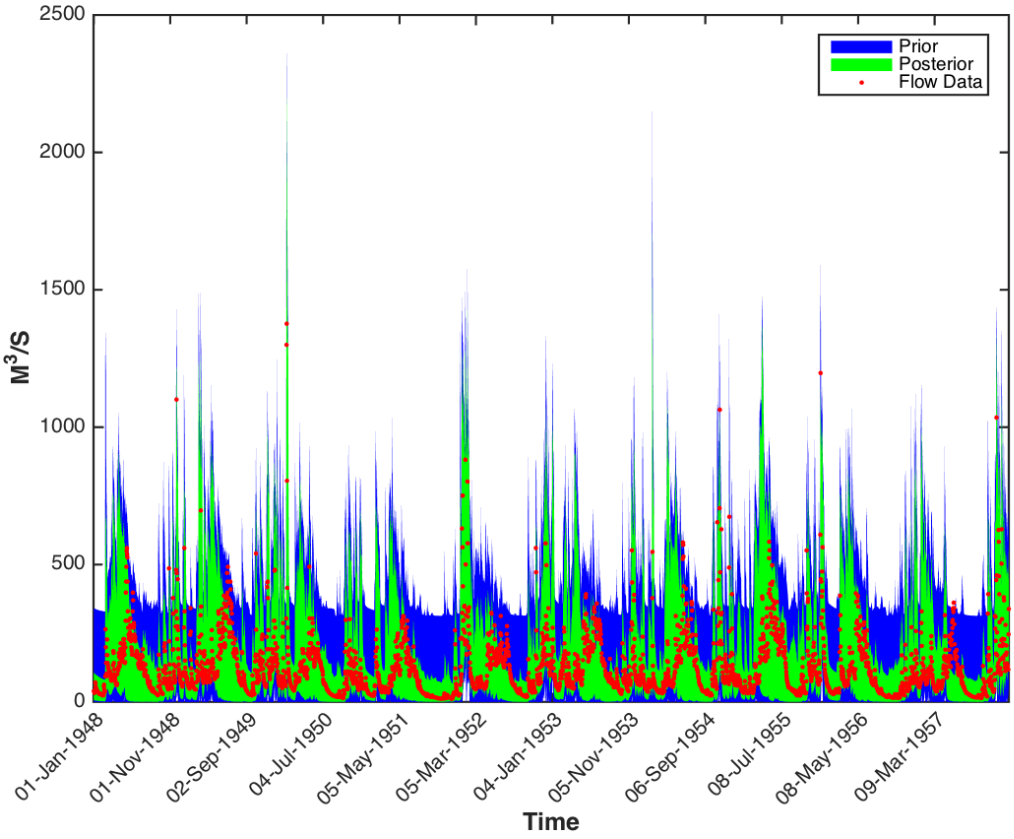
Prior
Posterior
Flow Data
2500
2000
1500
1000
500
0
M3/S
01-Jan-1948
01-Nov-1948
02-Sep-1949
04-Jul-1950
05-May-1951
05-Mar-1952
04-Jan-1953
05-Nov-1953
06-Sep-1954
08-Jul-1955
08-May-1956
09-Mar-1957
Time

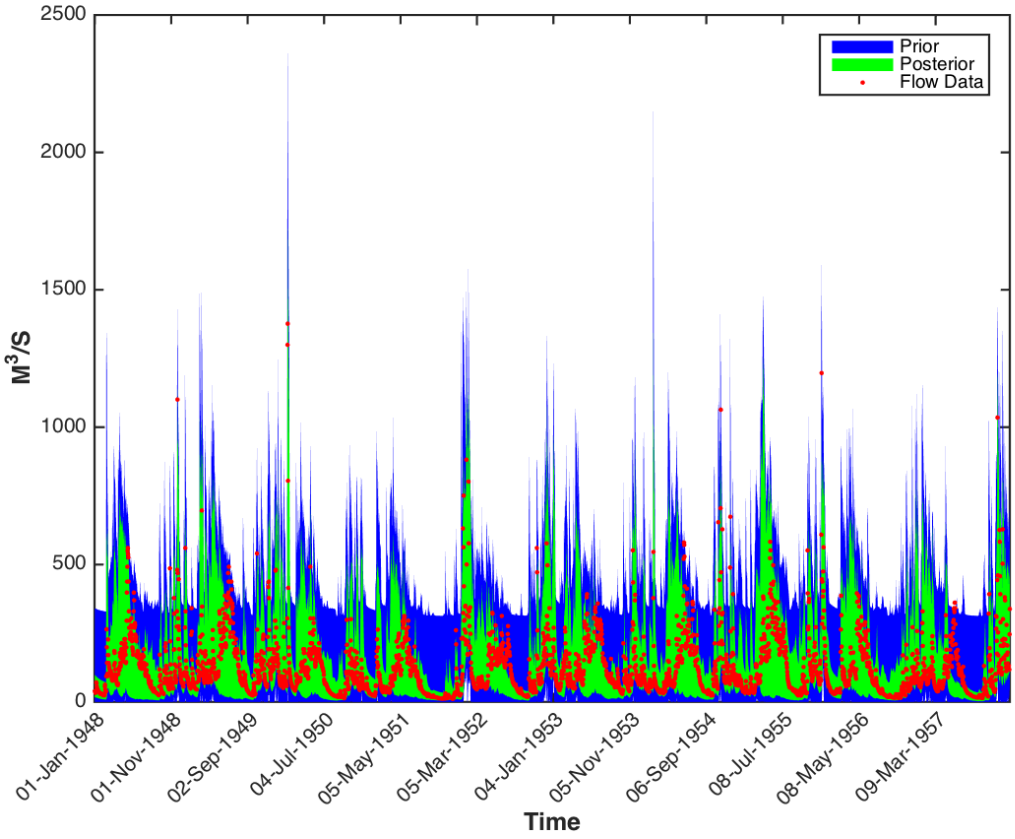

Figure 6.39. .Predictive uncertainty ranges of GR4J model constrained against Skykomish watershed (USGS ID 12134500) using Slope of Log FDC 5th & 95th Percentile (SL FDC Q5th&Q95th). Prior channel inflow in blue, posterior channel flow in green and observed data in red

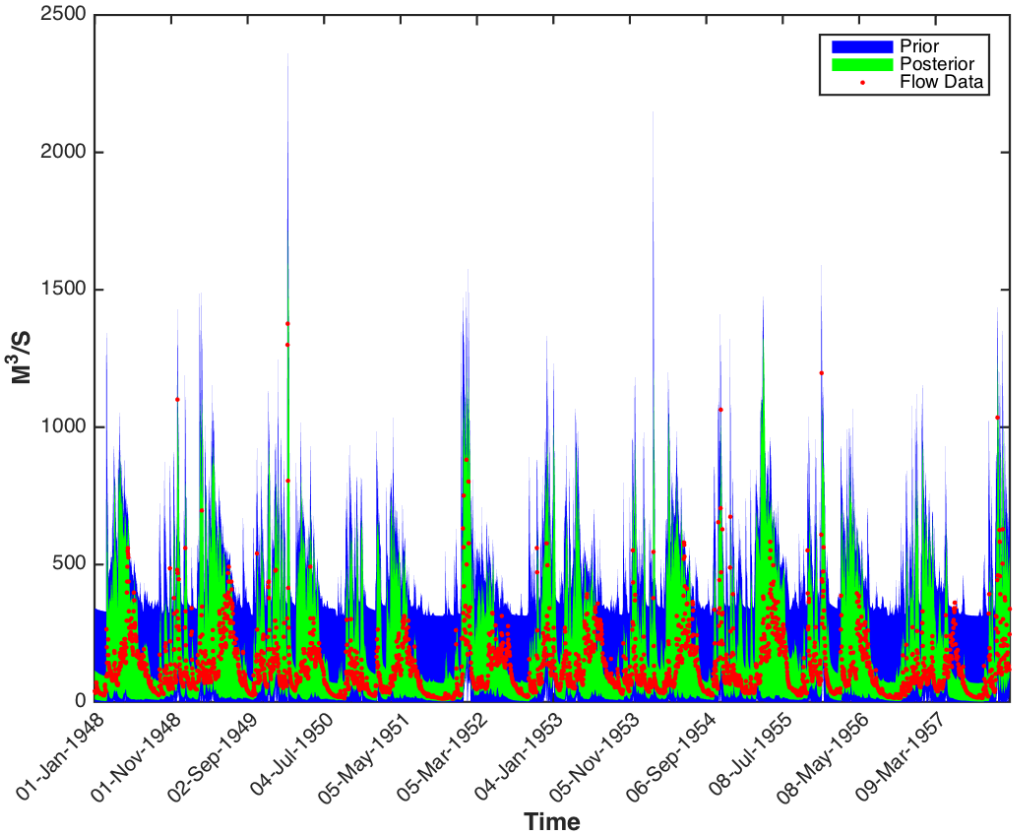

Figure 6.40. Predictive uncertainty ranges of GR4J model constrained against Skykomish watershed (USGS ID 12134500) using Slope of Log FDC 33 & 66 Percentile (SL FDC Q33th&Q66th). Prior channel inflow in blue, posterior channel flow in green and observed data in red

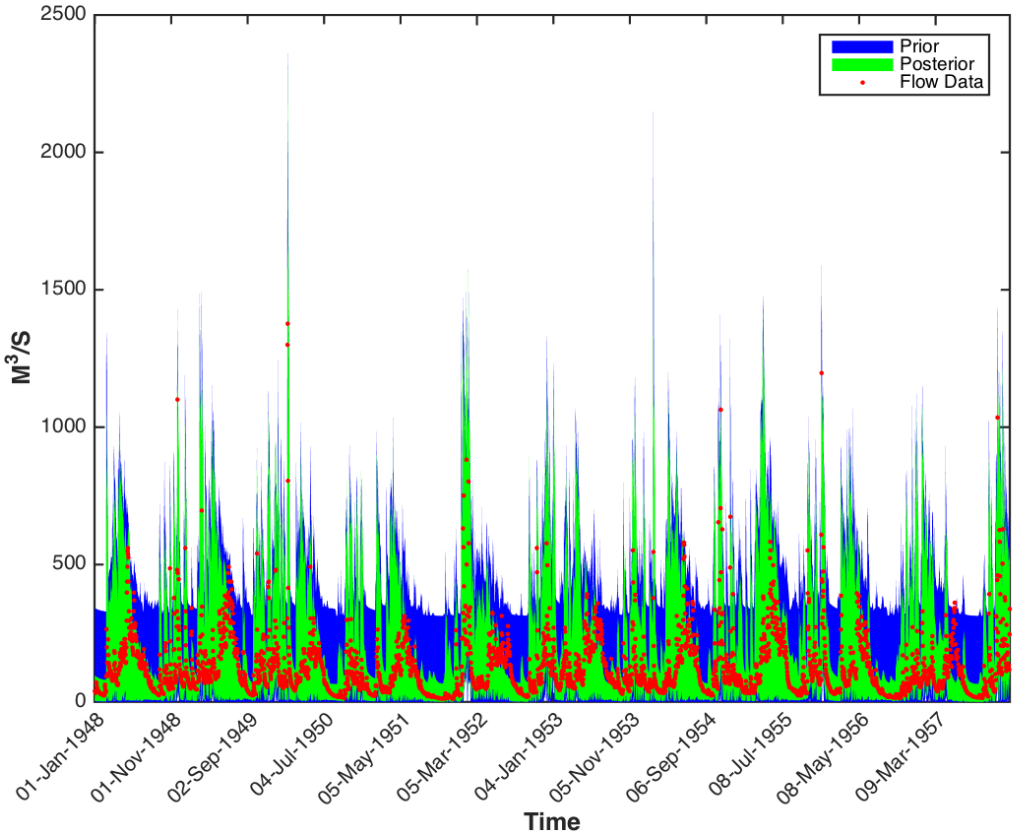

Figure 6.41. Predictive uncertainty ranges of GR4J model constrained against Skykomish watershed (USGS ID 12134500) using Slope of Log FDC 20 & 70 Percentile (SL FDC $Q20^{th}$&$Q70^{th}$). Prior channel inflow in blue, posterior channel flow in green and observed data in red

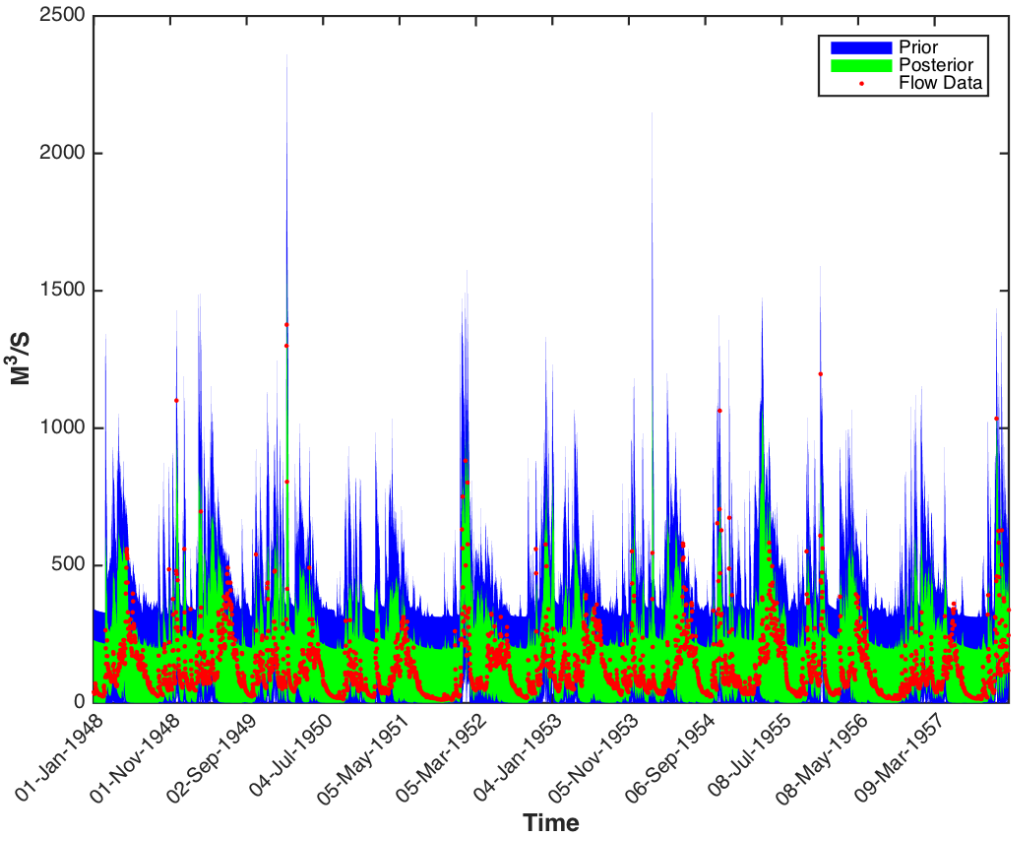
Prior
Posterior
Flow Data
M3/S
2500
2000
1500
1000
500
0
01-Jan-1948
01-Nov-1948
02-Sep-1949
04-Jul-1950
05-May-1951
05-Mar-1952
04-Jan-1953
05-Nov-1953
06-Sep-1954
08-Jul-1955
08-May-1956
09-Mar-1957
Time

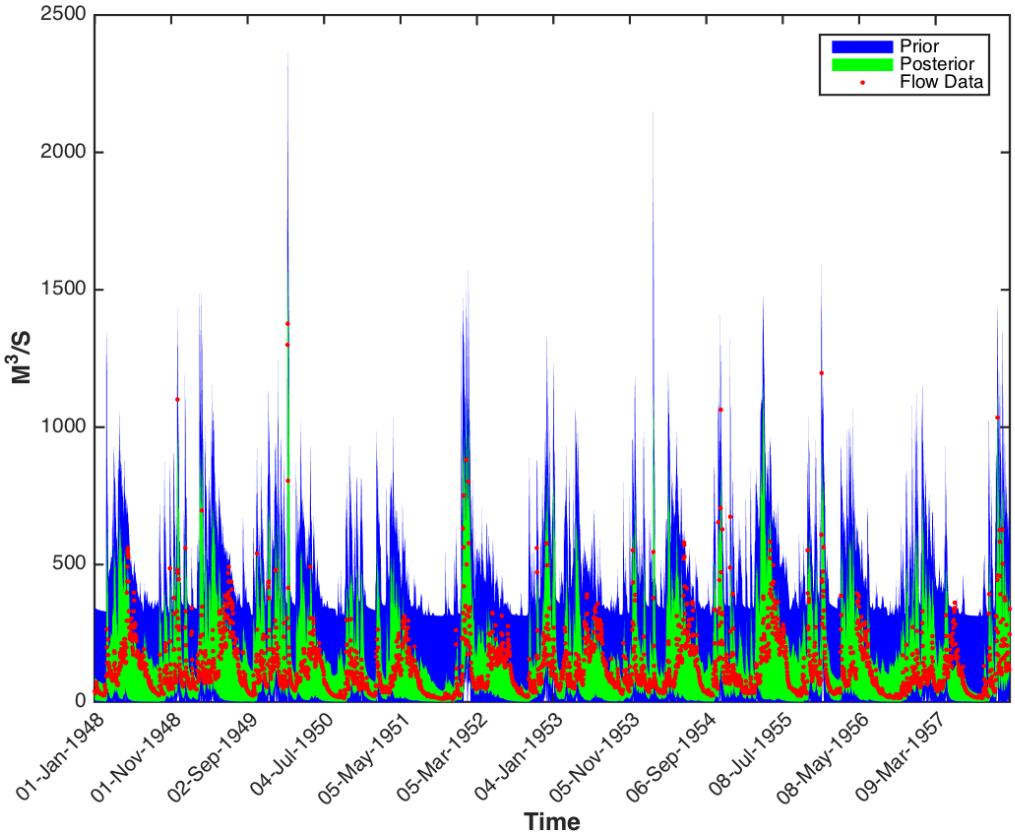

Figure 6.43. Predictive uncertainty ranges of GR4J model constrained against Skykomish watershed (USGS ID 12134500) using FDC Low Segment Volume less than 30 Percentile (FDC LSV Q30th) Prior channel inflow in blue, posterior channel flow in green and observed data in red

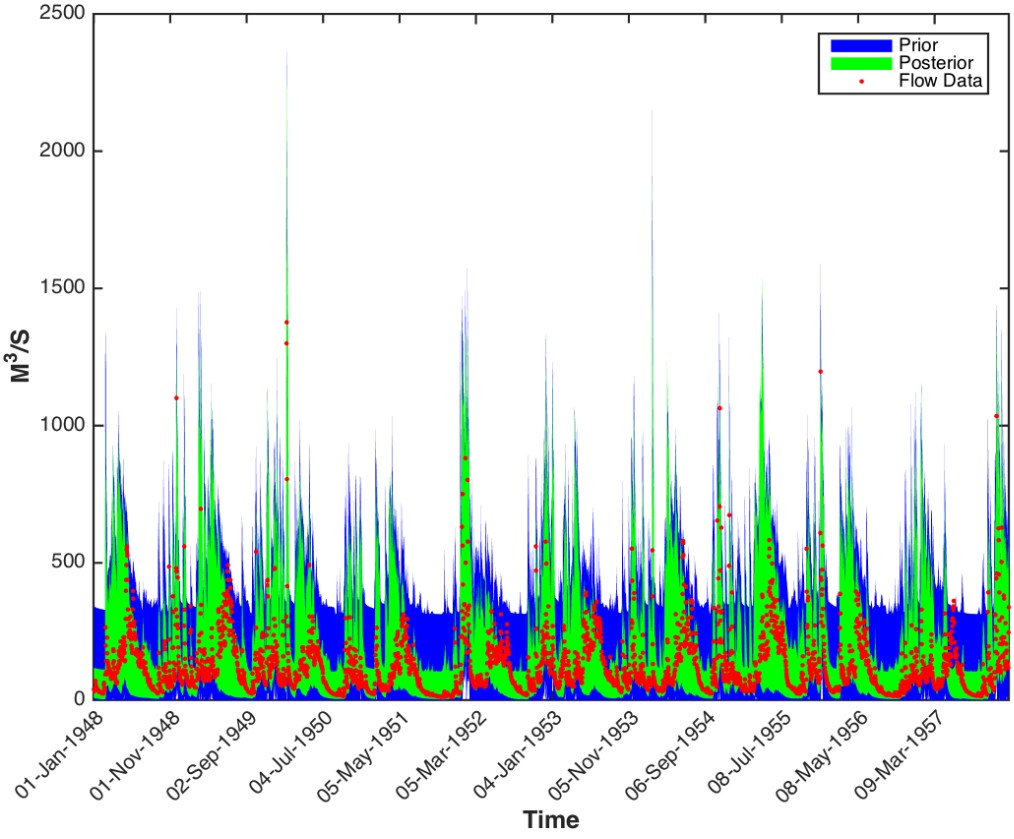
Prior
Posterior
Flow Data
2500
2000
1500
1000
500
0
M3/S
01-Jan-1948
01-Nov-1948
02-Sep-1949
04-Jul-1950
05-May-1951
05-Mar-1952
04-Jan-1953
05-Nov-1953
06-Sep-1954
08-Jul-1955
08-May-1956
09-Mar-1957
Time

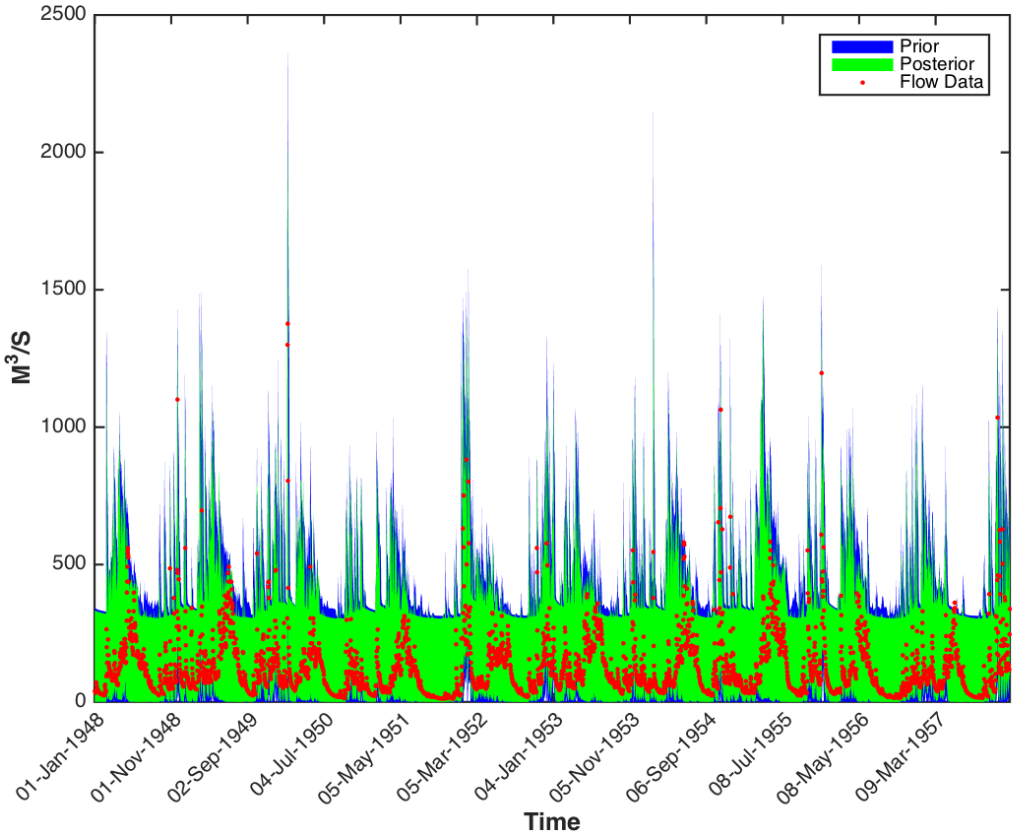

Figure 6.45. Predictive uncertainty ranges of GR4J model constrained against Skykomish watershed (USGS ID 12134500) using Auto Correlation of Hydrograph with 1 Day Lag (AC) Prior channel inflow in blue, posterior channel flow in green and observed data in red

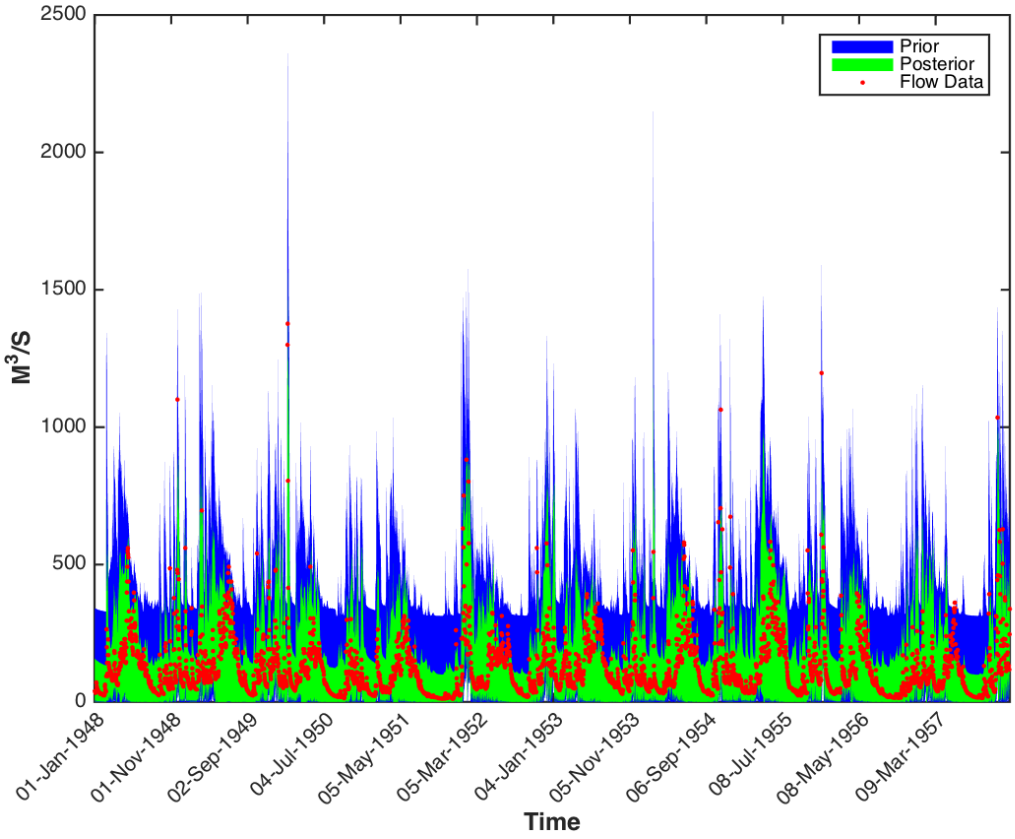

Figure 6.46. Predictive uncertainty ranges of GR4J model constrained against Skykomish watershed (USGS ID 12134500) Peak Distribution (Slope of Peak Flows) (PD) Prior channel inflow in blue, posterior channel flow in green and observed data in red

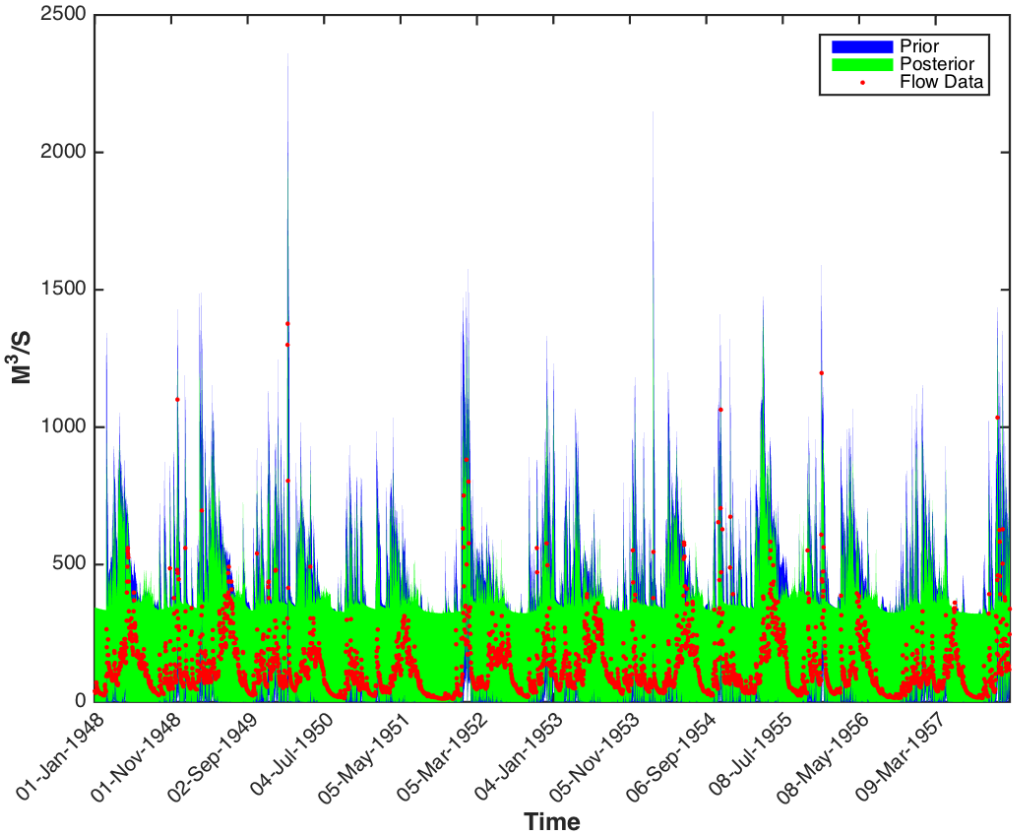

Figure 6.47. Predictive uncertainty ranges of GR4J model constrained against Skykomish watershed (USGS ID 12134500) using Reclining LIMB Destiny (RLD) Prior channel inflow in blue, posterior channel flow in green and observed data in red

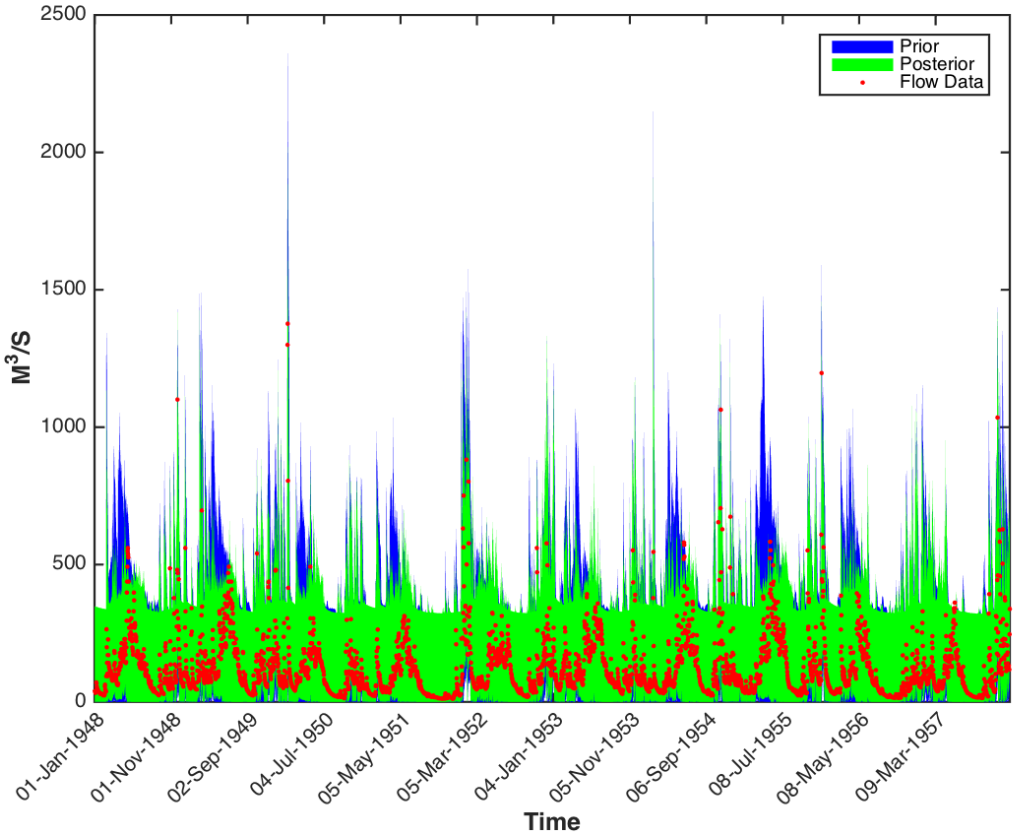

Figure 6.48.. Predictive uncertainty ranges of GR4J model constrained against Skykomish watershed (USGS ID 12134500) using Declining LIMB Destiny (DLD) Prior channel inflow in blue, posterior channel flow in green and observed data in red

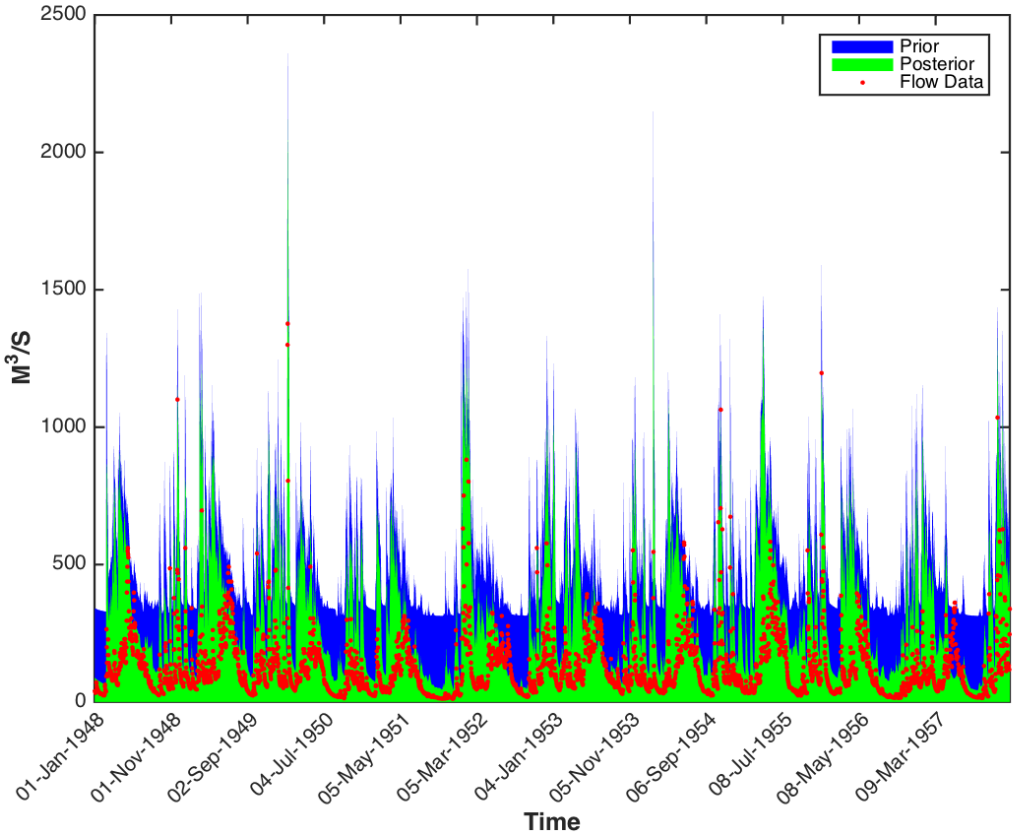

Figure6.49. Predictive uncertainty ranges of GR4J model constrained against Skykomish watershed (USGS ID 12134500) using 1st Flow Percentile (Q1st) Prior channel inflow in blue, posterior channel flow in green and observed data in red

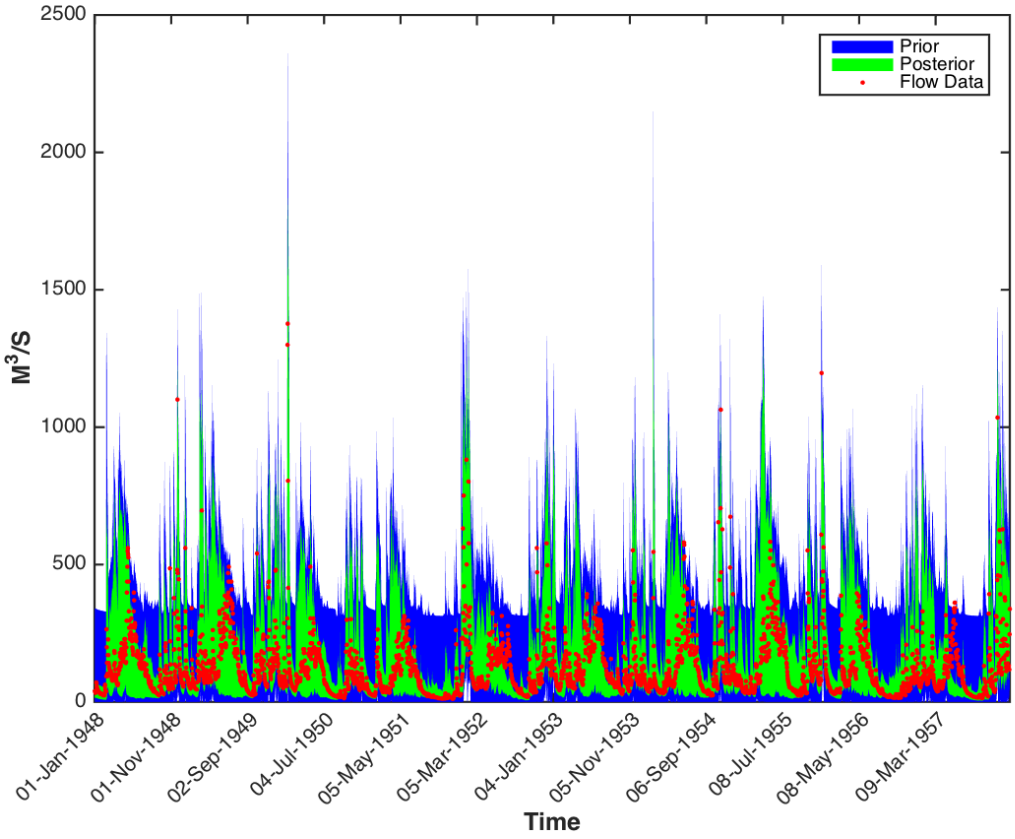

Figure 6.50. Predictive uncertainty ranges of GR4J model constrained against Skykomish watershed (USGS ID 12134500) using 5th Flow Percentile (Q5th) Prior channel inflow in blue, posterior channel flow in green and observed data in red

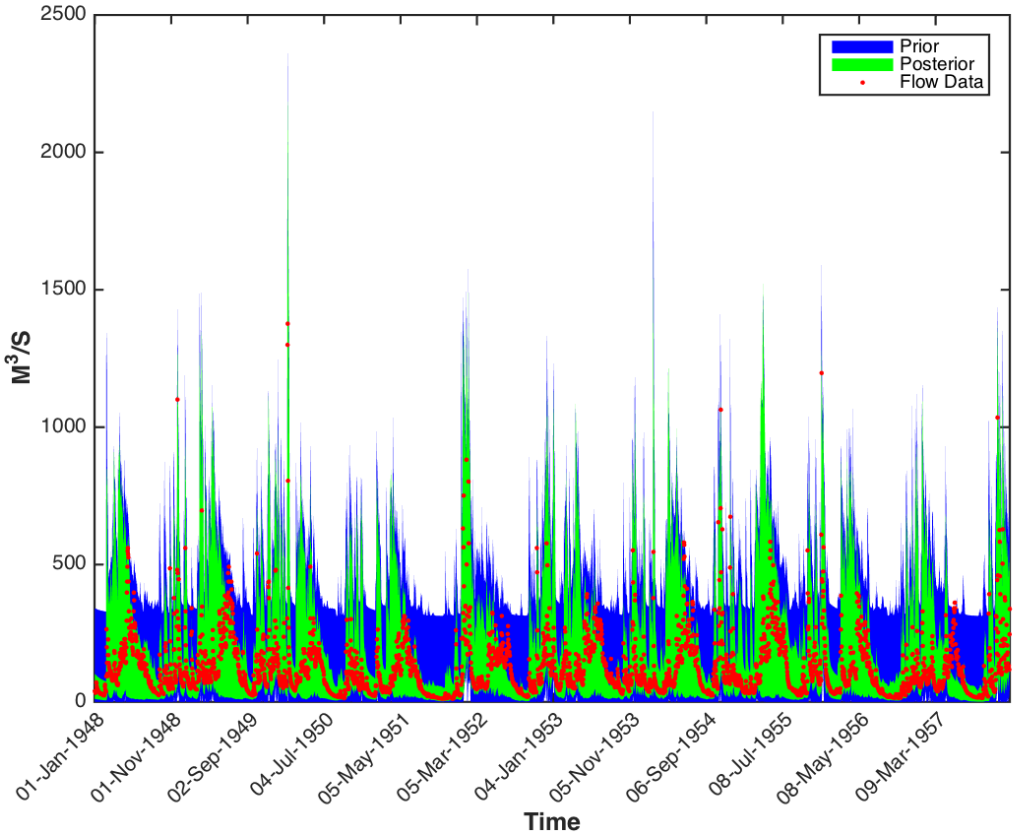

Figure 6.51. Predictive uncertainty ranges of GR4J model constrained against Skykomish watershed (USGS ID 12134500) using 15th Flow Percentile (Q15th) Prior channel inflow in blue, posterior channel flow in green and observed data in red

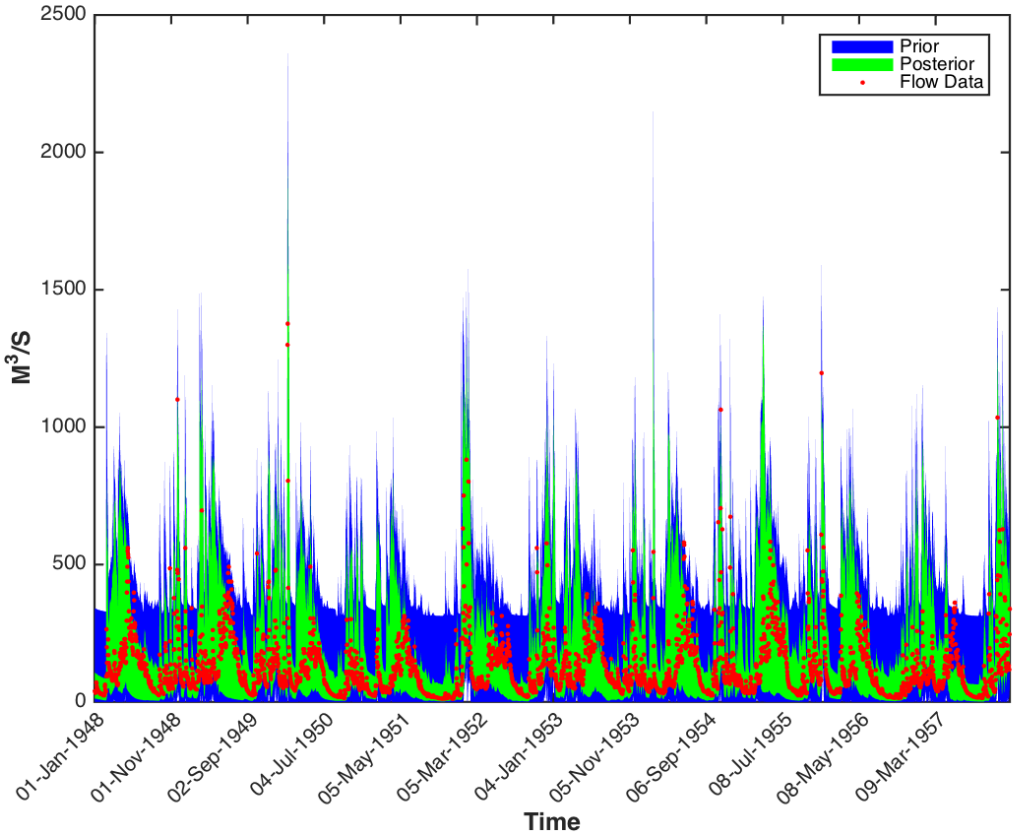

Figure 6.52. Predictive uncertainty ranges of GR4J model constrained against Skykomish watershed (USGS ID 12134500) using 50th Flow Percentile (Q50th) Prior channel inflow in blue, posterior channel flow in green and observed data in red

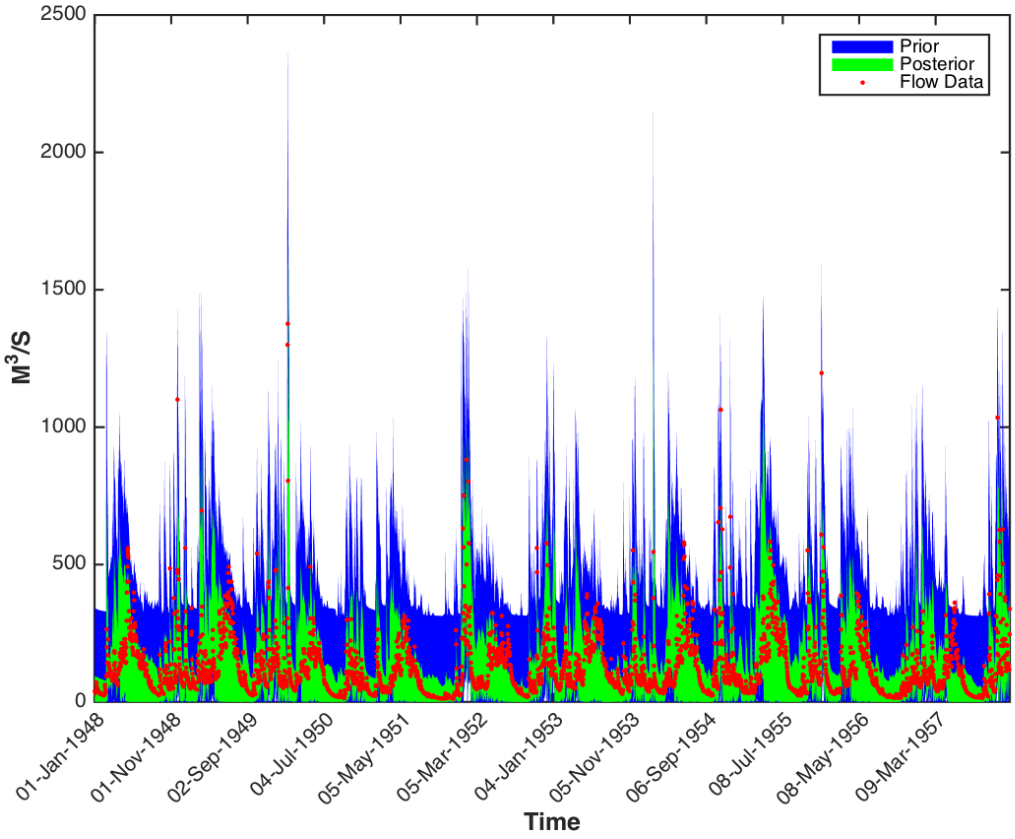

Figure 6.53 . Predictive uncertainty ranges of GR4J model constrained against Skykomish watershed (USGS ID 12134500) using 95th Flow Percentile (Q95th) Prior channel inflow in blue, posterior channel flow in green and observed data in red

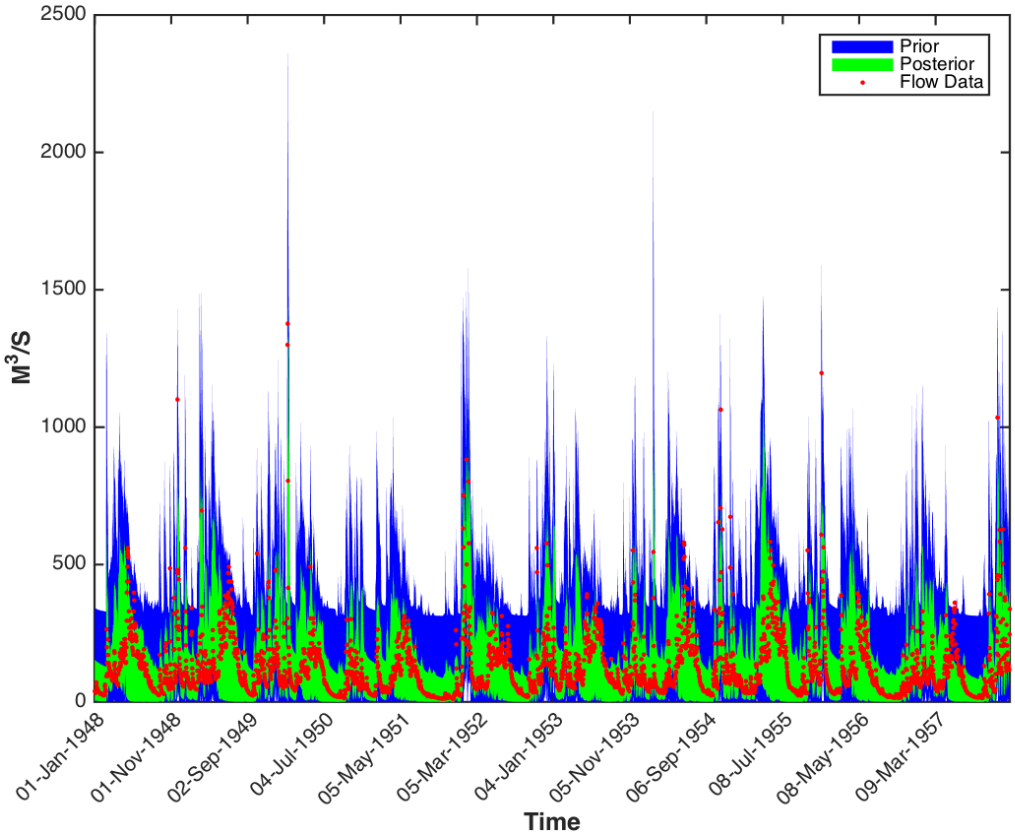

Figure 6.54. Predictive uncertainty ranges of GR4J model constrained against Skykomish watershed (USGS ID 12134500) using 99th Flow Percentile (Q99th) Prior channel inflow in blue, posterior channel flow in green and observed data in red

12134500 HYMOD

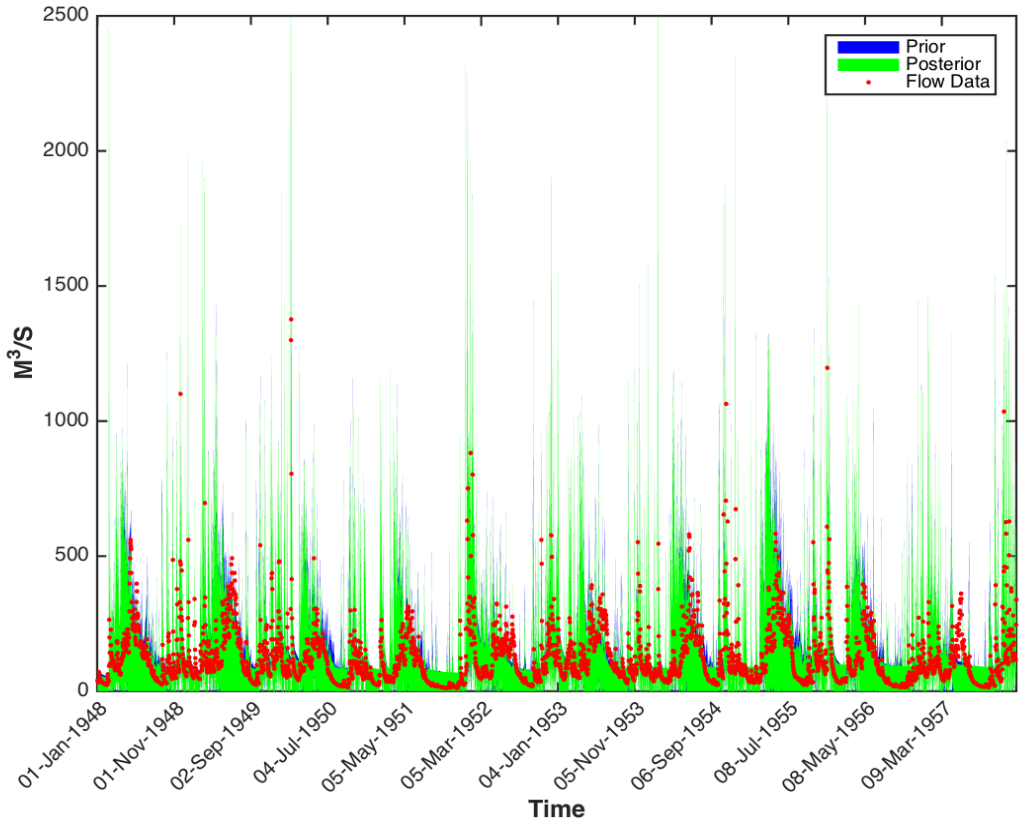

Figure 6.55. Predictive uncertainty ranges of HyMod model constrained against Skykomish watershed (USGS ID 12134500) using Runoff Ratio Metric (RR). Prior channel inflow in blue, posterior channel flow in green and observed data in red

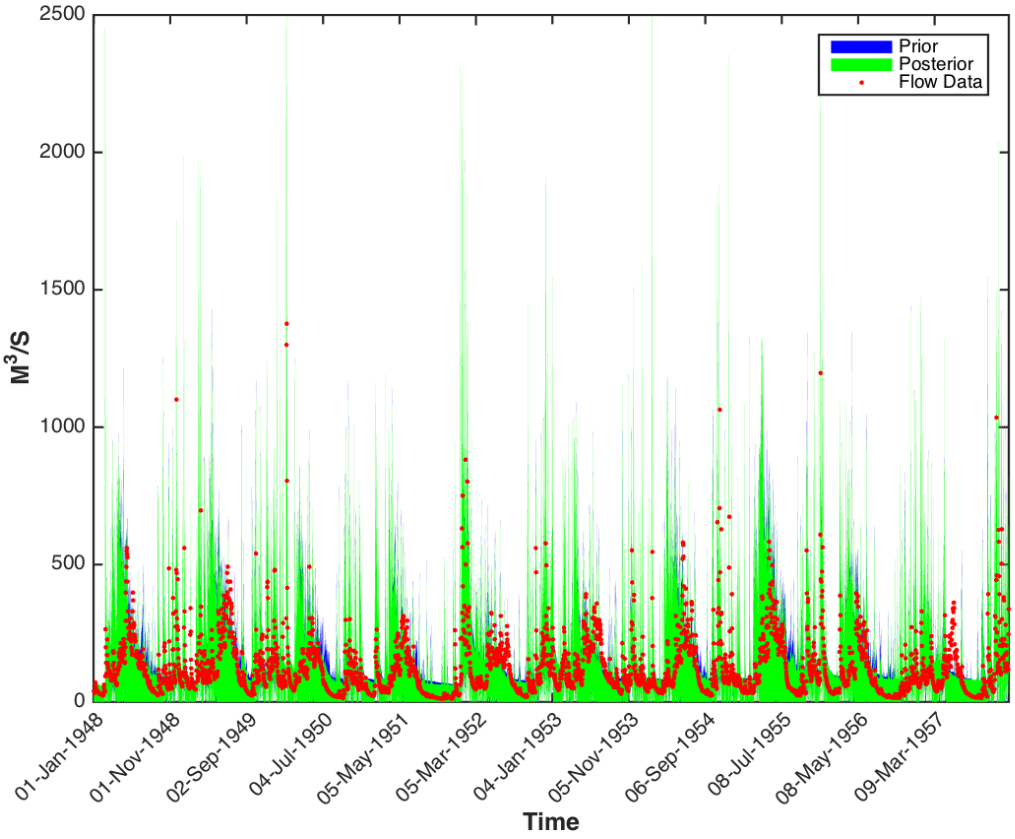

Figure 6.56. Predictive uncertainty ranges of HyMod model constrained against Skykomish watershed (USGS ID 12134500) using Base Flow Index (BFI). Prior channel inflow in blue, posterior channel flow in green and observed data in red

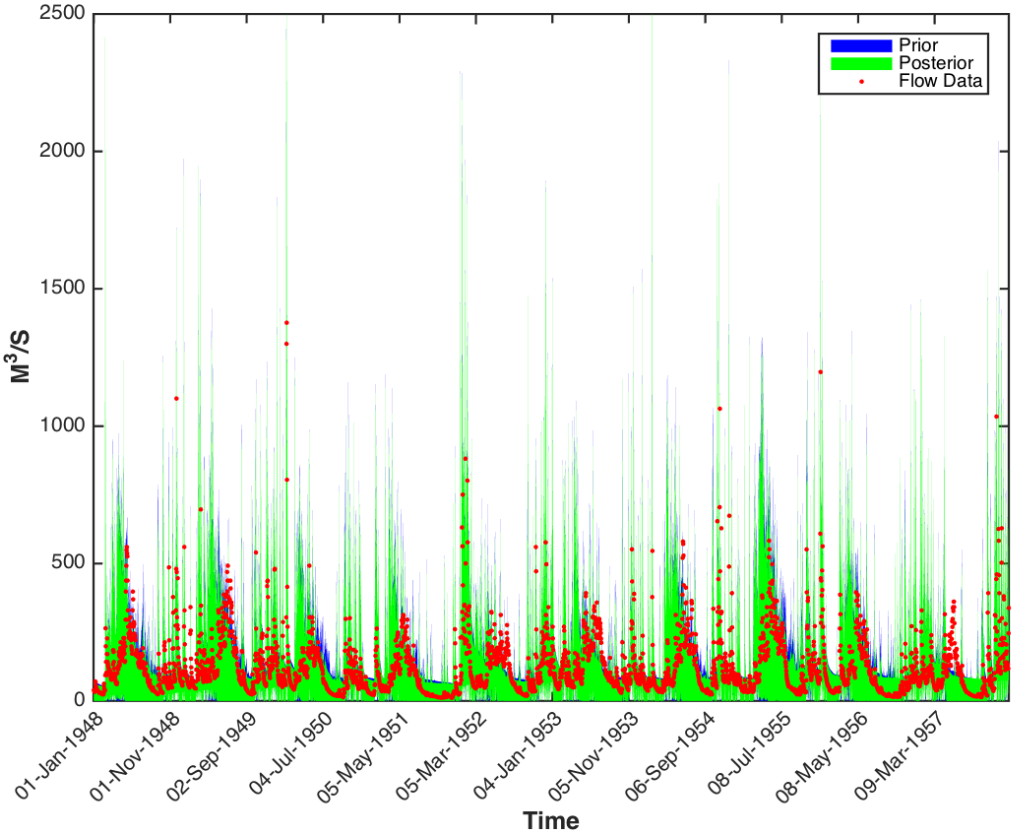
Prior
Posterior
Flow Data
M3/S
2500
2000
1500
1000
500
0
01-Jan-1948
01-Nov-1948
02-Sep-1949
04-Jul-1950
05-May-1951
05-Mar-1952
04-Jan-1953
05-Nov-1953
06-Sep-1954
08-Jul-1955
08-May-1956
09-Mar-1957
Time

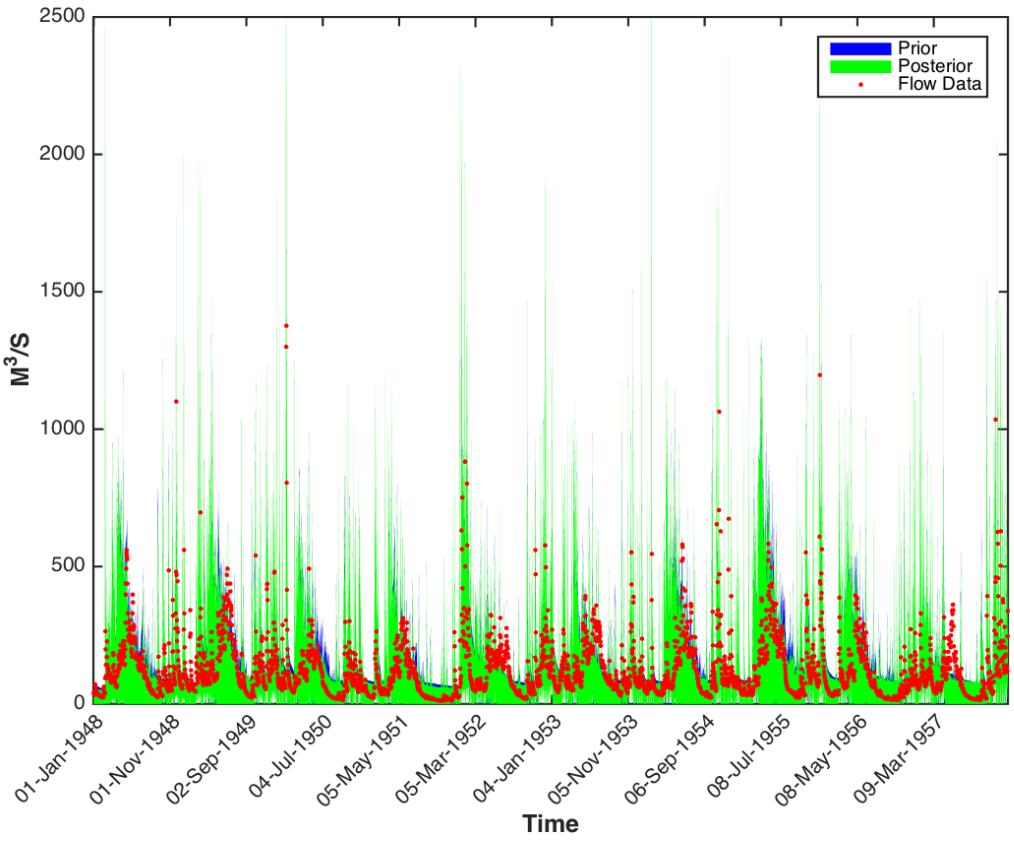
Prior
Posterior
Flow Data
M3/S
2500
2000
1500
1000
500
0
01-Jan-1948
01-Nov-1948
02-Sep-1949
04-Jul-1950
05-May-1951
05-Mar-1952
04-Jan-1953
05-Nov-1953
06-Sep-1954
08-Jul-1955
08-May-1956
09-Mar-1957
Time

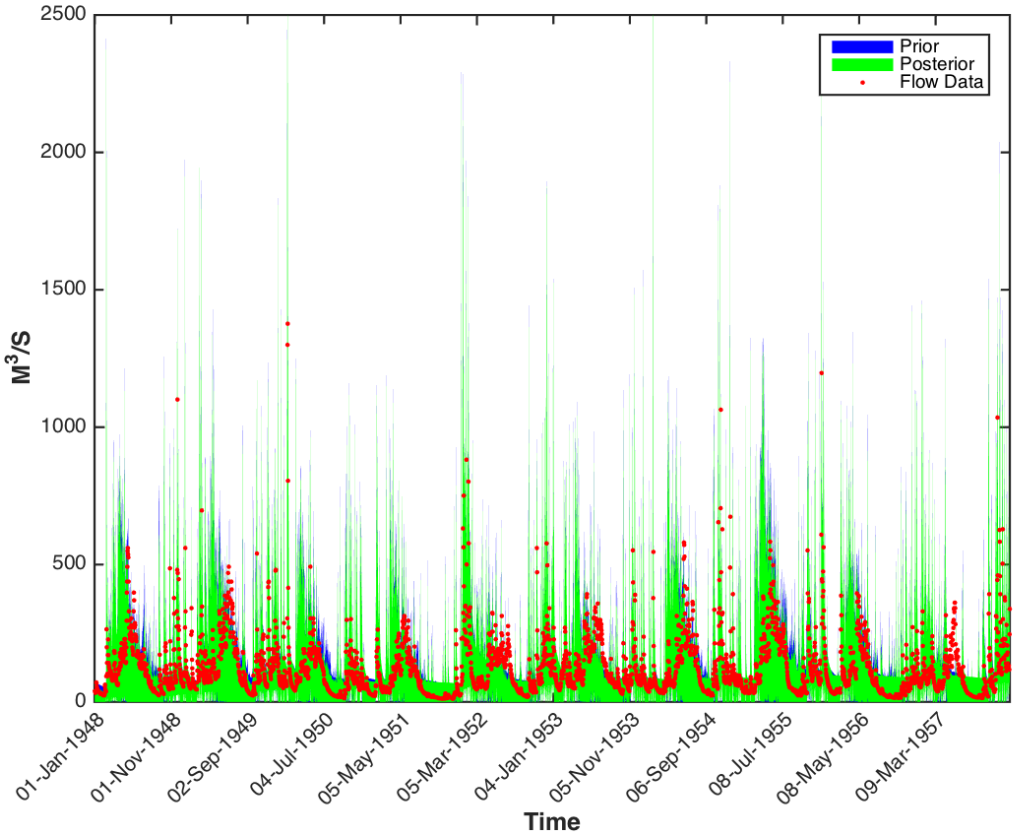

Figure 6.59. Predictive uncertainty ranges of HyMod model constrained against Skykomish watershed (USGS ID 12134500) using Slope of Log FDC 33 & 66 Percentile (SL FDC $Q33^{th}$&$Q66^{th}$). Prior channel inflow in blue, posterior channel flow in green and observed data in red

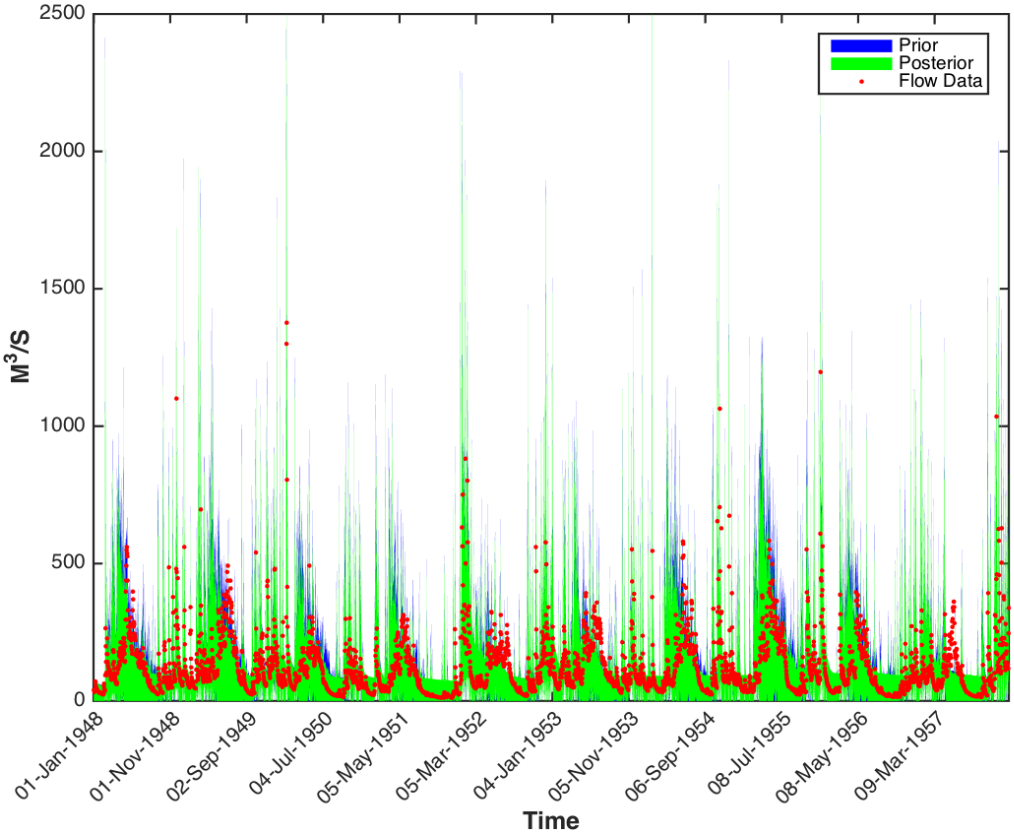
Prior
Posterior
Flow Data
2500
2000
1500
1000
500
0
M3/S
01-Jan-1948
01-Nov-1948
02-Sep-1949
04-Jul-1950
05-May-1951
05-Mar-1952
04-Jan-1953
05-Nov-1953
06-Sep-1954
08-Jul-1955
08-May-1956
09-Mar-1957
Time

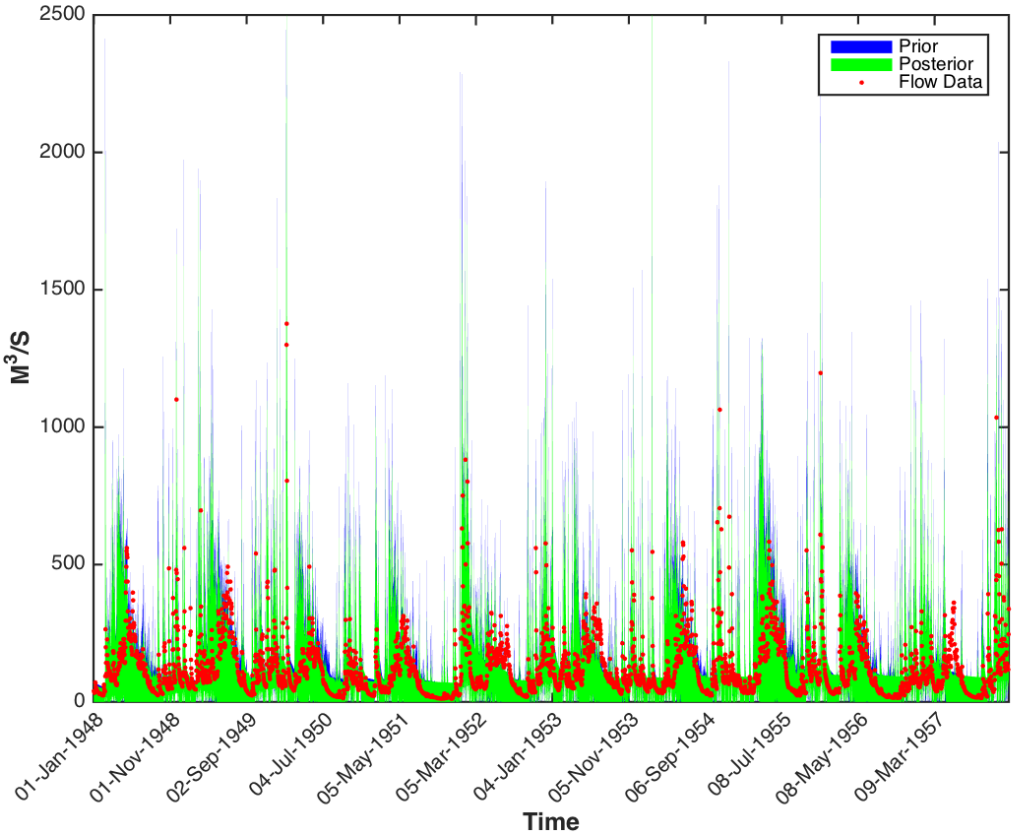

Figure 6.61 Predictive uncertainty ranges of HyMod model constrained against Skykomish watershed (USGS ID 12134500) using FDC High Segment Volume more than 90 Percentile (FDC HSV Q90th). Prior channel inflow in blue, posterior channel flow in green and observed data in red

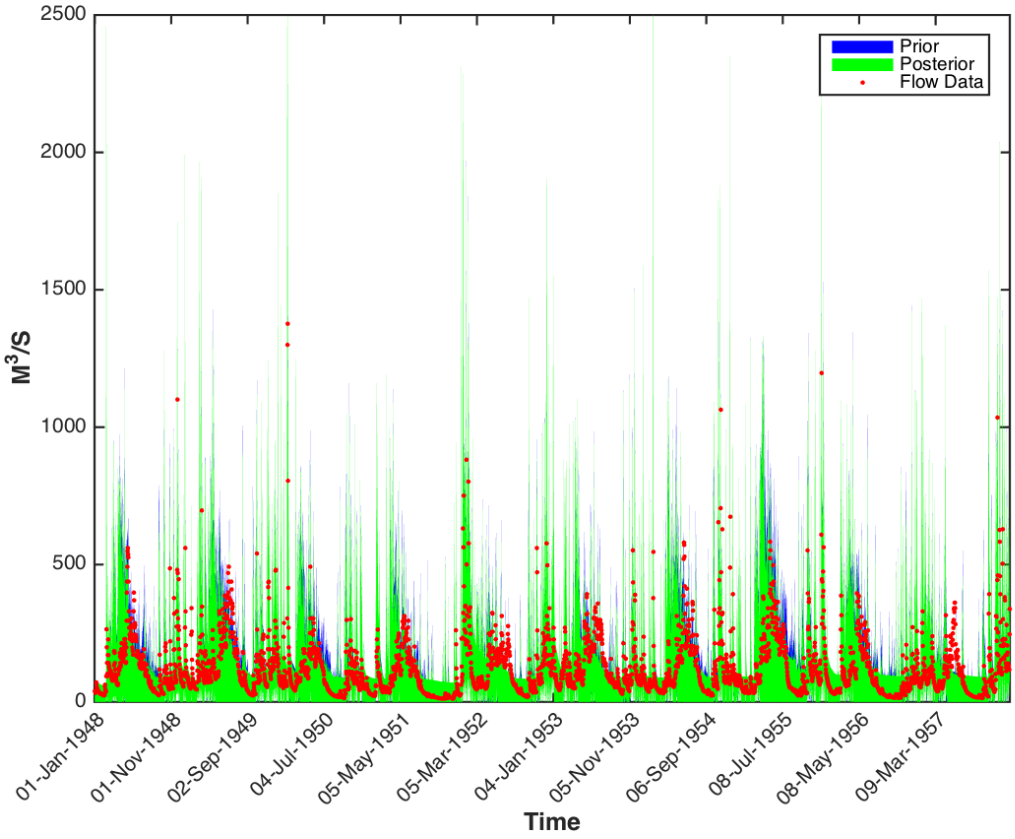

Figure 6.62 Predictive uncertainty ranges of HyMod model constrained against Skykomish watershed (USGS ID 12134500) using FDC Low Segment Volume less than 30 Percentile (FDC LSV Q30th) Prior channel inflow in blue, posterior channel flow in green and observed data in red

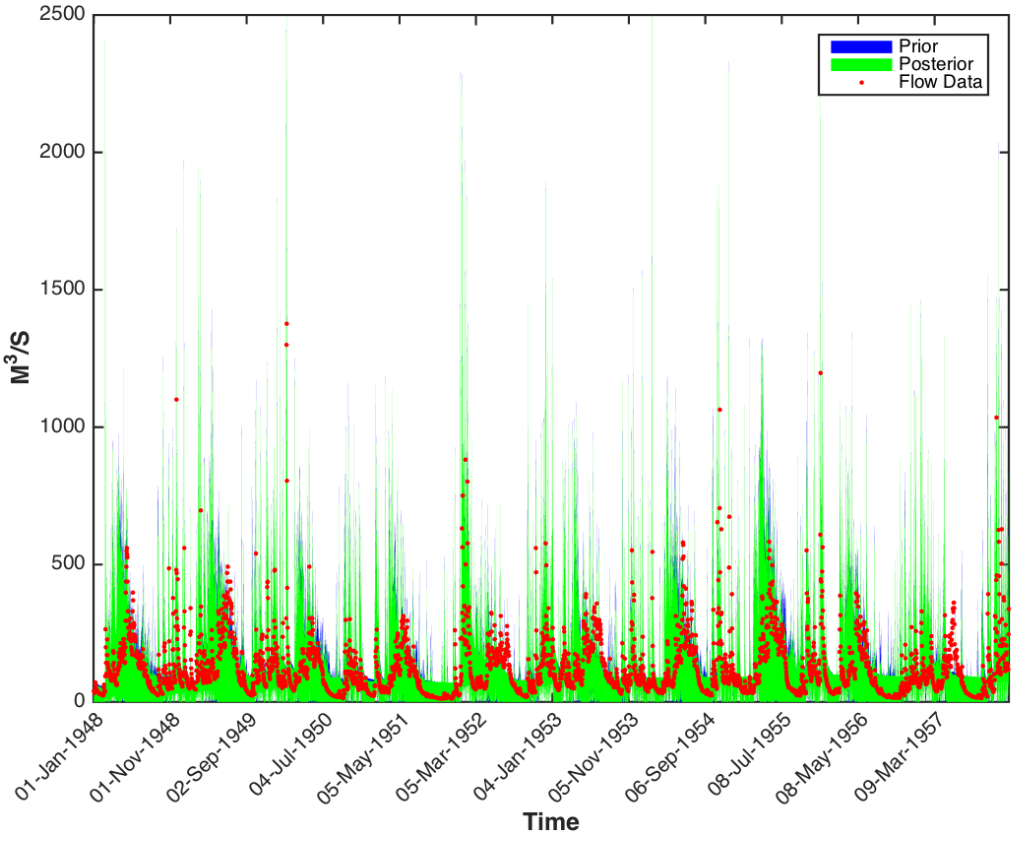
Prior
Posterior
Flow Data
M3/S
2500
2000
1500
1000
500
0
01-Jan-1948
01-Nov-1948
02-Sep-1949
04-Jul-1950
05-May-1951
05-Mar-1952
04-Jan-1953
05-Nov-1953
06-Sep-1954
08-Jul-1955
08-May-1956
09-Mar-1957
Time

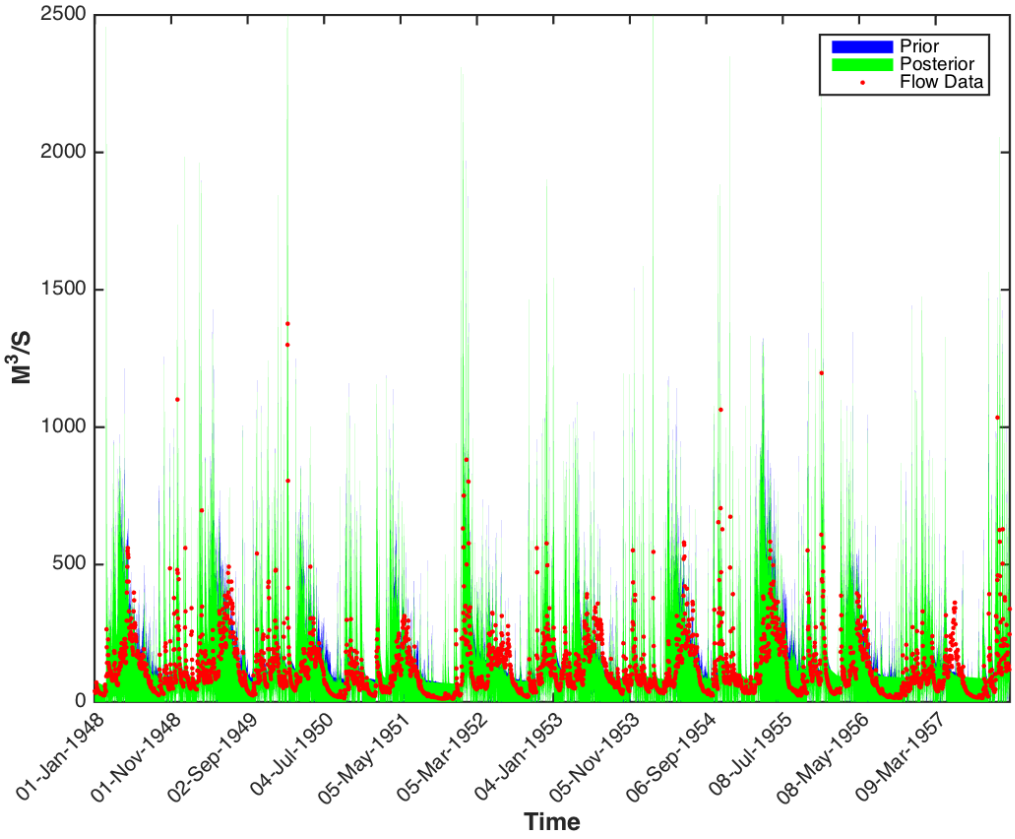

Figure 6.64. Predictive uncertainty ranges of HyMod model constrained against Skykomish watershed (USGS ID 12134500) using Auto Correlation of Hydrograph with 1 Day Lag (AC) Prior channel inflow in blue, posterior channel flow in green and observed data in red

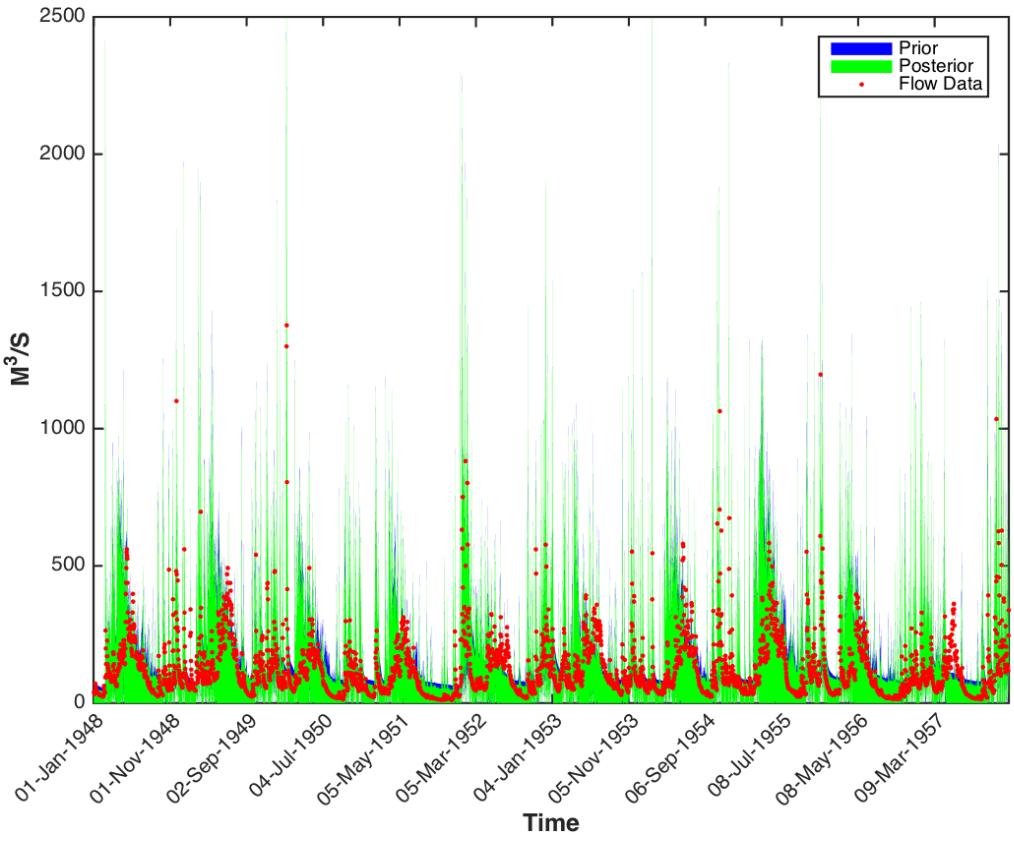
Prior
Posterior
Flow Data
2500
2000
1500
1000
500
0
M3/S
01-Jan-1948
01-Nov-1948
02-Sep-1949
04-Jul-1950
05-May-1951
05-Mar-1952
04-Jan-1953
05-Nov-1953
06-Sep-1954
08-Jul-1955
08-May-1956
09-Mar-1957
Time

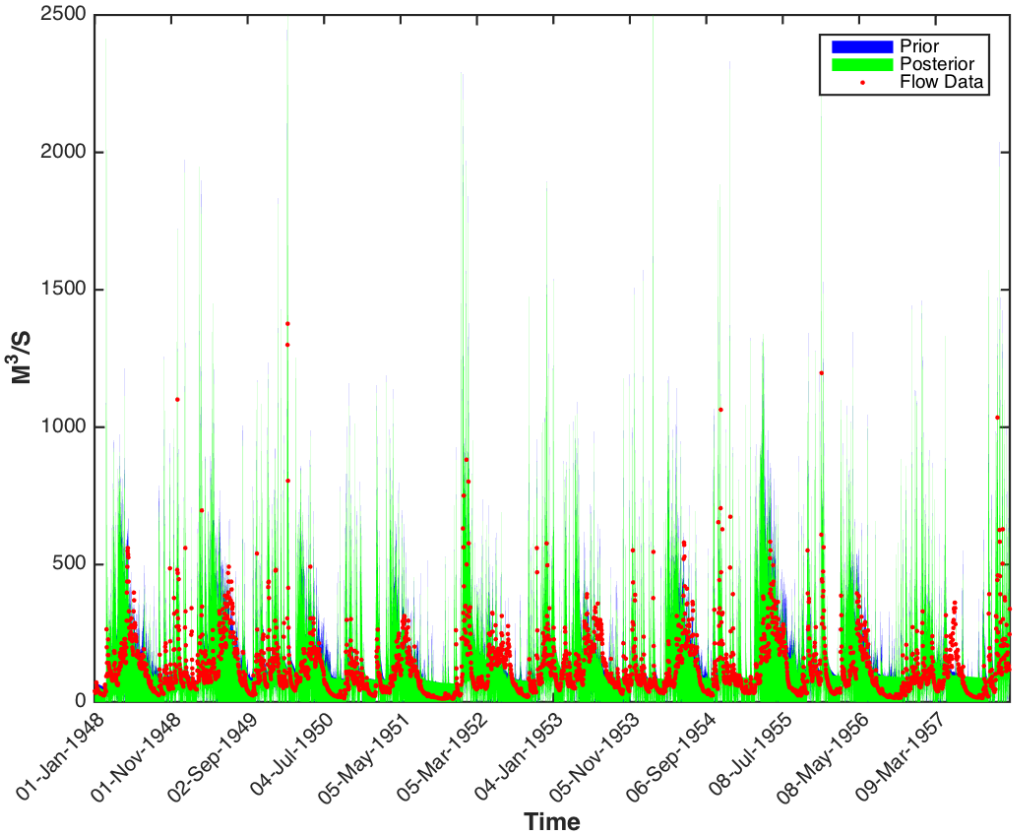

Figure 6.66. Predictive uncertainty ranges of HyMod model constrained against Skykomish watershed (USGS ID 12134500) using Reclining LIMB Destiny (RLD) Prior channel inflow in blue, posterior channel flow in green and observed data in red

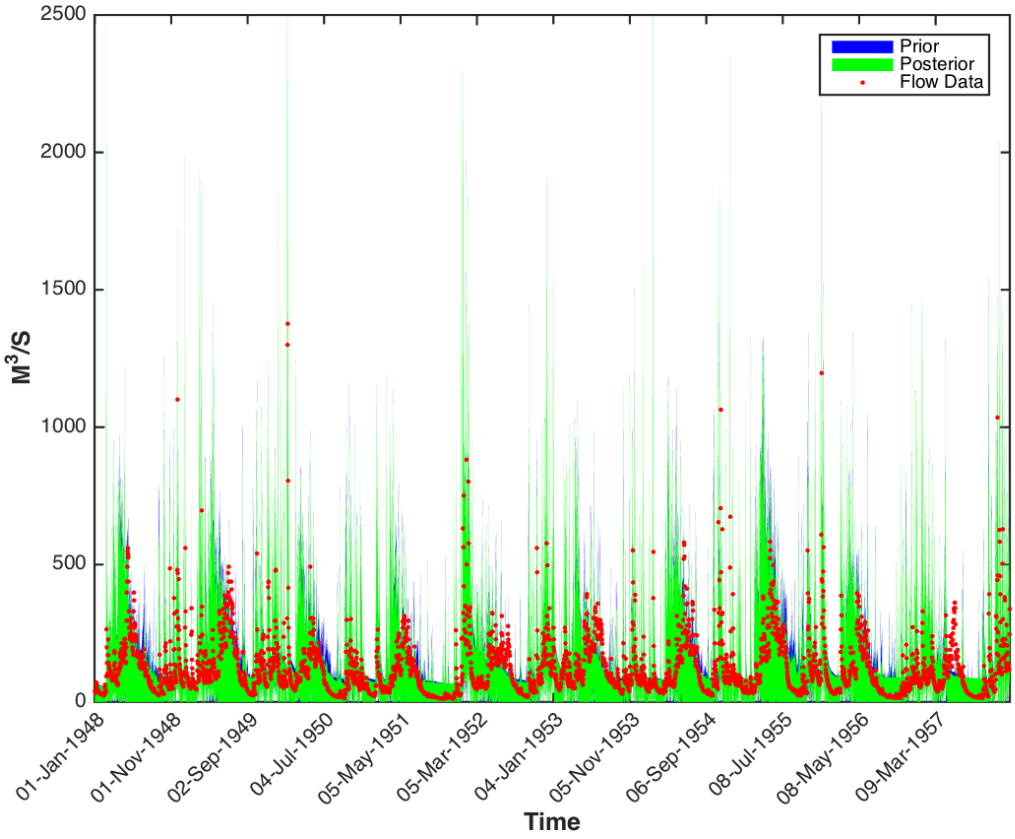

Figure 6.67. Predictive uncertainty ranges of HyMod model constrained against Skykomish watershed (USGS ID 12134500) using Declining LIMB Destiny (DLD) Prior channel inflow in blue, posterior channel flow in green and observed data in red

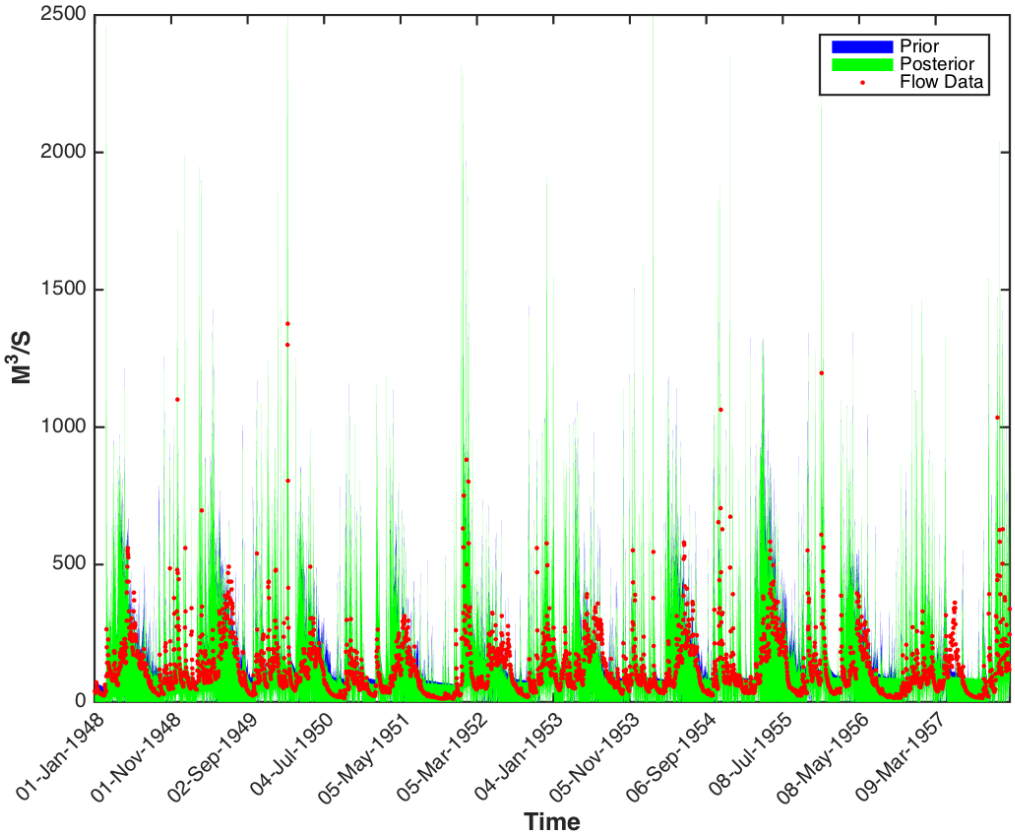

Figure 6.68. Predictive uncertainty ranges of HyMod model constrained against Skykomish watershed (USGS ID 12134500) using 1st Flow Percentile (Q1st) Prior channel inflow in blue, posterior channel flow in green and observed data in red

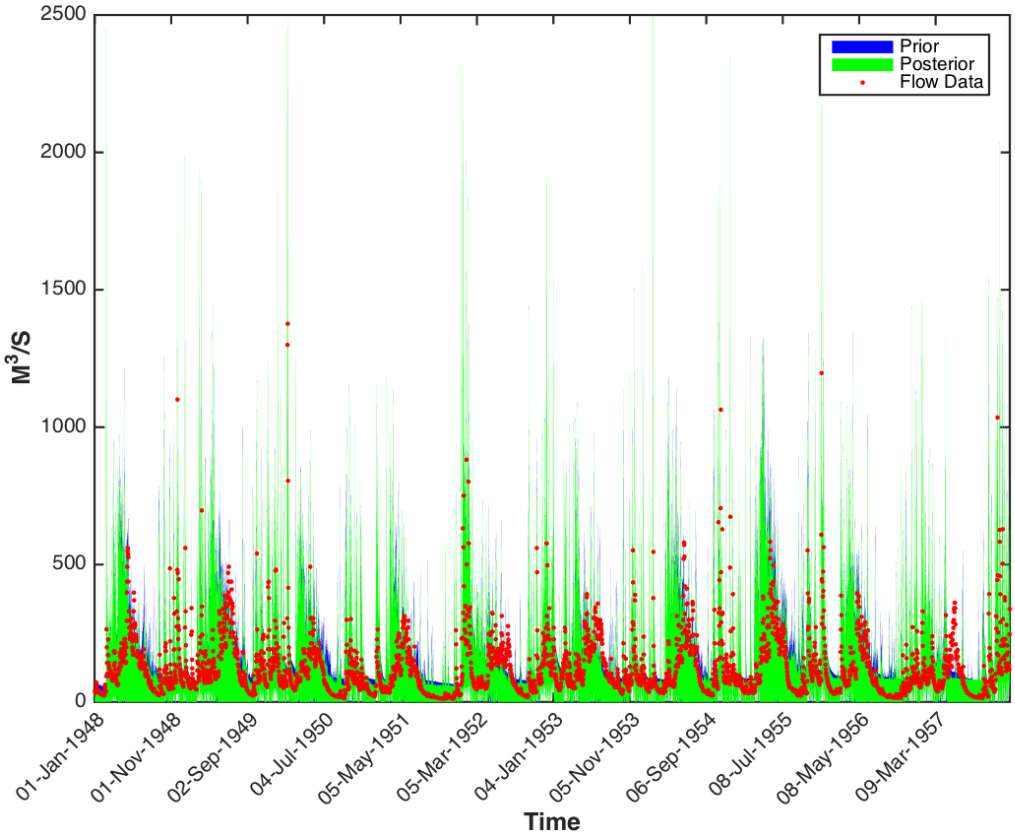

Figure 6.69. Predictive uncertainty ranges of HyMod model constrained against Skykomish watershed (USGS ID 12134500) using 5th Flow Percentile (Q5th) Prior channel inflow in blue, posterior channel flow in green and observed data in red

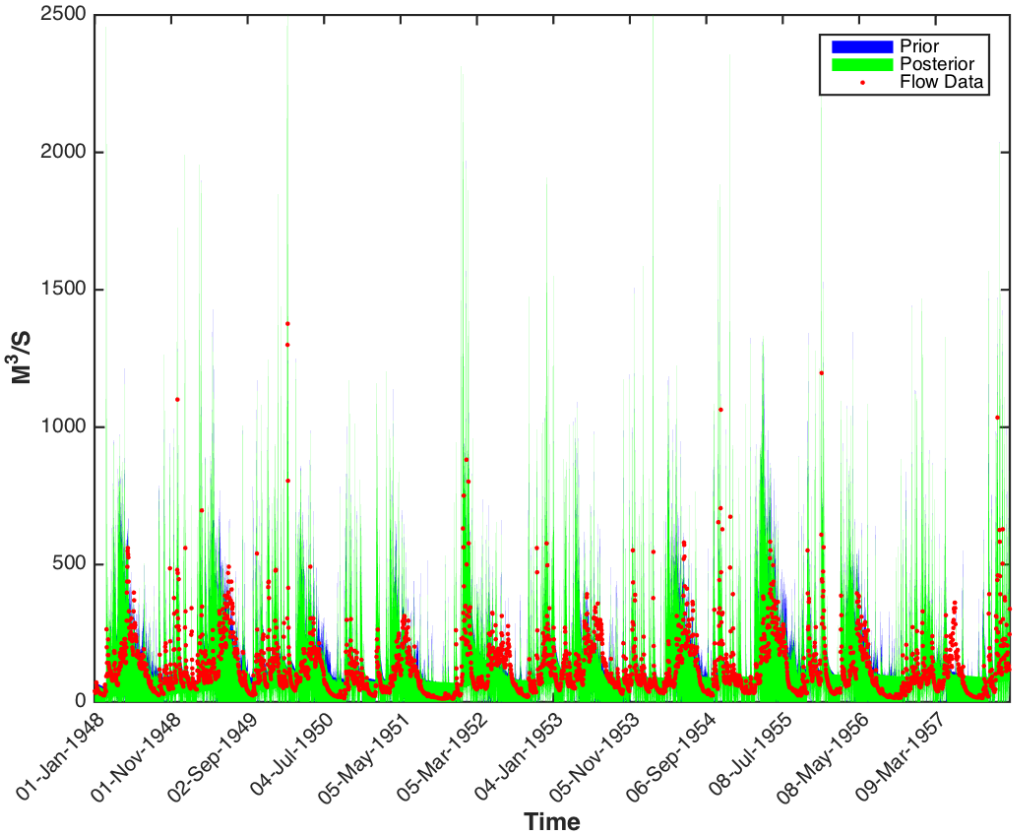

Figure 6.70. Predictive uncertainty ranges of HyMod model constrained against Skykomish watershed (USGS ID 12134500) using 15th Flow Percentile (Q15th) Prior channel inflow in blue, posterior channel flow in green and observed data in red

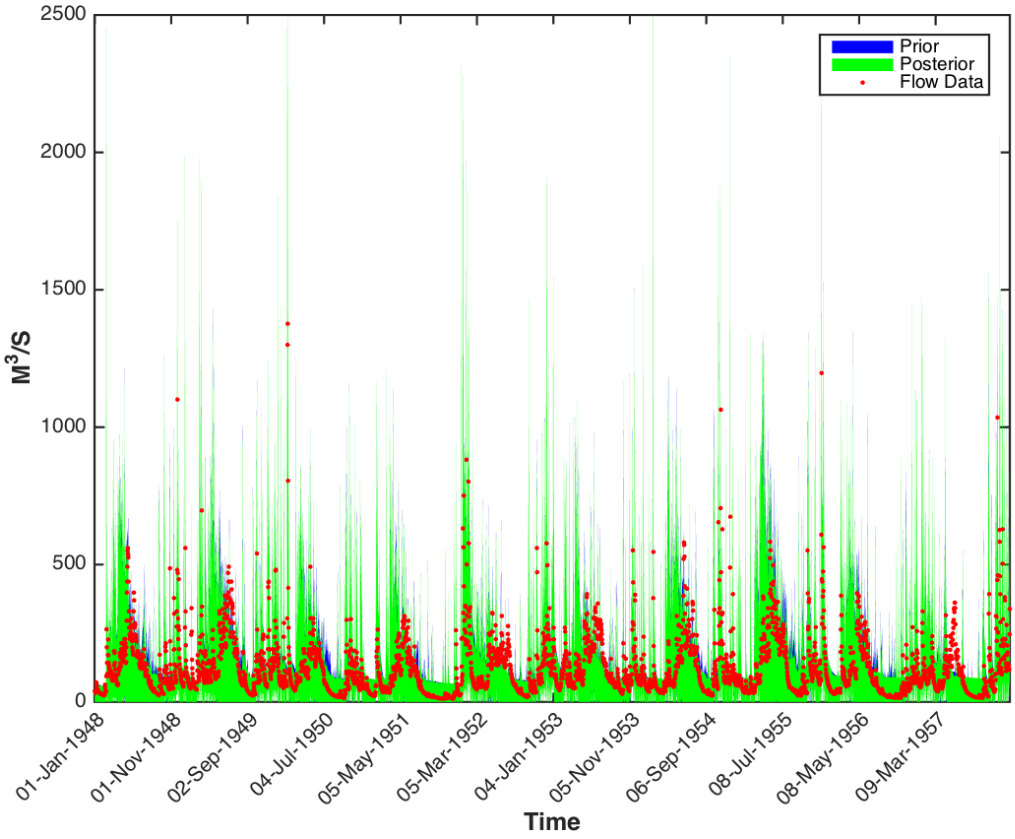

Figure 6.71. Predictive uncertainty ranges of HyMod model constrained against Skykomish watershed (USGS ID 12134500) using 50th Flow Percentile (Q50th) Prior channel inflow in blue, posterior channel flow in green and observed data in red

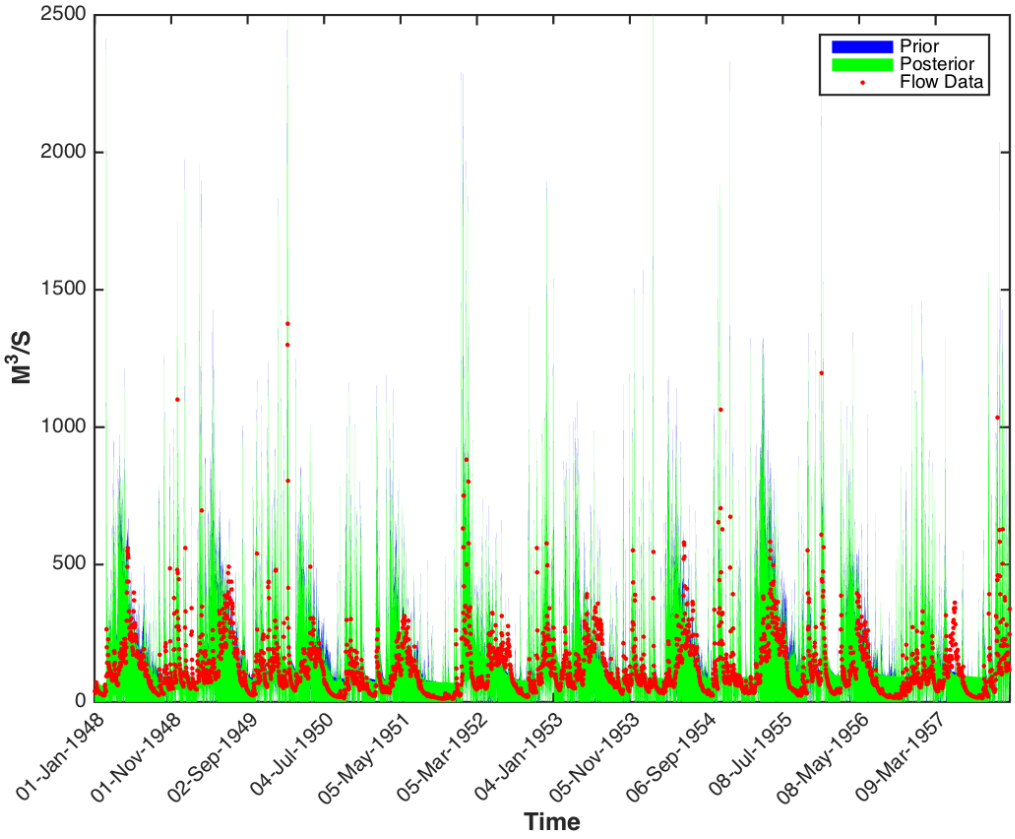

Figure 6.72. Predictive uncertainty ranges of HyMod model constrained against Skykomish watershed (USGS ID 12134500) using 95th Flow Percentile (Q95th) Prior channel inflow in blue, posterior channel flow in green and observed data in red

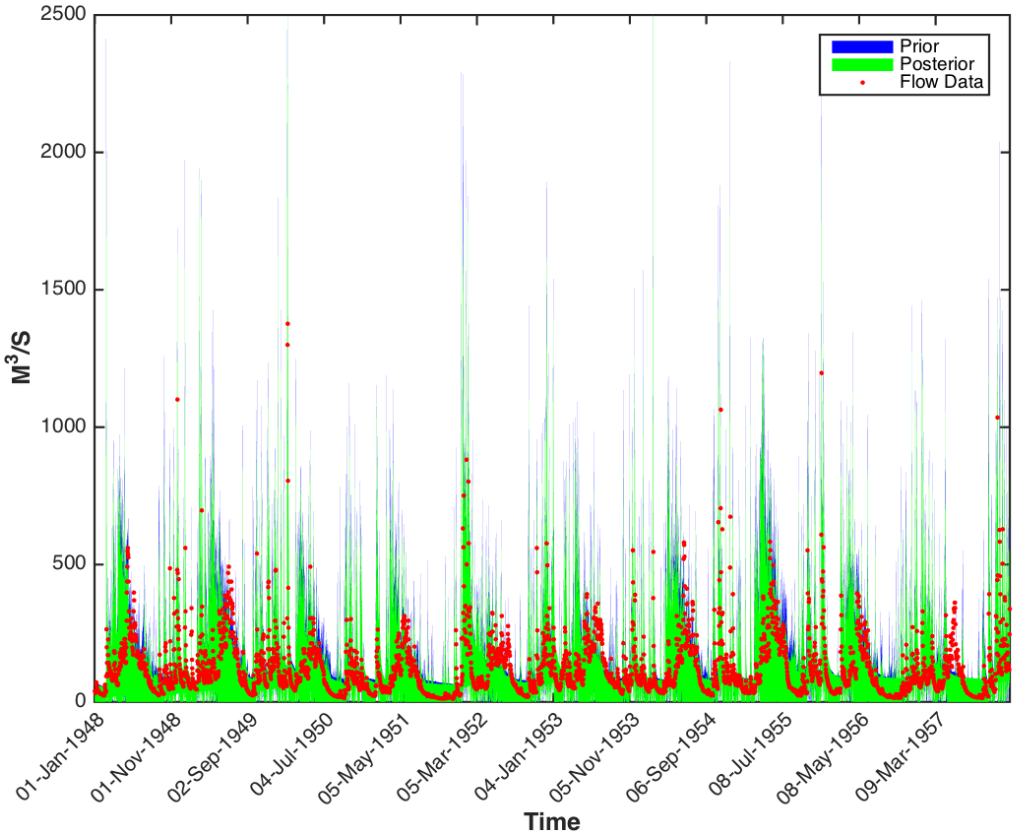

Figure 6.73. Predictive uncertainty ranges of HyMod model constrained against Skykomish watershed (USGS ID 12134500) using 99th Flow Percentile (Q99th) Prior channel inflow in blue, posterior channel flow in green and observed data in red

02143000 GR4J

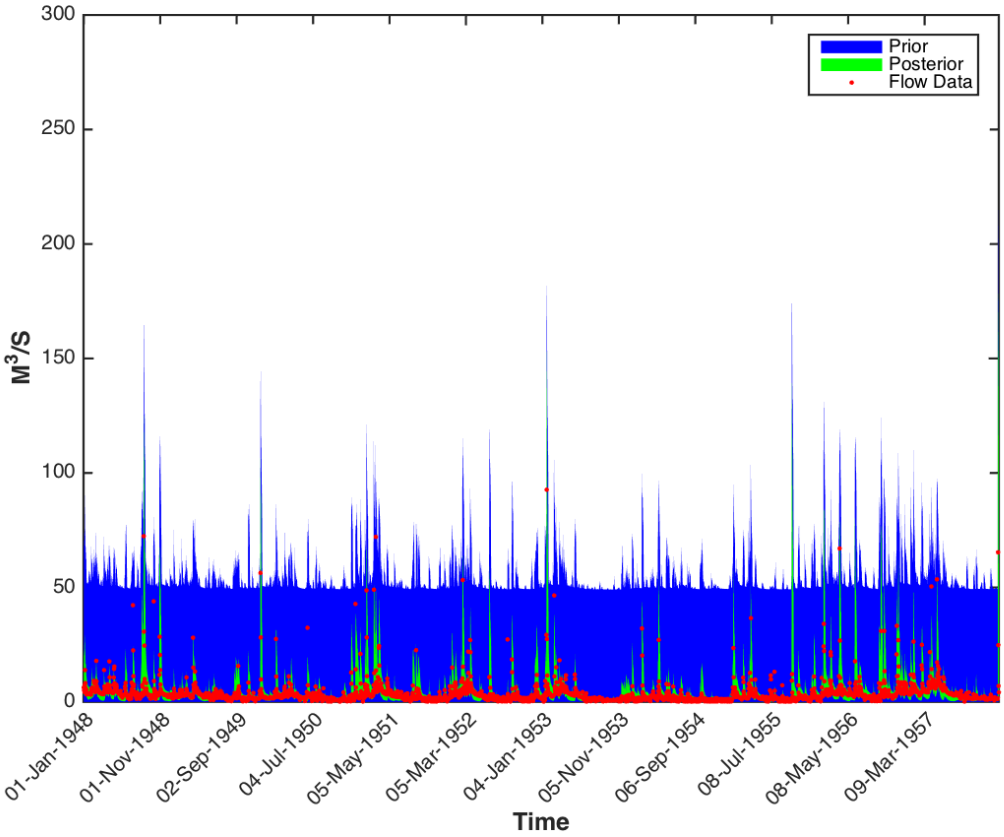

Figure 6.74. Predictive uncertainty ranges of GR4J model constrained against Henry Fork watershed (USGS ID 02143000) using Runoff Ratio Metric (RR). Prior channel inflow in blue, posterior channel flow in green and observed data in red

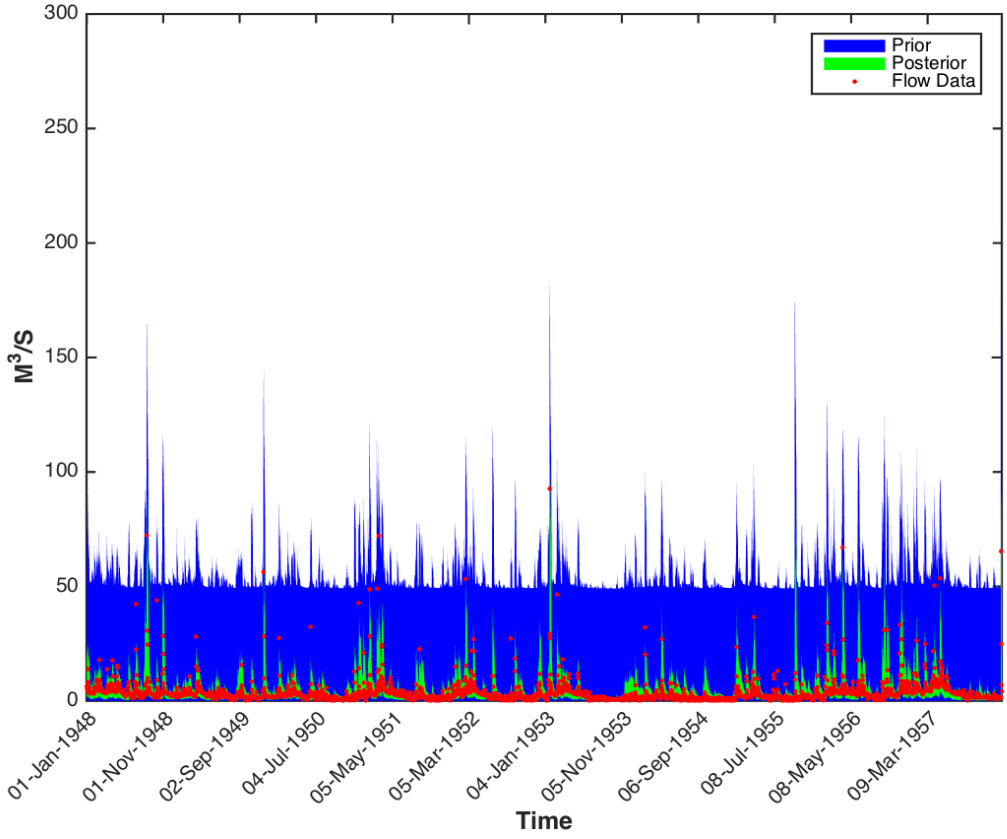
300
250
200
150
100
50
0
M3/S
Prior
Posterior
Flow Data
01-Jan-1948
01-Nov-1948
02-Sep-1949
04-Jul-1950
05-May-1951
05-Mar-1952
04-Jan-1953
05-Nov-1953
06-Sep-1954
08-Jul-1955
08-May-1956
09-Mar-1957
Time

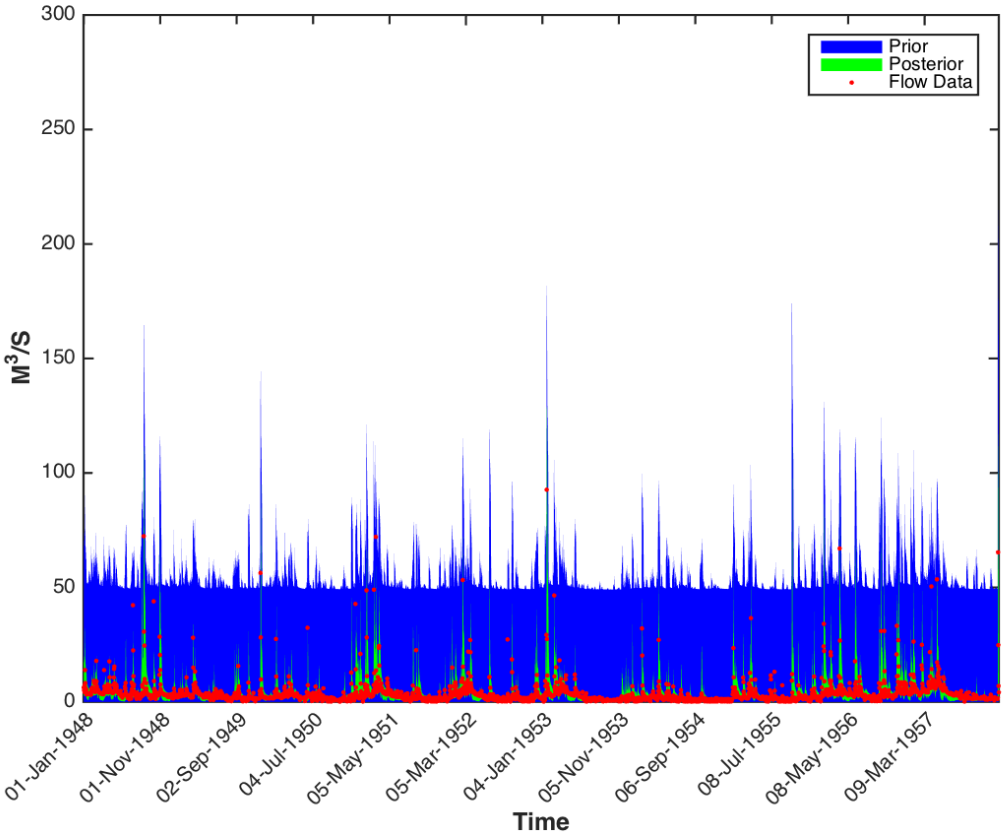

Figure 6.77. Predictive uncertainty ranges of GR4J model constrained against Henry Fork watershed (USGS ID 02143000) using Base Flow Runoff Ratio (BFR). Prior channel inflow in blue, posterior channel flow in green and observed data in red

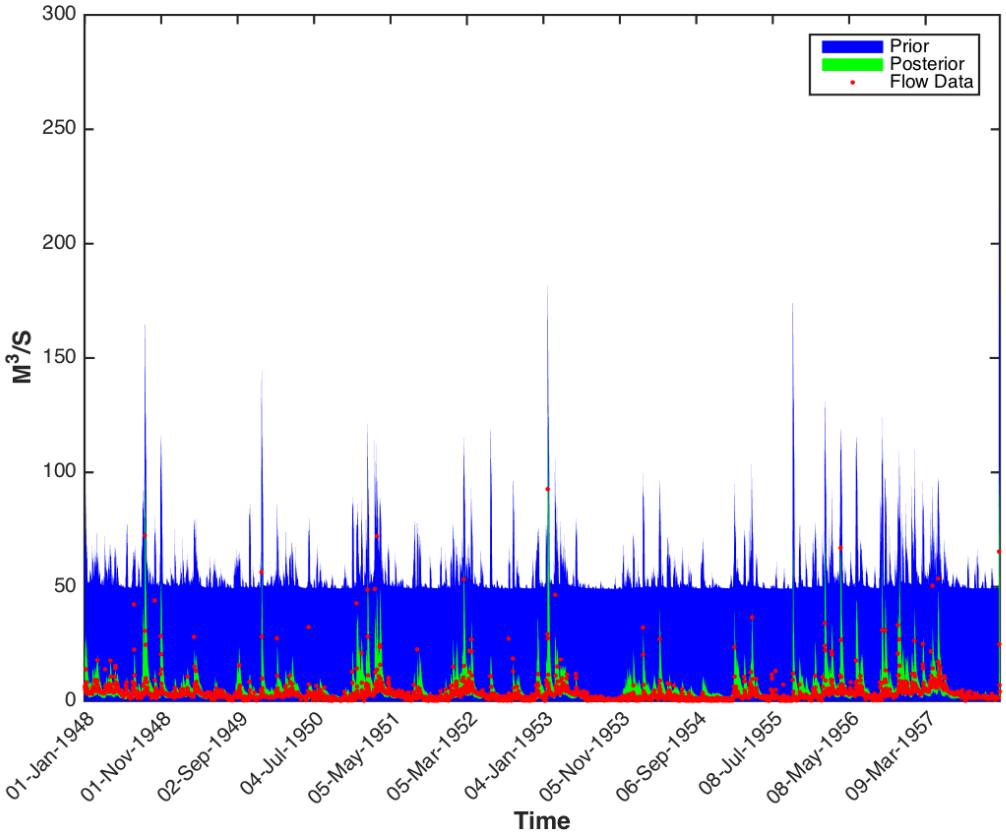
Prior
Posterior
Flow Data
M3/S
300
250
200
150
100
50
0
01-Jan-1948
01-Nov-1948
02-Sep-1949
04-Jul-1950
05-May-1951
05-Mar-1952
04-Jan-1953
05-Nov-1953
06-Sep-1954
08-Jul-1955
08-May-1956
09-Mar-1957
Time

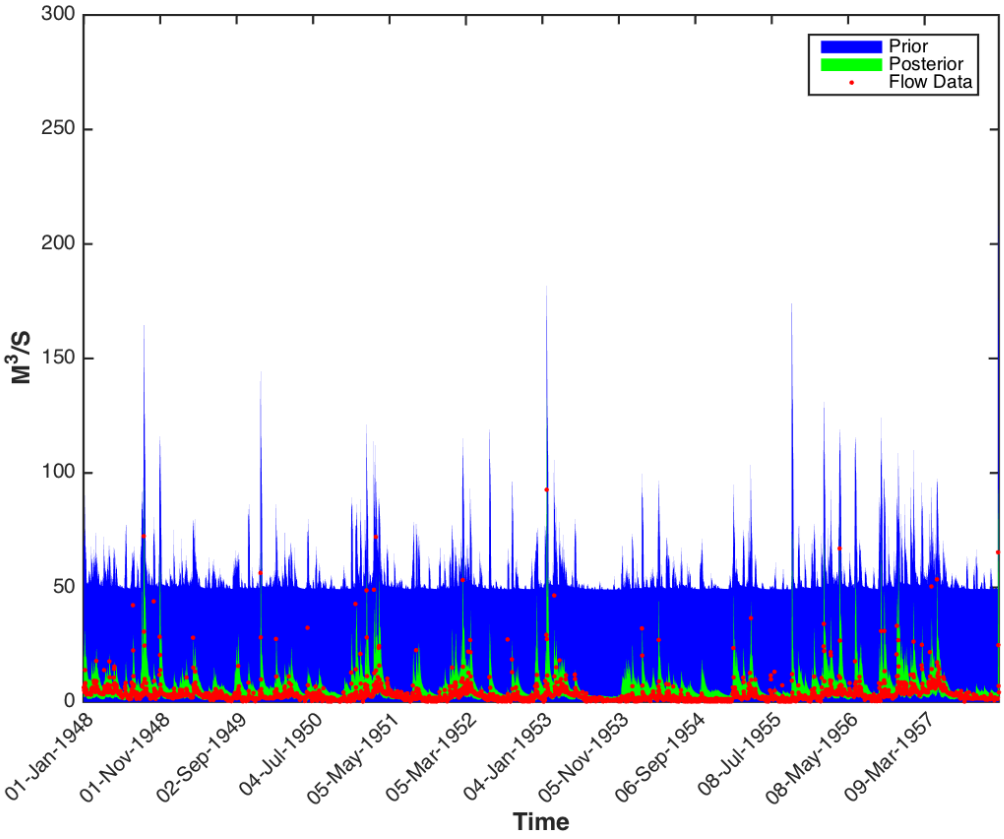

Figure 6.79. Predictive uncertainty ranges of GR4J model constrained against Henry Fork watershed (USGS ID 02143000) using Slope of Log FDC 33 & 66 Percentile (SL FDC Q33th&Q66th). Prior channel inflow in blue, posterior channel flow in green and observed data in red

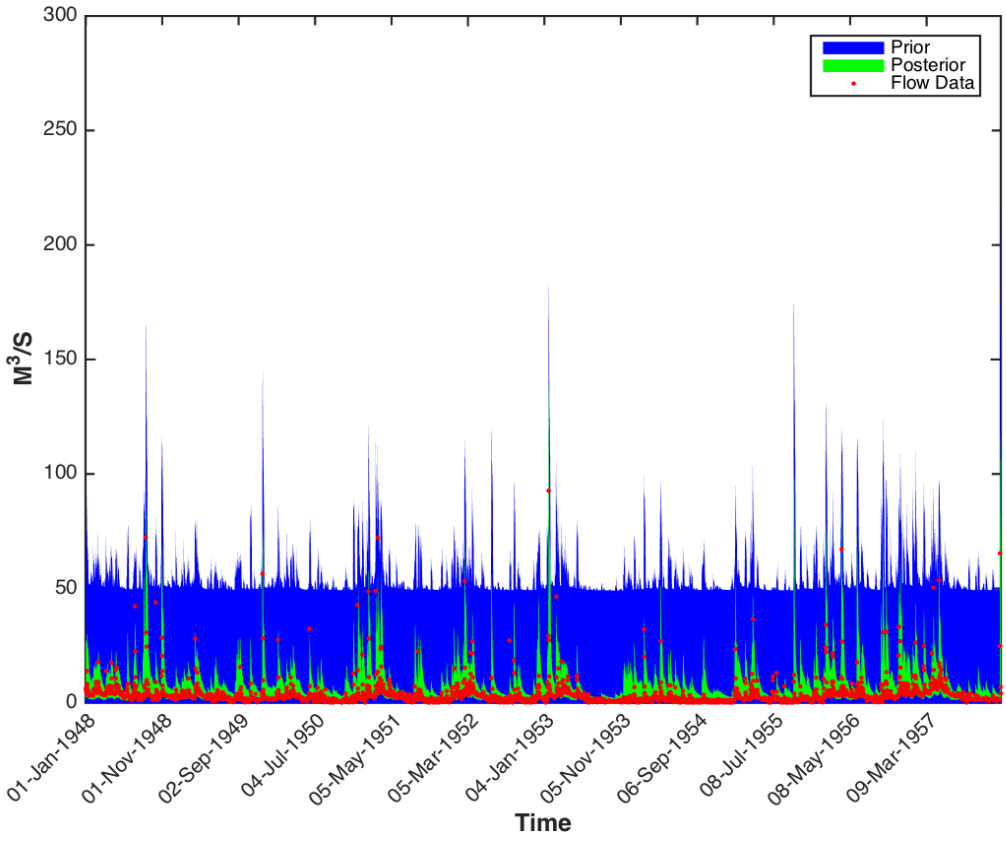
Prior
Posterior
Flow Data
M3/S
300
250
200
150
100
50
0
01-Jan-1948
01-Nov-1948
02-Sep-1949
04-Jul-1950
05-May-1951
05-Mar-1952
04-Jan-1953
05-Nov-1953
06-Sep-1954
08-Jul-1955
08-May-1956
09-Mar-1957
Time

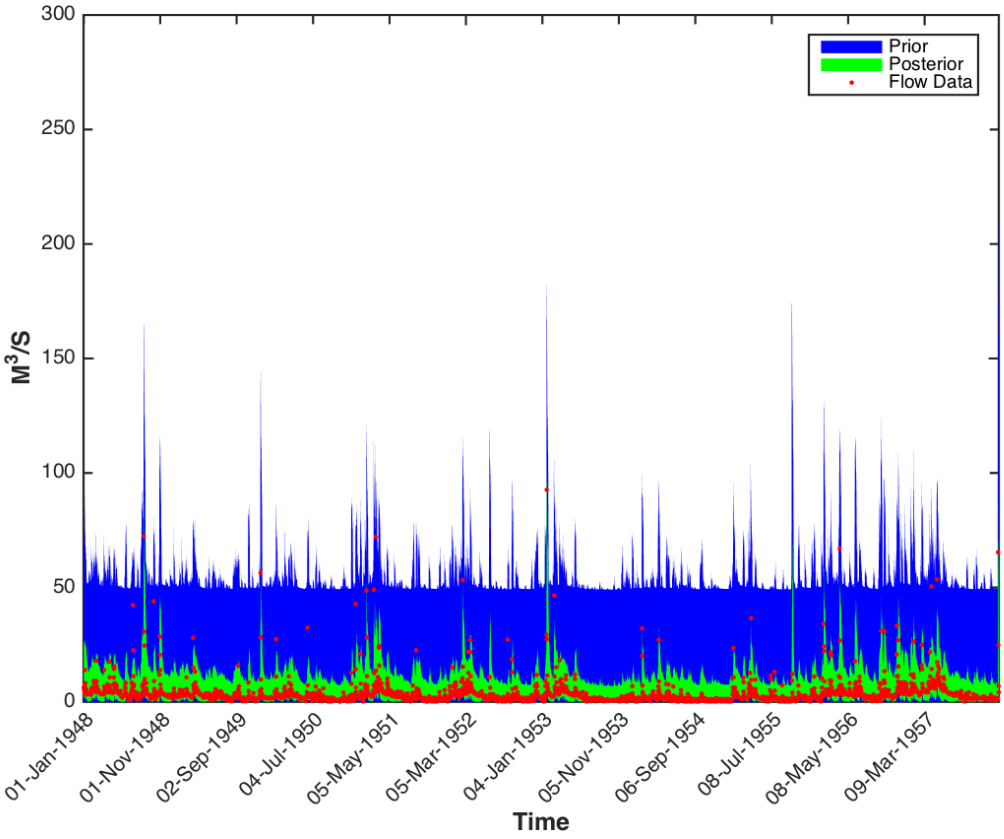

Figure 6.81. Predictive uncertainty ranges of GR4J model constrained against Henry Fork watershed (USGS ID 02143000) using FDC High Segment Volume more than 90 Percentile (FDC HSV Q90th). Prior channel inflow in blue, posterior channel flow in green and observed data in red

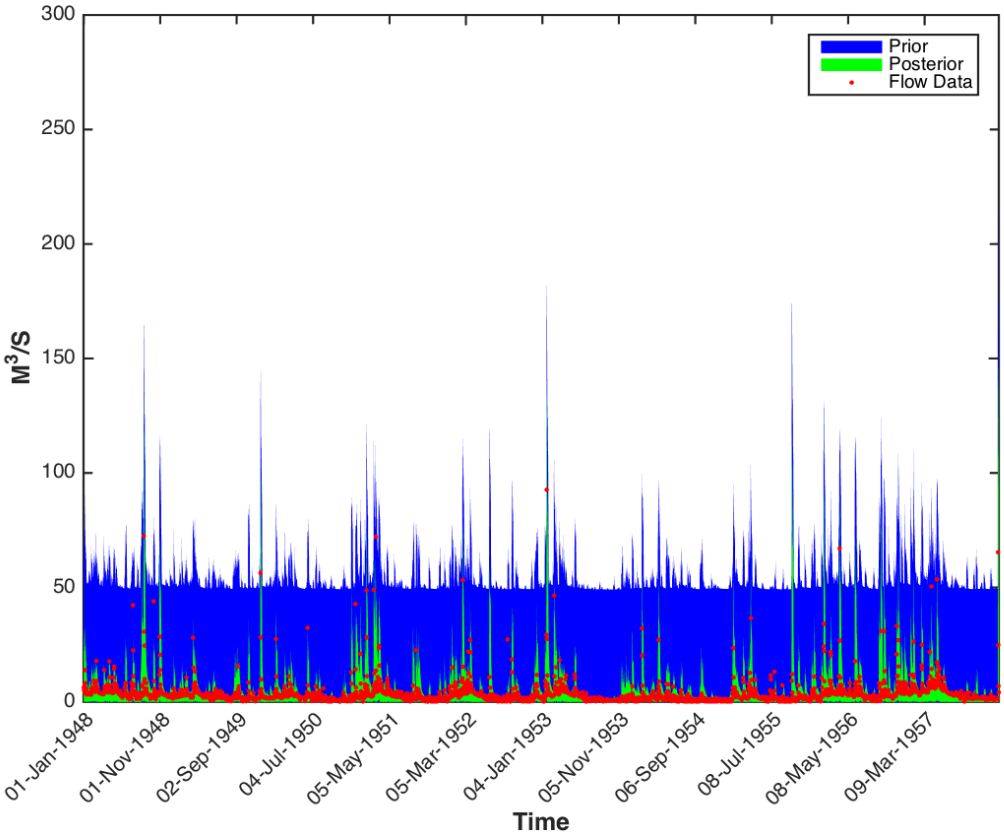
Prior
Posterior
Flow Data
300
250
200
150
100
50
0
M3/S
01-Jan-1948
01-Nov-1948
02-Sep-1949
04-Jul-1950
05-May-1951
05-Mar-1952
04-Jan-1953
05-Nov-1953
06-Sep-1954
08-Jul-1955
08-May-1956
09-Mar-1957
Time

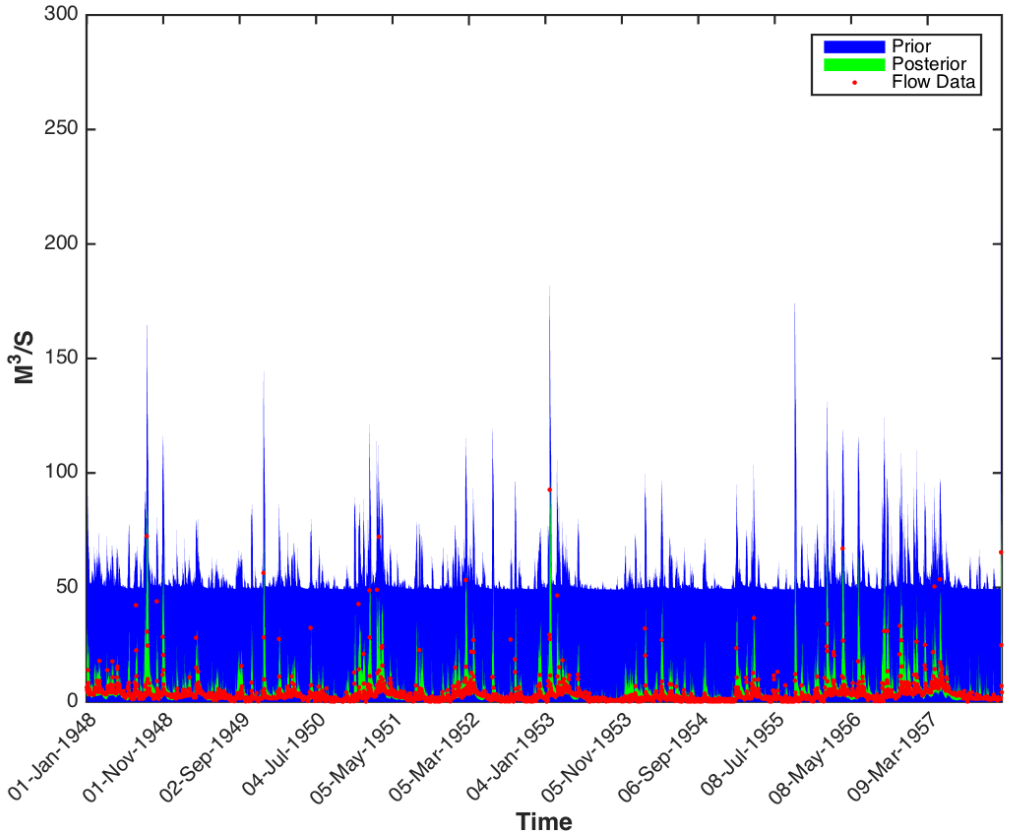

Figure 6.83. Predictive uncertainty ranges of GR4J model constrained against Henry Fork watershed (USGS ID 02143000) using FDC Medium Segment Volume (FDC MSV) Prior channel inflow in blue, posterior channel flow in green and observed data in red

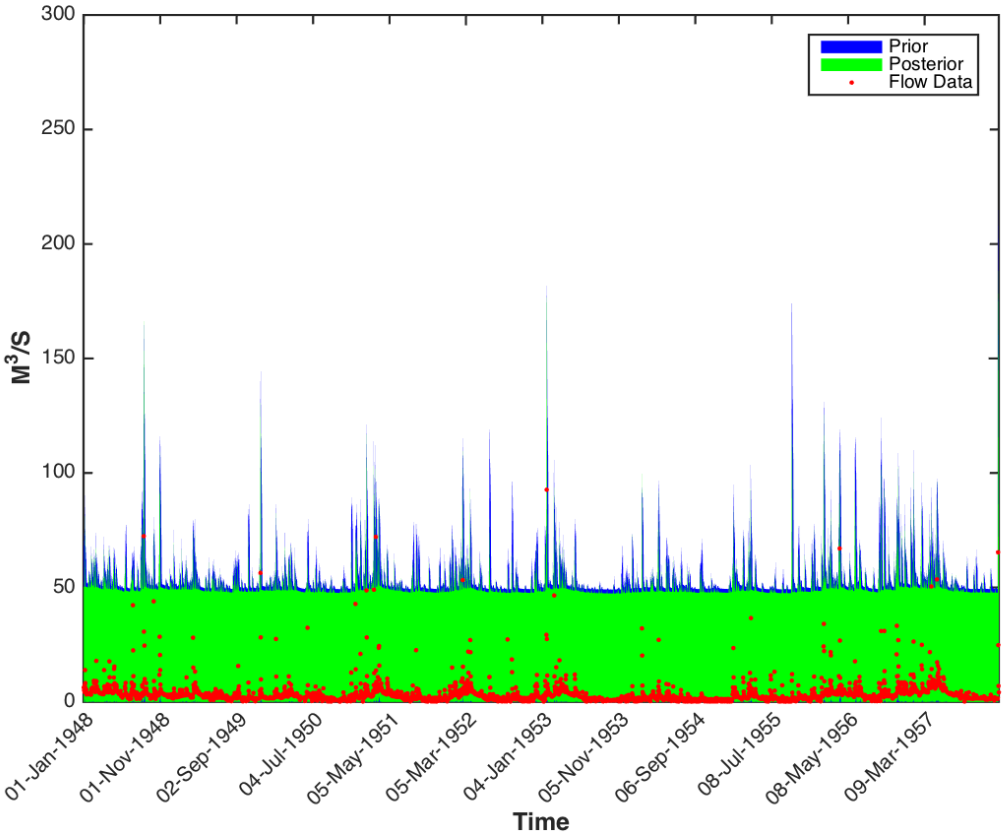

Figure 6.84. Predictive uncertainty ranges of GR4J model constrained against Henry Fork watershed (USGS ID 02143000) using Auto Correlation of Hydrograph with 1 Day Lag (AC) Prior channel inflow in blue, posterior channel flow in green and observed data in red

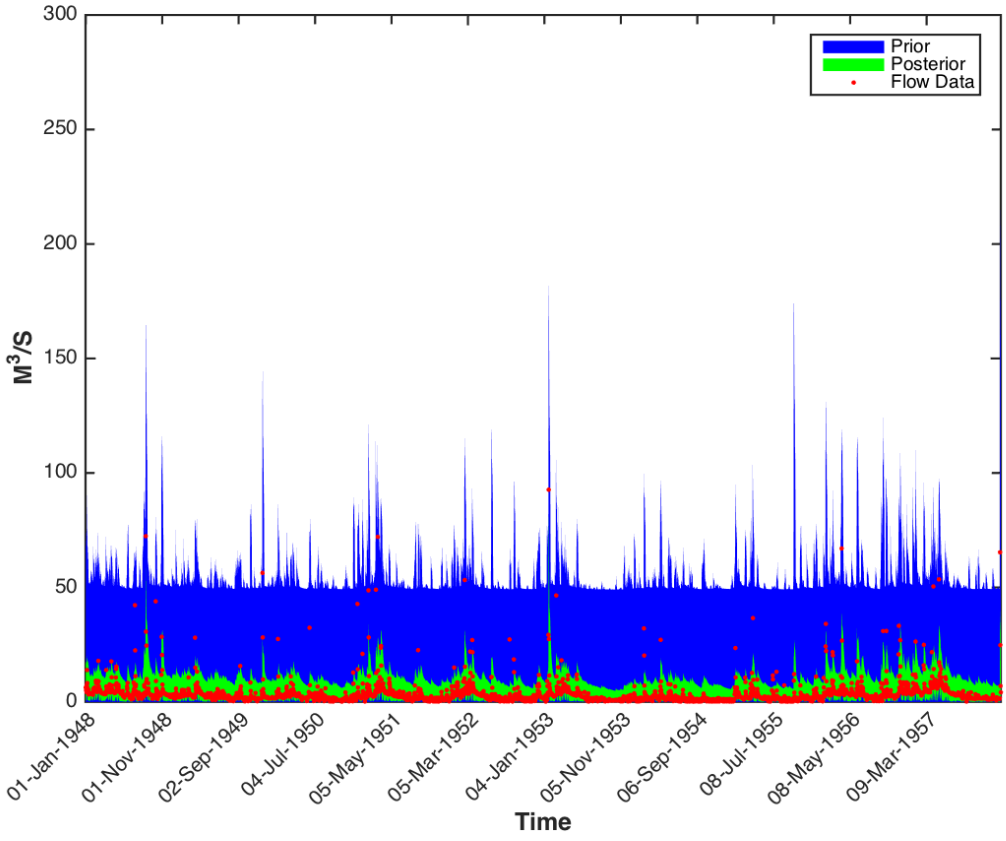
Prior
Posterior
Flow Data
M3/S
300
250
200
150
100
50
0
01-Jan-1948
01-Nov-1948
02-Sep-1949
04-Jul-1950
05-May-1951
05-Mar-1952
04-Jan-1953
05-Nov-1953
06-Sep-1954
08-Jul-1955
08-May-1956
09-Mar-1957
Time

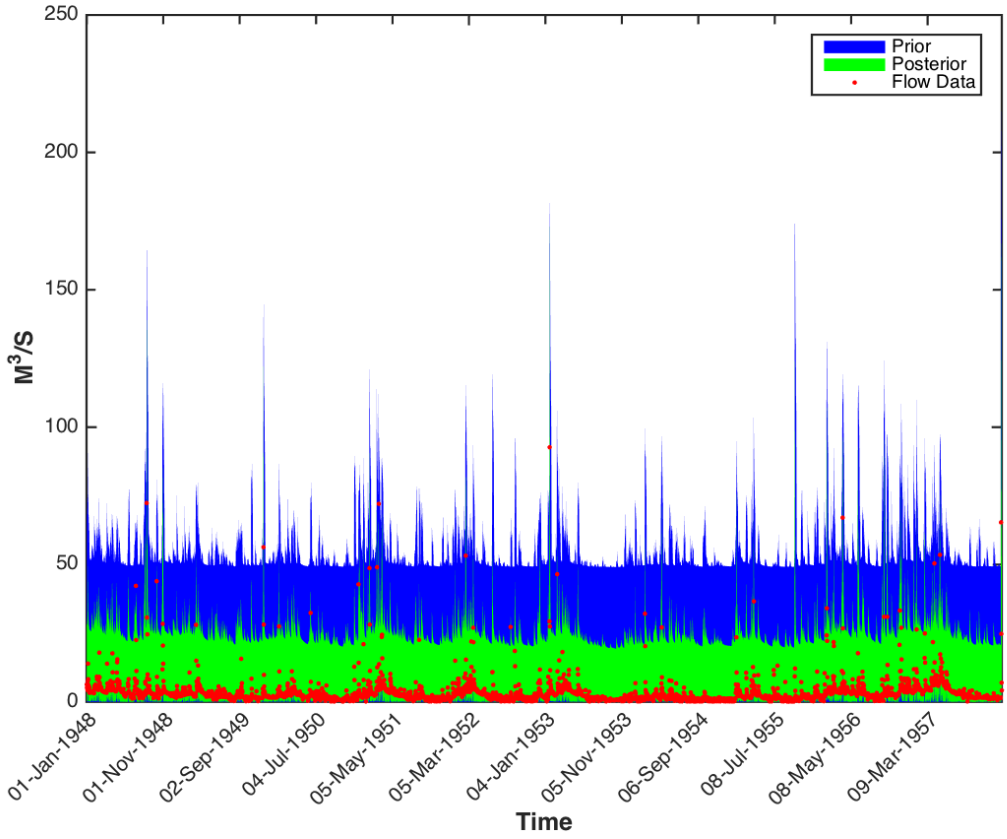

Figure 6.86. Predictive uncertainty ranges of GR4J model constrained against Henry Fork watershed (USGS ID 02143000) using Reclining LIMB Destiny (RLD) Prior channel inflow in blue, posterior channel flow in green and observed data in red

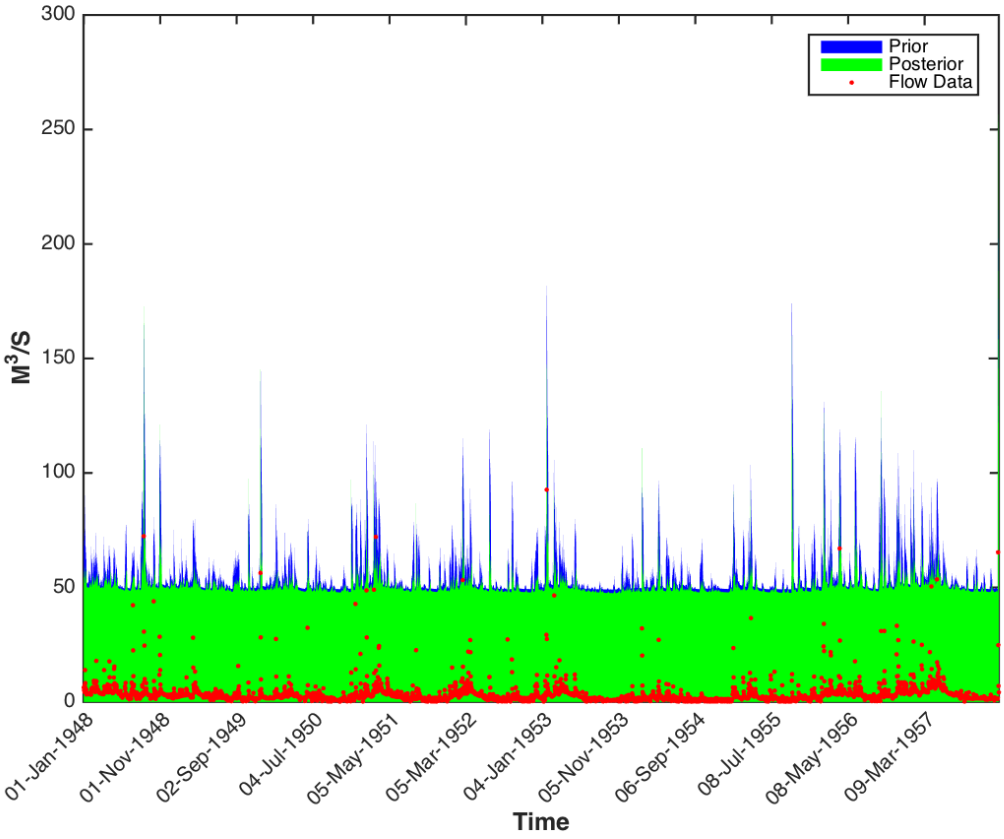

Figure 6.87. Predictive uncertainty ranges of GR4J model constrained against Henry Fork watershed (USGS ID 02143000) using Declining LIMB Destiny (DLD) Prior channel inflow in blue, posterior channel flow in green and observed data in red

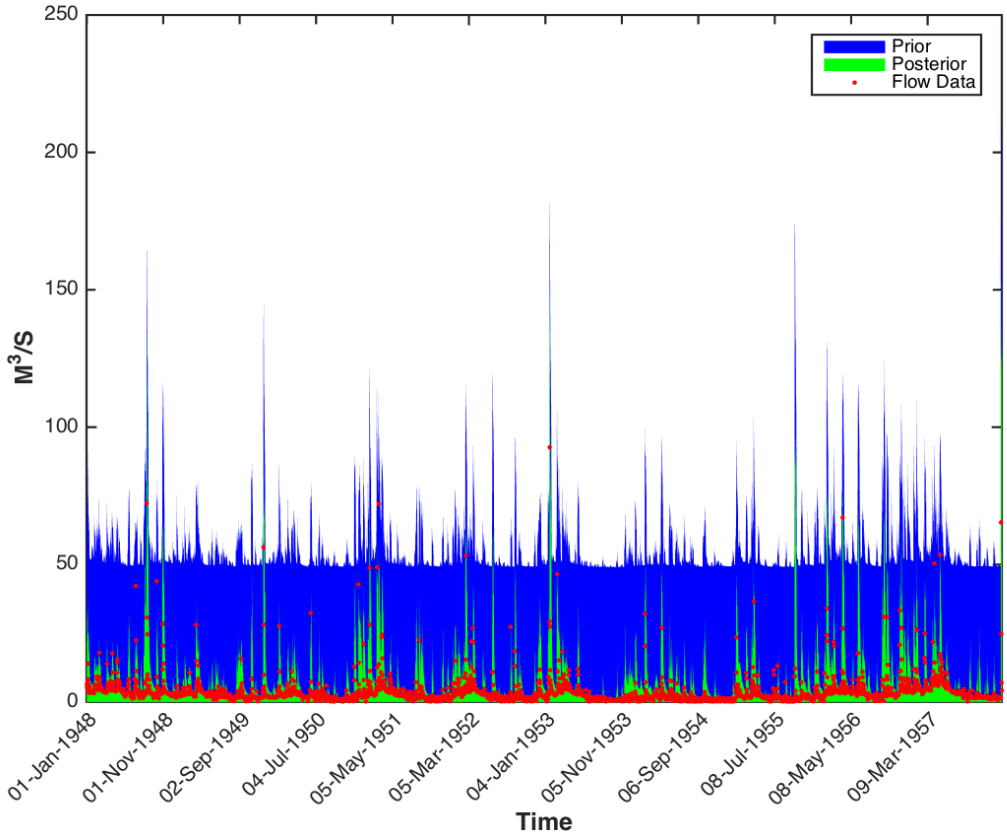

Figure 6.88. Predictive uncertainty ranges of GR4J model constrained against Henry Fork watershed (USGS ID 02143000) using 1st Flow Percentile (Q1st) Prior channel inflow in blue, posterior channel flow in green and observed data in red

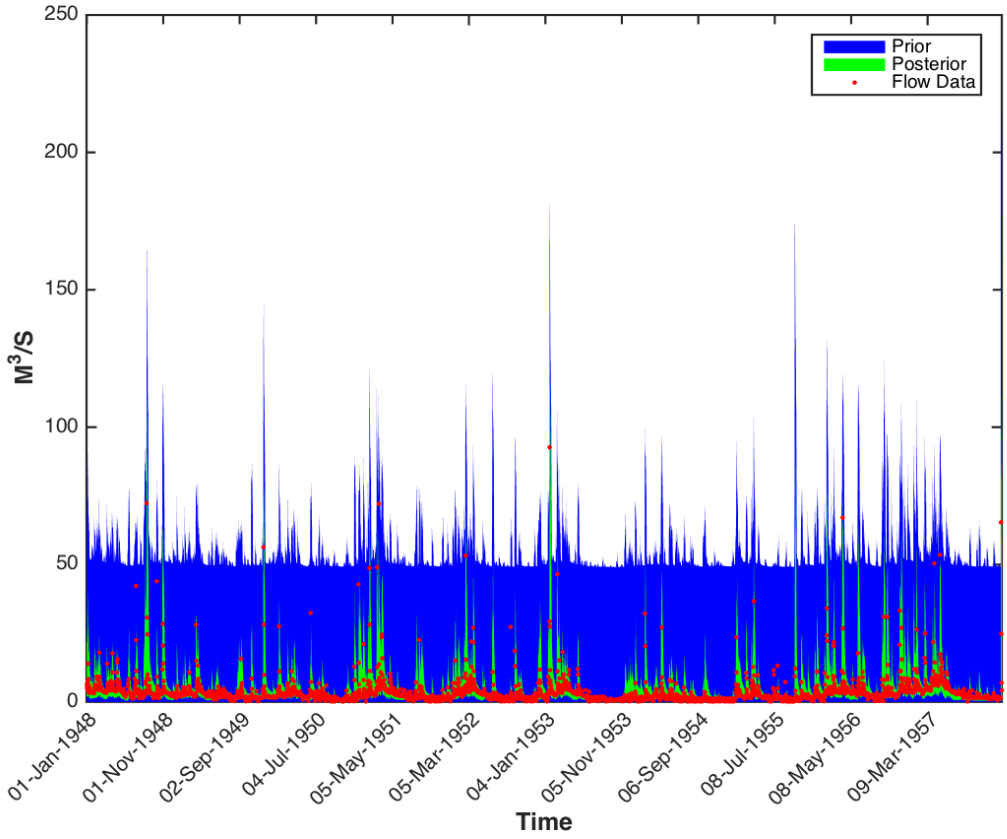

Figure 6.89. Predictive uncertainty ranges of GR4J model constrained against Henry Fork watershed (USGS ID 02143000) using 5th Flow Percentile (Q5th) Prior channel inflow in blue, posterior channel flow in green and observed data in red

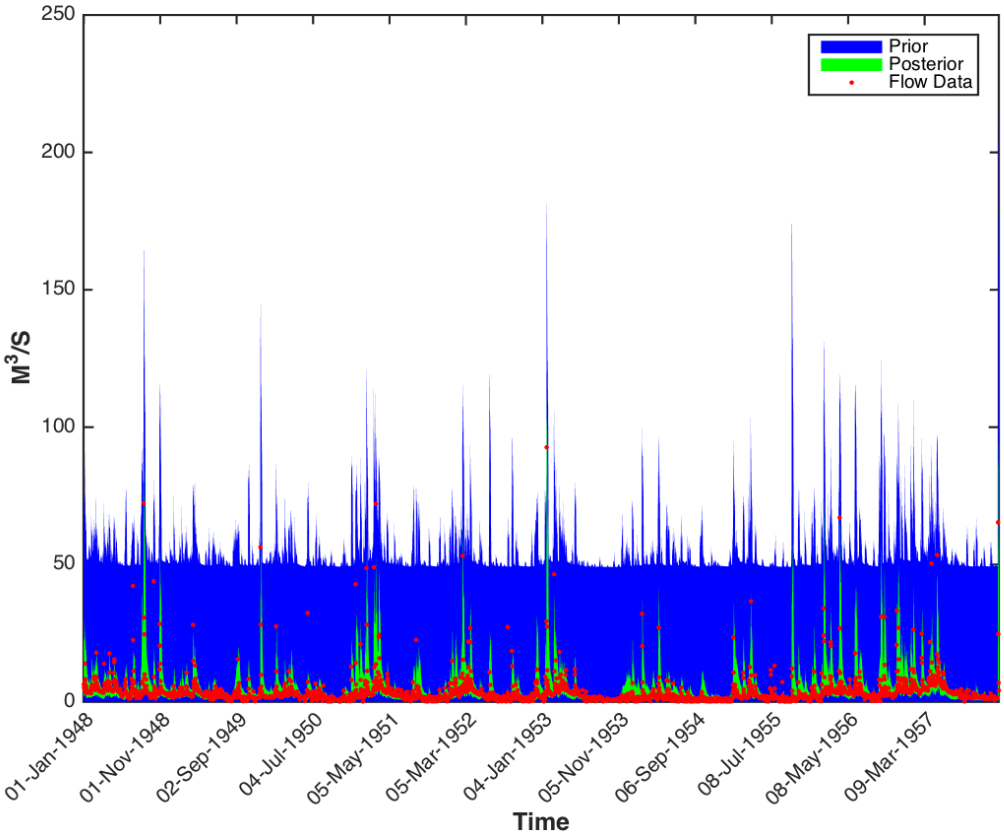

Figure 6.70. Predictive uncertainty ranges of GR4J model constrained against Henry Fork watershed (USGS ID 02143000) using 15th Flow Percentile (Q15th) Prior channel inflow in blue, posterior channel flow in green and observed data in red

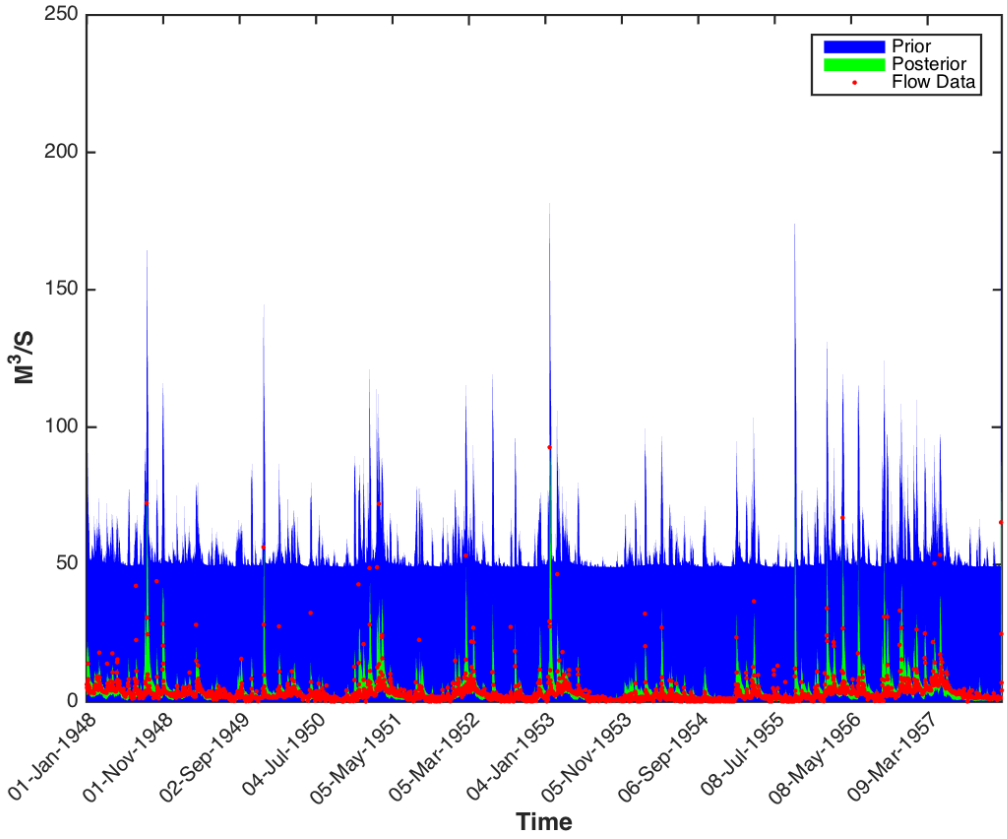

Figure 6.71.. Predictive uncertainty ranges of GR4J model constrained against Henry Fork watershed (USGS ID 02143000) using 50th Flow Percentile (Q50th) Prior channel inflow in blue, posterior channel flow in green and observed data in red

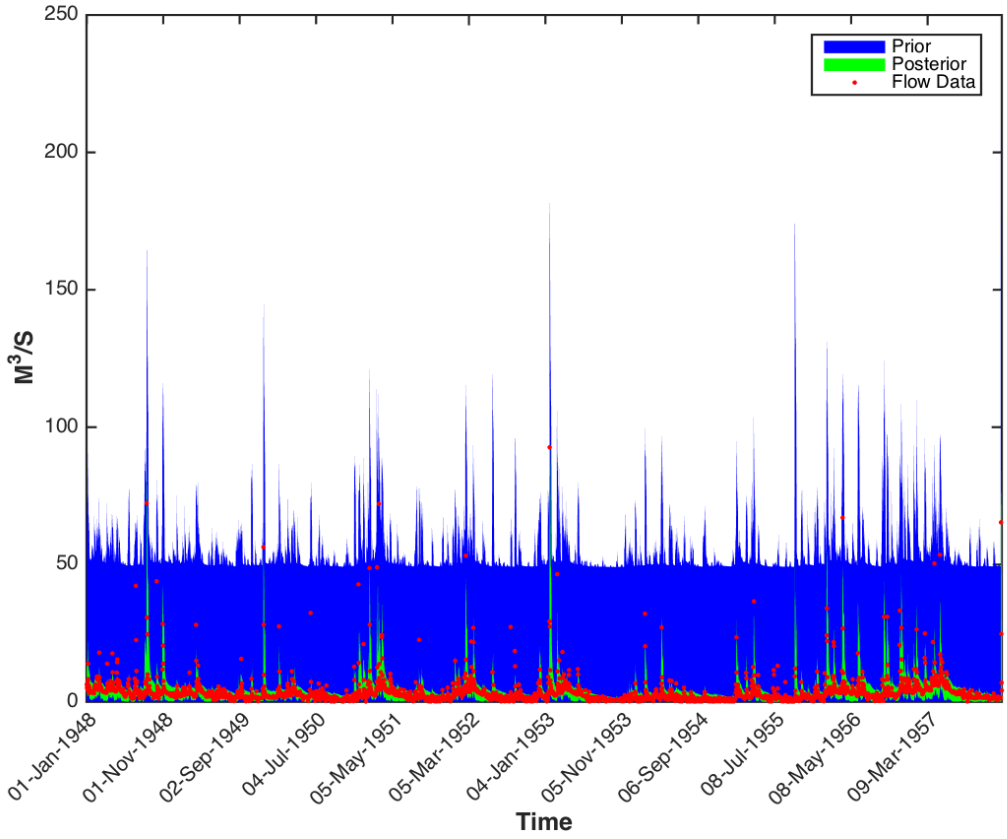

Figure 6.72. Predictive uncertainty ranges of GR4J model constrained against Henry Fork watershed (USGS ID 02143000) using 95th Flow Percentile (Q95th) Prior channel inflow in blue, posterior channel flow in green and observed data in red

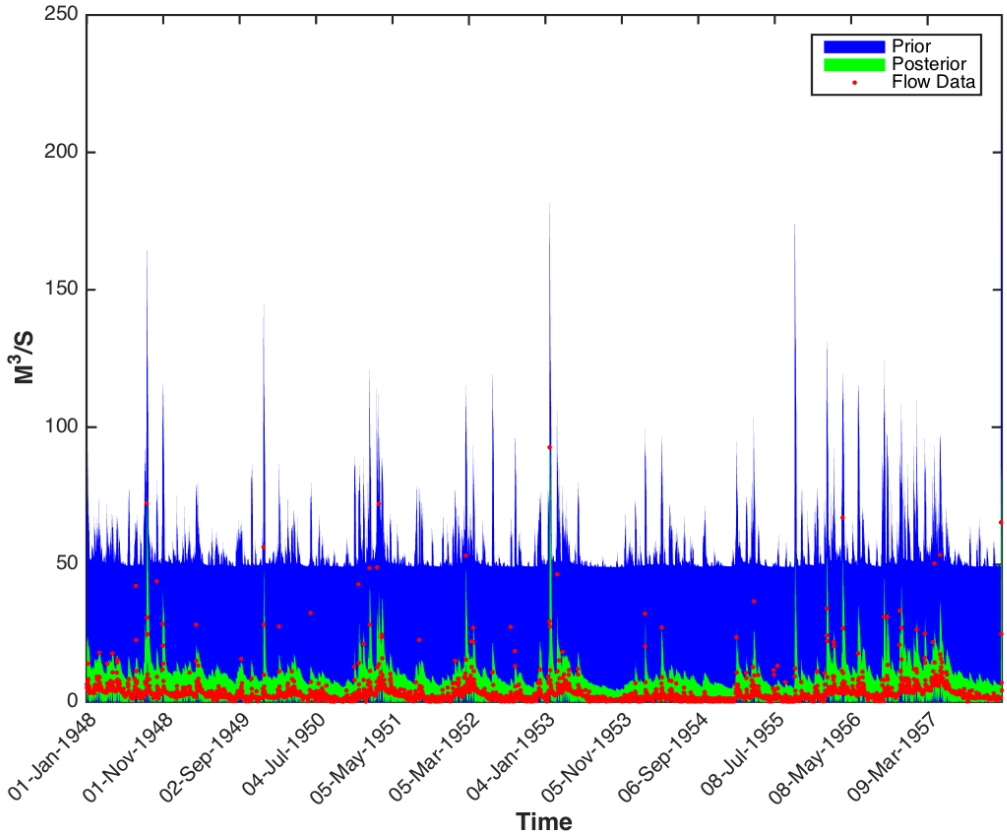

Figure 6.73 Predictive uncertainty ranges of GR4J model constrained against Henry Fork watershed (USGS ID 02143000) using 99th Flow Percentile (Q99th) Prior channel inflow in blue, posterior channel flow in green and observed data in red

02143000 HYMOD

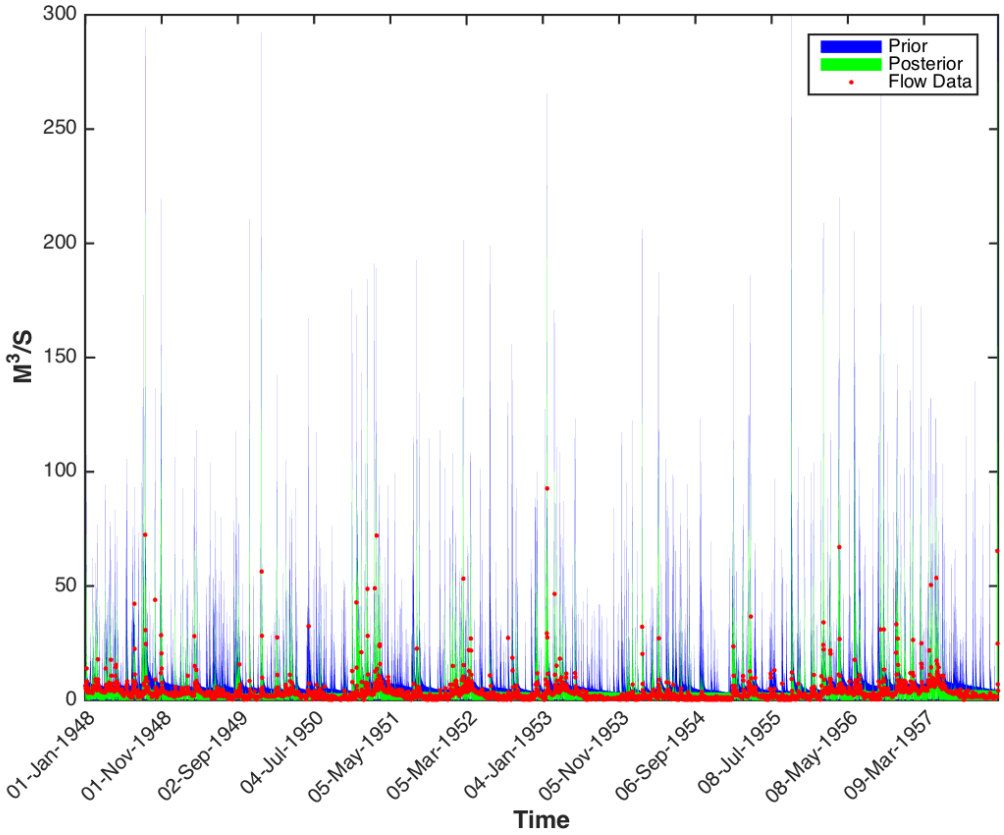

Figure 6.74. Predictive uncertainty ranges of HyModJ model constrained against Henry Fork watershed (USGS ID 02143000) using Runoff Ratio Metric (RR). Prior channel inflow in blue, posterior channel flow in green and observed data in red

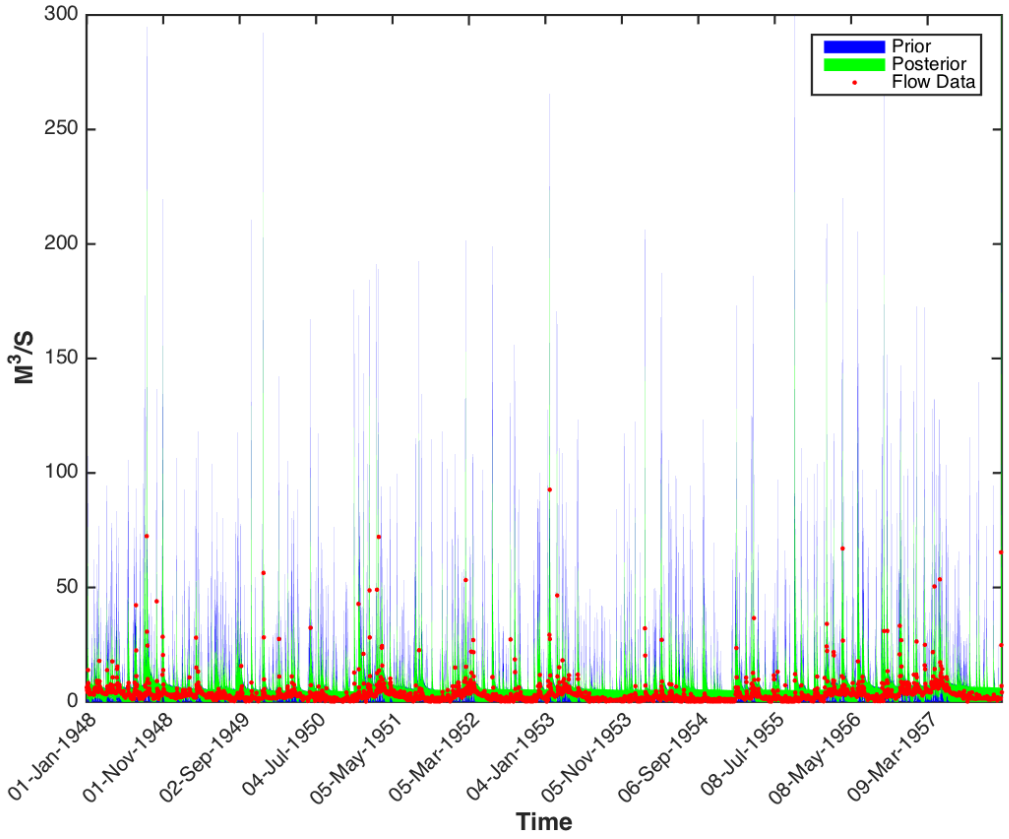

Figure 6.75. Predictive uncertainty ranges of HyModJ model constrained against Henry Fork watershed (USGS ID 02143000) using Base Flow Index (BFI). Prior channel inflow in blue, posterior channel flow in green and observed data in red

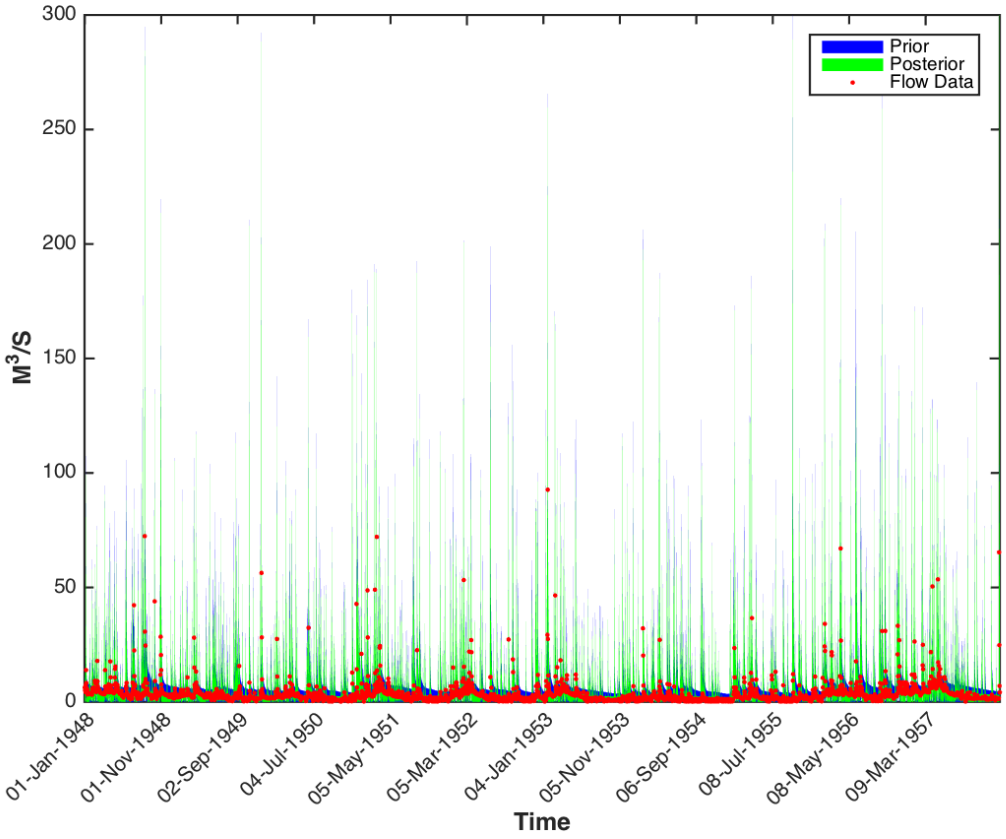

Figure 6.76. Predictive uncertainty ranges of HyModJ model constrained against Henry Fork watershed (USGS ID 02143000) using Base Flow Runoff Ratio (BFR). Prior channel inflow in blue, posterior channel flow in green and observed data in red

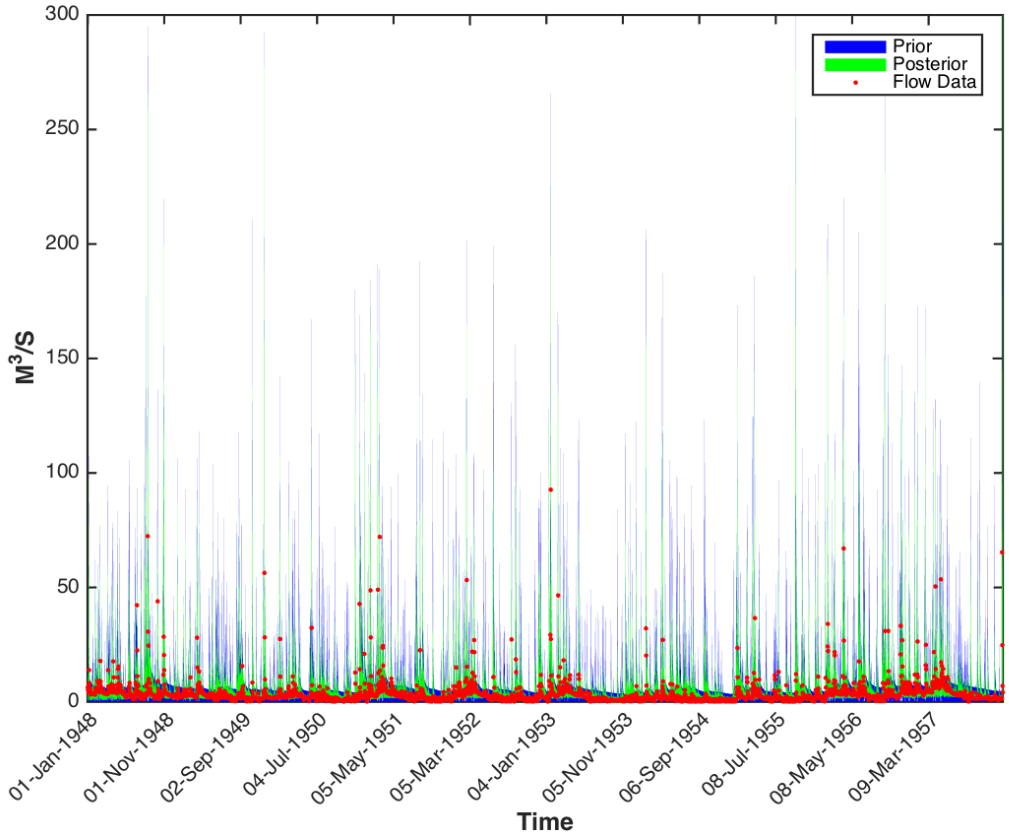

Figure 6.77. Predictive uncertainty ranges of HyModJ model constrained against Henry Fork watershed (USGS ID 02143000) using Slope of Log FDC 5th & 95th Percentile (SL FDC Q5th&Q95th). Prior channel inflow in blue, posterior channel flow in green and observed data in red

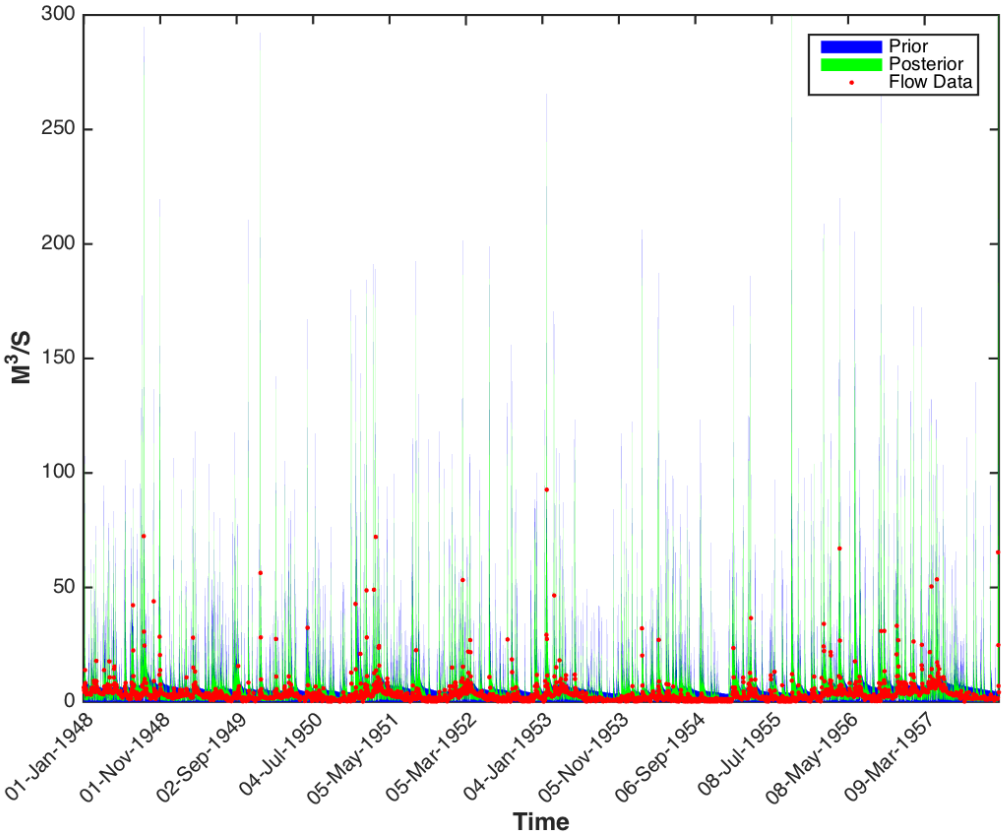

Figure 6.78. Predictive uncertainty ranges of HyModJ model constrained against Henry Fork watershed (USGS ID 02143000) using Slope of Log FDC 33 & 66 Percentile (SL FDC Q33th&Q66th). Prior channel inflow in blue, posterior channel flow in green and observed data in red

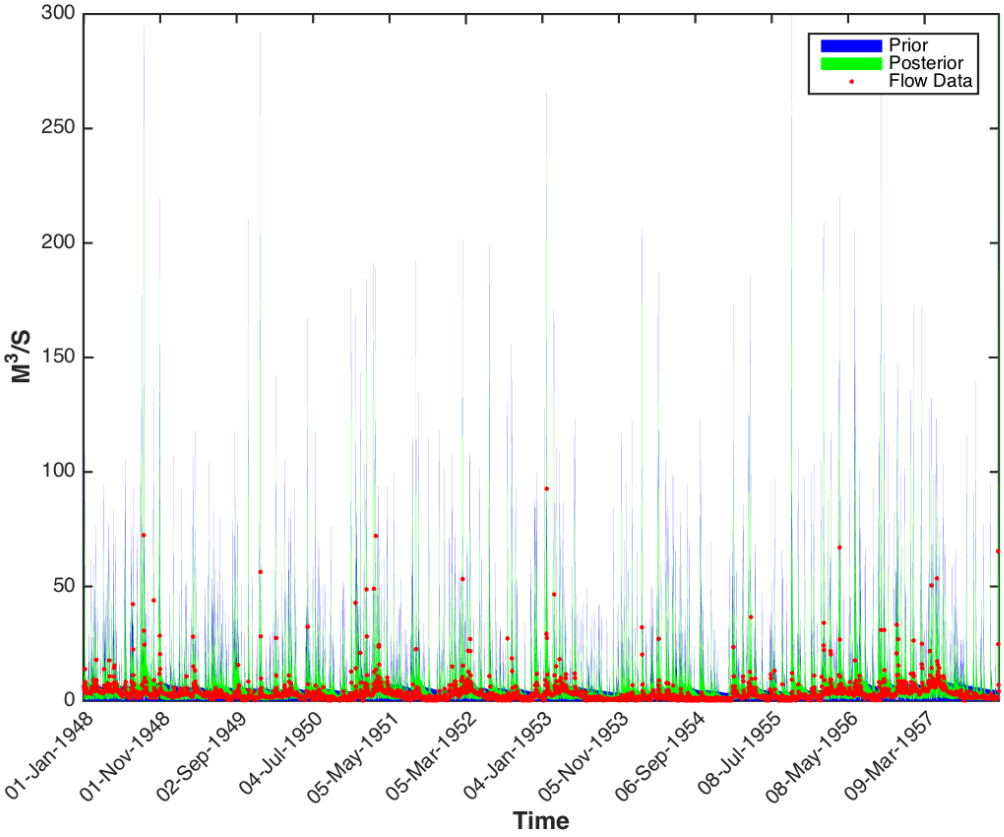
Prior
Posterior
Flow Data
M3/S
300
250
200
150
100
50
0
01-Jan-1948
01-Nov-1948
02-Sep-1949
04-Jul-1950
05-May-1951
05-Mar-1952
04-Jan-1953
05-Nov-1953
06-Sep-1954
08-Jul-1955
08-May-1956
09-Mar-1957
Time

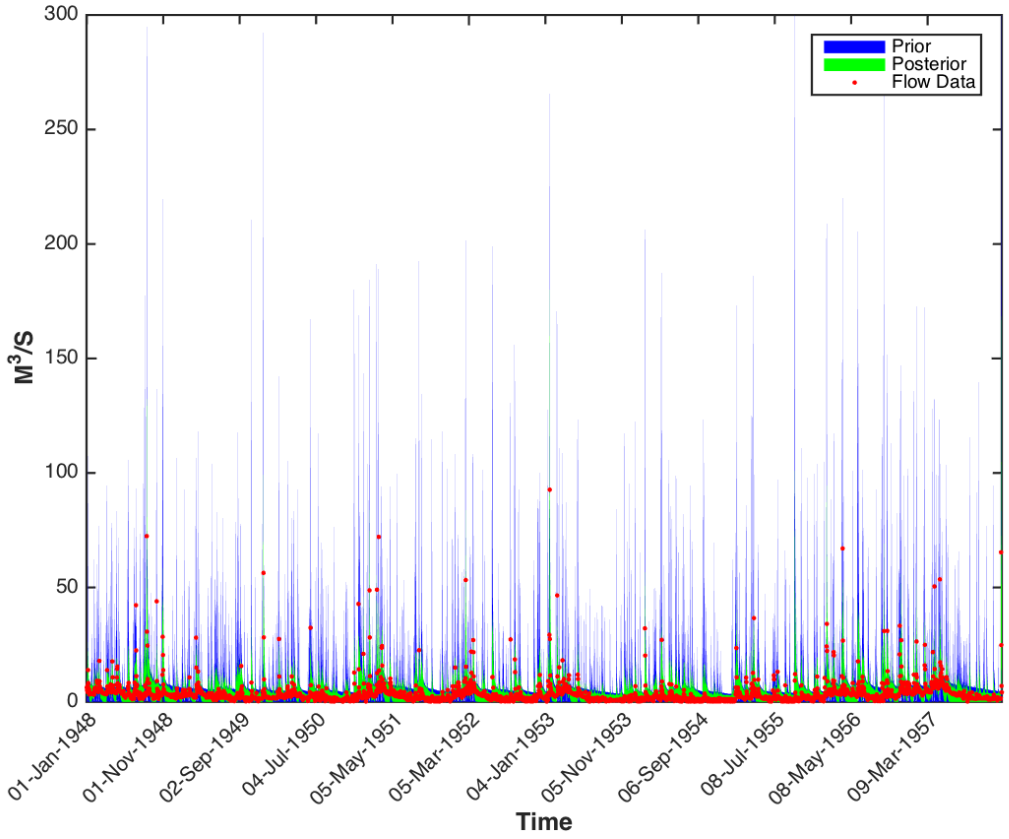

Figure 6.80. Predictive uncertainty ranges of HyModJ model constrained against Henry Fork watershed (USGS ID 02143000) using FDC High Segment Volume more than 90 Percentile (FDC HSV Q90th). Prior channel inflow in blue, posterior channel flow in green and observed data in red

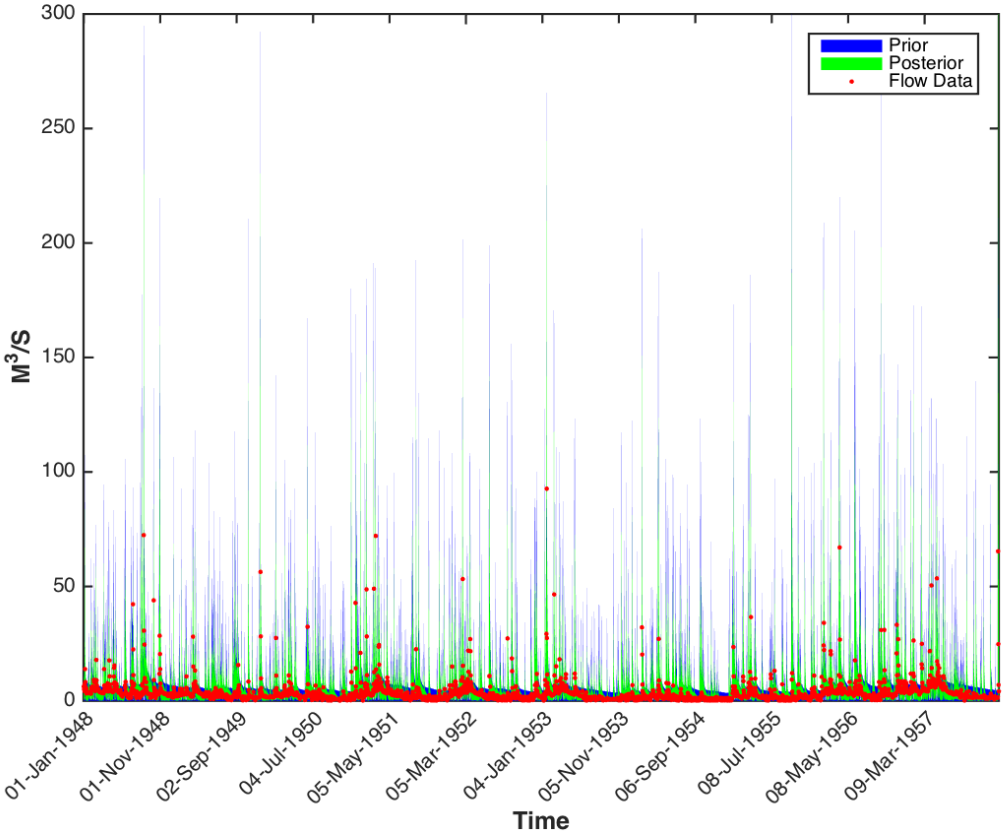
Prior
Posterior
Flow Data
300
250
200
150
100
50
0
M3/S
01-Jan-1948
01-Nov-1948
02-Sep-1949
04-Jul-1950
05-May-1951
05-Mar-1952
04-Jan-1953
05-Nov-1953
06-Sep-1954
08-Jul-1955
08-May-1956
09-Mar-1957
Time

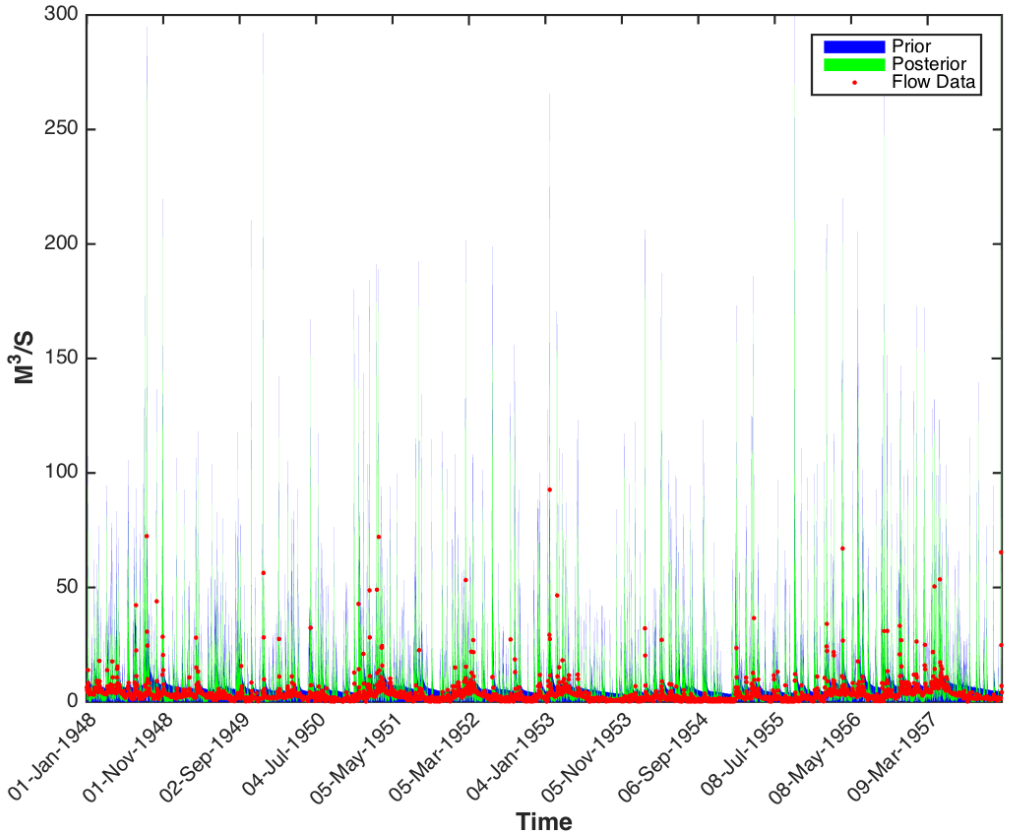

Figure 6.82. Predictive uncertainty ranges of HyModJ model constrained against Henry Fork watershed (USGS ID 02143000) using FDC Medium Segment Volume (FDC MSV) Prior channel inflow in blue, posterior channel flow in green and observed data in red

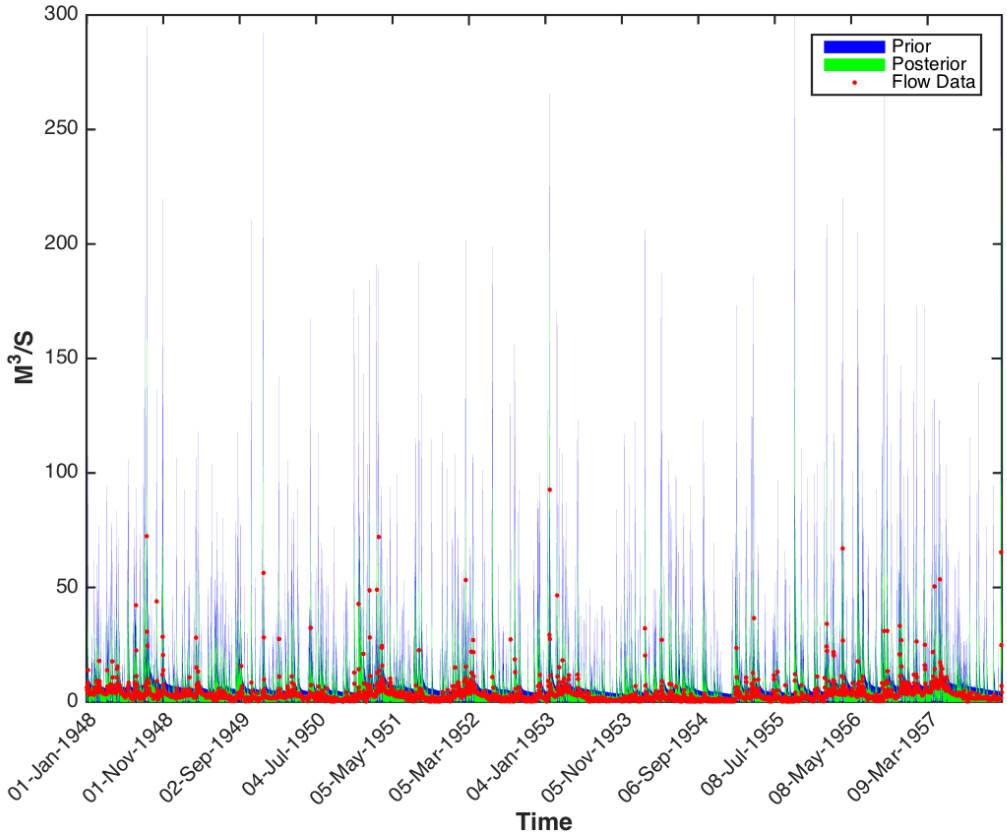
Prior
Posterior
Flow Data
300
250
200
150
100
50
0
M3/S
01-Jan-1948
01-Nov-1948
02-Sep-1949
04-Jul-1950
05-May-1951
05-Mar-1952
04-Jan-1953
05-Nov-1953
06-Sep-1954
08-Jul-1955
08-May-1956
09-Mar-1957
Time

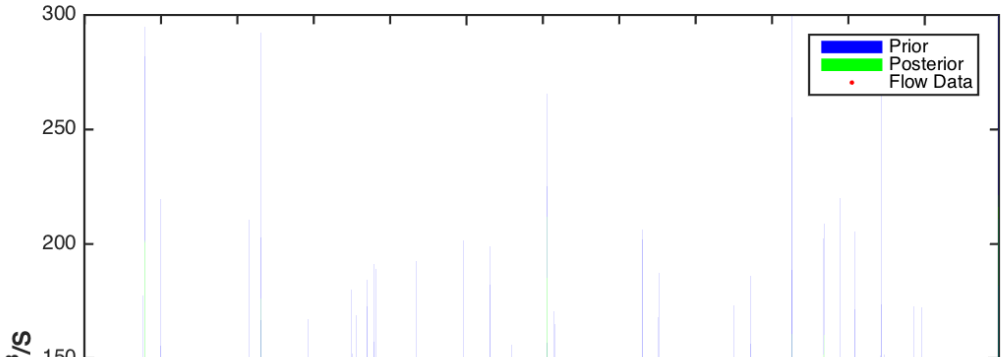

Figure 6.83. Predictive uncertainty ranges of HyModJ model constrained against Henry Fork watershed (USGS ID 02143000) using Auto Correlation of Hydrograph with 1 Day Lag (AC) Prior channel inflow in blue, posterior channel flow in green and observed data in red

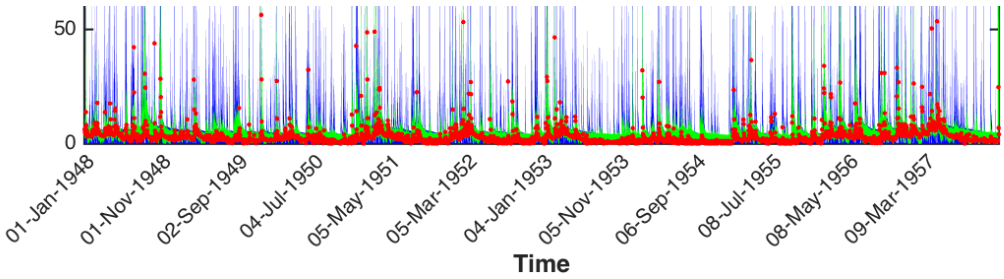

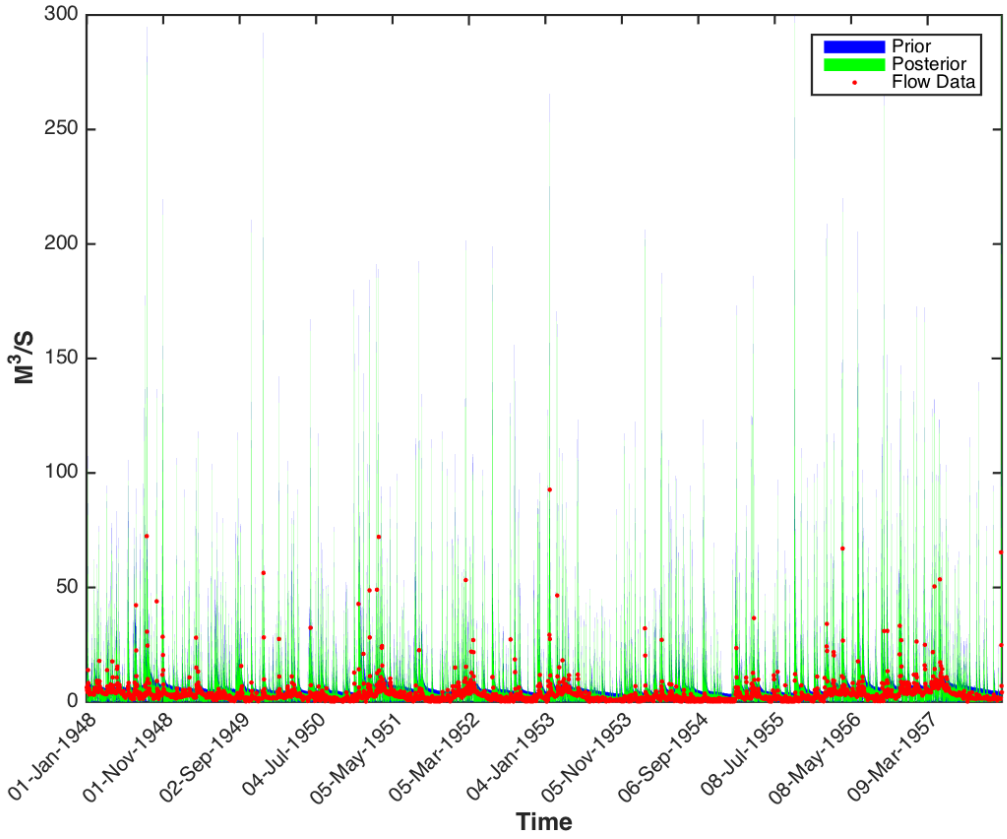
Prior
Posterior
Flow Data
M3/S
Time
300
250
200
150
100
50
0
01-Jan-1948
01-Nov-1948
02-Sep-1949
04-Jul-1950
05-May-1951
05-Mar-1952
04-Jan-1953
05-Nov-1953
06-Sep-1954
08-Jul-1955
08-May-1956
09-Mar-1957

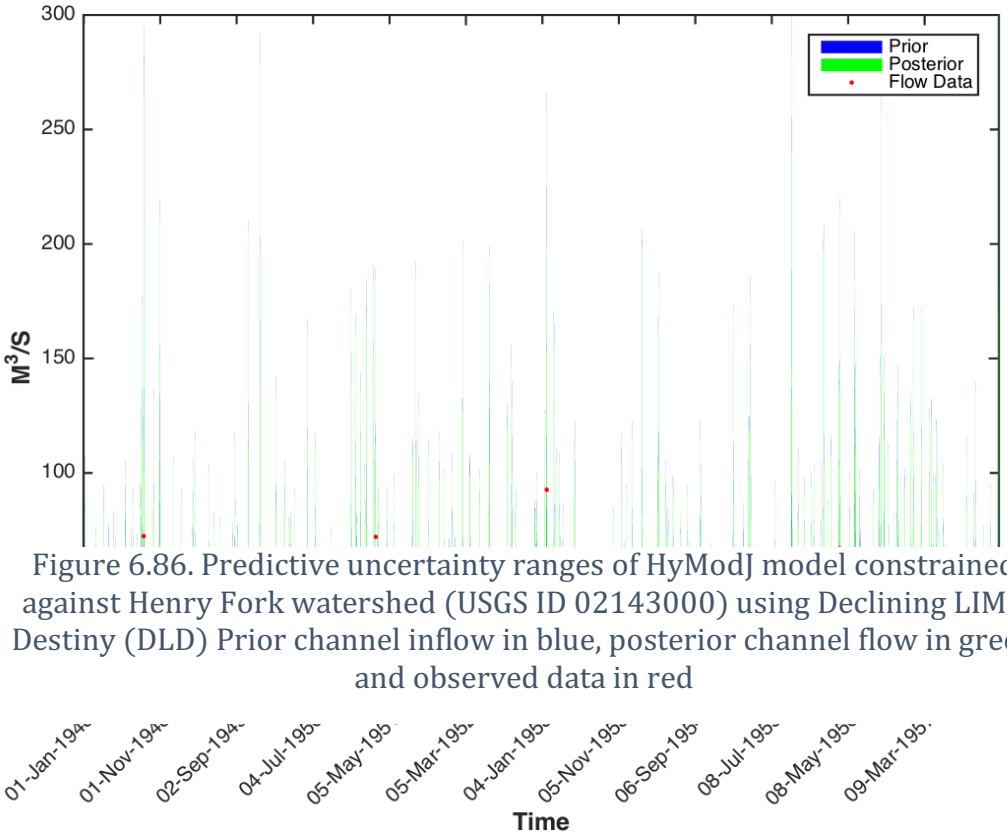

Figure 6.86. Predictive uncertainty ranges of HyModJ model constrained against Henry Fork watershed (USGS ID 02143000) using Declining LIMB Destiny (DLD) Prior channel inflow in blue, posterior channel flow in green and observed data in red

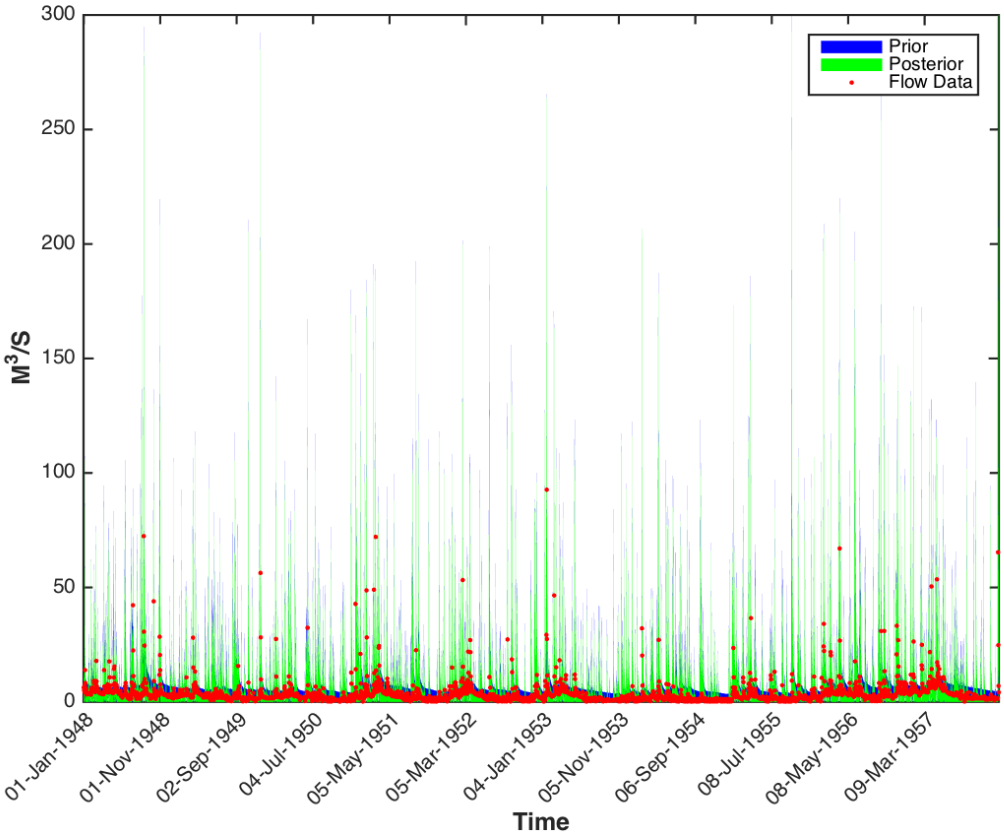

Figure 6.87. Predictive uncertainty ranges of HyModJ model constrained against Henry Fork watershed (USGS ID 02143000) using 1st Flow Percentile (Q1st) Prior channel inflow in blue, posterior channel flow in green and observed data in red

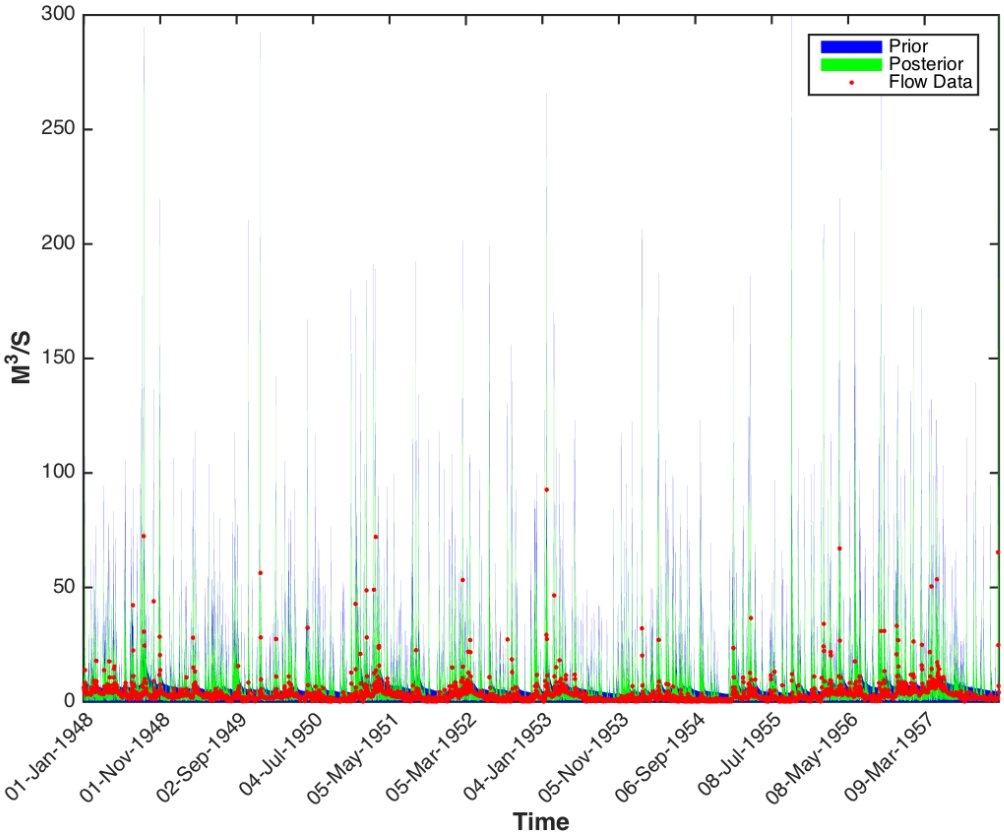

Figure 6.88. Predictive uncertainty ranges of HyModJ model constrained against Henry Fork watershed (USGS ID 02143000) using 5th Flow Percentile (Q5th) Prior channel inflow in blue, posterior channel flow in green and observed data in red

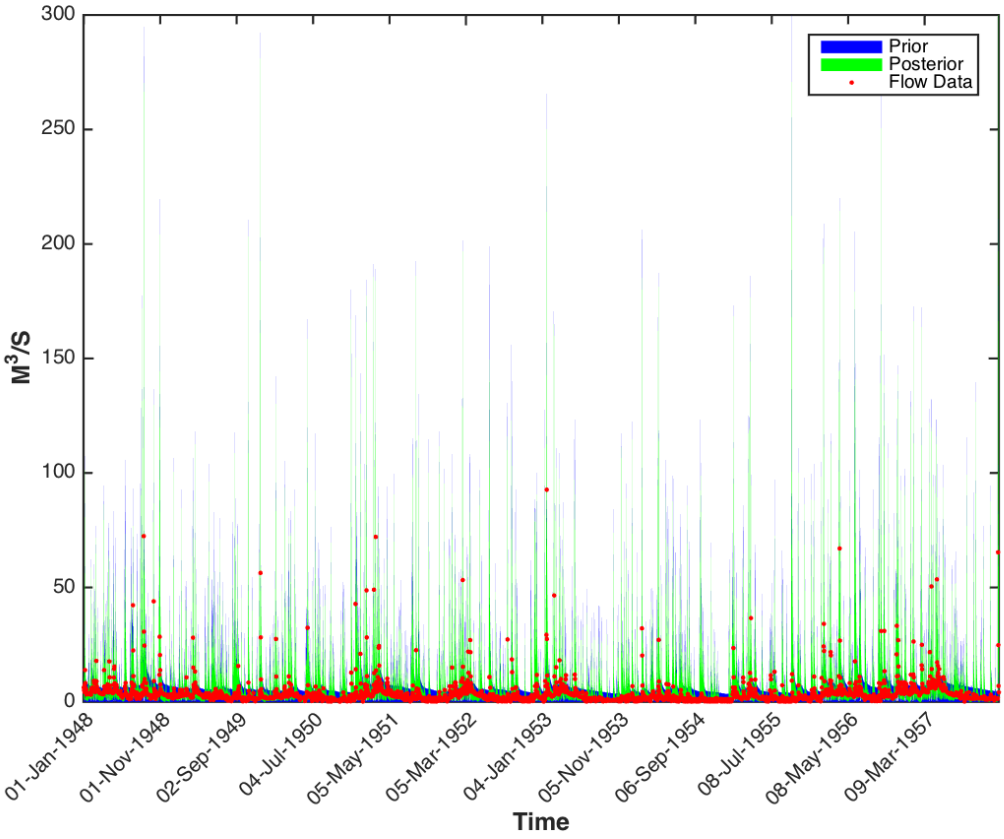

Figure 6.89. Predictive uncertainty ranges of HyModJ model constrained against Henry Fork watershed (USGS ID 02143000) using 15th Flow Percentile (Q15th) Prior channel inflow in blue, posterior channel flow in green and observed data in red

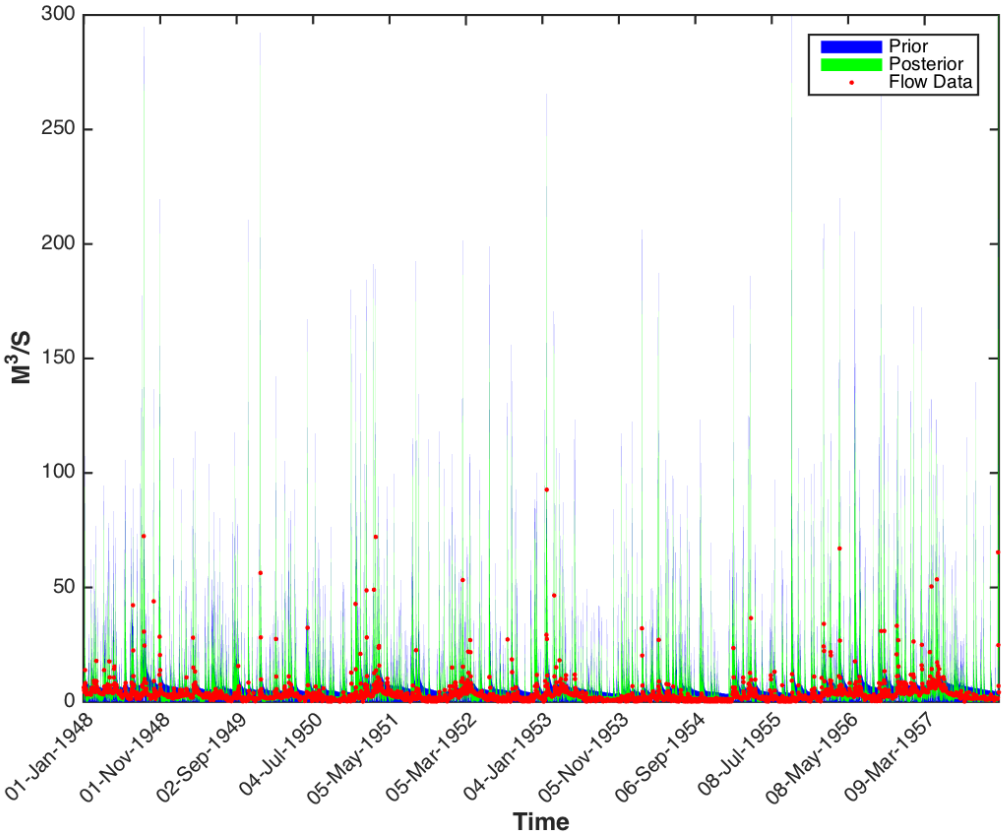

Figure 6.90. Predictive uncertainty ranges of HyModJ model constrained against Henry Fork watershed (USGS ID 02143000) using 50th Flow Percentile (Q50th) Prior channel inflow in blue, posterior channel flow in green and observed data in red

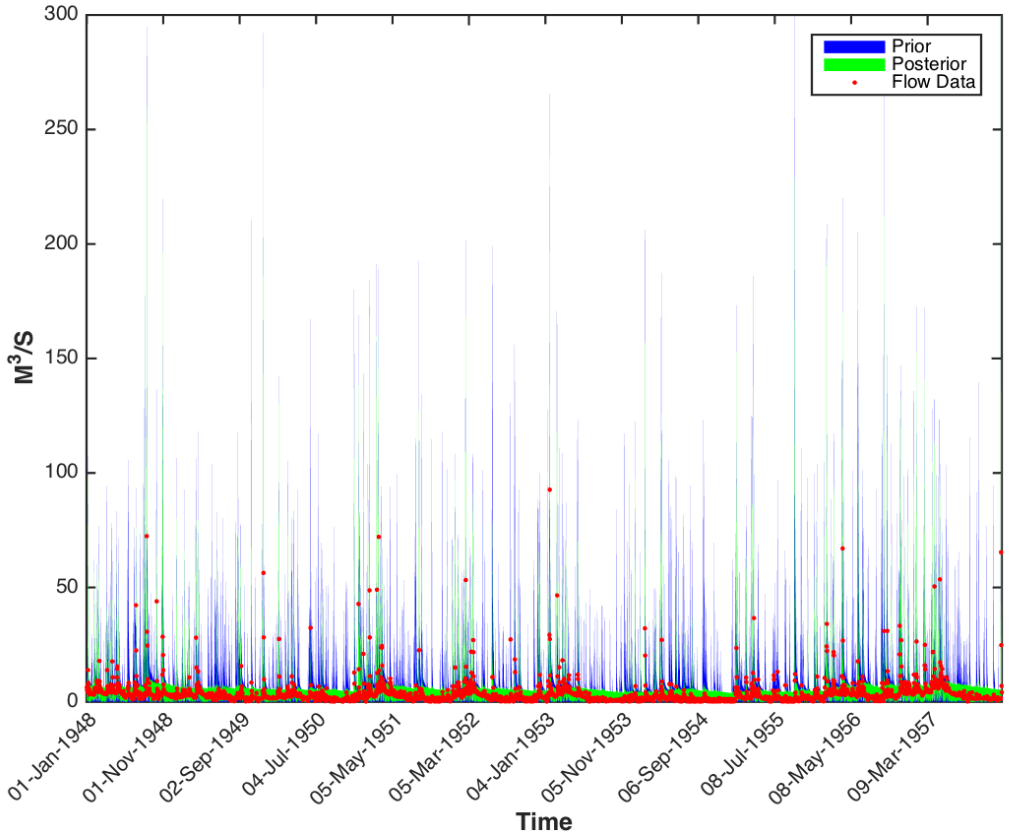

Figure 6.91. Predictive uncertainty ranges of HyMod model constrained against Henry Fork watershed (USGS ID 02143000) using 95th Flow Percentile (Q95th) Prior channel inflow in blue, posterior channel flow in green and observed data in red

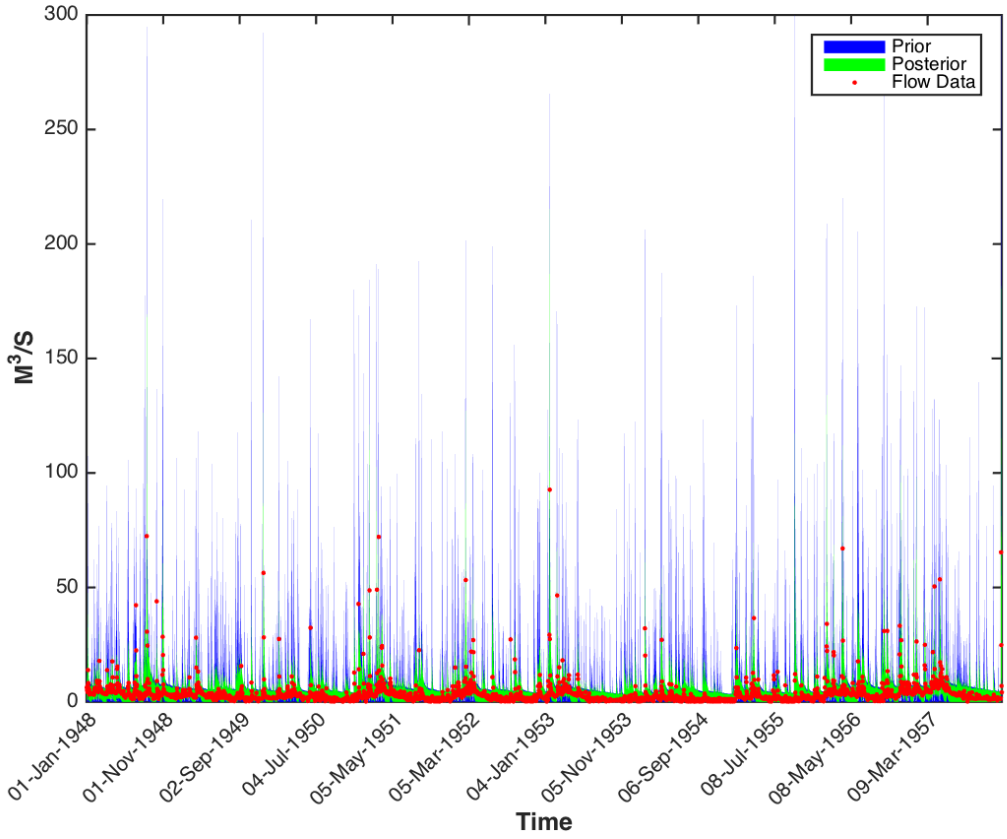

Figure 6.92. Predictive uncertainty ranges of HyMod model constrained against Henry Fork watershed (USGS ID 02143000) using 99th Flow Percentile (Q99th) Prior channel inflow in blue, posterior channel flow in green and observed data in red